

DISSERTATION

INDIRECT ELECTROCHEMICAL DETECTION OF DNA HYBRIDIZATION  
BASED ON CATALYTIC OXIDATION OF COBALT (II) AND CONCENTRATION  
GRADIENT FORMATION IN REDOX CONDUCTING POLYMERS

Submitted by

Di Xue

Department of Chemistry

In partial fulfillment of the requirements

for the Degree of Doctor of Philosophy

Colorado State University

Fort Collins, CO

Summer 2008

UMI Number: 3332717

## INFORMATION TO USERS

The quality of this reproduction is dependent upon the quality of the copy submitted. Broken or indistinct print, colored or poor quality illustrations and photographs, print bleed-through, substandard margins, and improper alignment can adversely affect reproduction.

In the unlikely event that the author did not send a complete manuscript and there are missing pages, these will be noted. Also, if unauthorized copyright material had to be removed, a note will indicate the deletion.

**UMI**<sup>®</sup>

---

UMI Microform 3332717

Copyright 2008 by ProQuest LLC.

All rights reserved. This microform edition is protected against unauthorized copying under Title 17, United States Code.

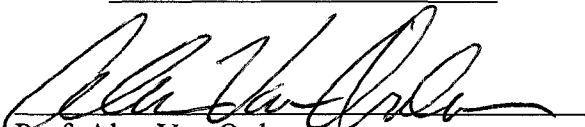
ProQuest LLC  
789 E. Eisenhower Parkway  
PO Box 1346  
Ann Arbor, MI 48106-1346

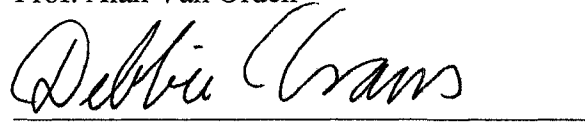
COLORADO STATE UNIVERSITY

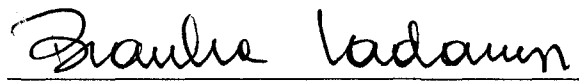
JULY 9, 2008

WE HEREBY RECOMMEND THAT THE DISSERTATION PREPARED UNDER OUR SUPERVISION BY DI XUE ENTITLED "INDIRECT ELECTROCHEMICAL DETECTION OF DNA HYBRIDIZATION BASED ON CATALYTIC OXIDATION OF COBALT (II) AND CONCENTRATION GRADIENT FORMATION IN REDOX CONDUCTING POLYMERS" BE ACCEPTED AS FULFILLING IN PART THE REQUIREMENTS FOR THE DEGREE OF DOCTOR OF PHILOSOPHY.

Committee on Graduate Work

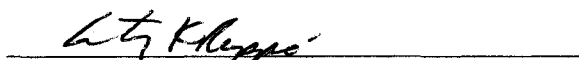
  
Prof. Alan Van Orden

  
Prof. Debbie Crans

  
Prof. Branka Ladanyi

  
Prof. Olve Peersen

  
Prof. C. Michael Elliott, Advisor

  
Prof. Anthony Rappé, Department Chair

## ABSTRACT OF DISSERTATION

### INDIRECT ELECTROCHEMICAL DETECTION OF DNA HYBRIDIZATION BASED ON CATALYTIC OXIDATION OF COBALT (II) AND CONCENTRATION GRADIENT FORMATION IN REDOX CONDUCTING POLYMERS

Since Millan and Mikkelsen introduced the new concept back in 1993, efforts to develop electrochemical methods for detecting nucleic acid hybridization (e.g., DNA) have mushroomed. At least four commercial products based on electrochemical methods are marketed. Compared with nearly all other analytical techniques, electrochemical instrumentation is inexpensive, robust, and relatively simple to operate.

The first part of the dissertation (Chapter 1 to Chapter 4) describes the development of a novel electrochemical DNA sensor based on catalytic oxidation of a cobalt bipyridine "mediator molecule" on an ITO electrode. Interaction of the surface bound DNA probe with the DNA target results in formation of hybrid duplex, which subsequently brings redox catalyst molecules from solution to the electrode surface. The mode of selective catalyst binding is intercalation between base pairs of ds-DNA. This surface-bound catalyst "turns on" the redox chemistry of the mediator molecule which is otherwise kinetically inert to oxidation on ITO. With this approach, we demonstrate detection of a 20-mer DNA target oligonucleotide at picomolar concentrations with outstanding signal-to-noise.

Chapter 2 is focused on identification of the best catalyst which exhibits efficient catalysis in the desired potential range where no oxidation of DNA occurs; Screening for the best probe immobilization approach is described in Chapter 3 and electrochemical sensing of DNA hybridization events in Chapter 4. Detections of the synthetic 20-mer target were performed at various concentrations ranging from micromolar to picomolar and even subpicomolar. The effect of the concentration of the Co(II) mediator is also investigated. The ITO sensing platform varies in area from  $0.5 \text{ cm}^2$  to  $0.1 \text{ mm}^2$ , including single electrodes of 7 mm diameter, 7x8 array electrodes of 3 mm diameter and 1x 8 microarray electrodes of 1 mm x 0.1 mm. This study also explores detection of a synthetic target DNA in a dilute blood serum matrix.

The second part of our research (Chapter 5) mainly concerns redox polymer films containing permanently locked concentration gradients. Upon redox gradient formation, the conducting polymer displays interesting properties, such as solid diode behavior and electroluminescence. Previous methods explored drying and/or cooling the film to physically immobilize its redox gradient. Unfortunately, this preservation was temporary, finite ionic motion and the subsequent degradation of the gradients could be induced over time. Our work is aimed to overcome limitations of the cooling/drying approach by covalently attaching counterions to the polymer backbone and thus permanently locking the redox gradients.

Both parts of this dissertation utilize heteroleptic metal complexes possessing redox potentials close to zero (vs SSCE). Compounds with highly negative potentials are strongly reducing and highly positive potentials means strong oxidizing capabilities,

which exerts strict requirements on supporting electrolytes and solvents, including high impurity, broad potential window as well as exclusion of environmental interference, for instance air and water. Thus, the closer the potential to zero (vs SSCE), the more stable (electrochemically) the complex and the easier the electrochemical measurements.

Di Xue  
Chemistry Department  
Colorado State University  
Fort Collins, CO 80526  
Summer 2008

## ACKNOWLEDGEMENT

I would like to thank my research advisor Dr. C. Michael Elliott and the members of Dr. Elliott's research group. Their patience and assistance made this work possible. Technical and financial support from Dr. David W. Grainger is also gratefully acknowledged.

## ABBREVIATION LIST

APS <sup>-</sup>	3-acryloyloxy-propane-1-sulfonate
ATA <sup>+</sup>	(2-acryloyloxy-ethyl)-tributyl-ammonium
bab-bipy	4,4'-bis(4-acryloyloxy-butyl)-2,2'-bipyridine
BPB	4,4'-bis(N-phenothiazinato)methyl-2,2'-bipyridine
C.E.	Counter Electrode
CV	cyclic voltammetry
DCB	4,4'-di-carboxyl-2,2'-bipyridine
DHAQ	dihydroxyanthraquinone
DMB	4,4'-dimethyl-2,2'-bipyridine
5,6-dmphen	5,6-dimethyl-1,10-phenanthroline
DTB	4,4'-di- <i>tert</i> -Butyl-2,2'-bipyridine
DPV	differential pulsed voltammetry
GC	glassy carbon
ITO	indium tin oxide
LBS	lithium 4-(10H-phenothiazin-10-yl)butane-1-sulfonate
MPB	4-methyl-4'-(N-phenothiazinato)methyl-2,2'-bipyridine
NEt <sub>3</sub>	triethyl amine
44POZ	4-methyl-4'-(4-(N-phenoxazinato)butyl)-2,2'-bipyridine
PTZ	phenothiazine
46PTZ	4-methyl-4'-(4-(N-phenothiazinato)hexyl)-2,2'-bipyridine

R. E.	reference electrode
sat.	saturated
SHE	standard hydrogen electrode
S.R.	scan rate
TBAPF <sub>6</sub>	tetrabutylammonium hexafluorophosphate
terpy	2,2':6',2''-terpyridine
TMAPF <sub>6</sub>	tetramethylammonium hexafluorophosphate
TPA	N,N,N',N'-tetramethyl-p-phenylene-diamine
TPT	4, 4', 4''-tris(N-phenothiazinato)methyl-2,2':4'2''-terpyridine
TTT	4,4',4''-tri- <i>tert</i> -Butyl-2,2':6',2''-terpyridine
W.E.	Working Electrode

# OUTLINE

## *Part I Electrochemical DNA Sensors (Chapter 1 to Chapter 4)*

Chapter 1 General Background of Electrochemical DNA Sensing .....	1
ABSTRACT.....	1
INTRODUCTION.....	1
ELECTROCHEMICAL SENSOR FABRICATION.....	3
TRANSDUCING PRINCIPLES.....	4
SIGNAL AMPLIFICATION.....	6
Stoichiometric signal amplification.....	6
Ferrocene–streptavidin conjugates.....	6
Polymeric osmium complex.....	6
Nanoparticles.....	7
Oligonucleotide-loaded gold nanoparticles and $[\text{Ru}(\text{NH}_3)_6]^{3+}$ .....	7
Non-stoichiometric signal amplification.....	8
Gold nanoparticles promoted deposition of silver.....	8
Electrocatalytic Oxidation of Ferricyanide with intercalative methylene blue.....	9
CONCLUSION.....	10
REFERENCES.....	11
Chapter 2 Investigation of Catalytic Oxidation of Co(II) Complexes for the Purpose of DNA Detection.....	15
INTRODUCTION.....	15
BACKGROUND.....	15
Redox chemistry of the Co(II) complexes .....	15
Detection strategies for DNA hybridization based on catalytic oxidation of the Co(II) complexes.....	17
EXPERIMENTAL.....	22

Chemicals and materials .....	22
Electrochemical experiments.....	23
ITO Electrodes fabrication.....	23
Single electrodes and array electrodes.....	23
Microarray electrodes.....	25
Synthesis of electrolyte TBAPF <sub>6</sub> .....	26
Synthesis of Co(II) complexes .....	28
[Co(DTB) <sub>3</sub> ]Cl <sub>2</sub> .....	28
[Co(TTT) <sub>2</sub> ]Cl <sub>2</sub> .....	29
[Co(TTT) <sub>2</sub> ](SO <sub>4</sub> ) .....	30
[Co(DTB) <sub>3</sub> ](ClO <sub>4</sub> ) <sub>2</sub> .....	31
[Co(DTB) <sub>3</sub> ](PF <sub>6</sub> ) <sub>2</sub> .....	32
[Co(TTT) <sub>2</sub> ](ClO <sub>4</sub> ) <sub>2</sub> .....	33
[Co(TTT) <sub>2</sub> ](PF <sub>6</sub> ) <sub>2</sub> .....	34
Synthesis of catalysts.....	35
<u>A, preparation of ligands</u> .....	35
4,4'-bis[(N-phenothiazinato)methyl]-2,2'-bipyridine.....	35
4,4',4''-tris[(N-phenothiazinato)methyl]-2,2':6,2''-terpyridine .....	39
<u>B, preparation of catalysts</u> .....	43
Fe (BPB) <sub>2</sub> (CN) <sub>2</sub> .....	43
Fe(DMB) <sub>2</sub> (CN) <sub>2</sub> .....	45
KFe(TPT)(CN) <sub>3</sub> .....	45
KFe(terpy)(CN) <sub>3</sub> .....	47
Ru(BPB) <sub>2</sub> (Cl) <sub>2</sub> .....	48
Ru (MPB) <sub>2</sub> (Cl) <sub>2</sub> .....	49
[NEt <sub>4</sub> ] <sub>2</sub> Ru(bpy)(CN) <sub>4</sub> .....	49
Catalytic Oxidation of [Co(DTB) <sub>3</sub> ] <sup>2+</sup> on the [Fe(DCB) <sub>3</sub> ] <sup>2+</sup> -modified ITO array Electrode.....	51
Functionalization of the ITO array electrode with (3-aminopropyl)-trimethoxysilane.....	51
Modification of the functionalized ITO array electrode with [Fe(DCB) <sub>3</sub> ] <sup>2+</sup> .....	51
Electrochemical catalysis of [Co(DTB) <sub>3</sub> ] <sup>2+</sup> Oxidation.....	52
RESULTS AND DISCUSSION.....	53
Catalytic oxidation of [Co(DTB) <sub>3</sub> ] <sup>2+</sup> on the [Fe(DCB) <sub>3</sub> ] <sup>2+</sup> modified ITO array electrode.....	53
Electrochemical properties of the Co(II) complexes .....	55
Effect of working electrodes .....	55
Electrolyte effect.....	56
Effect of coordinating ligand.....	59
Counterion effect.....	60
Summary.....	62

Catalytic oxidation of $\text{Co}(\text{DTB})_3^{2+}$ mediators.....	62
Catalytic oxidation of $[\text{Co}(\text{DBT})_3](\text{ClO}_4)_2$ by $(\text{NEt}_4)_2[\text{Ru}(\text{bipy})(\text{CN})_4]$ .....	63
Catalytic oxidation of $[\text{Co}(\text{DBT})_3](\text{ClO}_4)_2$ by LBS.....	65
Catalytic oxidation of $[\text{Co}(\text{DTB})_3](\text{ClO}_4)_2$ by thioridazine.....	67
Catalytic oxidation of $[\text{Co}(\text{DTB})_3](\text{ClO}_4)_2$ by phenothiazine.....	68
Catalytic oxidation of $[\text{Co}(\text{DTB})_3](\text{ClO}_4)_2$ by TPA.....	68
Catalytic oxidation of $[\text{Co}(\text{DTB})_3](\text{ClO}_4)_2$ by quinizarin.....	69
Catalytic oxidation of $[\text{Co}(\text{DBT})_3](\text{ClO}_4)_2$ by $\text{Fe}(\text{BPB})_2(\text{CN})_2$ ....	71
Catalytic oxidation of $[\text{Co}(\text{DBT})_3](\text{ClO}_4)_2$ by $\text{KFe}(\text{TPT})(\text{CN})_3$ ...73	
Catalytic oxidation of $[\text{Co}(\text{DBT})_3](\text{ClO}_4)_2$ by $\text{Ru}(44\text{POZ})_2\text{Cl}_2$ ....	74
Catalytic oxidation of $[\text{Co}(\text{DBT})_3](\text{ClO}_4)_2$ by $\text{Ru}(46\text{PTZ})_2\text{Cl}_2$ ....	75
Catalytic oxidation of $[\text{Co}(\text{DBT})_3](\text{ClO}_4)_2$ by $\text{Ru}(\text{MPB})_2(\text{Cl})_2$ ....	76
Catalytic oxidation of $[\text{Co}(\text{DBT})_3](\text{ClO}_4)_2$ by $\text{Ru}(\text{BPB})_2\text{Cl}_2$ .....	77
Summary.....	78
REFERENCES.....	81
Chapter 3 Probe ss-DNA attachment on ITO electrodes .....	84
INTRODUCTION.....	84
BACKGROUND.....	85
EXPERIMENTAL.....	87
Chemicals and materials.....	87
XPS experiments .....	88
Synthesis .....	88
12-phosphono-dodecanoic acid (PDA).....	88
11-phosphono-undecanoic acid (PUA).....	92
6-phosphono-hexanoic acid (PHA).....	95
5-phosphono-pentanoic acid (PPEA).....	98
Functionalization of the ITO electrodes.....	100
Electrode pretreatment.....	100
Functionalization of ITO with (3-aminopropyl)-trimethoxysilane.....	101
Succinylation of the silanized ITO surface.....	102
Functionalization of ITO with sebacic acid .....	102
Functionalization of ITO with $\omega$ -phosphonoalkyl carboxylic acid.....	103
Functionalization of ITO with $\alpha,\omega$ -dicarboxylic acid via $\text{ZrO}_2$ coupling.....	104
Functionalization of ITO with $\text{TiO}_2$ and tantalum-doped conducting $\text{TiO}_2$ .....	105

Electrochemical analysis of functionalized ITO surfaces.....	106
Probe DNA attachment on functionalized ITO electrodes.....	107
RESULTS AND DISCUSSION.....	108
Functionalization of ITO with (3-aminopropyl) trimethoxysilane.....	108
Acylation of the silanized ITO surface.....	109
Functionalization of ITO with sebacic acid .....	112
Functionalization of ITO with $\omega$ -phosphonoalkyl carboxylic acid.....	114
Modification of ITO with ZrO <sub>2</sub> .....	116
Functionalization of ITO with $\alpha,\omega$ -dicarboxylic acid via ZrO <sub>2</sub> coupling.....	118
Functionalization of ITO with TiO <sub>2</sub> and tantalum-doped conducting TiO <sub>2</sub> .....	120
Probe DNA attachment on Functionalized ITO electrodes.....	123
Summary.....	125
REFERENCES.....	127
Chapter 4 DNA Hybridization Detection .....	130
INTRODUCTION.....	130
EXPERIMENTAL.....	131
Materials.....	131
Sensor fabrication.....	131
Hybridization of single ITO biosensors with target DNA .....	132
Hybridization of array ITO biosensors with target DNA.....	133
Hybridization of microarray ITO biosensors with target .....	133
Fluorescence microscope imaging.....	134
DNA labeling with catalysts .....	134
Electrochemical experiments .....	134
Serum experiments.....	135
RESULTS AND DISCUSSION.....	137
Detection on silane-functionalized ITO surface .....	137
Detection on sebacic acid-functionalized ITO surface.....	139
Detection on PDA-functionalized ITO surface .....	140
Detection on PUA-functionalized ITO surface.....	142
Detection of 2 $\mu$ M complementary target Oligo2 using single ITO biosensors.....	142
Detection of 2 $\mu$ M complementary target Oligo2 using array ITO biosensors.....	143

Discrimination of 2 $\mu$ M complimentary target from mis-matched target .....	145
Fluorescence imaging.....	146
Detection of 3 nM target .....	147
Detection of 4 pM target.....	148
Detection of DNA target using microarray electrodes .....	149
Detection of DNA target in the presence of serum proteins.....	151
SUMMARY.....	156
REFERENCES.....	161

### *Part II Redox Conducting Polymers (Chapter 5)*

Chapter 5 Redox Conducting Polymers Containing Locked Redox Gradient: Preparation and Study.....	163
INTRODUCTION.....	163
BACKGROUND.....	163
EXPERIMENTAL.....	169
Chemicals and equipment .....	169
Electrodes and cells.....	169
Synthesis of polymerizable electrolytes.....	170
A. (2-hydroxy-ethyl)- tributyl-ammonium bromide.....	170
B. (2-acryloyloxy-ethyl)- tributyl-ammonium bromide .....	171
C. (2-acryloyloxy-ethyl)- tributyl-ammonium 3-acryloyloxy-propane-1-sulfonate .....	172
Synthesis of the coordinating bipyridine ligands.....	173
A. 3-bromopropanol.....	174
B. 2-(3-bromo-propoxy)-tetrahydropyran.....	175
C. 4,4'-bis[(tetrahydropyran-2-yloxy)-butyl]- -2,2'-bipyridine.....	175
D. 4,4'-bis(4-hydroxy-butyl)-2,2'-bipyridine.....	176
E. 4,4'-bis(4-acryloyloxy-butyl)-2,2'-bipyridine (bab-bipy).....	176
Synthesis of polypyrazolyborate ligands.....	177
A. 4-(3-hydroxypropyl)pyrazole.....	177
B. 4-(3-aminopropyl)pyrazole.....	179
C. potassim hydrotris(4-R-pyrazolyl)borate, where R stands for -3-hydroxypropyl or -3-aminopropyl).....	180
D. triethylammonium p-phenylene-di-(trispirazolyborate).....	181
Preparation of cyanoiron bipyridine complexes .....	182

Dicyano-bis-[4,4'-di(4-acryloyloxy-butyl)-2,2'-bipyridine]- Iron(II) (1).....	182
Potassium Tetracyano-mono-[4,4'-di(4-hydroxyl-butyl)-2,2'- -bipyridine] ferrate(II).....	182
Sodium tetracyano-mono-{4,4'-di[4-(2-methyl-acryloyloxy)- -butyl]-2,2'-bipyridine} ferrate(II) (2).....	183
Potassium Tetracyano-mono-[4,4'-di(4-hydroxyl-butyl) -2,2'-bipyridine] ferrate(III).....	184
(2-Acryloyloxy-ethyl)-tributyl-ammonium tetracyano-mono- [4,4'-di(4-acryloyloxy-butyl)-2,2'-bipyridine]ferrate(III) (3).....	184
Monomer film formation and initial polymerization.....	184
“Sandwich” electrode fabrication .....	185
Redox gradient formation and locking.....	186
<b>RESULTS AND DISCUSSION.....</b>	<b>187</b>
Synthesis of the bipyridine-based monomers .....	187
Solvatochromic behaviour of the Iron(II) Monomers.....	190
Synthesis of the polypyrazolyborate-based monomers and polymers.....	191
Coating solution preparation.....	192
Initial film polymerization.....	194
Cyclic voltammeteries of poly ( 1 ) .....	194
Cyclic voltammeteries of poly ( 2 ) .....	196
Dual mode CVs of the sandwich electrode GC/Poly ( 1 )/Au.....	198
Redox gradient formation in poly( 1 ) films sandwiched between GC and Au.....	198
Redox gradient formation in poly( 1&3 ) films coated on IDA electrodes.....	199
Locking of the redox gradients in the films.....	201
<b>SUMMARY.....</b>	<b>203</b>
<b>REFERENCES.....</b>	<b>205</b>

# ***Part I: Electrochemical DNA Sensors*** ***(Chapter 1 to Chapter 4)***

## **Chapter 1: General Background of Electrochemical DNA Sensing**

### **ABSTRACT**

DNA biosensors recognize Watson-Crick base pairing events utilizing a sequence-specific probe and a signal transducer.<sup>1</sup> Compared with almost any other analytical technique, electrochemical instrumentation is inexpensive, robust and relatively simple to operate. On this basis alone, if all else were equal, electrochemical based biosensors for DNA hybridization should hold one of the best prospects for real-world clinical applications; and it is this fact that is one of the primary drivers of interest in electrochemical detection of DNA hybridization.

This chapter presents a brief overview of electrochemical DNA sensors, including sensor fabrication, transducing principles and signal amplification strategies. Special emphasis will be given to the most interesting amplification strategies for a better understanding of numerous approaches to improve the sensitivity and/or selectivity of the sensors.

### **INTRODUCTION**

Nucleic acid analysis is frequently sought for diagnosis of disease, microbial contamination, forensics, biosecurity and basic research and development. These analyses

often use surface capture methods to identify a soluble DNA or RNA target analyte by selective or specific, complementary complexation with a matching probe nucleic acid oligomer immobilized on a capture surface. One popular commercialized method--nucleic acid microarray analyses--uses rapid robotic printing methods to place micrometer-sized spots of DNA target libraries onto activated solid supports in cataloged arrays. Exposure of these surfaces to samples containing unknown nucleic acid analytes permits simultaneous screening of up to tens of thousands of different complementary DNA or mRNA analytes or their single nucleotide polymorphisms (SNPs) in complex biological samples. While many modes of analyte detection of bound nucleic acid signal on the support are possible, measurement usually exploits image analysis of fluorescent emission from tags placed specifically on the captured analyte.<sup>2</sup> The fluorescent intensity of each microarray spot on the slide is then collected (via surface fluorescence scanning) and analyzed (see Figure 1.1).

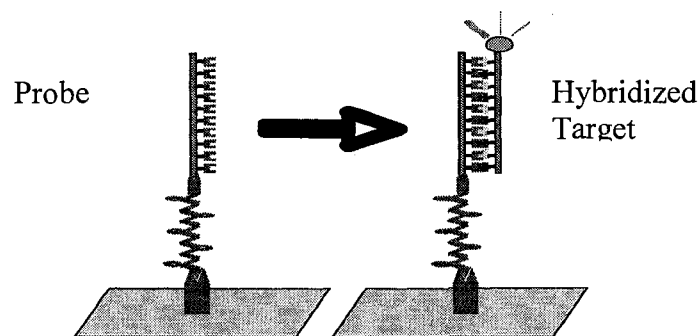


**Figure 1.1.** Schematic illustration of surface capture and detection by fluorescence of a soluble target nucleic acid complementary to an immobilized nucleic acid probe. Reprinted from Reference 2.

Fluorescence-based nucleotide microarray assays are technically attractive, currently the focus of a billion-dollar commercial effort, but exhibit significant limitations: (1) fluorescence has only relative correlation with natural DNA target

abundance without absolute reference to actual target concentrations, (2) fluorescence is relatively insensitive, requiring either pre-purification or amplification of DNA target to achieve reasonable assay detection limits (picomolar), (3) probe printing and target dye-labeling processes are expensive and time consuming, and (4) detection requires highly sophisticated optical scanners, laser excitation sources and post-assay image processing. As one alternative, electrochemical DNA detection has received substantial attention due to its intrinsically rapid response, ease of handling, compatibility with miniaturization technology and relatively low cost. By combining electrochemistry with the selectivity or specificity of biological recognition processes, electrochemical biosensors occupy an important analytical position.

## **ELECTROCHEMICAL SENSOR FABRICATION**

Sensitive DNA hybridization sensing requires selective and efficient binding between the surface-immobilized probe and the target in solution as well as efficient electrochemical signal transduction. Therefore, careful control of the probe layer on the electrode surface is imperative.

Briefly, DNA probes are either physically or chemically attached to bare or functionalized electrode surfaces. Physisorption is rapid and simple, however, suffers from low coverage and poor stability. Some of the most interesting immobilization approaches are listed in Table 1.1, including retention in a polymeric matrix, covalent attachment on a functionalized support, affinity immobilization and self-assembling. These chemistries allow capture probes to be immobilized via their end points. Through controlling of the surface coverage, such bio-architectures achieve hybridization

efficiencies as high as 100%, demonstrating full accessibility of the surface-bound probe to the solution-phase target.

**Table 1.1.** Well-established immobilization approaches.

Probe Attachment Mode	Sensing Substrate	References
retention in a polymeric matrix	ITO, Carbon, Au	ITO: <sup>3</sup> ; Carbon: <sup>4</sup> Au: <sup>5, 6</sup>
covalent attachment on a functionalized support	ITO, SiO <sub>2</sub> , Pt	ITO: <sup>7</sup> SiO <sub>2</sub> : <sup>8, 9</sup> Pt <sup>10</sup>
affinity immobilization	Carbon	11
self-assembling	Carbon, Au	Carbon: <sup>12</sup> Au: <sup>13, 14</sup>

## TRANSDUCING PRINCIPLES

In general, two signal transduction modes (direct and indirect) are involved in electrochemical DNA sensing. Direct signal transduction utilizes the intrinsic DNA electrochemical response, i.e, electro-oxidation of the guanine or adenine moieties in the hybridized target DNA. To minimize background, Wang and coworkers<sup>15</sup> used a guanine free (inosine-substituted) probe. Upon exposing to the DNA target solution, DNA hybrid formed on the electrode surface. Subsequent interrogation of the electrochemical signal due to guanine oxidation led to transduction of the hybridization events into readable electrochemical signals. To amplify the signals and thus improve detection limits, Ru(bpy)<sub>3</sub><sup>2+</sup> ion has been employed to catalyze the oxidation of guanine and adenine, where bpy stands for bipyridine.<sup>16, 17</sup> One of the inherent disadvantages of this sensor design is the electrochemical destruction of the DNA probe and target, preventing repeatable usage of the sensor. Indirect detection of hybridization, on the other hand,

exploits enzyme labels,<sup>5, 11, 18-20</sup> or other redox mediators<sup>1, 21</sup> such as ferrocene,<sup>22-27</sup>  $\text{Fe}(\text{CN})_6^{4-}$ ,<sup>28</sup>  $\text{Ru}(\text{bpy})_3^{2+}$ ,<sup>29</sup>  $\text{Os}(\text{bpy})_3^{2+}$ ,<sup>30</sup>  $\text{Co}(\text{NH}_3)_6^{3+}$ ,<sup>31</sup>  $\text{Co}(\text{phen})_3^{3+}$ ,<sup>32</sup>  $\text{Co}(\text{bpy})_3^{3+}$ ,<sup>32</sup> and  $\text{Ru}(\text{NH}_3)_6^{3+}$ ,<sup>33, 34</sup> or intercalating organic compounds including daunomycin,<sup>35, 36</sup> methylene blue<sup>36</sup> and Hoechst 33258.<sup>37, 38</sup>

Enzyme and ferrocene labels are usually pre-attached to the target oligonucleotide sequence. Hybridization of the labeled target with the surface immobilized probe subsequently brings the labels to the electrode surface. Enzyme functions as a catalyst to promote production of redox active species from redox inactive substrates present in solution. Interrogation of the redox chemistry of the enzymatic product or intrinsically redox active ferrocene produced a signal (usually current) which is proportionally to the hybridization event.

Covalent attachment of enzyme and ferrocene however, is laborious and time-consuming. Alternative methods utilize solution-phase metal complexes and organic dyes mentioned above, exposing the target challenged DNA to selected label solutions. As hybridization proceeds, increasing amounts of targets are specifically accumulated at the electrode surface. The resulting electrostatic attraction (repulsion) between the cationic (anionic) metal complexes and the polyanionic backbone of the targets thus lead to increasing the redox current generated by redox mediators (increasing charge transfer resistance values). Organic dyes recognize the hybridized DNA by selectively binding to the grooves of the helix and/or reversibly and selectively intercalating into the double-stranded DNA. For sensitive, accurate and reliable determination of DNA target hybridization, these redox species must interact more efficiently with ds-DNA than with ss-DNA targets.

## SIGNAL AMPLIFICATION

According to Lucarelli et al.,<sup>1</sup> a detection limit of attomolar or femtomolar is required to sense a single DNA copy. Tremendous efforts have been made to further increase the sensitivity of the DNA hybridization biosensors.<sup>39-42</sup> A common strategy is to improving the electron stoichiometry.

### **Stoichiometric Signal Amplification**

*Ferrocene–streptavidin conjugates:* One straightforward method to improve signal is to increase the surface concentration of the redox labels. Liu et al.<sup>22</sup> observed a detection limit of 10 pM (2 fmol, with signal to noise > 3) for a 12-mer oligonucleotide target, utilizing a modified streptavidin (Strep) labeled with multiple ferrocene (Fc) units. Hybrid duplex formed on the electrode surface upon challenging the surface-immobilized probes with the biotinylated targets. Subsequent labeling with the Fc-conjugated Strep, allowed electrochemical monitoring of the hybridization events. Each Strep molecule carried at least nine Fc markers. Consequently, the electrochemical response was significantly enhanced.

*Polymeric osmium complex:* Liu and Anzai<sup>43</sup> employed a polymeric Os complexes as the hybridization indicator. The poly(4-vinylpyridine) labeled with ca. 120 units of  $[\text{Os}(5,6\text{-dmphen})_2\text{Cl}]^{2+}$  exhibited ~1000 times higher sensitivity than the monomeric analogue,  $[\text{Os}(5,6\text{-dmphen})_3]^{2+}$ , where 5,6-dmphen stands for 5,6-dimethyl-1,10-phenanthroline. Owing to the polymeric structure of the indicator, intercalation of the first Os complex brought adjacent redox units proximal to the double helix, facilitating

the overall interaction. Such a polymeric osmium label allowed detection of a 25-mer synthetic target as few as 1 pM.

*Nanoparticles:* Recently, significant signal amplifications have been reported by labeling the target DNA with metal nanoparticles (e.g., gold).<sup>44</sup> An HBr/Br<sub>2</sub> solution is used to dissolve the gold which is then detected by electrochemical stripping analysis. Each gold particle, depending on its size, can yield thousands of Au<sup>3+</sup> ions giving rise to impressive stoichiometric signal amplification.

*Oligonucleotide-loaded gold nanoparticles and [Ru(NH<sub>3</sub>)<sub>6</sub>]<sup>3+</sup>:* Figure 1.2 shows a “sandwich” type assay developed by Fan and co-workers.<sup>34</sup> The cationic complex [Ru(NH<sub>3</sub>)<sub>6</sub>]<sup>3+</sup> was used as the redox label owing to its strong electrostatic interaction with the anionic DNA backbone. The target hybridized with the probe followed with a detection probe loaded on a gold nanoparticle (AuNP). This “sandwich” architecture was heavily charged since each AuNP carried hundreds of anionic DNA strands, leading to a signal amplification of two to three orders of magnitude. As a result, the sensor could detect target of femtomolar concentrations.

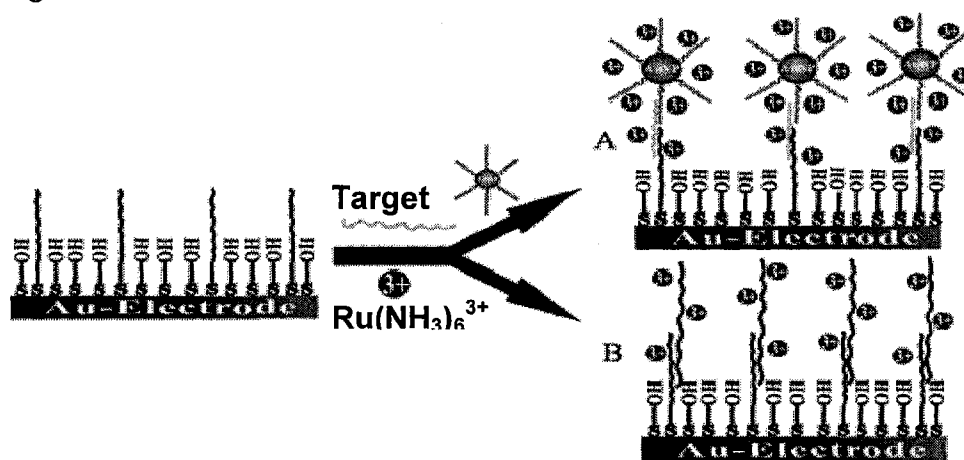


**Figure 1.2.** Schematic illustration of Fan and co-workers' strategy for DNA sensing. (A) AuNPs amplified detection; (B) Nonamplified detection. Reprinted from Reference 34.

## Non-Stoichiometric Signal Amplification

Stoichiometric electrochemical assays have achieved notable detection levels, but amplification of the hybridization signal is finite and limited by the stoichiometry. Once all the electrons/holes of the multiple redox labels are extracted, or once all of the gold atoms are stripped into solution, there is no more signal! Non-stoichiometric signal amplification, on the other hand, overcomes this inherent limitation. Enzymatic catalysis has been widely used.<sup>5, 11, 18-20, 45-47</sup> To avoid laborious enzymatic labeling, alternative methods utilize chemical/electrochemical catalysis.

*Gold nanoparticles (AuNP) promoted deposition of silver:* As discussed earlier, labeling the target DNA with AuNP produced a decent signal amplification. The electrochemical response was further improved with AuNP promoted deposition of silver.<sup>3, 48</sup> Figure 1.3 schematically illustrates the strategy employed by Yeung et al.<sup>3</sup> Electro-deposition of silver onto the AuNPs was achieved in a silver nitrate solution (1 mM AgNO<sub>3</sub>/1 M KNO<sub>3</sub>). Subsequent electrochemical interrogation of the silver shell allowed detection of an asymmetric PCR (i.e., polymerase chain reaction) product as few as 100 cells sample<sup>-1</sup>.

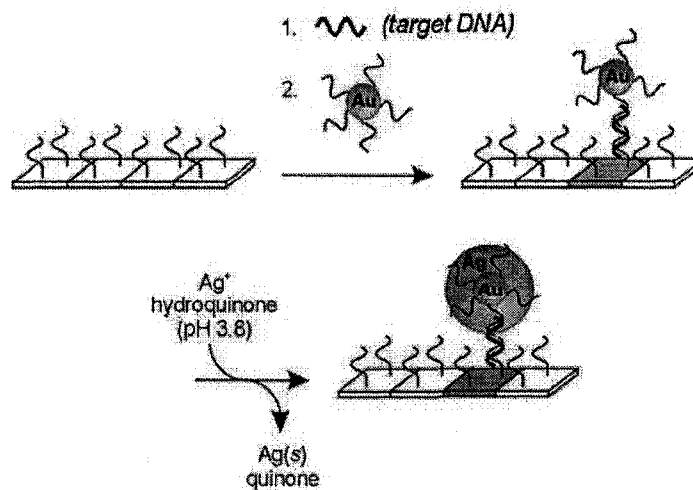


**Figure 1.3.** Schematically illustration of AuNP catalyzed electrochemical deposition of silver. Reprinted from Reference 3.

*Electrocatalytic reduction of ferricyanide with intercalative methylene blue (MB):*

Barton and co-workers<sup>49</sup> took advantage of the DNA duplex's electrical conductivity to detect single-nucleotide polymorphisms. A close-packed DNA duplex monolayer sterically and electrostatically blocks ferricyanide anion from accessing the gold electrode surface. Addition of a small amount of methylene blue (MB) to solution leads to catalytic electro-reduction of  $[\text{Fe}(\text{CN})_6]^{3-}$ . MB is bound to the electrode surface via intercalation into the ds-DNA strand, which serves as a molecular wire conducting electrons to or from MB. And reduced MB is regenerated by transferring electrons to the solution-phase  $[\text{Fe}(\text{CN})_6]^{3-}$ , thus entering a catalytic cycle (see Figure 1.4 A). Interestingly, any mismatch located within the duplex wire results in decreased electron transfers, impeding the catalytic process (see Figure 1.4 B).

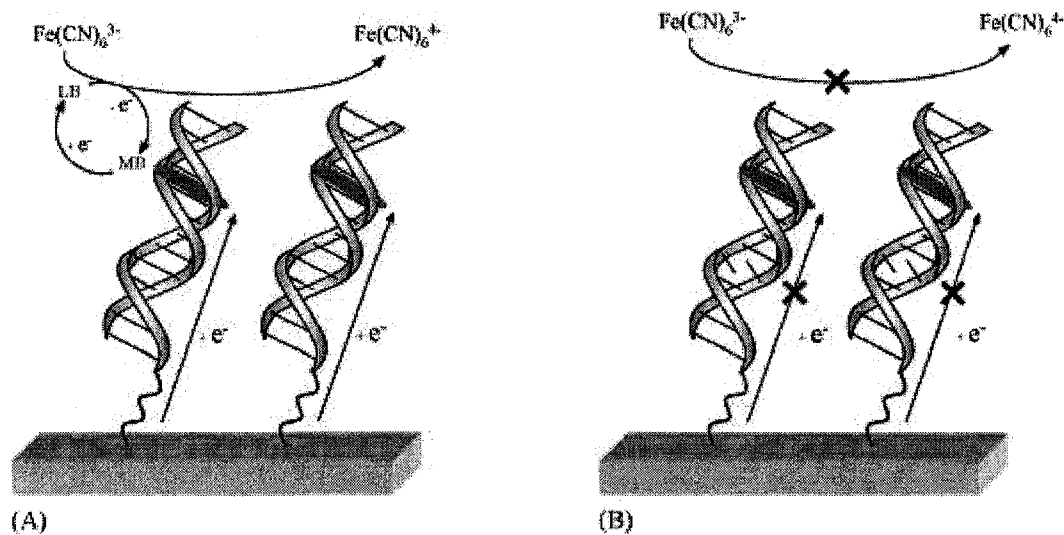


**Figure 1.4.** Exploiting DNA-mediated charge transport for the detection of single-base mismatches. (A) Perfectly matched duplex. When applying a negative potential, the intercalated MB underwent electrochemical reduction, generating leucomethylene blue (LB). MB was then re-generated through the chemical oxidation of LB by the solution-phase ferricyanide. (B) Mismatched duplex. Any mismatch located within the immobilized duplexes inhibited the whole process, being the first electro-reduction step impeded. Adapted from Reference 1.

## CONCLUSION

To date, femtomolar detection limits have been achieved with successful employment of signal amplification strategies. Tremendous efforts, however, have to be made to avoid non-specific interactions.<sup>50, 51</sup> Research to develop new sensitive and reliable analytical protocols is still open.

In this study, a new electrochemical approach for detecting target DNA is developed. The scheme involves the catalytic oxidation of a cobalt bipyridine "mediator molecule" in solution. Probe/target DNA duplexes (ds-DNA), bound on an ITO electrode, selectively recruit redox catalyst molecules from solution. This surface-bound catalyst "turns on" the redox chemistry of the mediator molecule which is otherwise kinetically inert to oxidation on ITO. The mode of selective catalyst binding is intercalation between base pairs of ds-DNA. With this approach, we demonstrate detection of a 20-mer DNA target oligonucleotide at picomolar concentrations with outstanding signal-to-noise.

1. Lucarelli, F.; Tombelli, S.; Minunni, M.; Marrazza, G.; Mascini, M., Electrochemical and piezoelectric DNA biosensors for hybridization detection. *Analytica Chimica Acta* **2008**, 609, (2), 139-159.
2. Elliott, C. M.; Bignozzi, C. A.; Xue, D.; Grainger, D. W.; Caramori, S.; Dissette, V. Electrochemical detection of complex formation using probes immobilized on electrode surfaces, *U.S. Pat. Appl. Publ.* **2008**. 2006-536478, 2008081329, 20060928.
3. Yeung, S. W.; Lee, T. M. H.; Cai, H.; Hsing, I., A DNA biochip for on-the-spot multiplexed pathogen identification. *Nucleic Acids Research* **2006**, 34, (18), e118.
4. Teh, H. F.; Gong, H.; Dong, X.-D.; Zeng, X.; Lai Kuan Tan, A.; Yang, X.; Tan, S. N., Electrochemical biosensing of DNA with capture probe covalently immobilized onto glassy carbon surface. *Analytica Chimica Acta* **2005**, 551, (1-2), 23-29.
5. Dominguez, E.; Rincon, O.; Narvaez, A., Electrochemical DNA Sensors Based on Enzyme Dendritic Architectures: an Approach for Enhanced Sensitivity. *Anal. Chem.* **2004**, 76, (11), 3132-3138.
6. Garnier, F.; Bouabdallaoui, B.; Srivastava, P.; Mandrand, B.; Chaix, C., Conjugated polymer-based DNA chip with real time access and femtomol detection threshold. *Sensors and Actuators B: Chemical* **2007**, 123, (1), 13-20.
7. Popovich, N. D.; Eckhardt, A. E.; Mikulecky, J. C.; Napier, M. E.; Thomas, R. S., Electrochemical sensor for detection of unmodified nucleic acids. *Talanta* **2002**, 56, (5), 821-828.
8. Ingebrandt, S.; Han, Y.; Nakamura, F.; Poghossian, A.; Schöning, M. J.; Offenhäusser, A., Label-free detection of single nucleotide polymorphisms utilizing the differential transfer function of field-effect transistors. *Biosensors and Bioelectronics* **2007**, 22, (12), 2834-2840.
9. Gao, Z.; Agarwal, A.; Trigg, A. D.; Singh, N.; Fang, C.; Tung, C. H.; Fan, Y.; Buddharaju, K. D.; Kong, J., Silicon Nanowire Arrays for Label-Free Detection of DNA. *Anal. Chem.* **2007**, 79, (9), 3291-3297.
10. Hang, T. C.; Guiseppi-Elie, A., Frequency dependent and surface characterization of DNA immobilization and hybridization. *Biosensors and Bioelectronics* **2004**, 19, (11), 1537-1548.
11. Metfies, K.; Huljic, S.; Lange, M.; Medlin, L. K., Electrochemical detection of the toxic dinoflagellate *Alexandrium ostenfeldii* with a DNA-biosensor. *Biosensors and Bioelectronics* **2005**, 20, (7), 1349-1357.
12. Gorodetsky, A. A.; Barton, J. K., Electrochemistry Using Self-Assembled DNA Monolayers on Highly Oriented Pyrolytic Graphite. *Langmuir* **2006**, 22, (18), 7917-7922.
13. Elsholz, B.; Worl, R.; Blohm, L.; Albers, J.; Feucht, H.; Grunwald, T.; Jurgen, B.; Schweder, T.; Hintsche, R., Automated Detection and Quantitation of Bacterial RNA by Using Electrical Microarrays. *Anal. Chem.* **2006**, 78, (14), 4794-4802.
14. Flechsig, G. U.; Reske, T., Electrochemical Detection of DNA Hybridization by Means of Osmium Tetroxide Complexes and Protective Oligonucleotides. *Anal. Chem.* **2007**, 79, (5), 2125-2130.

15. Wang, J.; Rivas, G.; Fernandes, J. R.; Lopez Paz, J. L.; Jiang, M.; Waymire, R., Indicator-free electrochemical DNA hybridization biosensor. *Analytica Chimica Acta* **1998**, 375, (3), 197-203.
16. Johnston, D. H.; Glasgow, K. C.; Thorp, H. H., Electrochemical Measurement of the Solvent Accessibility of Nucleobases Using Electron Transfer between DNA and Metal Complexes. *Journal of the American Chemical Society* **1995**, 117, (35), 8933-8938.
17. Gore, M. R.; Szalai, V. A.; Ropp, P. A.; Yang, I. V.; Silverman, J. S.; Thorp, H. H., Detection of attomole quantities of DNA targets on gold microelectrodes by electrocatalytic nucleobase oxidation. *Anal. Chem* **2003**, 75, (23), 6586-6592.
18. Carpini, G.; Lucarelli, F.; Marrazza, G.; Mascini, M., Oligonucleotide-modified screen-printed gold electrodes for enzyme-amplified sensing of nucleic acids. *Biosensors and Bioelectronics* **2004**, 20, (2), 167-175.
19. Miranda-Castro, R.; de-los-Santos-Alvarez, P.; Lobo-Castanon, M. J.; Miranda-Ordieres, A. J.; Tunon-Blando, P., Hairpin-DNA Probe for Enzyme-Amplified Electrochemical Detection of *Legionella pneumophila*. *Anal. Chem.* **2007**, 79, (11), 4050-4055.
20. DelGiallo, M. L.; Lucarelli, F.; Cosulich, E.; Pistarino, E.; Santamaria, B.; Marrazza, G.; Mascini, M., Steric Factors Controlling the Surface Hybridization of PCR Amplified Sequences. *Anal. Chem.* **2005**, 77, (19), 6324-6330.
21. Lucarelli, F.; Marrazza, G.; Turner, A. P. F.; Mascini, M., Carbon and gold electrodes as electrochemical transducers for DNA hybridisation sensors. *Biosensors and Bioelectronics* **2004**, 19, (6), 515-530.
22. Liu, J.; Tian, S.; Tiefenauer, L.; Nielsen, P. E.; Knoll, W., Simultaneously Amplified Electrochemical and Surface Plasmon Optical Detection of DNA Hybridization Based on Ferrocene-Streptavidin Conjugates. *Anal. Chem.* **2005**, 77, (9), 2756-2761.
23. Yu, C. J.; Wan, Y.; Yowanto, H.; Li, J.; Tao, C.; James, M. D.; Tan, C. L.; Blackburn, G. F.; Meade, T. J., Electronic Detection of Single-Base Mismatches in DNA with Ferrocene-Modified Probes. *J. Am. Chem. Soc.* **2001**, 123, (45), 11155-11161.
24. Jenkins, D. M.; Chami, B.; Kreuzer, M.; Presting, G.; Alvarez, A. M.; Liaw, B. Y., Hybridization Probe for Femtomolar Quantification of Selected Nucleic Acid Sequences on a Disposable Electrode. *Anal. Chem.* **2006**, 78, (7), 2314-2318.
25. Ricci, F.; Lai, R. Y.; Heeger, A. J.; Plaxco, K. W.; Sumner, J. J., Effect of Molecular Crowding on the Response of an Electrochemical DNA Sensor. *Langmuir* **2007**, 23, (12), 6827-6834.
26. Umek, R. M.; Lin, S. W.; Vielmetter, J.; Terbrueggen, R. H.; Irvine, B.; Yu, C. J.; Kayyem, J. F.; Yowanto, H.; Blackburn, G. F.; Farkas, D. H., Electronic Detection of Nucleic Acids A Versatile Platform for Molecular Diagnostics. In ASIP: 2001; Vol. 3, pp 74-84.
27. Nakayama, M.; Ihara, T.; Nakano, K.; Maeda, M., DNA sensors using a ferrocene-oligonucleotide conjugate. *Talanta* **2002**, 56, (5), 857-866.
28. Liu, J.; Tian, S.; Nielsen, P. E.; Knoll, W., In situ hybridization of PNA/DNA studied label-free by electrochemical impedance spectroscopy. *Chemical Communications* **2005**, 2005, (23), 2969-2971.

29. Armistead, P. M.; Thorp, H. H., Modification of Indium Tin Oxide Electrodes with Nucleic Acids: Detection of Attomole Quantities of Immobilized DNA by Electrocatalysis. *Anal. Chem.* **2000**, *72*, (16), 3764-3770.
30. Ropp, P. A.; Holden Thorp, H., Site-selective electron transfer from purines to electrocatalysts: voltammetric detection of a biologically relevant deletion in hybridized DNA duplexes. *Chemistry & Biology* **1999**, *6*, (9), 599-605.
31. Kerman, K.; Vestergaard, M.; Nagatani, N.; Takamura, Y.; Tamiya, E., Electrochemical genosensor based on peptide nucleic acid-mediated PCR and asymmetric PCR techniques: electrostatic interactions with a metal cation. *Anal. Chem* **2006**, *8*, 2182-2189.
32. Millan, K. M.; Mikkelsen, S. R., Sequence-selective biosensor for DNA based on electroactive hybridization indicators. *Analytical Chemistry* **1993**, *65*, (17), 2317-2323.
33. Steichen, M.; Decrem, Y.; Godfroid, E.; Buess-Herman, C., Electrochemical DNA hybridization detection using peptide nucleic acids and [Ru(NH<sub>3</sub>)<sub>6</sub>]<sup>3+</sup> on gold electrodes. *Biosensors and Bioelectronics* **2007**, *22*, (9-10), 2237-2243.
34. Zhang, J.; Song, S.; Zhang, L.; Wang, L.; Wu, H.; Pan, D.; Fan, C., Sequence-Specific Detection of Femtomolar DNA via a Chronocoulometric DNA Sensor (CDS): Effects of Nanoparticle-Mediated Amplification and Nanoscale Control of DNA Assembly at Electrodes. *J. Am. Chem. Soc.* **2006**, *128*, (26), 8575-8580.
35. Shana O. Kelley, N. M. J. M. G. H. J. K. B., Long-Range Electron Transfer through DNA Films. *Angewandte Chemie International Edition* **1999**, *38*, (7), 941-945.
36. Kelley, S. O.; Boon, E. M.; Barton, J. K.; Jackson, N. M.; Hill, M. G., Single-base mismatch detection based on charge transduction through DNA. *Nucl. Acids Res.* **1999**, *27*, (24), 4830-4837.
37. Hashimoto, K.; Ito, K.; Ishimori, Y., Sequence-Specific Gene Detection with a Gold Electrode Modified with DNA Probes and an Electrochemically Active Dye. *Anal. Chem.* **1994**, *66*, (21), 3830-3833.
38. Hashimoto, K.; Ito, K.; Ishimori, Y., Microfabricated disposable DNA sensor for detection of hepatitis B virus DNA. *Sensors and Actuators B: Chemical* **1998**, *46*, (3), 220-225.
39. Drummond, T. G.; Hill, M. G.; Barton, J. K., Electrochemical DNA sensors. *Nature Biotechnology* **2003**, *21*, (10), 1192-1199.
40. Kerman, K.; Kobayashi, M.; Tamiya, E., Recent trends in electrochemical DNA biosensor technology. *Meas. Sci. Technol* **2004**, *15*, R1-R11.
41. de-los-Santos-Alvarez, P.; Lobo-Castanon, M. J.; Miranda-Ordieres, A. J.; Tunon-Blanco, P., Current strategies for electrochemical detection of DNA with solid electrodes. *Analytical and Bioanalytical Chemistry* **2004**, *378*, (1), 104-118.
42. Merkoçi, A.; Aldavert, M.; Mari'n, S.; Alegret, S., New materials for electrochemical sensing V: Nanoparticles for DNA labeling. *Trends in Analytical Chemistry* **2005**, *24*, (4), 341-349.
43. Liu, A.; Azai, J. i., Use of Polymeric Indicator for Electrochemical DNA Sensors: Poly(4-vinylpyridine) Derivative Bearing [Os(5,6-dimethyl-1,10-phenanthroline)2Cl]<sup>2+</sup>. *Anal. Chem.* **2004**, *76*, (10), 2975-2980.

44. Fritzsche, W.; Taton, T. A., Metal nanoparticles as labels for heterogeneous, chip-based DNA detection. *Nanotechnology* **2003**, 14, (12), R63-R73.
45. Brett, A. M. O., DNA-based biosensors. *Biosensors and Modern Biospecific Analytical Techniques* **2005**.
46. Hwang, S.; Kim, E.; Kwak, J., Electrochemical Detection of DNA Hybridization Using Biometallization. *Anal. Chem.* **2005**, 77, (2), 579-584.
47. Munge, B.; Liu, G.; Collins, G.; Wang, J., Multiple Enzyme Layers on Carbon Nanotubes for Electrochemical Detection Down to 80 DNA Copies. *Anal. Chem.* **2005**, 77, (14), 4662-4666.
48. Taton, T. A.; Mirkin, C. A.; Letsinger, R. L., Scanometric DNA Array Detection with Nanoparticle Probes. *Science* **2000**, 289, (5485), 1757-1760.
49. Boon, E. M.; Ceres, D. M.; Drummond, T. G.; Hill, M. G.; Barton, J. K., Mutation detection by electrocatalysis at DNA-modified electrodes. *Nature Biotechnology* **2000**, 18, 1096-1100.
50. Wang, J., Electrochemical biosensors: Towards point-of-care cancer diagnostics. *Biosensors and Bioelectronics* **2006**, 21, (10), 1887-1892.
51. Lucarelli, F.; Marrazza, G.; Mascini, M., Dendritic-like Streptavidin/Alkaline Phosphatase Nanoarchitectures for Amplified Electrochemical Sensing of DNA Sequences. *Langmuir* **2006**, 22, (9), 4305-4309.

# Chapter 2: Investigation of Catalytic Oxidation of Co(II) Complexes for the Purpose of DNA Detection

## INTRODUCTION

Electrochemical biosensors are of considerable current interest. Herein we propose a new electrochemical approach to detect target DNA molecules based on the catalytic oxidation of mediator molecule,  $\text{Co}(\text{DTB})_3^{2+}$  where DTB is 4,4'-di-*t*-butyl-2,2'-bipyridine. In this chapter, the electrochemical properties of a number of N-heterocyclic-multipyridine coordinated Co(II) complexes and the results of catalytic oxidation of the  $\text{Co}(\text{DTB})_3^{2+}$  complex by a wide variety of redox active catalysts dissolved in solution are reported. Our work has been aimed to identify the best catalytic system which exhibits efficient catalysis in the desired potential range where no oxidation of DNA occurs, which is imperative for sensitive, non-damaging DNA hybridization detection.

This work also explores catalytic oxidation of Co(II) complexes by redox active catalysts immobilized on ITO array electrodes. Previous investigation was carried out using single ITO electrodes modified with  $[\text{Fe}(\text{DCB})_3]^{2+}$ , where DCB stands for 4,4'-dicarboxyl-2,2'-bipyridine.<sup>1</sup> Array detection can provide parallel comparison and is a fundamental concept for DNA detection. Here, catalytic oxidation of  $[\text{Co}(\text{DTB})_3]^{2+}$  was investigated using  $[\text{Fe}(\text{DCB})_3]^{2+}$  modified ITO array electrodes.

## BACKGROUND

### Redox Chemistry of Co(II) Complexes

In previous studies on dye-sensitized solar cells, it has been observed and reported

that certain cobalt bipyridine complexes can serve as reasonable replacements for the commonly employed  $I^-/I^{3-}$  redox mediator couple.<sup>2-6</sup> Two reasons why these cobalt complexes are successful at mediating electron transfers in  $TiO_2$  cells are that (1) their heterogeneous electron transfer both on bare  $TiO_2$  and on the fluoride-doped tin oxide electron collector is extremely slow and (2) the reaction with the photo-oxidized “ $N_3$  dye”, i.e., *cis*-diisothiocyanato bis(2,2'-bipyridine-4,4'-carboxylic acid)ruthenium(II), on the  $TiO_2$  surface is fast. Following these studies, the electrochemistry of  $[Co(DTB)_3]^{2+}$  has been examined on unmodified and  $[Fe(DCB)_3]^{2+}$ -modified ITO surfaces.<sup>1</sup> It is demonstrated that the complex  $[Co(DTB)_3]^{2+}$  is essentially electrochemically inert on the unmodified ITO surfaces, as show in Figure 2.1 (compare the dashed curve with the solid curve).

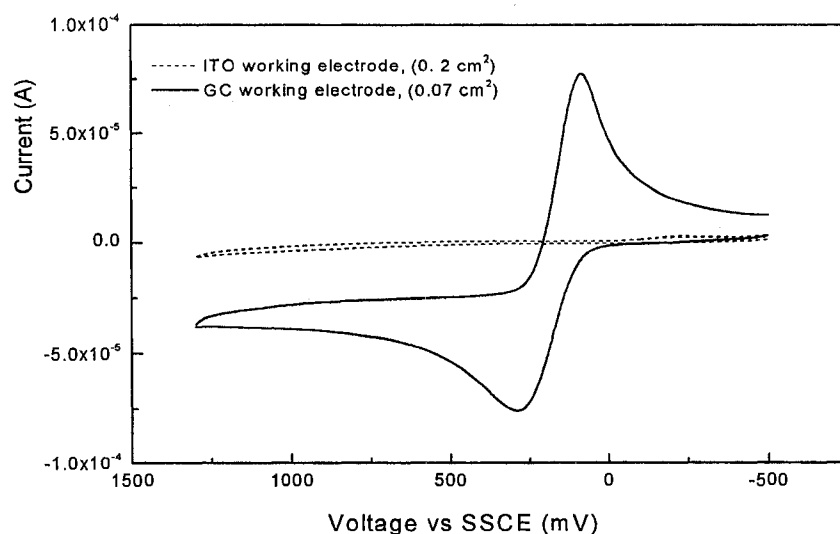
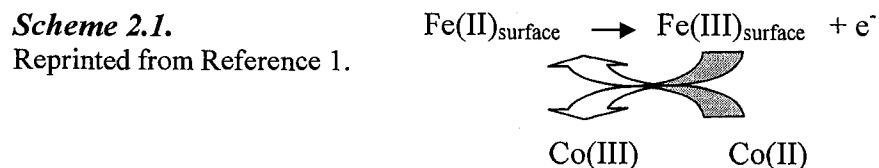


**Figure 2.1.** CVs of approximately  $1 \times 10^{-3}$  M  $Co(DTB)_3^{2+}$  in acetonitrile on GC (solid line), and on ITO (dotted line). Electrolyte, 100 mM TBAPF<sub>6</sub>/acetonitrile; R.E., SSCE; C.E., platinum; S.R., 100 mV/s. Current on GC is normalized to that on the ITO electrode based on differences in area. Reprinted from Reference 1.

However, if the ITO electrode surface is modified with the  $[Fe(DCB)_3]^{2+}$  complex,

the oxidation of the cobalt complex can be “turned on” via an  $E_{\text{surface}}C'$  mechanism (Scheme 2.1):<sup>1</sup>



The catalysis is sufficiently efficient that the peak current for  $[\text{Co}(\text{DTB})_3]^{2+}$  oxidation exceeds the  $i_p$  for the oxidation of surface trapped  $[\text{Fe}(\text{DCB})_3]^{2+}$  by  $> \times 100$ , as shown in Figure 2.2. This dramatic on-off behavior led us to investigate this chemistry for sensitive DNA detection.

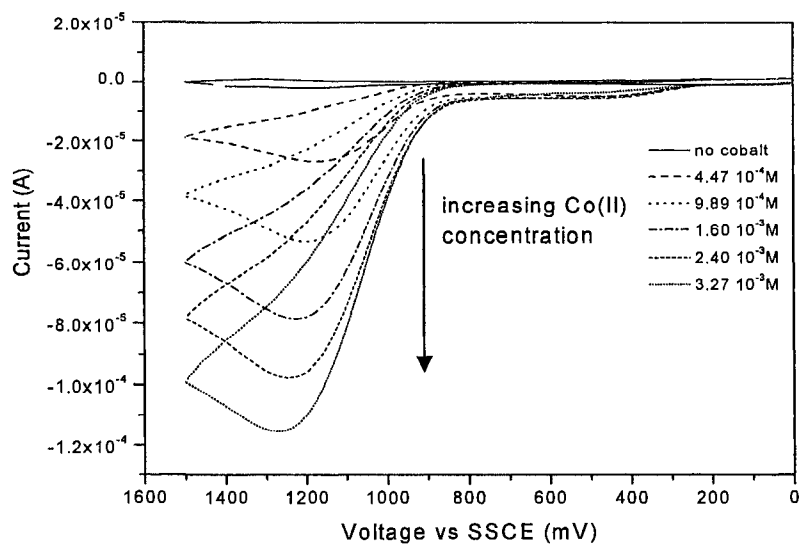


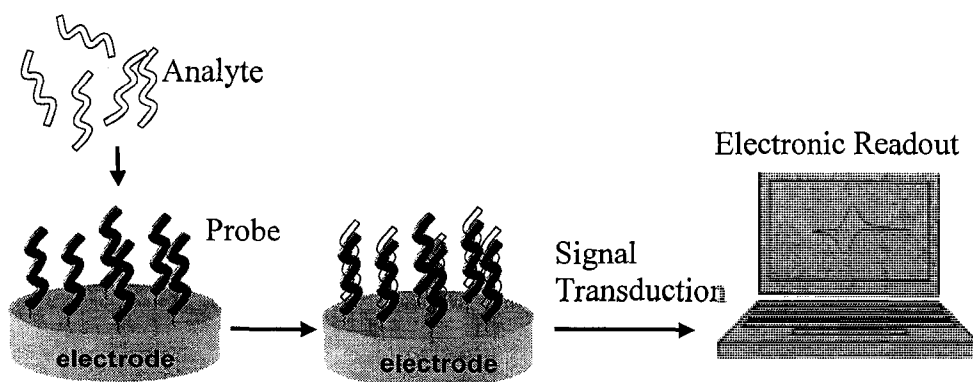
**Figure 2.2.** Catalytic oxidation of  $[\text{Co}(\text{DTB})_3]^{2+}$  on  $[\text{Fe}(\text{DCB})_3]^{2+}$  modified ITO electrodes. Electrolyte, 100 mM TBAPF<sub>6</sub>/acetonitrile; R.E., SSCE; C.E., platinum; S.R., 100 mV/s. Reprinted from Reference 1.

### DNA detection strategies based on catalytic oxidation of Co(II)

Scheme 2.2 illustrates, in the most general terms, the principles of electrochemical DNA analyte capture detection via double-strand hybridization on electrode surfaces.

Usually, a probe molecule consisting of a single strand oligonucleotide (ss-DNA) is first chemically attached to an electrode surface; the probe modified electrode is then challenged with a solution containing the target DNA to form a surface bound duplex (ds-DNA). For electrochemical detection, the hybridization event must produce some sort of an electrochemical signal—usually a current. Only guanine and adenine bases are inherently electrochemically active at practical potentials. At ca. 1.0 and 1.3 V vs. Ag/AgCl, respectively, G and A can undergo oxidation but only when the solution and electrode conditions are precisely controlled.<sup>7, 8</sup> Furthermore, because these oxidation processes are chemically irreversible, the sensing event necessarily destroys the DNA. For these reasons, much of the effort in developing electrochemical DNA sensors has pursued indirect sensing approaches.<sup>7, 9-13</sup> Because the DNA is not destroyed, the prospect for multiuse is an obvious advantage of indirect sensing. More importantly, however, the detection signal is not limited by the A and G composition of the probe/target complex; consequently, the potential for significantly enhanced (over the stoichiometric G and A content) signals is possible.

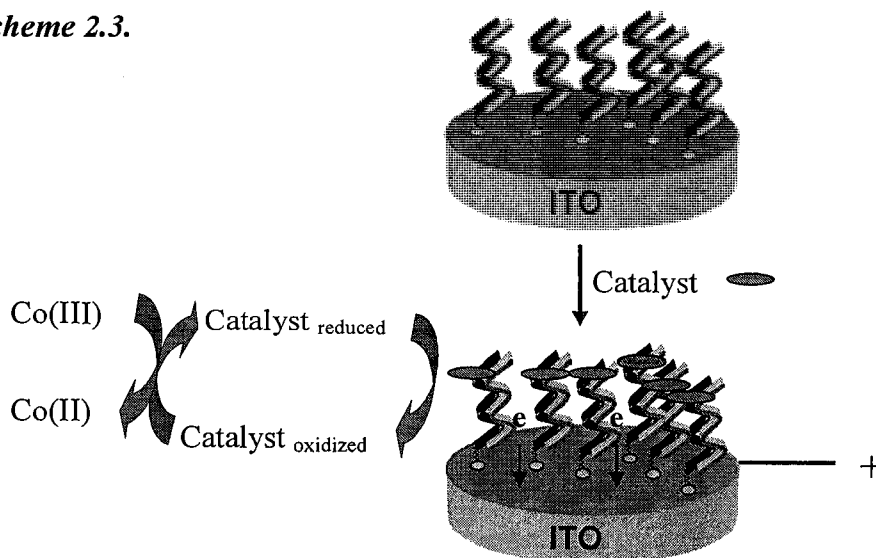
**Scheme 2.2.**



Herein, the development of a new electrochemical approach to detection of target DNA molecules based on the catalytic oxidation of a mediator molecule, Co(II) complex

is described. The signal transduction and amplification are illustrated in Scheme 2.3.

*Scheme 2.3.*



The probe/target duplex modified ITO electrode is treated with a redox catalyst solution. The DNA duplex recruits the catalyst onto the ITO electrode surface. Some appropriate potential program (e.g., a linear voltage sweep) is applied to the catalyst-treated electrode in the electrolyte solution containing the Co(II) complex. At the oxidation potential of the catalyst, it is electrochemically oxidized. And the oxidized catalyst will immediately oxidize Co(II) to Co(III) —a process that is kinetically inert on bare ITO; at the same time, the catalyst is reduced back to its original oxidation state. The recovered catalyst is re-oxidized by the ITO electrode. The cycle repeats continuously oxidizing the Co(II) complex. The redox catalyst “turns on” the redox chemistry of the mediator molecule. On the other hand, if the electrochemical experiment is done without the Co(II) complex, the current measured by the ITO electrode will be much less since the oxidized catalyst is not recovered. Therefore, the presence of the Co(II) complex in the electrolyte solution significantly increases the current (over the

catalyst alone) and thus improve the signal-to-noise ratio for DNA hybridization detection.

Based on this detection strategy, the chemistry used to recruit the catalyst molecule to the electrode surface must discriminate strongly between ss- and ds-DNA. The double helix of the DNA is shown in Figure 2.3 along with details of how the bases, sugars and phosphates connect to form the structure of the molecule.<sup>14</sup>

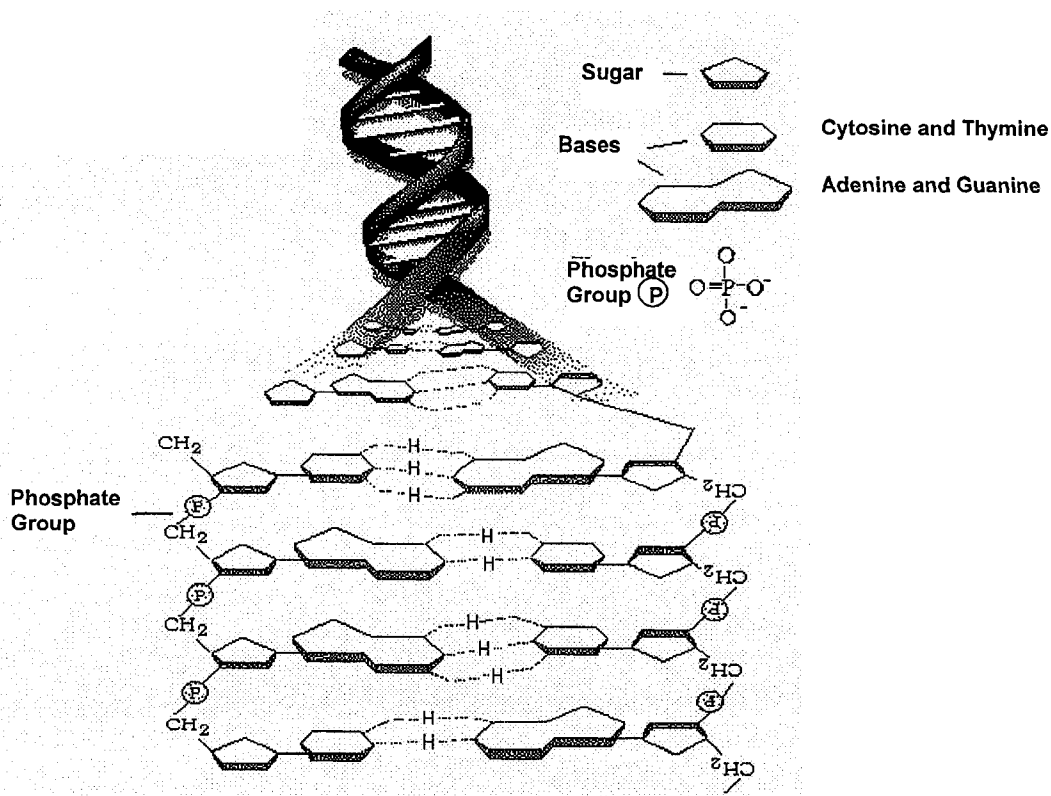


**Figure 2.3.** Molecular structure of ds-DNA. Reprinted from Reference 14.

Each spiraling strand of the DNA molecule, comprised of a sugar-phosphate backbone and attached bases, is connected to a complementary strand by non-covalent hydrogen bonding between paired bases. The bases are adenine (A), thymine (T), cytosine (C) and guanine (G). A and T are connected by two hydrogen bonds. G and C are connected by three hydrogen bonds. All the base pairs are aligned to stay parallel to

each other via  $\pi$ -stacking. Such an orderly structure allows aromatic planar groups to intercalate into the parallel base pairs along the DNA double strands.<sup>15-18</sup> On the other hand, the intercalation into the DNA single strands is much weaker due to the structure disorder along the ss-DNA. Thus, intercalation of planar molecules between the base pairs of ds-DNA, in principle, meets the requirement to discriminate strongly between ss- and ds-DNA. This discrimination mechanism can be introduced by incorporation of non-polar aromatic groups, such as phenothiazine (PTZ)<sup>15-17</sup>, phenoxazine (POZ)<sup>18</sup> or daunomycin<sup>19</sup> into the catalyst structure.

Moreover, the redox potential of the catalyst is very important. The reason to choose a catalyst with the proper redox potential is simple. If the redox potential is too low, the oxidized catalyst won't be able to oxidize the Co(II) complex ( $E_{1/2} = 155$  mV on GC vs SSCE); on the other hand, at high potentials, the DNA molecule will be partially or totally oxidized (G and A bases undergo oxidation around 1.0 and 1.3 V versus Ag/AgCl, respectively). Thus, the desired potential of the redox catalyst should be in the range from 160 mV to 650 mV vs SSCE.

In summary, for sensitive DNA hybridization detection, the current due to the redox chemistry of the mediator molecule, the Co(II) complex on the bare ITO electrode surface, should be as small as possible on the bare ITO surface to avoid noise; meanwhile, to increase the signal, the catalyst should possess not only high efficiency toward catalytic oxidation of the Co(II) complex at non-damaging potentials, but also a strong ability to discriminate between ss- and ds-DNA. Based on these requirements, the catalyst is designed to have the following properties:

1. Being redox active on the ITO electrode with formal potential ranging from 160 mV to 650 mV vs SSCE,
2. Consisting of planar aromatic groups such as PTZ or POZ to discriminate between ss- and ds-DNA, and
3. Negatively or zero charged to avoid non-specific electrostatic interaction between the catalyst and the negatively charged DNA backbone.

During this research, a wide variety of Co(II) complexes and catalysts were prepared/purchased and tested in order to optimize catalytic efficiency and to improve signal/noise.

## **EXPERIMENTAL**

### **Chemicals and Materials**

Hydrochloric and nitric acids of analytical grade were obtained from Mallinckrodt. Photoresist AZ 1512 was obtained from Clariant Corp., and photo-epoxy UVE4050-4 was from Star Technology, Waterloo, IN. Low resistance (4-8  $\Omega$ ) ITO glass slides were purchased from Delta Technologies, Ltd., Stillwater, MN. Reagents used for complex synthesis, electrode preparation, and functionalization [acetone, acetonitrile (ACN), dimethylformamide (DMF), ethanol, 2-propanol, and sodium hydroxide] were all ACS grade purchased from Fisher. Optima grade ACN from Fisher was used for the electrochemical studies. Cobalt(II) perchlorate hydrate was obtained from GFS Chemical Co.  $[\text{Fe}(\text{DCB})_3](\text{ClO}_4)_2$  was prepared according to the literature procedure.<sup>1</sup> Other Chemicals were purchased from Aldrich. Unless otherwise indicated, all reagents were used without further purification.

## **Electrochemical Experiments**

Electrochemical studies were performed using a Bioanalytical System BAS 100 B Potentiostat-Galvanostat controlled by BAS 100 W software resident on an IBM-compatible personal computer. All the electrochemistry was run in a one-compartment electrochemical cell. The counter electrode was a platinum wire, and a sodium saturated calomel electrode (SSCE) or a silver wire was used as the reference electrode or quasi-reference electrode. The working electrode was either an ITO electrode ( $0.5 \text{ cm}^2$ ) or a conventional electrode as specified. Unless otherwise stated,  $0.1 \text{ M TMAPF}_6$  in acetonitrile was employed as the supporting electrolyte.

## **ITO Electrodes Fabrication**

Three different ITO electrodes were fabricated and used during this research; including single electrodes ( $0.5 \text{ cm}^2$ ), array electrodes ( $7 \text{ mm}^2 \times 56$  or  $24$ ) and microarray electrodes ( $0.1 \text{ mm}^2 \times 8$ ).

### **1) Single Electrodes and Array Electrodes**

Conductive ITO glass pieces were cleaned by rinsing with acetone, ethanol, and 2-propanol, to remove any oil and grease on the surface. After drying the electrodes under a nitrogen stream, positive Photoresist AZ 1512 was spin-coated onto the ITO surface at 2500 rpm for 40 s and baked in an oven at  $100 \text{ }^\circ\text{C}$  for 20 min. An opaque mask (vide infra) of the desired shape and size was placed onto the electrodes which were then exposed to UV light generated by a Blak Ray 100 AP Long Wavelength UV lamp for about 2 min. The exposed photoresist is soluble in basic aqueous solution and was removed by immersion of the electrodes in a 0.5% NaOH solution for 20-30 s. The UV-unexposed photoresist remains intact protecting the underlying ITO from the next step.

ITO was removed from the unprotected surface by immersion of the electrode in an “Aqua Regia solution” made of 45% concentrated HCl, 5% concentrated HNO<sub>3</sub>, and 50% water for 30 min. To ensure that the ITO layer was totally removed from the underlying insulating glass surface, the conductivity of the etched regions was checked. When the resistance was larger than 20 MΩ the etch was deemed complete. After etch, the protecting photoresist layer was removed with acetone, leaving a conductive ITO pattern of well-defined geometry on the glass surface. Figure 2.4 a and b show scaled representations of the obtained single electrode and array electrode, respectively.

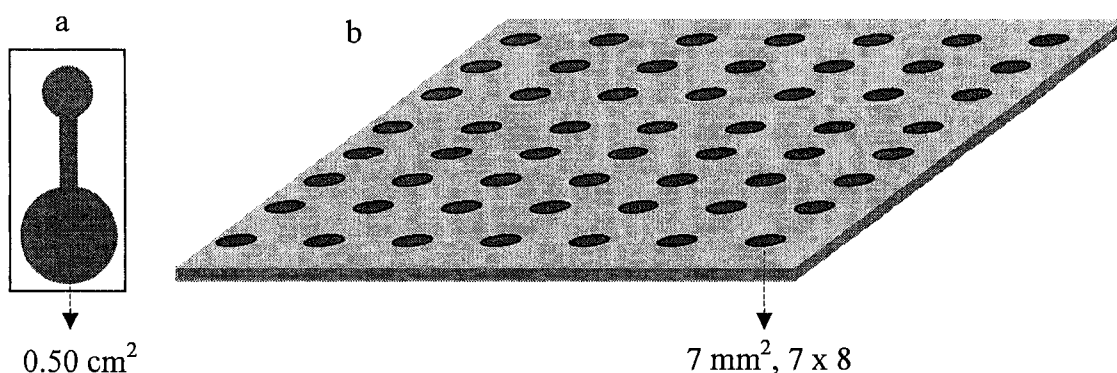


**Figure 2.4.** a) Single electrode: the big circle ( $0.5 \text{ cm}^2$ ) is the DNA sensing area; the small circle is used for making electrical contact with potentiostat. b) ITO array electrode consisting of  $7 \times 8$  ITO spots; each ITO spot has an area of  $7 \text{ mm}^2$ .

The single electrode consists of two circles. The big circle ( $0.5 \text{ cm}^2$ ) represents the active area for DNA hybridization sensing. The small one (4.0 mm diameter) is used to make electrical contact via an alligator clip. These two circles are connected with a narrow ITO rectangle (1.2 mm width x 12 mm length). Resistance between the two circles is  $\sim 50 \Omega$ . The array electrode consists of  $7 \times 8$  electrically isolated ITO spots (or  $7 \times 4$  in some cases); each spot has an active area of  $7 \text{ mm}^2$ . The technique for making

electrical contact of each ITO spot with the potentiostat will be addressed later in section “*Experimental: Catalytic Oxidation of  $[Co(DTB)_3]^{2+}$  on the  $[Fe(DCB)_3]^{2+}$  Modified ITO array Electrode*”.

## 2) Microarray ITO electrode (1 x 0.1 mm<sup>2</sup>, 8 electrodes) fabrication

Following the same procedure as described above, a preliminary ITO array (Figure 2.5 a) was prepared with a mask consisting of eight individual ITO patterns. The masks used to fabricate microarray electrodes were graphically created with CorelDraw 9.0 software and then digitally printed onto a transparency with the help of the Communications and Creative Services at Colorado State University. Onto the preliminary ITO array was added a drop of a UV-curable, negative photo-epoxy UVE4050-4 and a ~ 1 in. x 1 in. piece of clear Teflon film was placed over the glass and the epoxy. The epoxy was then smear-coated on the glass and under the Teflon by carefully dragging a microscope slide over the Teflon film until a uniform layer was obtained (Figure 2.5 b). An opaque mask (Figure 2.5 c) was then positioned over the Teflon and the assembly was then exposed to a near-UV flood source (INTELLI-RAY 400, Professor C. S. Henry’s property) for 90 seconds. The coated ITO plate was baked at 65 °C for 3 min and 95 °C for 6 min; it was then developed in propylene glycol methyl ether acetate leaving a positive relief pattern on the ITO surface (Figure 2.5 d). Upon UV-light illumination, the UVE4050-4 epoxy polymerized and hardened to protect the ITO underneath, while the un-illuminated epoxy under the opaque mask was removed by the developer solution.

Figure 2.5 d shows the structure of the obtained microarray electrode. It has eight individual ITO electrodes, each consists of four ITO rectangles (1<sup>st</sup> to 4<sup>th</sup>). The exposed

area (0.1 x 1 mm<sup>2</sup>) of the 4<sup>th</sup> rectangle is the DNA sensing platform; the 1<sup>st</sup> rectangle is used to make electrical contact with the potentiostat through a lab-made clip. The 1<sup>st</sup> (2 x 3 mm<sup>2</sup>) and 3<sup>rd</sup> (2 x 10 mm<sup>2</sup>) ITO rectangles are “wired” by the 2<sup>nd</sup> rectangle which exhibits smaller dimensions (0.5 x 2 mm<sup>2</sup>). The epoxy film has much higher affinity for the glass surface than for the ITO surface. Such a design allows the edge of the epoxy film to have more glass area to hold on to, which greatly increases the film’s stability.

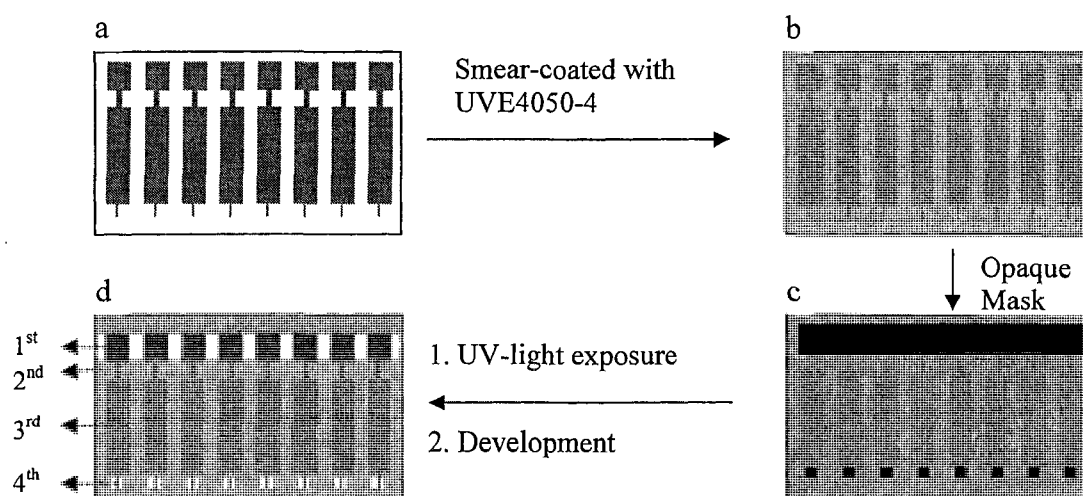
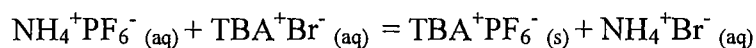


**Figure 2.5** Schematic illustration of microarray ITO electrode fabrication.

### Synthesis of Electrolyte TBAPF<sub>6</sub>



To a solid mixture of TBA<sup>+</sup>Br<sup>-</sup> (5.63g, 17.3 mMol) and NH<sub>4</sub><sup>+</sup>PF<sub>6</sub><sup>-</sup> (2.82g, 17.3 mMol), 100 ml water was added and the suspension was stirred thoroughly for half an hour. The white solid was collected by filtering and washed thoroughly with water. The dried solid was recrystallized from ethanol. The recrystallized product was dissolved in

100 ml methylene chloride. Into the methylene chloride solution 1 g of silver sulfate was added and stirred overnight. Trace amount of the bromide impurities (from reactants or solvents) were trapped on the surfaces of the silver sulfate particles. Solids were removed by centrifuge and filtering and the solution was dried with sodium sulfate. Methylene chloride was removed under reduced pressure. Purity of the product at different stage of the preparation and purification procedure (crude, recrystallized and  $\text{Ag}_2\text{SO}_4$ -treated) was electrochemically analyzed. As shown in Figure 2.6, the crude product (solid curve) contains bromide impurities, which had an  $E_{1/2}$  of 640 mV vs SSCE. The bromide impurities were effectively removed through recrystallization (dashed curve). And the silver-sulfate-treatment (dotted curve) removed trace amount of the impurities (compare the dotted curve with the dashed curve).

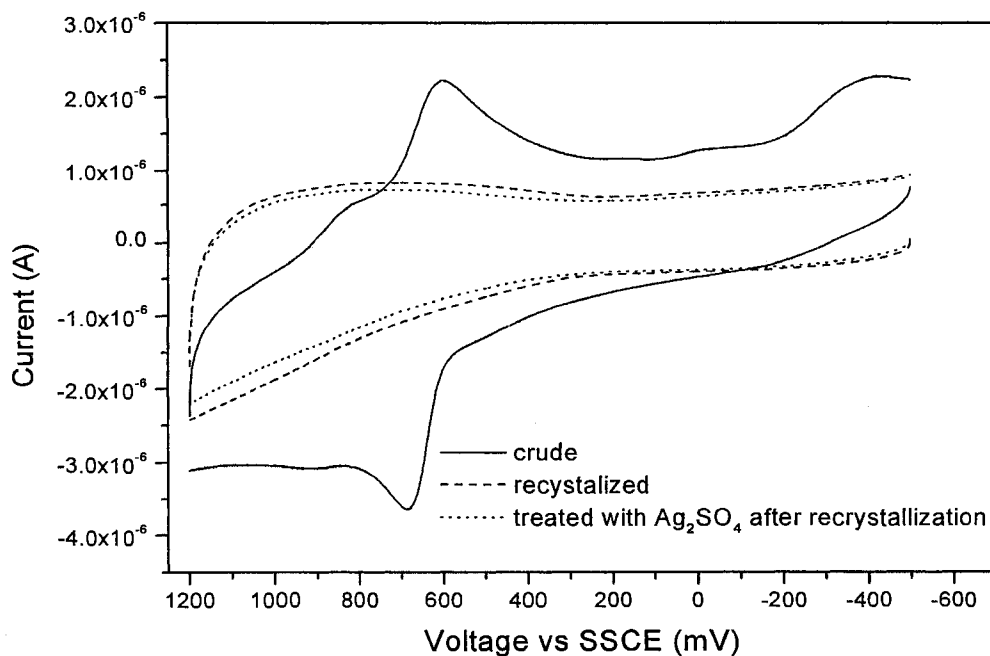
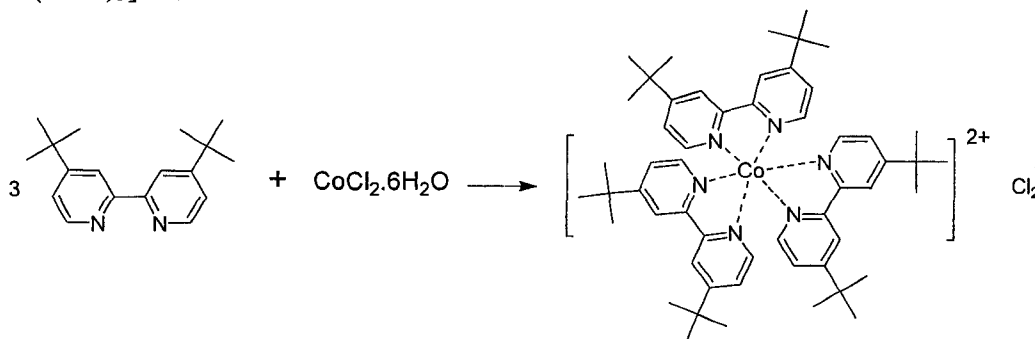


**Figure 2.6.** CVs of 100 mM  $\text{TBAPF}_6$  in acetonitrile on GC ( $0.07 \text{ cm}^2$ ) electrode, scan rate 100 mV/s.

## Synthesis of the Co(II) Complexes

### 1) $[\text{Co}(\text{DTB})_3]\text{Cl}_2$



A solution of 1.1 g DTB (3.9 mMol) and 0.24 g  $\text{CoCl}_2 \cdot 6\text{H}_2\text{O}$  (1.0 mMol) in 50 ml methanol was refluxed under nitrogen for 2 hours, cooled to room temperature. Volatiles were removed under reduced pressure. The solids were dissolved in 5ml methylene chloride and ether was slowly added to this solution to precipitate the crude product as a fine gray powder. The product was collected by filtering, rinsed thoroughly with ether, dried in vacuum (yield 0.69 g, 74%). CVs on ITO and GC are shown in Figure 2.7.

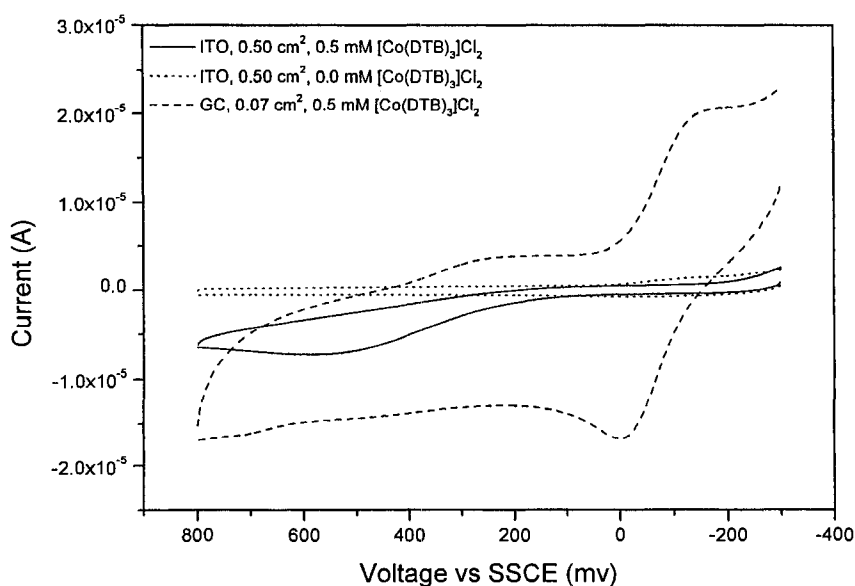
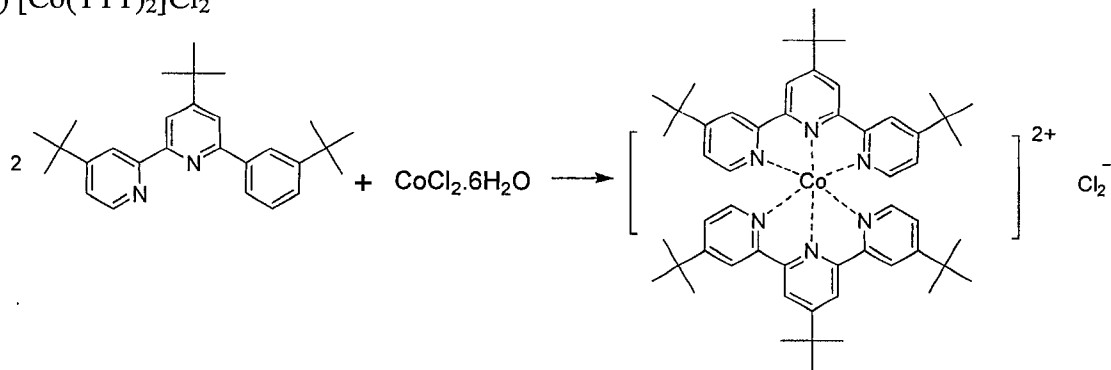


**Figure 2.7.** CVs of  $[\text{Co}(\text{DTB})_3]\text{Cl}_2$  on ITO (0.5 cm<sup>2</sup>) and GC (0.07 cm<sup>2</sup>) electrodes along with a background CV on ITO. The current of GC was scaled by an area factor of 0.5/0.07. Electrolyte 100 mM NaCl/H<sub>2</sub>O, scan rate 100 mV/s.

2)  $[\text{Co}(\text{TTT})_2]\text{Cl}_2$



A solution of 1.2 g TTT (3.0 mMol) and 0.23 g  $\text{CoCl}_2 \cdot 6\text{H}_2\text{O}$  (0.97 mMol) in 90 ml methanol was refluxed under nitrogen for 2 hours, cooled to room temperature. Volatiles were removed under reduced pressure. The solids were taken by 10ml methylene chloride; ether was slowly added to precipitate the crude product. The product was collected by filtering, rinsed thoroughly with ether, dried in vacuum (yield 0.38g). CVs of  $[\text{Co}(\text{TTT})_2]\text{Cl}_2$  on ITO and GC are shown in Figure 2.8.

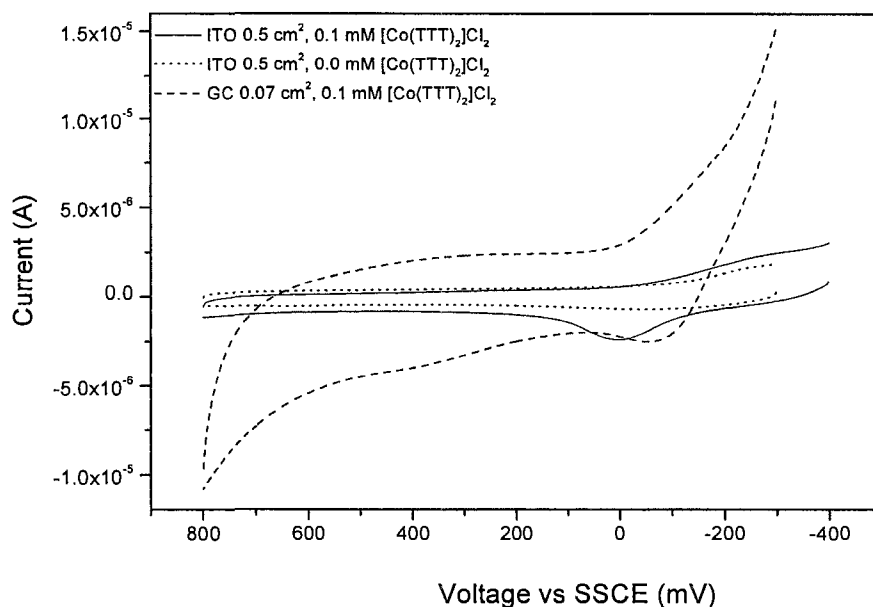
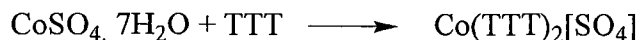
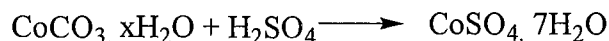
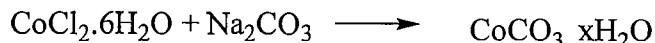


**Figure 2.8.** CVs of  $[\text{Co}(\text{TTT})_2]\text{Cl}_2$  on ITO (0.5 cm<sup>2</sup>) and GC (0.07 cm<sup>2</sup>) electrodes along with a background CV on ITO. The current of GC was scaled by an area factor of 0.5/0.07. Electrolyte 100 mM NaCl/H<sub>2</sub>O, scan rate 100 mV/s.

3) [Co(TTT)<sub>2</sub>](SO<sub>4</sub>)



a) CoCO<sub>3</sub>

Equivalent amount of CoCl<sub>2</sub>·6H<sub>2</sub>O and Na<sub>2</sub>CO<sub>3</sub> were dissolved separately in water, the two aqueous solutions were mixed together with stirring and the solid was collected by filtering, rinsed thoroughly with water, dried in vacuum overnight.

b) CoSO<sub>4</sub>·7H<sub>2</sub>O

H<sub>2</sub>SO<sub>4</sub> (96.5%, 9.1 mMol) of 0.5 ml was dissolved in 50 ml water, and the powder of CoCO<sub>3</sub> (1.2g, 10 mMol) was added slowly with stirring at 40°C. The mixture was stirred at 40°C for 30 minutes, cooled to 3°C. Excess CoCO<sub>3</sub> was removed by filtering and volatiles were evaporated under reduced pressure. The solids were rinsed thoroughly with acetone, dried in vacuum.

c) [Co(TTT)<sub>2</sub>](SO<sub>4</sub>)

A solution of CoSO<sub>4</sub>·7H<sub>2</sub>O (0.22g, 0.78 mMol) and TTT (1.1 g, 2.7 mMol) in 140 ml methanol was refluxed under nitrogen for 14 hours. Volatiles were removed under reduced pressure. The solids were dissolved in methylene chloride (10 ml). Excess ethyl ether was added. The precipitate was collected with filtering, rinsed thoroughly with ether, dried in the air (yield 0.40g, 53%). Cyclic voltammetries of [Co(TTT)<sub>2</sub>](SO<sub>4</sub>) are shown in Figure 2.9.

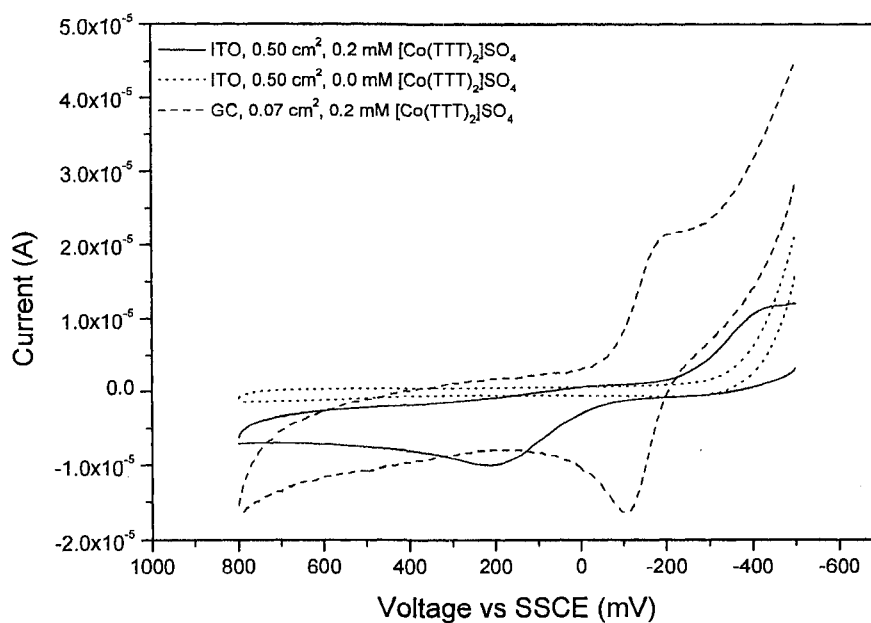
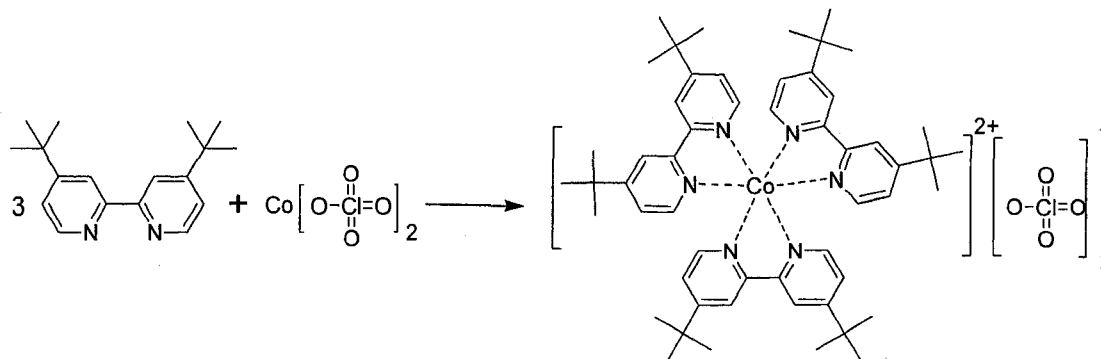


**Figure 2.9.** CVs of  $[\text{Co}(\text{TTT})_2]\text{SO}_4$  on ITO ( $0.5 \text{ cm}^2$ ) and GC ( $0.07 \text{ cm}^2$ ) electrodes along with a background CV on ITO. The current of GC was scaled by an area factor of 0.5/0.07. Electrolyte  $100 \text{ mM Na}_2\text{SO}_4/\text{H}_2\text{O}$ , scan rate  $100 \text{ mV/s}$ .

#### 4) $[\text{Co}(\text{DTB})_3](\text{ClO}_4)_2$



A solution of DTB (5.90 g, 21.5 mMol) and  $\text{Co}(\text{ClO}_4)_2 \cdot 6 \text{ H}_2\text{O}$  (2.38g, 6.50 mMol) in 150 ml methanol was refluxed under nitrogen overnight, cooled to room temperature. Volatiles were removed. And the solids were dissolved in 30 ml methanol, and 100 ml

ether was slowly added. The solid was collected by filtering, and washed thoroughly with ether, dried in vacuum (yield 5.85 g, 85%). CVs are shown in Figure 2.10.

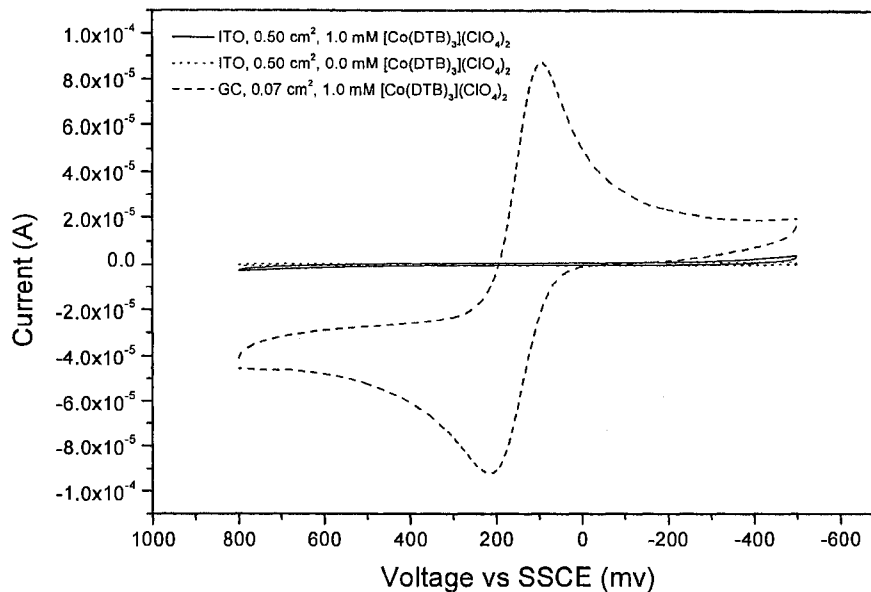
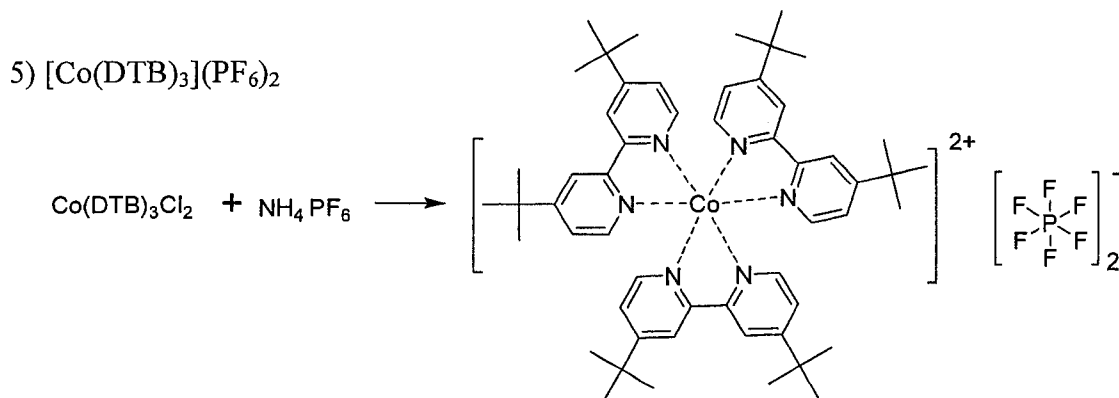


**Figure 2.10.** CVs of  $[\text{Co}(\text{DTB})_3](\text{ClO}_4)_2$  on ITO ( $0.5 \text{ cm}^2$ ) and GC ( $0.07 \text{ cm}^2$ ) electrodes along with a background CV on ITO. The current of GC was scaled by an area factor of  $0.5/0.07$ . Electrolyte  $100 \text{ mM TMAPF}_6/\text{acetonitrile}$ , scan rate  $100 \text{ mV/s}$ .



$\text{Co}(\text{DTB})_3\text{Cl}_2$  (0.31g, 0.33 mMol) was dissolved in 15 ml water and a solution of ammonium hexafluorophosphate (0.11g, 0.66 mMol) in 2 ml water was added while stirring. The solid was collected by filtering and washed thoroughly with water, dried in

vacuum (yield 0.31g, 80%). Cyclic voltammeteries of  $[\text{Co}(\text{DTB})_3](\text{PF}_6)_2$  on GC and ITO are shown in Figure 2.11.

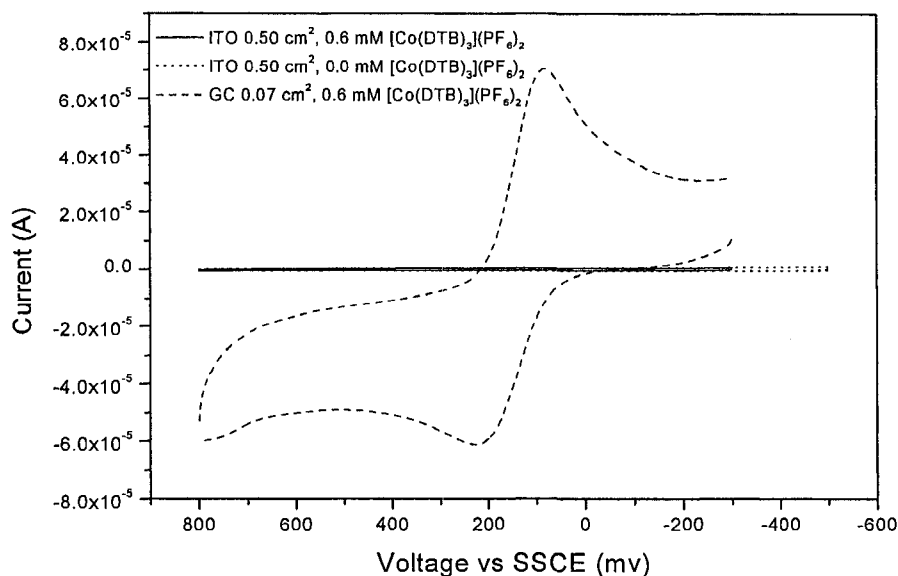
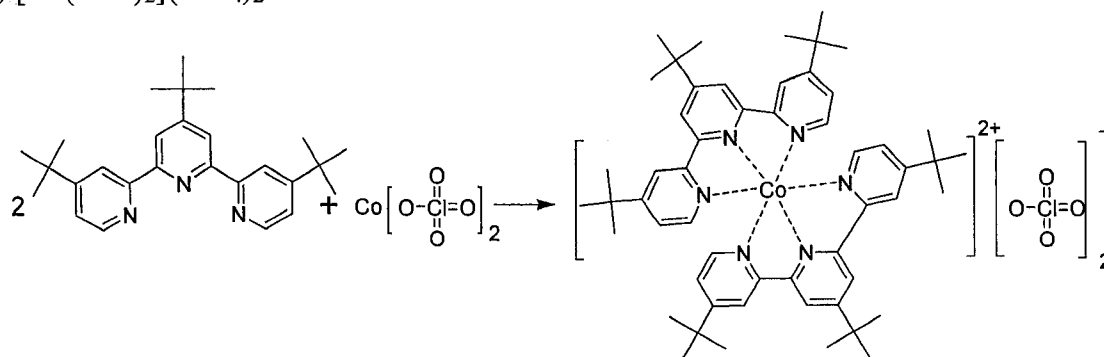


**Figure 2.11.** CVs of  $[\text{Co}(\text{DTB})_3](\text{PF}_6)_2$  on ITO ( $0.5 \text{ cm}^2$ ) and GC ( $0.07 \text{ cm}^2$ ) electrodes along with a background CV on ITO. The current of GC was scaled by an area factor of  $0.5/0.07$ . Electrolyte  $100 \text{ mM TMAPF}_6/\text{acetonitrile}$ , scan rate  $100 \text{ mV/s}$ .

6)  $[\text{Co}(\text{TTT})_2](\text{ClO}_4)_2$



A solution of TTT (1.4 g, 3.3 mMol) and  $\text{Co}(\text{ClO}_4)_2 \cdot 6 \text{ H}_2\text{O}$  (0.38g, 1.0 mMol) in 100 ml methanol was refluxed under nitrogen overnight, cooled to room temperature. Volatiles were removed. ethyl ether 100 ml was added to dissolve the excess TTT. The

solid was collected by filtering, washed thoroughly with ether, dried in vacuum (yield 1.1g, 100%). Cyclic voltammeteries are shown in Figure 2.12.

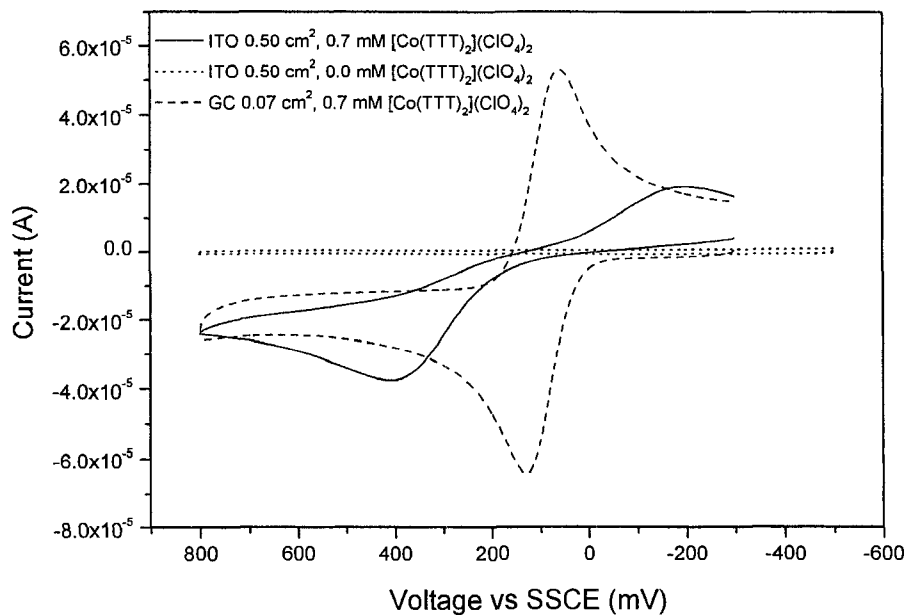
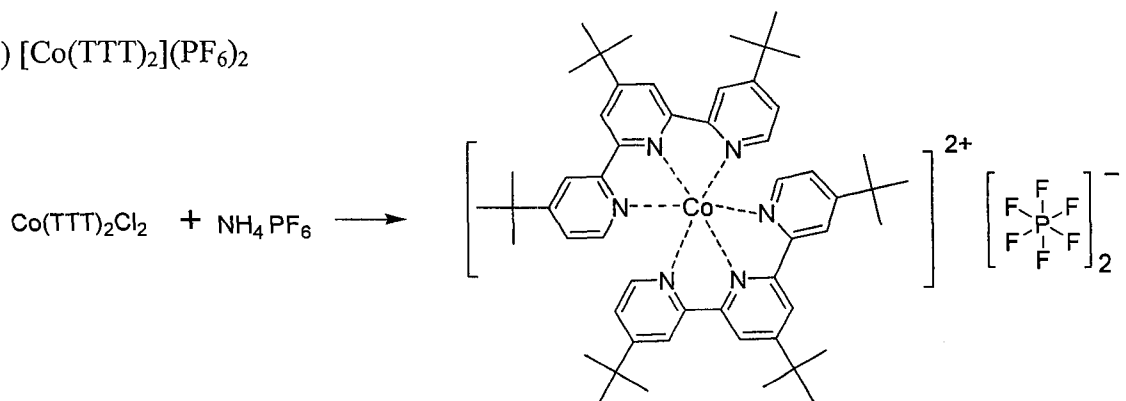


**Figure 2.12.** CVs of )  $[\text{Co}(\text{TTT})_2](\text{ClO}_4)_2$  on ITO ( $0.5 \text{ cm}^2$ ) and GC ( $0.07 \text{ cm}^2$ ) electrodes along with a background CV on ITO. The current of GC was scaled by an area factor of  $0.5/0.07$ . Electrolyte  $100 \text{ mM TMAPF}_6/\text{acetonitrile}$ , scan rate  $100 \text{ mV/s}$ .

7)  $[\text{Co}(\text{TTT})_2](\text{PF}_6)_2$



$\text{Co}(\text{TTT})_2\text{Cl}_2$  ( $0.31 \text{ g}$ ,  $0.33 \text{ mMol}$ ) was dissolved in  $15 \text{ ml}$  water and a solution of ammonium hexafluorophosphate ( $0.11 \text{ g}$ ,  $0.66 \text{ mMol}$ ) in  $2 \text{ ml}$  water was added while stirring. The solid was collected by filtering and washed thoroughly with water, dried in vacuum (yield  $0.31 \text{ g}$ ,  $80\%$ ). Cyclic voltammeteries are shown in Figure 2.13.

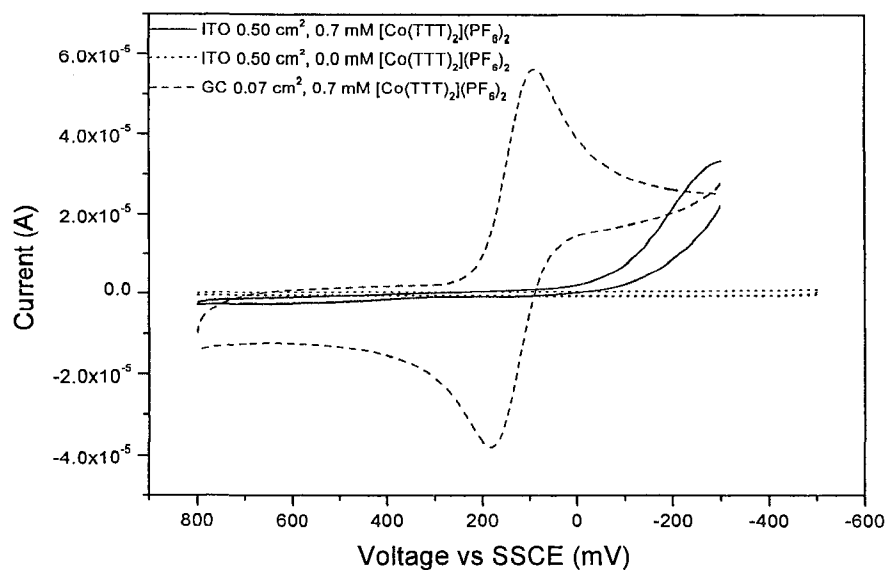


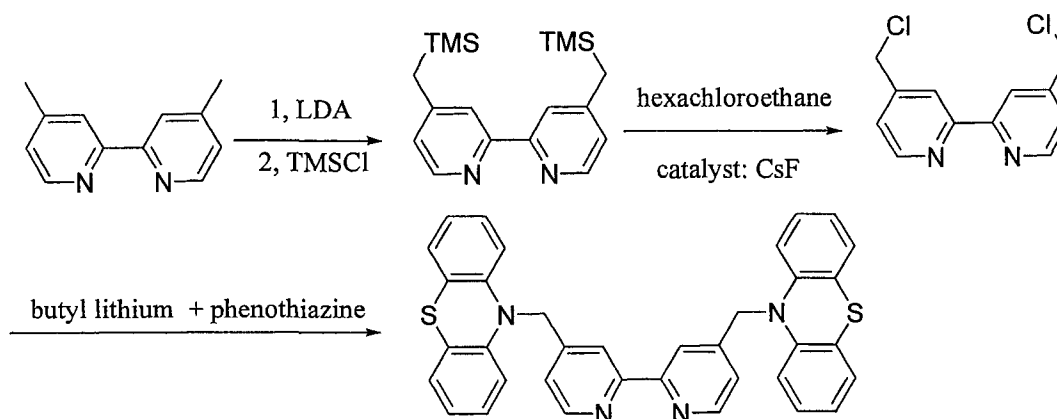
**Figure 2.13.** CVs of  $[\text{Co}(\text{TTT})_2](\text{PF}_6)_2$  on ITO ( $0.5 \text{ cm}^2$ ) and GC ( $0.07 \text{ cm}^2$ ) electrodes along with a background CV on ITO. The current of GC was scaled by an area factor of  $0.5/0.07$ . Electrolyte  $100 \text{ mM TMAPF}_6/\text{acetonitrile}$ , scan rate  $100 \text{ mV/s}$ .

## Synthesis of Catalysts

To prepare the catalysts capable of intercalating into DNA duplex, the coordinating ligands containing aromatic planar groups were first synthesized.

### A. preparation of ligands

#### 1) 4,4'-bis[(N-phenothiazinato)methyl]-2,2'-bipyridine (BPB)



a) 4,4'-Bis[(trimethylsilyl)methyl]-2,2'-bipyridine was prepared according to Smith et al.<sup>20</sup> A solution of diisopropylamine (9.8 ml, 70 mMol) in 90 ml dry THF was cooled to -78°C under nitrogen, then 39 mL 1.6M N-butyl-lithium in hexane (62 mMol) was added dropwise via syringe. The mixture was stirred for 10 mins, and warmed up to room temperature and stirred for another 30 mins, cooled to 0°C. A solution of 4,4'-dimethylbipyridine (5.1g, 28 mMol) in 130 ml dry THF was added via cannula after being degassed. The solution was stirred at 0°C for 30 mins, cooled to -78°C, 8.9 ml trimethylsilyl chloride (70 mMol) was added via syringe all at once, stirred vigorously for 11 seconds, and quickly quenched with methanol. The cold mixture was added to 200 ml aqueous saturated NaHCO<sub>3</sub> solution. The product was extracted with methylene chloride, dried over Na<sub>2</sub>SO<sub>4</sub>. Methylene chloride was removed with rotatory evaporation, obtaining 8.8 g off white solid (yield 96%). <sup>1</sup>H NMR spectrum is shown in Figure 2.14.

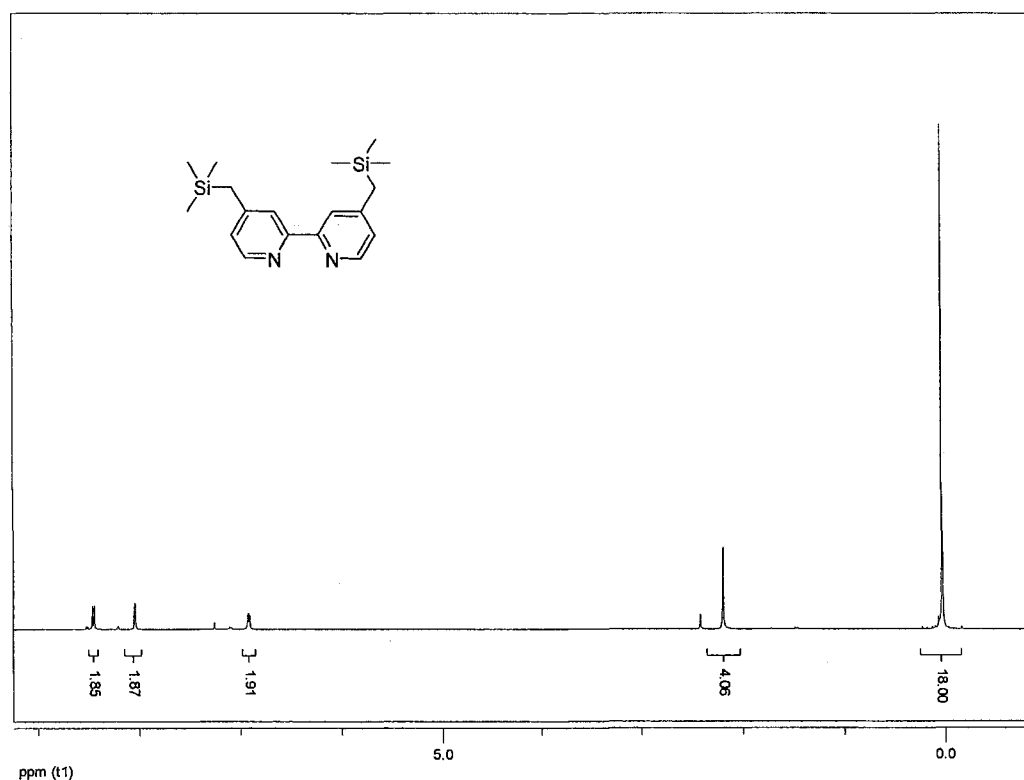


**Figure 2.14.** <sup>1</sup>H NMR spectrum of 4,4'-bis[(trimethylsilyl)methyl]-2,2'-bipyridine in CDCl<sub>3</sub>.

b) *4,4'-Bis(chloromethyl)-2,2'-bipyridine* was prepared according to literature procedures.<sup>20</sup> The mixture of 4,4'-Bis[(trimethylsilyl)methyl]-2,2'-bipyridine (8.15 g, 24.8 mMol), hexachloroethane (23.5g, 99.2 mMol) and Cesium fluoride (15.1g, 99.2 mMol) in 400 ml dry acetonitrile was degassed and heated to 60°C under nitrogen for 4 hs. The reaction mixture was cooled to room temperature and was added to a separatory funnel containing 150 ml water and 150 ml ethyl acetate. The product was extracted with 3 x 100 ml ethyl acetate. The organic phase was collected, extracted with brine, dried over Na<sub>2</sub>SO<sub>4</sub>, and was evaporated under reduced pressure. The product was purified by silica column with gradient ethyl acetate/hexane as eluent (yield 4.13g, 66%). Silica columns were deactivated by flushing with 1% triethylamine in hexanes and then were washed with hexanes prior to use. <sup>1</sup>H NMR spectrum of the product is shown in Figure 2.15.

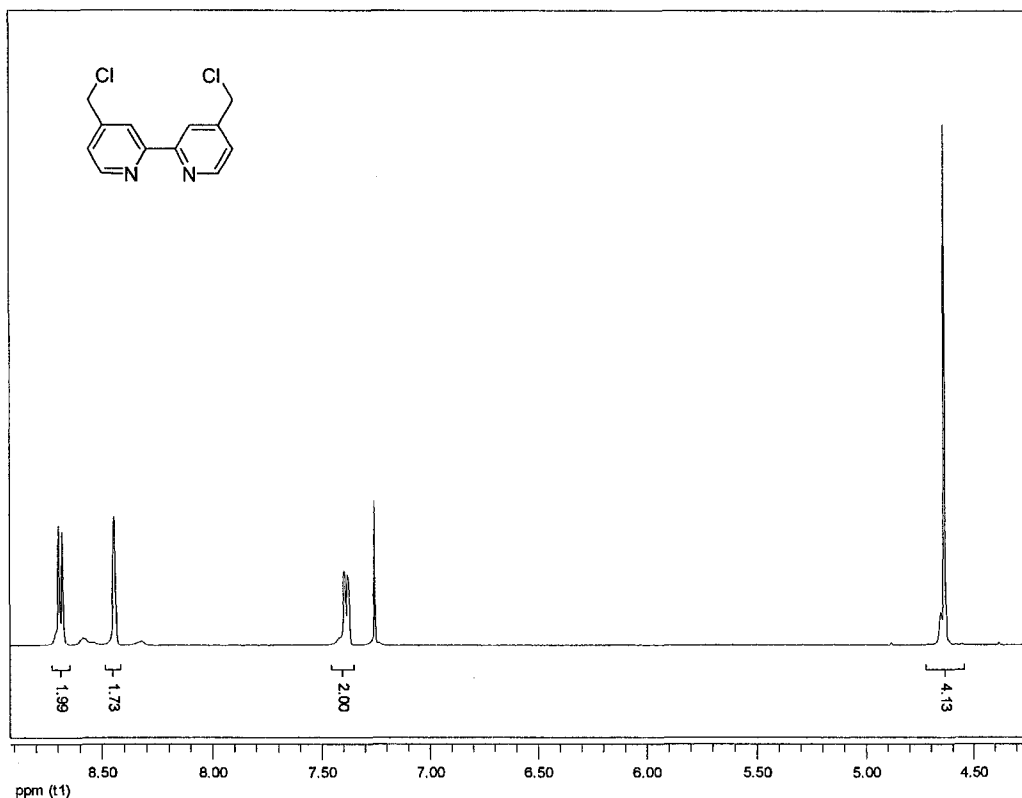


**Figure 2.15.** <sup>1</sup>H NMR spectrum of 4,4'-bis(chloromethyl)-2,2'-bipyridine in CDCl<sub>3</sub>.

c) 4,4'-bis[*((N-phenothiazinato))methyl*]-2,2'-bipyridine (BPB) was prepared by modification of literature procedures.<sup>21</sup> Under nitrogen, n-butyl lithium (1.6 M in hexane, 13 ml, 20mMol) was added dropwise by syringe into a solution of phenothiazine (4.2g, 21 mMol) in 200 ml dry THF. During this process, the solution was kept at 0°C by ice bath. The bright yellow solution was stirred at 0°C under nitrogen for one hour. A solution of 4,4'-Bis(chloromethyl)-2,2'-bipyridine (0.53g, 2.1 mMol) in 25 ml dry THF was added slowly under nitrogen via cannula. The mixture was stirred and was allowed to warm from 0°C to room temperature overnight. The solvent was removed by rotatory evaporation. 30 ml water was added, the product was extracted with methylene chloride. The product was purified by silica column (15g) with gradient hexane/ether as eluent, weighed 0.46 g (yield 37%). <sup>1</sup>H NMR spectrum is shown in Figure 2.16.

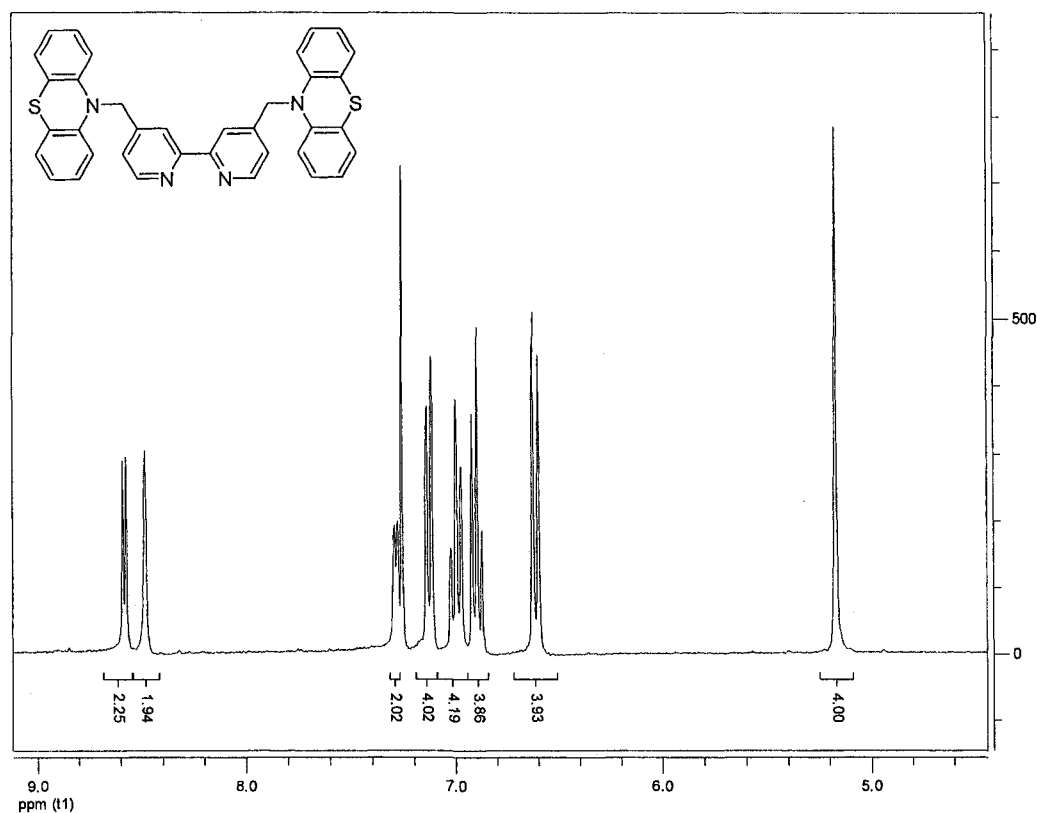
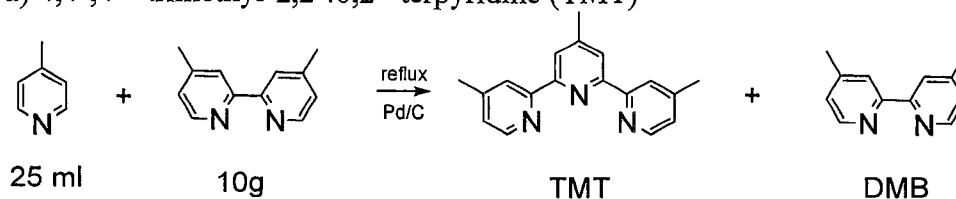


**Figure 2.16.** <sup>1</sup>H NMR spectrum of 4,4'-bis[*((N-phenothiazinato))methyl*]-2,2'-bipyridine in CDCl<sub>3</sub>.

2) 4,4',4''-tris[(N-phenothiazinato)methyl]-2,2':6,2''-terpyridine (TPT)

a) 4,4',4''-trimethyl-2,2':6,2''-terpyridine (TMT)



TMT was prepared by modification of literature procedures<sup>22</sup>. Before use, picoline was distilled under reduce pressure (~3 mmHg) over KOH at 60°C. The freshly distilled picoline 17 g was mixed with 3.4 g 10% Pd/C and 7g bipyridine. The mixture was degassed and refluxed under nitrogen for 91 hours, cooled to room temperature, dissolved in methylene chloride. Solid was removed by filtering. The solution was dried by rotatory evaporation and the resulting solid contains TMT and DMB. DMB was removed by vacuum sublimation overnight. The remaining solid was dissolved in methylene chloride and filtered. The solvent of the filtrate was removed to obtain 2.5g product (Rf = 0.1 with 1:5 methanol/methylene chloride, <sup>1</sup>H NMR spectrum is shown in Figure 2.17).

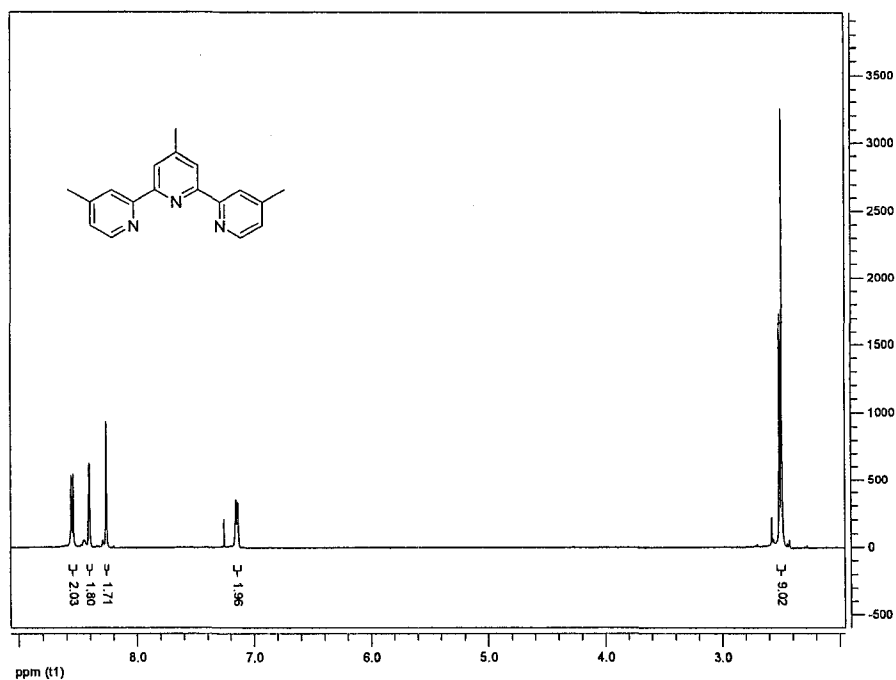
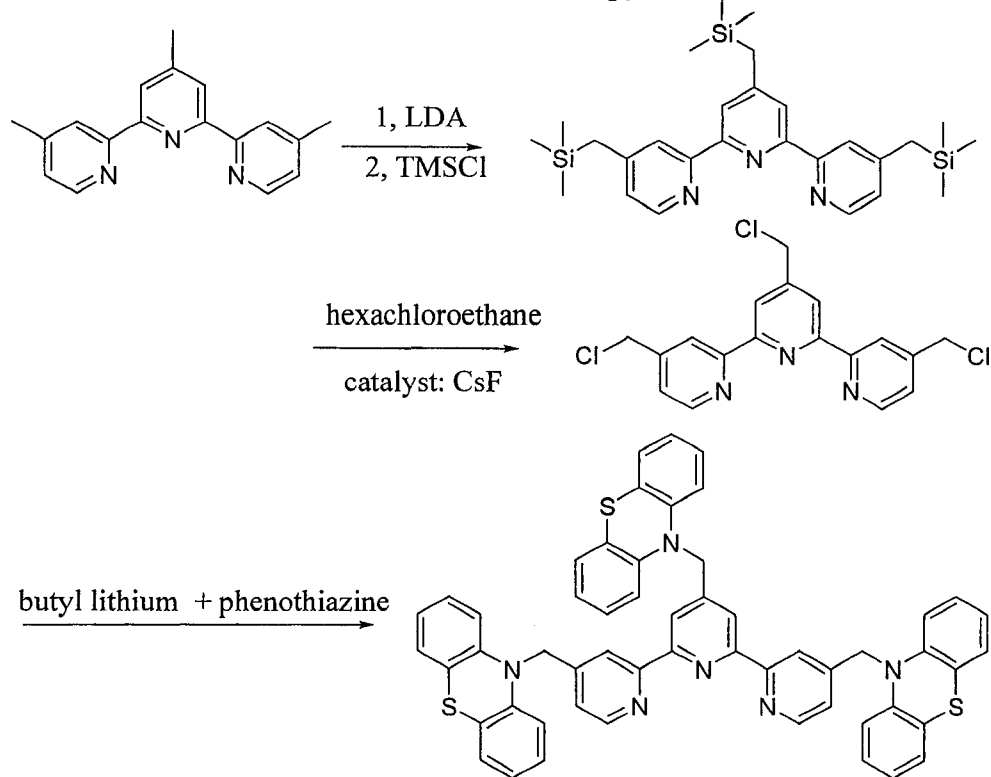


**Figure 2.17.** <sup>1</sup>H NMR spectrum of 4,4',4''-trimethyl-2,2':6,2''-terpyridine in CDCl<sub>3</sub>.

b) 4,4',4''-tris[(trimethylsilyl)methyl]-2,2':6,2''-terpyridine



Under nitrogen, a solution of diisopropylamine (1.1ml, 7.8 mMol) in 20 ml dry THF was cooled to 0°C. N-butyl lithium (1.6M in hexane, 4.2 ml, 6.7 mMol) was added slowly via syringe. The solution was stirred at 0°C for 30 mins. Then a solution of 4, 4', 4''-trimethyl-2, 2':6, 2''-terpyridine (0.53 g, 1.9 mMol) in 20 ml THF was added via cannula. The solution was stirred and allowed to warm from 0°C to room temperature over three hours, cooled to -78°C, and trimethylsilyl chloride (0.98 ml, 7.7 mMol) was added via syringe all at once. The mixture was stirred for 15 seconds, quenched with 10 ml absolute ethanol, and poured into 50 ml saturated sodium bicarbonate aqueous solution. When warmed to room temperature, the product was extracted with methylene chloride. The organic portion was washed with brine, dried with sodium sulfate, and volatiles were removed by rotatory evaporation, obtaining off white solid (yield 0.96g, 100 %). <sup>1</sup>H NMR spectrum is shown in Figure 2.18.

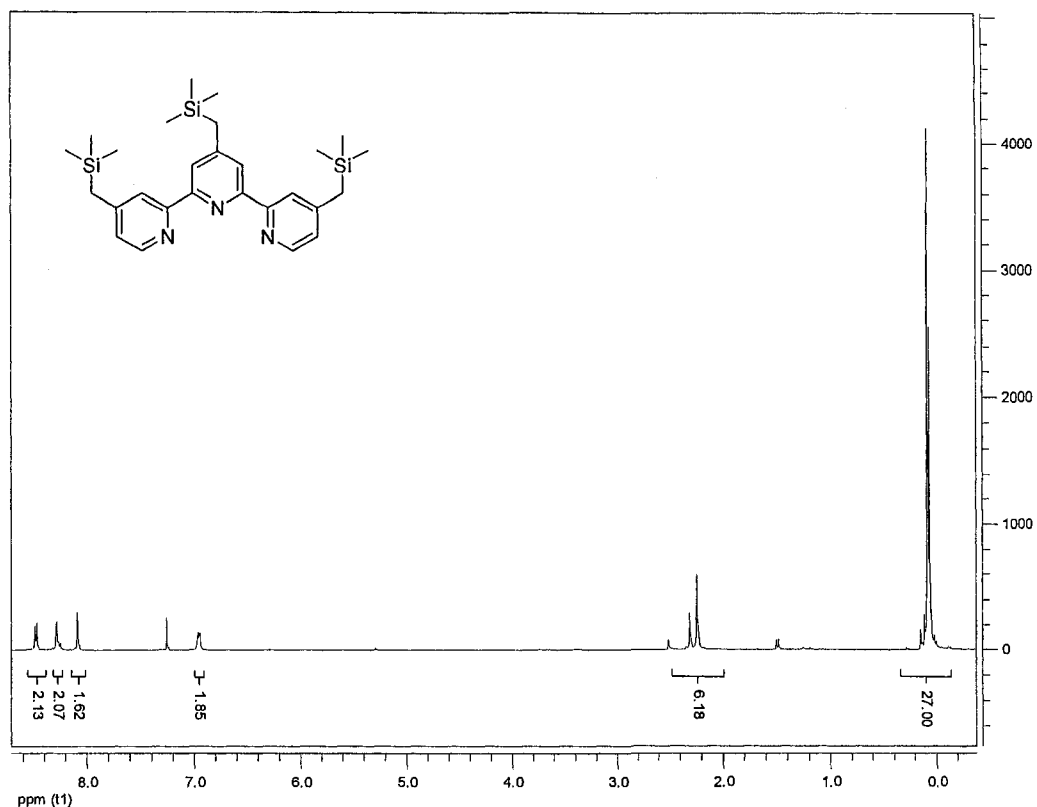


**Figure 2.18.**  $^1\text{H}$  NMR spectrum of 4,4',4''-tris[(trimethylsilyl)methyl]-2,2':6,2''-terpyridine in  $\text{CDCl}_3$ .

c) 4,4',4''-tris(chloromethyl)-2,2':6,2''-terpyridine

Under nitrogen, the suspension of 4,4',4''-tris(chloromethyl)-2,2':6,2''-terpyridine (0.96g, 1.9 mMol), hexachloroethane (2.77g, 11.6 mMol) and cesium fluoride (1.8g, 12 mMol) in 50 ml dry THF was stirred at  $60^\circ\text{C}$  for three hours, then poured into the separatory funnel containing 100 ml water and 100 ml ethyl acetate. The product was extracted with ethyl acetate, and the organic portion was washed with brine, dried over sodium sulfate. After the solvent was removed, the product was purified by silica column (30g) with 3:7 ethyl acetate / hexane, (yield 0.50g, 69%),  $^1\text{H}$  NMR spectrum is shown in Figure 2.19.

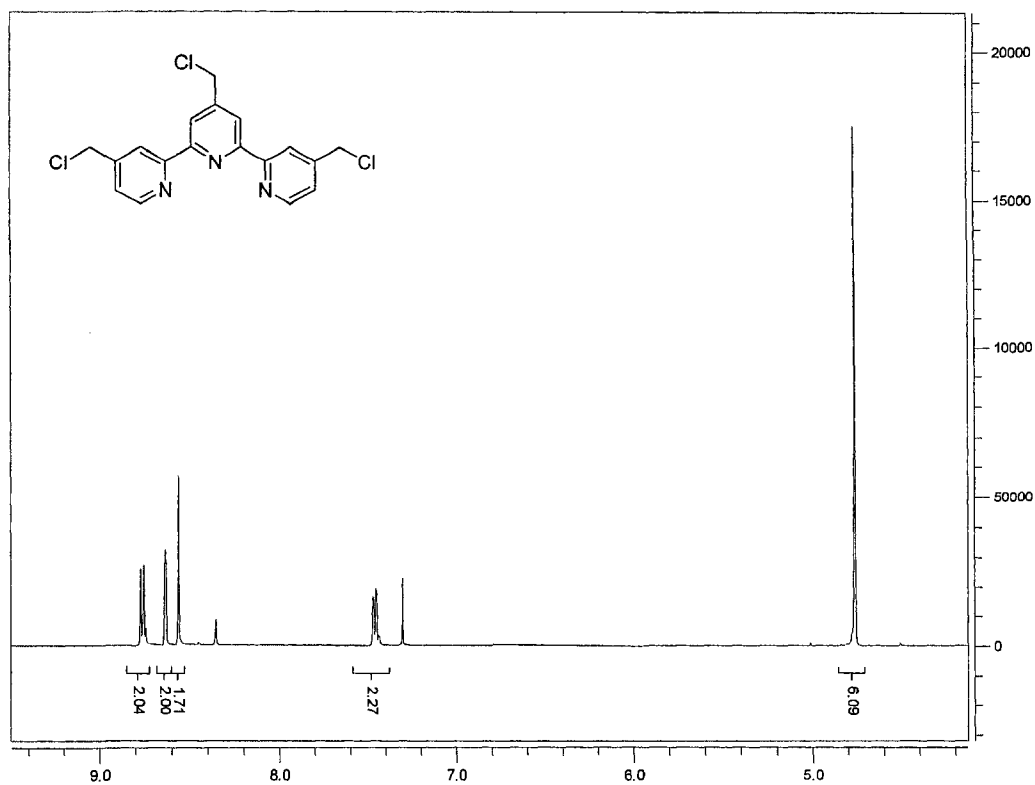


**Figure 2.19.** <sup>1</sup>H NMR spectrum of 4,4',4''-tris(chloromethyl)-2,2':6,2''-terpyridine in CDCl<sub>3</sub>.

d) 4,4',4''-tris[(N-phenothiazinato)methyl]-2,2':6,2''-terpyridine (TPT)

Under nitrogen, n-butyl lithium (1.6 M in hexane, 7.5 ml, 12mMol) was added by syringe into a solution of phenothiazine (4.2g, 21mMol) in 100 ml dry THF. During this process, the solution was kept at -78 °C. The yellow suspension was stirred at 0 °C under nitrogen for one hour. The solution of 4,4',4''-tris(chloromethyl)-2,2':6,2''-bipyridine 0.45g, 1.2 mMol) in 25 ml dry THF was added slowly through cannula. The mixture was stirred from 0 °C to room temperature for 30 hours. 10 ml methanol was added to quench the reaction and 100 ml water was added. The product was extracted into ethyl acetate, dried over sodium sulfate. The product was purified by column (silica, 15g) with gradient hexane/ethyl acetate as eluent (yield 0.52 g, 50%); <sup>1</sup>H NMR spectrum is shown in Figure 2.20.

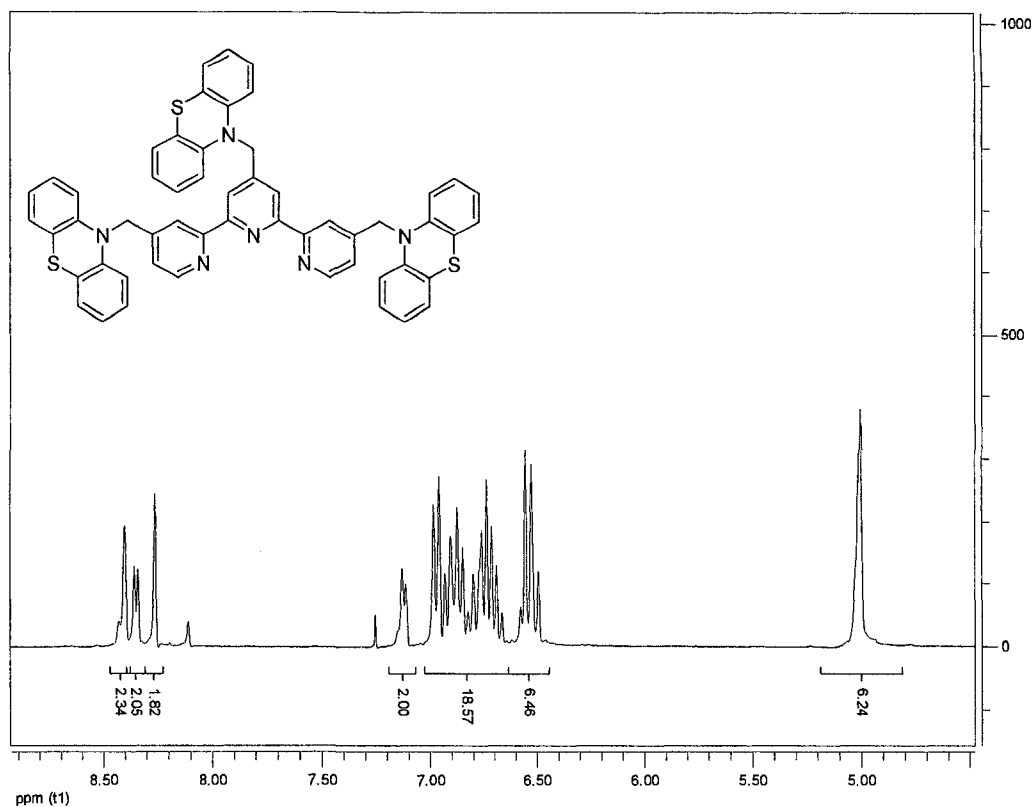
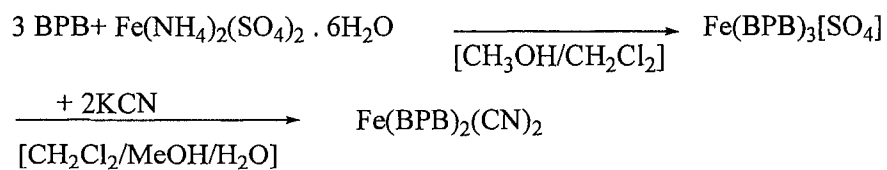
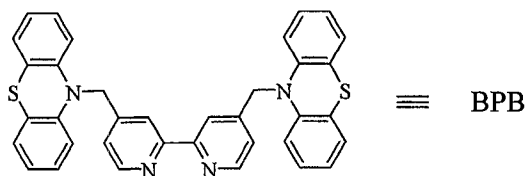


**Figure 2.20.**  $^1\text{H}$  NMR spectrum of 4,4',4''-tris[(N-phenothiazinato)methyl]-2,2':6,2''-terpyridine in  $\text{CDCl}_3$ .

*B. preparation of catalysts*

1)  $\text{Fe}(\text{BPB})_2(\text{CN})_2$



$\text{Fe}(\text{BPB})_2(\text{CN})_2$  was prepared by modification of literature procedures.<sup>23, 24</sup> A mixture of 24 mg ferrous ammonium sulfate hexahydrate (60  $\mu\text{mol}$ ) and 0.10 mg (0.18

mmol) 4,4'-bis(N-phenothiazinato)methyl-2,2'-bipyridine (BPB), in 105 ml 1:1:3 (v:v:v)water / chloroform / methanol was refluxed under nitrogen for 30 mins, and the freshly prepared solution of potassium cyanide (1.2g, 18 mmol) in 5 ml water was added all at once. The mixture was refluxed under nitrogen for 14 hours, cooled to room temperature. The solids were removed by filtering. The filtrate was dried by rotatory evaporation, and product was dissolved in 50 ml methylene chloride. The methylene chloride solution was washed with 10ml x3 water, dried over sodium sulfate, and dried by rotatory evaporation. The product was purified by silica column (10 g). Silica chromatography columns were deactivated by flushing with 1% triethylamine in methylene chloride and then were washed with methylene chloride prior to use. The product was separated with gradient methanol/methylene chloride as eluent (yield 69 mg, 91%). The cyclic voltammetry is shown in Figure 2.21.

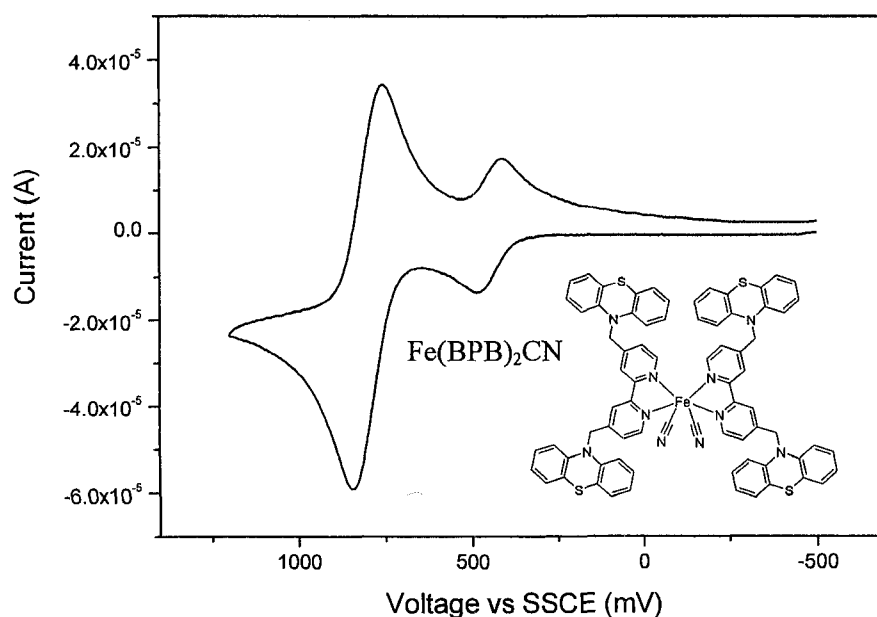


**Figure 2.21.** CV of Fe(BPB)<sub>2</sub>CN<sub>2</sub> in 100 mM TMAPF<sub>6</sub>/ACN. W.E., ITO (0.5 cm<sup>2</sup>); R.E., SSCE; C.E., Pt; S.R. = 100 mV/sec.

2)  $\text{Fe}(\text{DMB})_2(\text{CN})_2$

The preparation of  $\text{Fe}(\text{DMB})_2(\text{CN})_2$  is similar to  $\text{Fe}(\text{BPB})_2(\text{CN})_2$  except ligand DMB was used instead of BPB. The cyclic voltammetry is shown in Figure 2.22.

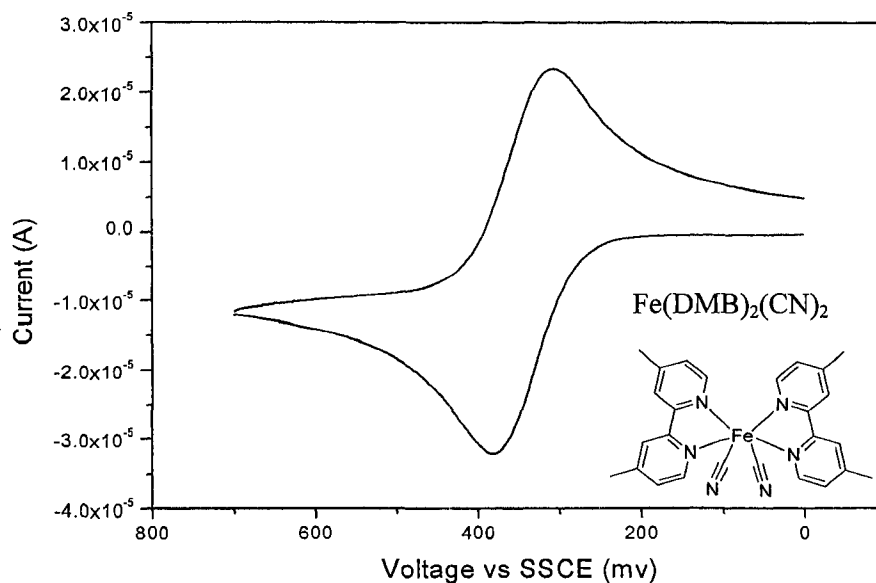
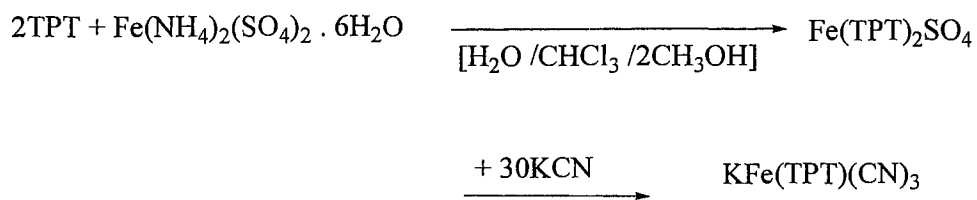
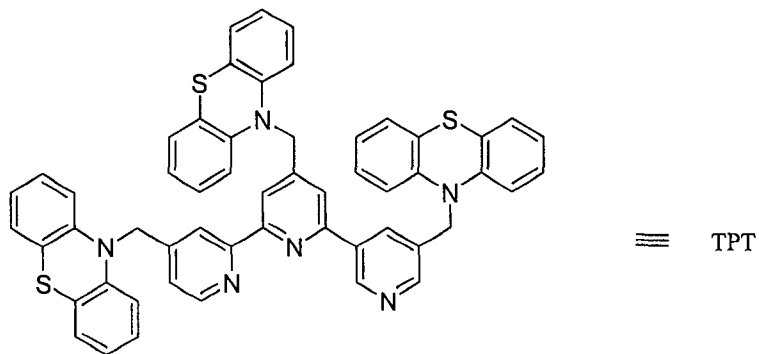


**Figure 2.22.** CV of  $\text{Fe}(\text{DMB})_2(\text{CN})_2$  in 100 mM  $\text{TMAPF}_6/\text{ACN}$ . W.E., ITO ( $0.5 \text{ cm}^2$ ); R.E., SSCE; C.E., Pt; S.R. = 100 mV/sec.

3)  $\text{KFe}(\text{TPT})(\text{CN})_3$



The mixture of 4, 4', 4''-tris(N-phenothiazinato)methyl-2,2':6, 2''-terpyridine (TPT) 93.0 mg (107  $\mu\text{mol}$ ) and ferrous ammonium sulfate hexahydrate 21.4 mg (54.5  $\mu\text{mol}$ ) in 55 ml 2:3:6 (v:v:v) water/chloroform/methanol was refluxed under nitrogen till a homogenous purple solution formed, and a freshly prepared solution of potassium cyanide (105 mg, 1.62 mmol) in 5 ml water was added all at once. The mixture was refluxed under nitrogen for 35 mins, cooled to room temperature. The product was extracted with methylene chloride. The methylene chloride solution was dried over sodium sulfate, and volatiles were removed by rotatory evaporation. The product was purified by silica column (10g) with gradient methanol/methylene chloride as eluent (yield 57.8 mg, 100%). Silica chromatography columns were deactivated by flushing with 1% triethylamine in methylene chloride and then were washed with methylene chloride prior to use. The cyclic voltammetry of  $\text{KFe}(\text{TPT})(\text{CN})_3$  is shown in Figure 2.23. The small surface wave at potentials around 450 mV indicates an surface bound impurity with an peak separation of  $\sim 20$  mV.

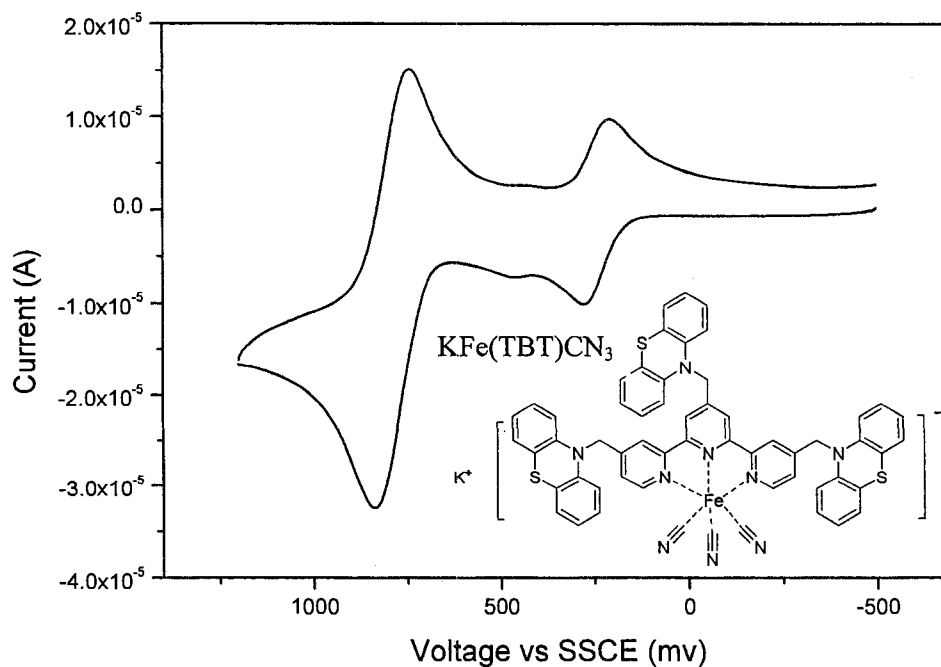
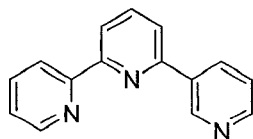
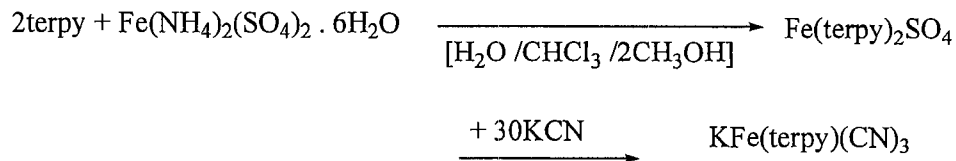


**Figure 2.23.** CV of  $\text{KFe}(\text{TBT})\text{CN}_3$  in 100 mM  $\text{TMAPF}_6/\text{ACN}$ . W.E., ITO ( $0.5 \text{ cm}^2$ ); R.E., SSCE; C.E., Pt; S.R. = 100 mV/sec.

4)  $\text{KFe(terpy)(CN)}_3$



≡ terpy



$\text{KFe(terpy)(CN)}_3$  was prepared similarly as above except unsubstituted terpy instead of TPT was used. Cyclic voltammetry of  $\text{KFe(terpy)(CN)}_3$  in 100 mM NaCl on ITO electrode was shown in Figure 2.24.

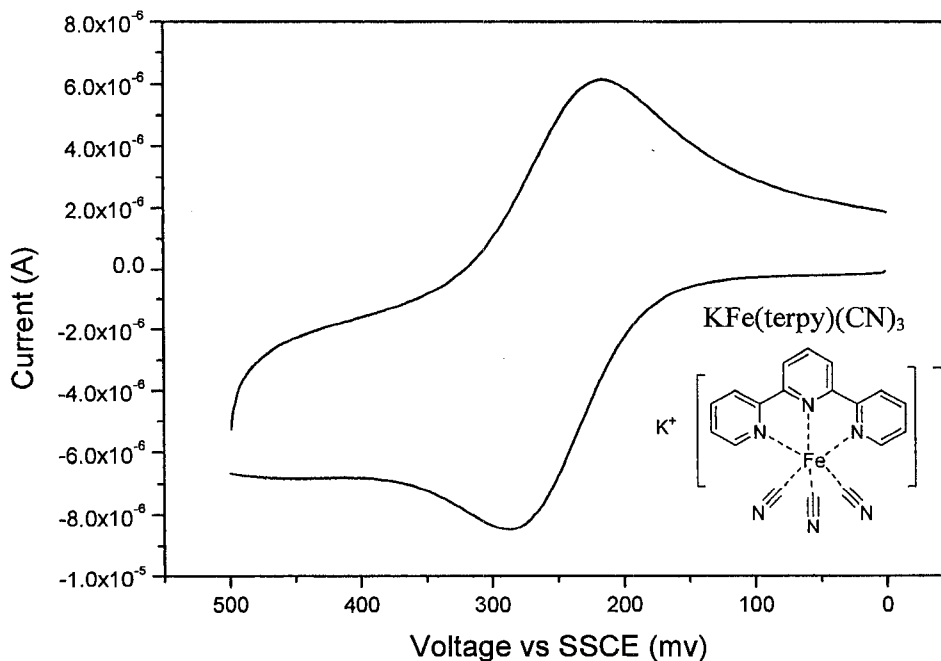
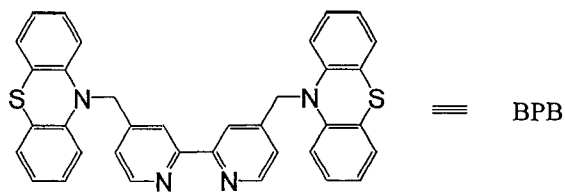


**Figure 2.24.** CV of  $\text{KFe(terpy)(CN)}_3$  in 100 mM TMAPF<sub>6</sub>/ACN. W.E., ITO (0.5 cm<sup>2</sup>); R.E., SSCE; C.E., Pt; S.R. = 100 mV/sec.

5) Ru(BPB)<sub>2</sub>(Cl)<sub>2</sub>



Ru(BPB)<sub>2</sub>(Cl)<sub>2</sub> was prepared by modification of literature procedures.<sup>25</sup> One equivalent Ru(DMSO)<sub>4</sub>(Cl)<sub>2</sub> (0.075 mMol), two equivalent BPB (0.15 mMol) and 10 equivalent LiCl (1.5 mMol) were mixed in 100 mL dry DMF and degassed, the mixture was refluxed under nitrogen for 1 h, DMF was removed by rotatory evaporation, The product was dissolved in methylene chloride, and the solution was washed with water, brine, dried over sodium sulfate. The product was purified through a silica column with gradient methanol/methylene chloride as the eluent (yield 32 mg, 33%). The cyclic voltammetry is shown in Figure 2.25.

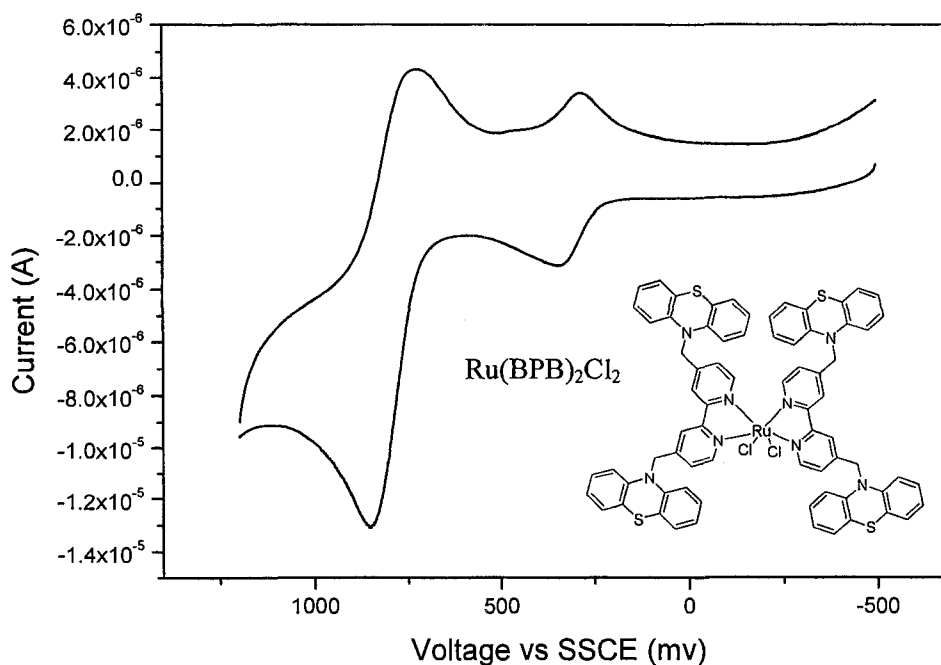
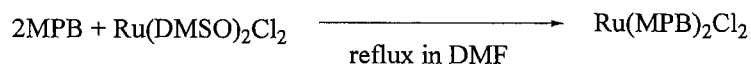
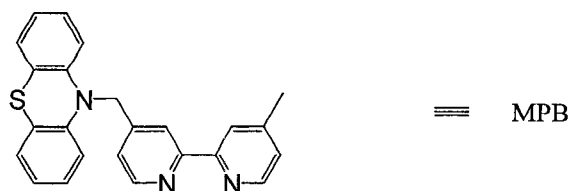


**Figure 2.25.** CV of Ru(BPB)<sub>2</sub>Cl<sub>2</sub> in 100 mM TMAPF<sub>6</sub>/ACN. W.E., ITO (0.5 cm<sup>2</sup>); R.E., SSCE; C.E., Pt; S.R. = 100 mV/sec.

6) Ru (MPB)<sub>2</sub>(Cl)<sub>2</sub>



MPB was prepared according to literature procedures.<sup>21</sup> Ru (MPB)<sub>2</sub>(Cl)<sub>2</sub> was prepared similarly as Ru(BPB)<sub>2</sub>(Cl)<sub>2</sub>, except that MPB was used instead of BPB. The cyclic voltammetry is shown in Figure 2.26.

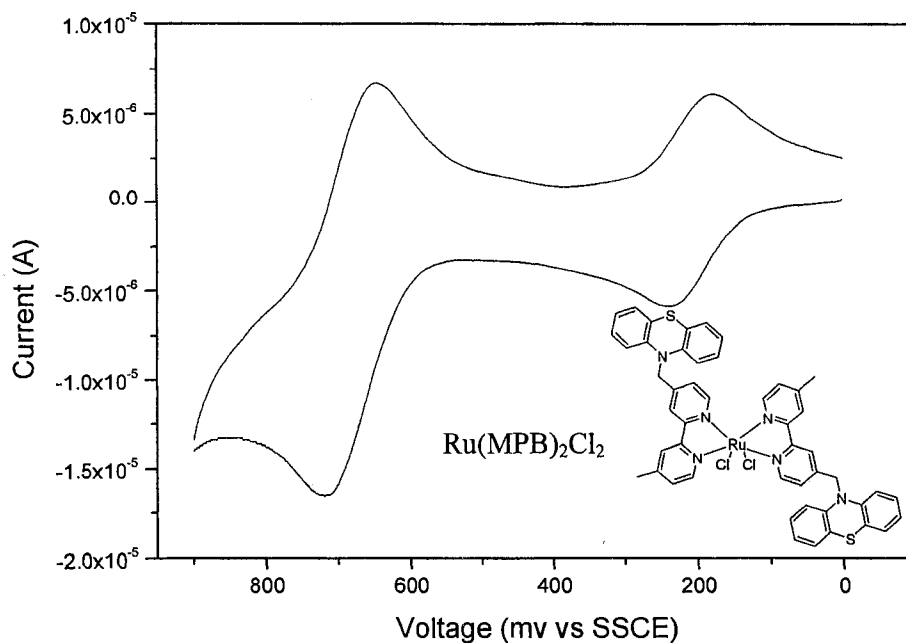
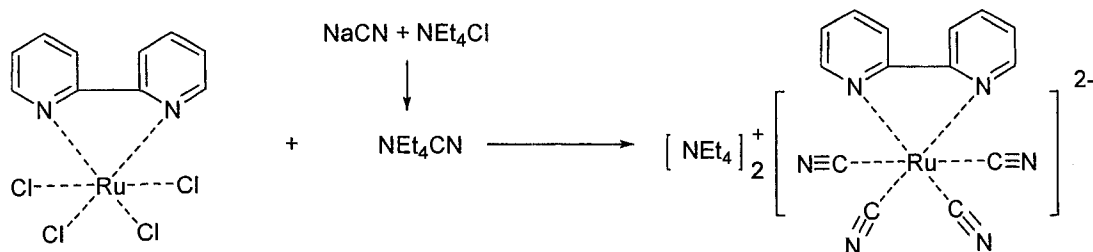


**Figure 2.26.** CV of Ru(MPB)<sub>2</sub>Cl<sub>2</sub> in 100 mM TMAPF<sub>6</sub>/ACN. W.E., ITO (0.5 cm<sup>2</sup>); R.E., SSCE; C.E., Pt; S.R. = 100 mV/sec.

7) [NEt<sub>4</sub>]<sub>2</sub> Ru(bpy)(CN)<sub>4</sub>



$NEt_4CN$  was prepared according to Andreades et al.<sup>26</sup> A flask with stirrer was charged with 10 g  $NEt_4Cl \cdot xH_2O$  and 20 ml methanol. The solution was stirred. Under nitrogen, a solution of 5g sodium cyanide in 150 ml methanol was added dropwise via cannula and stirred for one hour. The content of the flask was filtered and the filtrate was dried under vacuum. 50 ml x 3 acetonitrile was used to extract the product. Crystals formed after the acetonitrile solution was concentrated to ~15 ml, was allowed to mature at  $-30^\circ C$  for 30 mins before warming up to room temperature. The crystals were collected by filtration, washed with 2 ml acetonitrile, dried in vacuum (1.9g, yield 12%).

$[NEt_4]_2 Ru(bpy)(CN)_4$  was prepared according to Kato et al.<sup>27</sup> A solution of 0.51 g  $NEt_4CN$  (3.3 mMol) and 0.18g  $Ru(bpy)Cl_4$ <sup>28</sup> (0.45mMol) in 100 ml 4:1  $H_2O$ /ethanol was refluxed under nitrogen for 10 days, the solvents were removed under vacuum. The product was purified by silica column with gradient methanol/methylene chloride as eluent (yield 69 mg, 91%). CV of the product is shown in Figure 2.27.

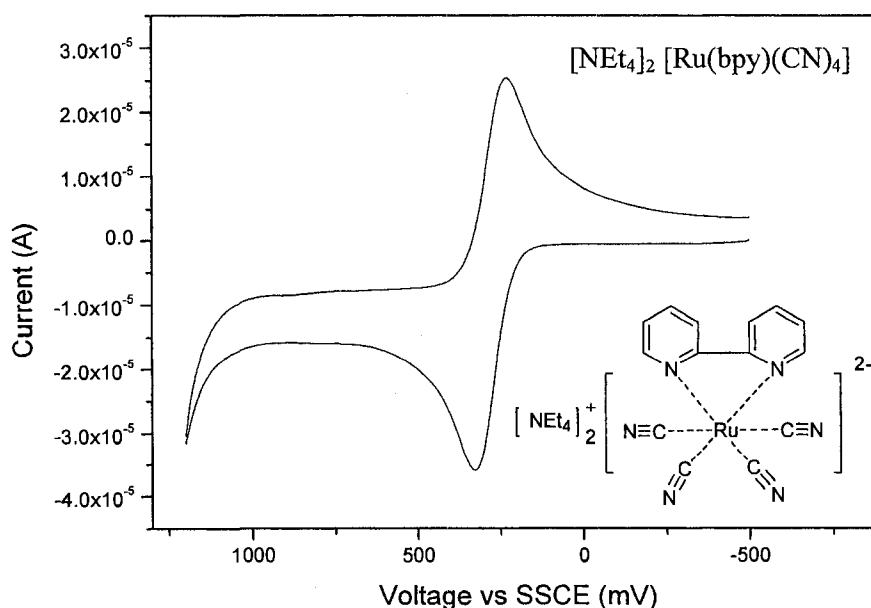


**Figure 2.27.** CV of  $[NEt_4]_2 [Ru(bpy)(CN)_4]$  in 100 mM TMAPF<sub>6</sub>/ACN. W.E., ITO (0.5 cm<sup>2</sup>); R.E., SSCE; C.E., Pt; S.R. = 100 mV/sec.

## **Catalytic Oxidation of $[\text{Co}(\text{DTB})_3]^{2+}$ on the $[\text{Fe}(\text{DCB})_3]^{2+}$ Modified ITO Array Electrode**

### 1) Functionalization of ITO array electrode with (3-aminopropyl)trimethoxysilane

The ITO array electrode consisting of 7 x 4 ITO spots (3 mm diameter) was vigorously cleaned by sonication in an Alconox/water solution (approximately 30 g/L) for 15 min, rinsed with water and iso-propanol, sonicated in iso-propanol for 15 min, rinsed again with iso-propanol and water, followed by sonication twice in water, and dried at 115°C. Finally, the surfaces were cleaned in air plasma for 35 minutes using a Harrick PDC3XG plasma cleaner.

The freshly cleaned ITO array was immediately soaked in 2M NaOH aqueous solution of 24 hours, rinsed with 18 MΩ water, sonicated in 18 MΩ water for 15 minutes, dried at 115°C for 4 hours. The dried ITO array electrode was refluxed under nitrogen in 10 ml (3-aminopropyl)trimethoxysilane / 100 ml toluene overnight. The array was rinsed under nitrogen with toluene, iso-propanol and 18 MΩ water, cured at 115°C for 4 hours. As the zoom-in view of the gray spot schematically shown in Figure 2.6, at this point, all the ITO spots were functionalized with terminal amine groups through the silane chemistry.

### 2) Modification of the functionalized ITO array electrode with $[\text{Fe}(\text{DCB})_3]^{2+}$

50 μl of the solution containing  $[\text{Fe}(\text{DCB})_3](\text{ClO}_4)_2$  (22.5 μM) and the coupling agent (EDC 60 mM and NHS 15 mM) in MES buffer (pH=6.0, 0.1M MES with 0.25 M NaCl) was carefully applied to alternate functionalized ITO spots. And the array was allowed to incubate in 75% humidity at room temperature for 21 hours. The electrode was rinsed with water and dried in the air. As shown in Figure 2.28, half of the ITO spots

(gray circles with square pattern) were treated with the  $[\text{Fe}(\text{DCB})_3](\text{ClO}_4)_2$  solution. Through EDC/NHS coupling, the complex  $[\text{Fe}(\text{DCB})_3]^{2+}$  was chemically attached to the ITO surface.

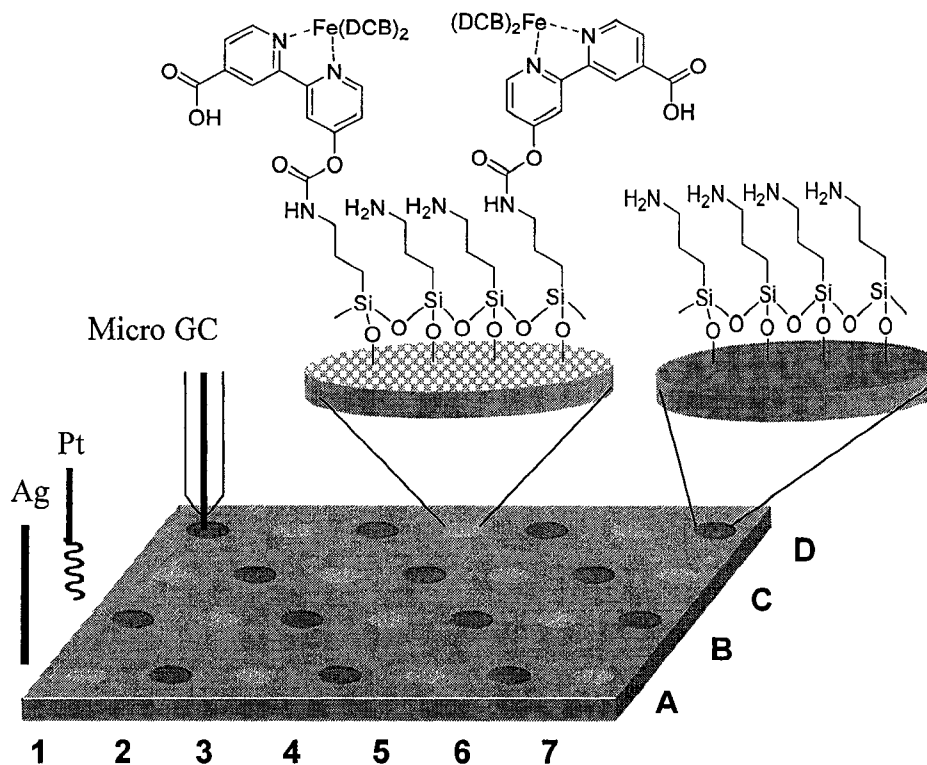


**Figure 2.28.** Schematic illustration of surface functionalization of ITO array electrode and the electrochemical cell configuration.

### 3) Electrochemical Catalysis of $[\text{Co}(\text{DTB})_3]^{2+}$ Oxidation

A three-electrode configuration (see Figure 2.28) was used for the electrochemical experiments. The electrochemical cell is a glass Petri dish. The counter electrode was a platinum coil and a silver wire was used as the quasi-reference electrode. The solution of 0.1 M TMAPF<sub>6</sub> in acetonitrile was employed as supporting electrolyte. The electrolyte solution also contained the redox-inert mediator,  $[\text{Co}(\text{DTB})_3](\text{ClO}_4)_2$  (0.1 mM). A micro GC electrode (100  $\mu\text{m}$ ) was pushed onto the ITO spot to make electrical contact between the ITO and the potentiostat. A DPV was obtained for each ITO spot by scanning the GC

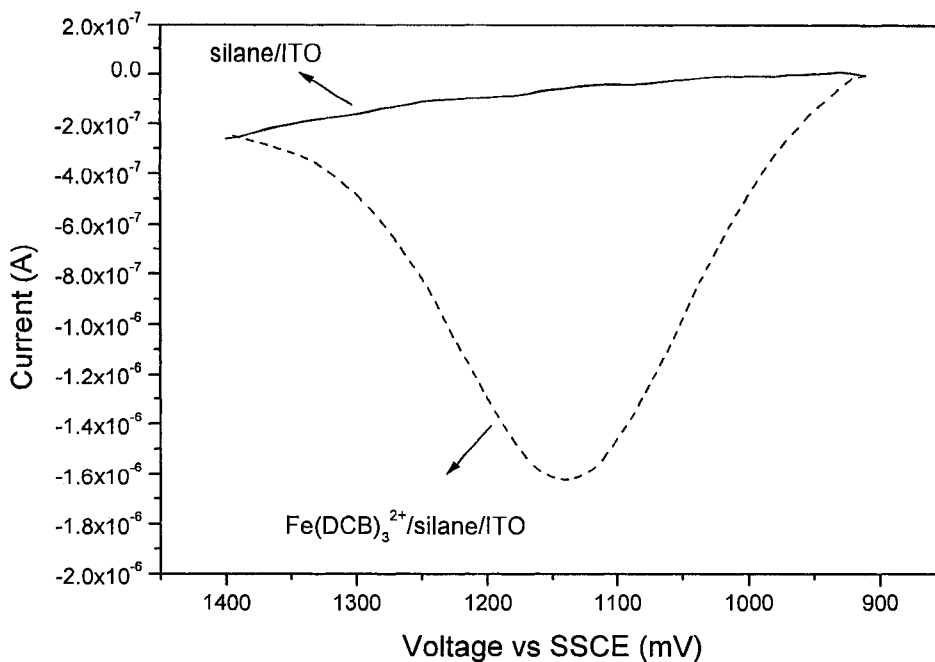
electrode from spot to spot (S.R. = 50 mV/sec; Sample Width = 17 msec; Pulse Amplitude = 50 mV; Pulse Width = 100 msec; Pulse Period = 200 msec).

## RESULTS AND DISCUSSION

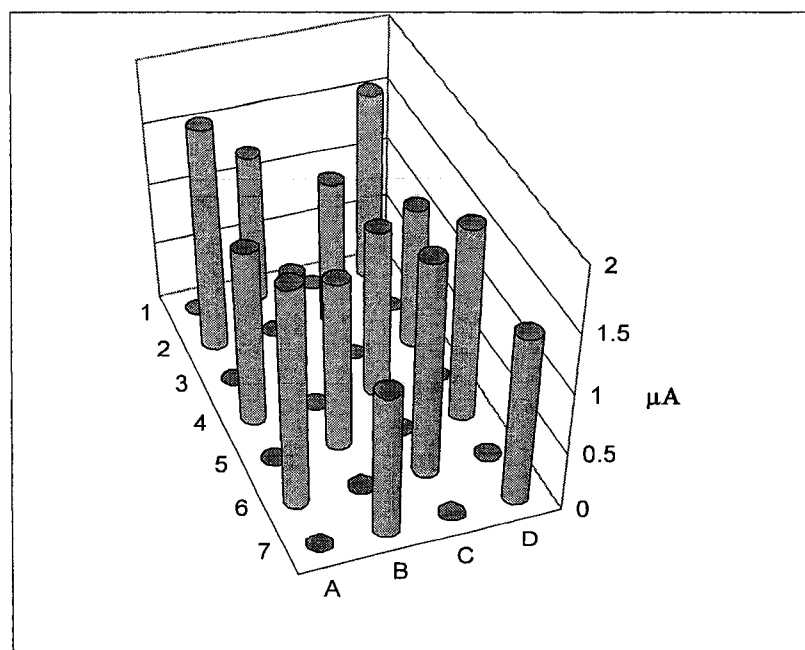
### Catalytic Oxidation of $[\text{Co}(\text{DTB})_3]^{2+}$ on the $[\text{Fe}(\text{DCB})_3]^{2+}$ Modified ITO Array Electrode

Figure 2.29A shows typical, representative DPVs of an ITO spot modified with silane and that was subsequently modified with  $[\text{Fe}(\text{DCB})_3]^{2+}$ . The DPV oxidation peak current was plotted versus the ITO spot position and a 3D graph is shown in Figure 2.29B. Each ITO spot modified with  $[\text{Fe}(\text{DCB})_3]^{2+}$  produces a significant oxidation current; the average current for all the  $[\text{Fe}(\text{DCB})_3]^{2+}$  modified ITO spots was 1.43  $\mu\text{A}$  with a standard deviation 0.28  $\mu\text{A}$ . On the other hand, no evident peak current was detected on the rest of the ITO spots, which were not modified with the complex  $[\text{Fe}(\text{DCB})_3]^{2+}$ .

It can be seen that catalytic oxidation of the mediator molecule,  $[\text{Co}(\text{DTB})_3](\text{ClO}_4)_2$ , provides a sensitive and parallel method to probe the ITO electrode surface composition. An electrochemical signal, the current, is detected if the ITO surface is modified with a redox active catalyst, such as  $[\text{Fe}(\text{DCB})_3]^{2+}$ ; while no signal is detected on the ITO surface free of the redox active catalyst. It is also revealed that functionalization of the ITO surface with an organic monolayer provides a stable platform for redox catalyst attachment.



**Figure 2.29 A.** Representative DPVs of an ITO spot modified with silane and that was subsequently modified with  $[\text{Fe}(\text{DCB})_3]^{2+}$ . Measurements were taken in 0.1 mM  $[\text{Co}(\text{DTB})_3](\text{ClO}_4)_2$ . S.R. = 50 mV/sec; Sample Width = 17 msec; Pulse Amplitude = 50 mV; Pulse Width = 100 msec; Pulse Period = 200 msec).



**Figure 2.29 B.** DPV peak current vs. ITO spot position. Alternate ITO spots A2, A4, A6, B1, B3, B5, B7, C2, C4, C6, D1, D3, D5, D7 were modified with  $[\text{Fe}(\text{DCB})_3]^{2+}$ .

## Electrochemical Properties of the Co(II) Complexes

As discussed earlier, a wide variety of Co(II) complexes were prepared and studied as possible redox mediators for electrochemical DNA detection, with CVs on ITO and GC shown in Figure 2.7 to 2.13. Electrochemical properties of these complexes are summarized in Table 2.1. Effects of the electrochemical experimental conditions (i.e., working electrodes, electrolytes) and the chemical compositions of these Co(II) complexes (i.e., coordinating-ligands and charge compensating counterions) were discussed.

Table 2.1: Electrochemical properties of the Co (II) complexes (scan rate: 100 mV/s; R.E. SSCE; C.E. Pt.; ACN acetonitrile)

Complex	Co(DTB) <sub>3</sub> <sup>2+</sup>			Co(TTT) <sub>2</sub> <sup>2+</sup>			
	ClO <sub>4</sub> <sup>-</sup>	PF <sub>6</sub> <sup>-</sup>	Cl <sup>-</sup>	ClO <sub>4</sub> <sup>-</sup>	PF <sub>6</sub> <sup>-</sup>	Cl <sup>-</sup>	SO <sub>4</sub> <sup>2-</sup>
Electrolyte	TMAPF <sub>6</sub> /ACN	TBAPF <sub>6</sub> /ACN	NaCl /H <sub>2</sub> O	TMAPF <sub>6</sub> /ACN	TBAPF <sub>6</sub> /ACN	NaCl /H <sub>2</sub> O	Na <sub>2</sub> SO <sub>4</sub> /H <sub>2</sub> O
E <sub>1/2, GC</sub>	153	153	-67	94	133	/	-147
ΔE <sub>p, GC</sub>	118	141	129	66	91	/	79
E <sub>1/2, ITO</sub>	/	/	/	104	/	/	-107
ΔE <sub>p, ITO</sub>	/	/	/	606	/	/	648

### 1) Effects of working electrodes

From Figure 2.8 - 2.14, it can be seen that all the seven Co(II) complexes exhibit heterogeneous electron-transfer properties that are electrode surface dependent. At the scan rate of 100 mV/s, except for Co(TTT)<sub>2</sub>Cl<sub>2</sub> that is redox irreversible in the NaCl aqueous solution, all of the remaining cobalt complex are quasi-reversible on the GC electrode; all of them however, exhibit sluggish electron transfer on the ITO electrode. Compounds of

particular interest are  $[\text{Co}(\text{DTB})_3](\text{ClO}_4)_2$  and  $[\text{Co}(\text{DTB})_3](\text{PF}_6)_2$ . These two complexes were essentially redox inert on the ITO electrode although they produced normal quasi-reversible CVs on the GC electrode. Therefore, little or no noise due to Co(II) oxidation will be produced if either of them is used as the redox mediator for the ITO-based biosensors.

## 2) Electrolyte effect

Figure 2.30 shows the CVs of 1mM  $[\text{Co}(\text{DTB})_3](\text{ClO}_4)_2$  on the ITO electrode. The dashed curve is the CV obtained in the acetonitrile solution of TBAPF<sub>6</sub>. At the scan rate of 100 mV/s, it exhibits a very broad oxidation peak and a relatively sharp reduction peak, implying a slow electron transfer rate from the Co(II) center to the ITO surface but a relatively faster rate from the Co(III) center to the ITO surface. However, the redox activity of  $[\text{Co}(\text{DTB})_3](\text{ClO}_4)_2$  on ITO was reduced when TMAPF<sub>6</sub> was used as the supporting electrolyte. The solid curve shows the CV obtained in the solution of TMAPF<sub>6</sub>/acetonitrile. Apparently, the choice of the electrolyte played a big role here. Both its oxidation and the reduction current were significantly suppressed.

To explain this electrolyte effect, a more systematic study were carried out utilizing  $\text{Li}^+ \text{ClO}_4^-$ ,  $\text{TMA}^+ \text{ClO}_4^-$ ,  $\text{TEA}^+ \text{ClO}_4^-$  and  $\text{TBA}^+ \text{ClO}_4^-$  as the electrolytes. The obtained CVs of 1 mM  $[\text{Co}(\text{DTB})_3](\text{ClO}_4)_2$  on ITO are shown in Figure 2.31. It can be seen that the magnitude of the redox current increases as the electrolyte changes according to the sequence  $\text{Li}^+ \text{ClO}_4^- < \text{TMA}^+ \text{ClO}_4^- < \text{TEA}^+ \text{ClO}_4^- < \text{TBA}^+ \text{ClO}_4^-$ . Since all the electrolytes have the same anion  $\text{ClO}_4^-$ , the current variation must be induced by the cation change. There are two possible explanations, either the small-sized cation “turns off” the current by strongly absorbing onto the electrode surface<sup>3</sup> and driving off the positively charged

$\text{Co}(\text{DTB})_3^{2+}$  via electrostatic repulsion, or the large-size and greasy cation “turns on” the current by attracting the  $\text{Co}(\text{DTB})_3^{2+}$  molecules onto the electrode surface via hydrophobic interaction with the greasy ligands of the complex.

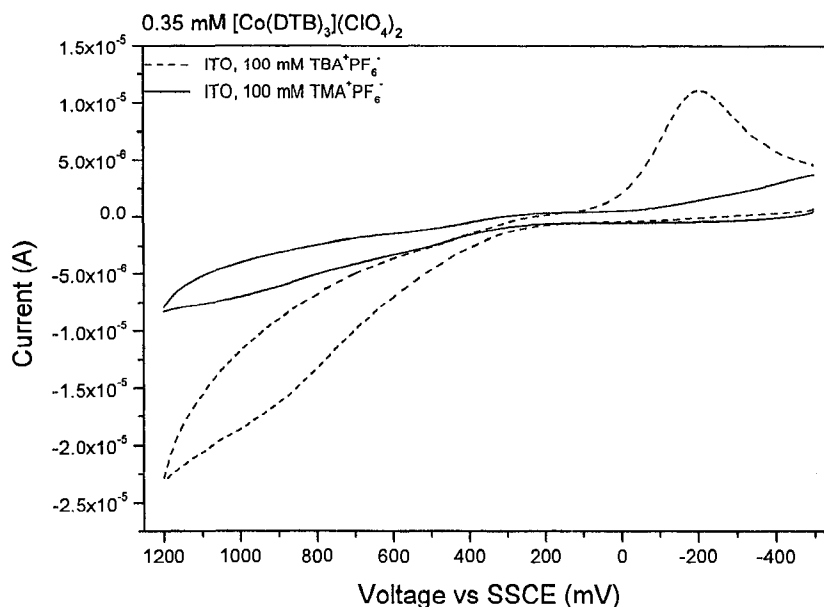


**Figure 2.30.** CVs of 1mM  $[\text{Co}(\text{DTB})_3](\text{ClO}_4)_2$  in different electrolyte solutions. W.E., ITO ( $0.5 \text{ cm}^2$ ); R.E., SSCE; C.E., Pt; 100 mV/s.

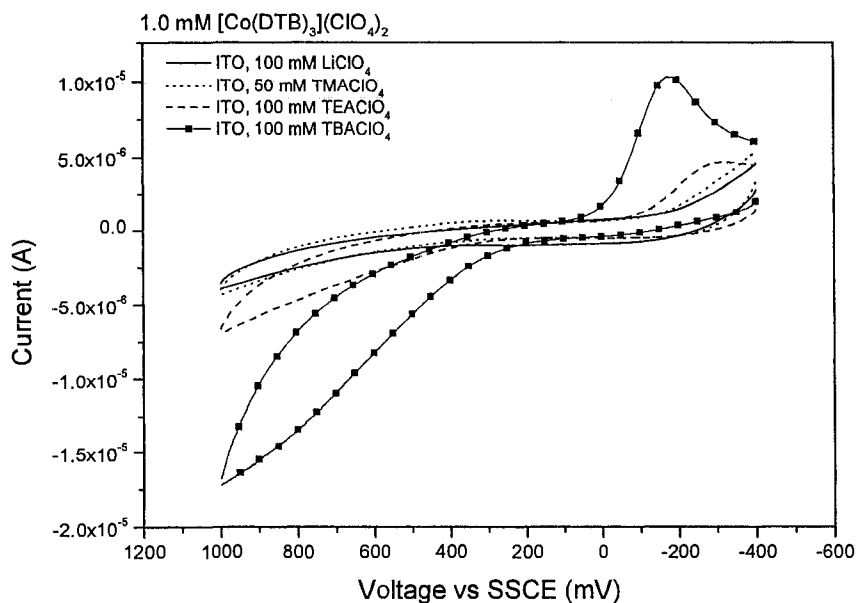


**Figure 2.31.** CVs of  $[\text{Co}(\text{DTB})_3](\text{ClO}_4)_2$  (1 mM) in different electrolyte solutions. W.E., ITO ( $0.5 \text{ cm}^2$ ); R.E., SSCE; C.E., Pt; 100 mV/s.

To have a better understanding, the following control experiments were done and the results were shown in Figure 2.32. First, a CV (black curve) of 1 mM  $[\text{Co}(\text{DTB})_3](\text{ClO}_4)_2$  on ITO was obtained in an acetonitrile solution containing 100 mM  $\text{LiClO}_4$ . Then, solid  $\text{TBAClO}_4$  was added with stirring into the electrolyte solution till its concentration reached 100 mM. A second CV (red curve) was subsequently obtained on the same ITO electrode. After that, the ITO electrode was taken out of solution, rinsed thoroughly with acetonitrile and was used to obtain a third CV (green curve) in a separate acetonitrile solution containing 1 mM  $[\text{Co}(\text{DTB})_3](\text{ClO}_4)_2$  and 100 mM  $\text{TBAClO}_4$ . Similarly, solid  $\text{LiClO}_4$  was then added into this new solution till its concentration reached 100 mM and was stirred, and a fourth CV (blue curve) was obtained.

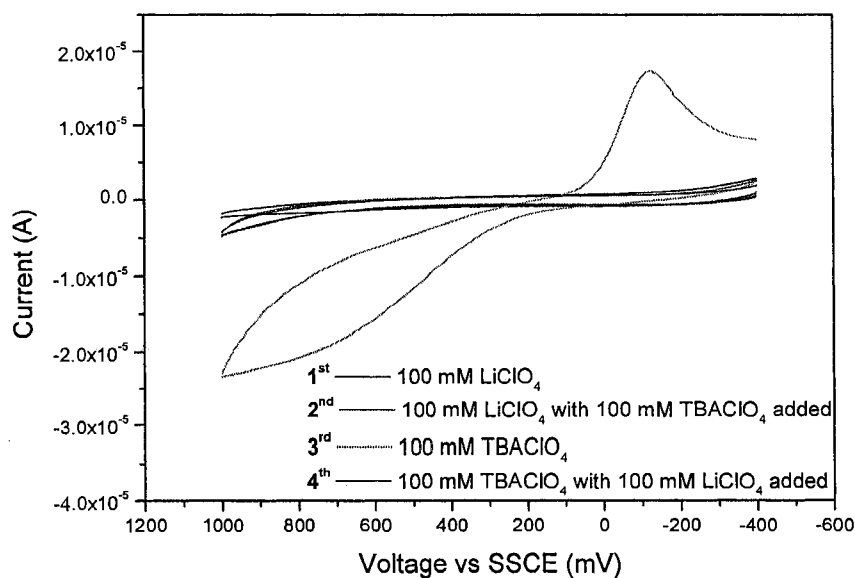


**Figure 2.32.** CVs of  $[\text{Co}(\text{DTB})_3](\text{ClO}_4)_2$  (1 mM) in different electrolyte solutions. W.E., ITO ( $0.5 \text{ cm}^2$ ); R.E., SSCE; C.E., Pt; 100 mV/s.

As it can be seen from Figure 2.32, the current magnitude of the CV obtained in the solution containing 100 mM  $\text{TBAClO}_4$  (the 4<sup>th</sup> CV) is much higher than that obtained in

100 mM LiClO<sub>4</sub> solution (the 1<sup>st</sup> CV), which is consistent with previous result. The meaningful discovery here, is that addition of solid LiClO<sub>4</sub> into the TBAClO<sub>4</sub> solution gave rise to a significant current decrease (compare the 4<sup>th</sup> and the 3<sup>rd</sup> CV); but addition of solid TBAClO<sub>4</sub> into the LiClO<sub>4</sub> solution produced only a small degree of current increase (compare the 2<sup>nd</sup> and the 1<sup>st</sup> CV). Thus, it can be concluded that the deactivation effect of Li<sup>+</sup> overpowered the activation effect of TBA<sup>+</sup>. However, the Li<sup>+</sup> effect was not permanent. Once the LiClO<sub>4</sub>-treated ITO surface was cleaned by rinsing with solvent, the redox chemistry of [Co(DTB)<sub>3</sub>](ClO<sub>4</sub>)<sub>2</sub> “returned” in the electrolyte of 100 mM TBAClO<sub>4</sub> (compare the 3<sup>rd</sup> and the 2<sup>nd</sup> CV).

In summary, electrolytes containing small cations, such as LiClO<sub>4</sub> and TMAPF<sub>6</sub>, are desired for sensitive DNA detection due to the fact that, in these electrolyte solutions, the redox mediator [Co(DTB)<sub>3</sub>](ClO<sub>4</sub>)<sub>2</sub> is essentially redox inert on the bare ITO electrode.

### 3) Effect of coordinating ligand

Figure 2.33 shows the CV of 1.0 mM [Co(TTT)<sub>2</sub>](ClO<sub>4</sub>)<sub>2</sub> (solid curve) and that of 1.0 mM [Co(DTB)<sub>3</sub>](ClO<sub>4</sub>)<sub>2</sub> (dashed curve) on ITO obtained in the acetonitrile solution of 100 mM TMAPF<sub>6</sub>. It can be observed that at the scan rate 100 mV/s, the complex Co(TTT)<sub>2</sub><sup>2+</sup> displayed evident oxidation and reduction processes on the ITO electrode, despite that its CV had a huge peak separation 606 mV; on the other hand, Co(DTB)<sub>3</sub><sup>2+</sup> showed little if any, redox activity at all. This suggests that the heterogeneous electron transfer rate of [Co(TTT)<sub>2</sub>]<sup>2+</sup> on the ITO surface is relatively faster than that of [Co(DTB)<sub>3</sub>]<sup>2+</sup>. According to the well accepted Marcus-Hush theory, this difference means that either [Co(TTT)<sub>2</sub>]<sup>2+/3+</sup> has a better electronic coupling with the electrode

surface or  $[\text{Co}(\text{DTB})_3]^{2+/3+}$  has a higher intrinsic Frank-Condon factor which is a measure of the nuclear motion involved in the electron transfer process.

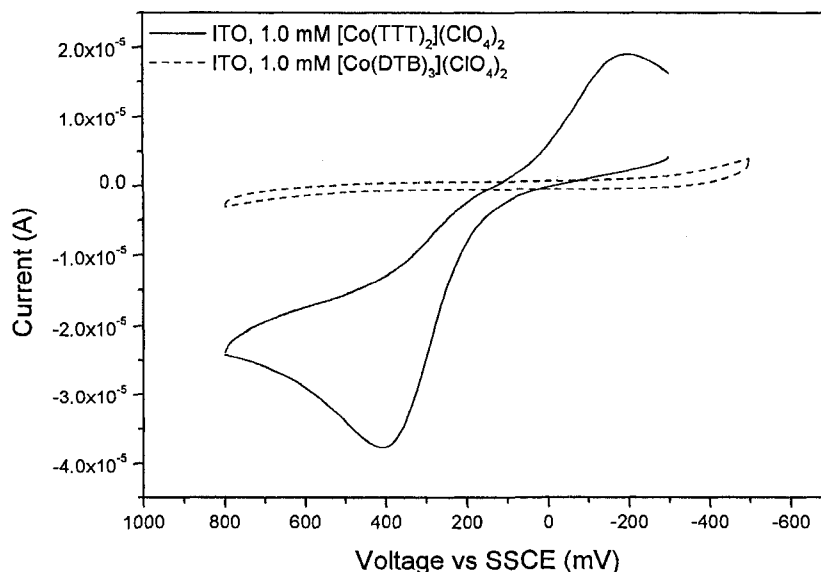


**Figure 2.33.** CVs of 1 mM  $[\text{Co}(\text{TTT})_2](\text{ClO}_4)_2$  and 1 mM  $[\text{Co}(\text{DTB})_3](\text{ClO}_4)_2$  in 100 mM TMAPF<sub>6</sub>/ACN electrolyte solutions. W.E., ITO (0.5 cm<sup>2</sup>); R.E., SSCE; C.E., Pt; 100 mV/s.

#### 4) Counterion effect

The neutralizing counterions can also influence the redox properties of the positively charge cobalt complexes. Figure 2.34 shows the CVs of 1 mM  $[\text{Co}(\text{DTB})_3](\text{ClO}_4)_2$  (dotted curve) and 1 mM  $[\text{Co}(\text{DTB})_3](\text{PF}_6)_2$  (dashed curve) in 100 mM TMAPF<sub>6</sub>/acetonitrile along with a background CV (solid curve) on the ITO electrode. For potentials from 350 mV to -300 mV,  $[\text{Co}(\text{DTB})_3](\text{ClO}_4)_2$  is essentially kinetically inert on the bare ITO surface; while  $[\text{Co}(\text{DTB})_3](\text{PF}_6)_2$  exhibits redox inactivity within a even broader potential range from -300 mV to 800 mV.

Similar counterion effect is also observed for the complex  $[\text{Co}(\text{TTT})_2]^{2+}$ . As shown in Figure 2.35, the CV of 1 mM  $[\text{Co}(\text{TTT})_2](\text{ClO}_4)_2$  (dotted line) shows obvious oxidation and reduction peaks with a peak separation of 606 mV; however, the complex

$[\text{Co}(\text{TTT})_2](\text{PF}_6)_2$  is kinetically inert to oxidation for potentials higher than 50 mV. At this point, there isn't a clear explanation for this counterion effect. But this might be relevant to the association strength of the counterions to the cationic cobalt complexes or to the electrode surface.

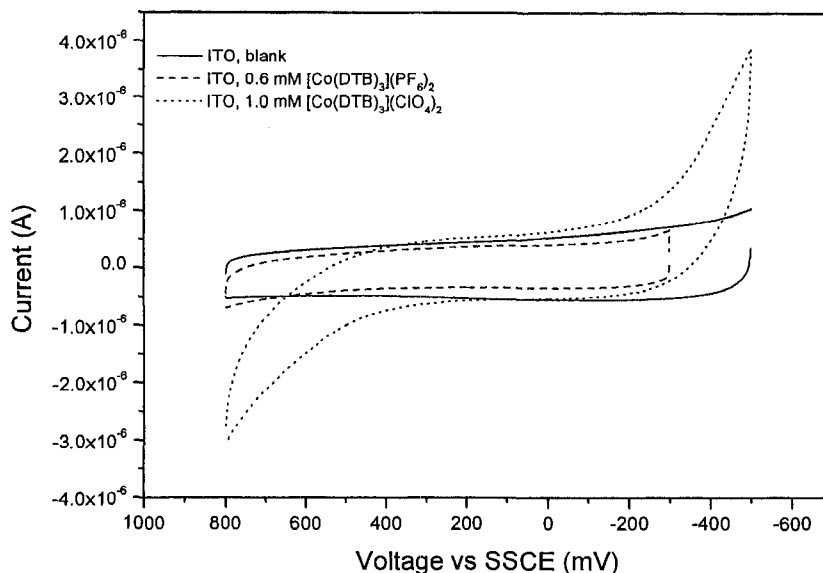


**Figure 2.34.** CVs of 1 mM  $[\text{Co}(\text{DTB})_3](\text{ClO}_4)_2$  and 1 mM  $[\text{Co}(\text{DTB})_3](\text{PF}_6)_2$  in 100 mM TMAPF<sub>6</sub>/ACN electrolyte solutions. W.E., ITO (0.5 cm<sup>2</sup>); R.E., SSCE; C.E., Pt; 100 mV/s.

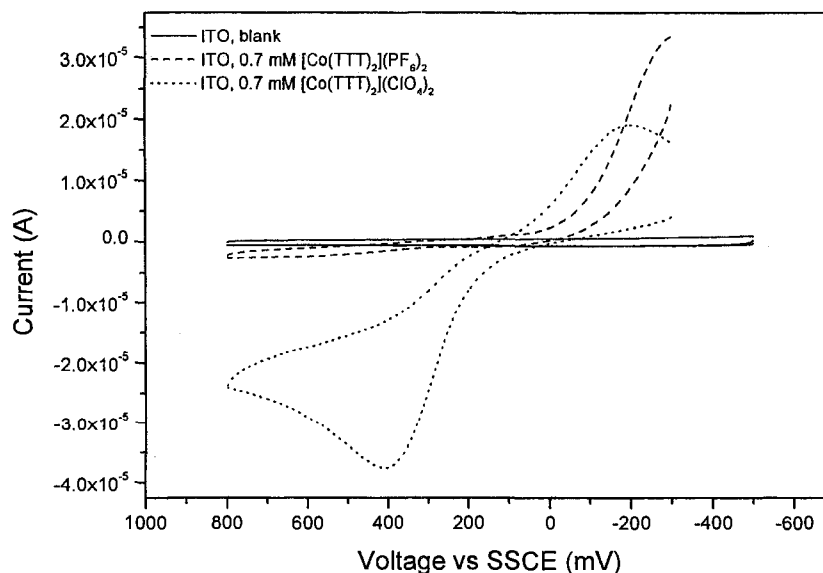


**Figure 2.35.** CVs of 1 mM  $[\text{Co}(\text{TTT})_2](\text{ClO}_4)_2$  and 1 mM  $[\text{Co}(\text{TTT})_2](\text{PF}_6)_2$  in 100 mM TMAPF<sub>6</sub>/ACN electrolyte solutions. W.E., ITO (0.5 cm<sup>2</sup>); R.E., SSCE; C.E., Pt; 100 mV/s.

## 5) Summary

Seven cobalt complexes of substituted polypyridine ligands were carefully examined as possible signal amplifying mediators for electrochemical DNA hybridization sensing. As suggested by electrochemical results, the redox chemistry of the cobalt complexes can be tuned as a function of their molecular structures as well as the electrochemical experimental conditions. Screening assessment was conducted by which qualified mediators exhibited little or no redox activity on the bare ITO electrodes. The electrochemical results led to the discovery that electrolytes of small cation outperform those of large cation. Furthermore,  $[\text{Co}(\text{DTB})_3](\text{ClO}_4)_2$  and  $[\text{Co}(\text{DTB})_3](\text{PF}_6)_2$  were found to be essentially redox inert in a reasonable potential range on the bare ITO electrode in the electrolyte solution of TMAPF<sub>6</sub>/acetonitrile.

### **Catalytic Oxidation of $\text{Co}(\text{DTB})_3^{2+}$ Mediators**

Compounds listed in Table 2.2 (vide infra) are all redox active on the ITO electrode, which is a necessary attribute for a reporter molecule to sense and amplify the DNA hybridization signal via catalytic oxidation of  $\text{Co}(\text{DTB})_3^{2+}$  on ITO. Besides, all the compounds were designed to have zero or negative electrostatic charge to minimize non-specific interaction with the negatively charged DNA backbone and hence prevent false-positive signal.

However, the redox potential of methylene blue (-0.41 V) is found to be too negative for catalyzing the oxidation of  $\text{Co}(\text{DTB})_3^{2+}$ ; and the redox potential of triphenylamine (0.93 V) is too positive to avoid DNA damage. The redox potentials of the rest of the compounds listed in Table 2.2 (ranging from 180 mV to 640 mV vs SSCE) were

considered proper for catalytic oxidation of  $\text{Co}(\text{DTB})_3^{2+}$  via an EC' mechanism. The following report details their catalytic performance.

**Table 2.2.** Electrochemical properties of the catalysts. W.E., ITO (0.5  $\text{cm}^2$ ); R.E., SSCE; C.E., Pt; electrolyte, 100 mM  $\text{TMA}^+\text{PF}_6^-/\text{ACNE}$ ; \* electrolyte: 100 mM NaCl in water; scan rate: 100 mV/s.

Catalyst	$E_{1/2}$ vs SSCE (V)	$\Delta E_p$ (mV)
$\text{Fe}(\text{DMB})_2(\text{CN})_2$	0.34	75
$\text{KFe}(\text{terpy})(\text{CN})_3$	0.25	62
$\text{KFe}(\text{terpy})(\text{CN})_3^*$	0.46	247
$[\text{NEt}_4]_2[\text{Ru}(\text{bipy})(\text{CN})_4]$	0.28	86
LBS@	0.62	66
Quinizarin	/	/
Thioridazine	0.64	96
Phenothiazine	0.58	190
TPA@	0.19 (1 <sup>st</sup> redox)	520 (1 <sup>st</sup> redox)
	0.71 (2 <sup>nd</sup> redox)	195 (2 <sup>nd</sup> redox)
Methylene Blue	-0.41	297
Ferrocene	0.56	907
triphenylamine	0.93	84
$\text{Fe}(\text{BPB})_2(\text{CN})_2$	0.44	73
$\text{KFe}(\text{TPT})(\text{CN})_3$	0.24	69
$\text{Ru}(\text{MPB})_2(\text{Cl})_2$	0.18	69
$\text{Ru}(\text{BPB})_2\text{Cl}_2$	0.32	59
$\text{Ru}(\text{46PTZ})_2\text{Cl}_2^{\#}$	0.18	70
$\text{Ru}(\text{44POZ})_2\text{Cl}_2^{\#}$	0.60	82

@: LBS stands for lithium 4-(10H-phenothiazin-10-yl)butane-1-sulfonate; TPA stands for N,N,N',N'-tetramethyl-p-phenylenediamine; 46PTZ stands for 4-methyl-4'-(4-(N-phenothiazinato)hexyl)-2,2'-bipyridine; 44POZ stands for 4-methyl-4'-(4-(N-phenoxazinato)butyl)-2,2'-bipyridine.

#:  $\text{Ru}(\text{46PTZ})_2\text{Cl}_2$  was prepared according to Reference 25;  $\text{Ru}(\text{44POZ})_2\text{Cl}_2$  was prepared according to Reference

### 1) Catalytic oxidation of $[\text{Co}(\text{DBT})_3](\text{ClO}_4)_2$ by $(\text{NEt}_4)_2[\text{Ru}(\text{bipy})(\text{CN})_4]$

As shown in Figure 2.27,  $(\text{NEt}_4)_2[\text{Ru}(\text{bipy})(\text{CN})_4]$  displayed a quasi-reversible CV on ITO with an  $\text{Ru}^{3+/2+}$   $E_{1/2}$  at 280 mV vs SSCE, which is higher than the  $E_{1/2}$  of  $[\text{Co}(\text{DBT})_3](\text{ClO}_4)_2$  on GC (155 mV vs SSCE). From the perspective of thermodynamic

energy,  $[\text{Ru}^{\text{III}}(\text{bipy})(\text{CN})_4]^+$  should possess enough driving force to oxidize  $[\text{Co}^{\text{II}}(\text{DBT})_3]^{2+}$ , and be simultaneously reduced to  $[\text{Ru}^{\text{II}}(\text{bipy})(\text{CN})_4]^{2+}$  which will enter the next EC' cycle. In other words, addition of  $[\text{Co}(\text{DBT})_3](\text{ClO}_4)_2$  to the solution containing  $(\text{NEt}_4)_2[\text{Ru}(\text{bipy})(\text{CN})_4]$  is assumed to produce a current amplification around the  $\text{Ru}^{2+}$  oxidation peak.

Figure 2.36 shows the DPVs of  $(\text{NEt}_4)_2[\text{Ru}(\text{bipy})(\text{CN})_4]$  in the absence (solid curve) or presence of  $[\text{Co}(\text{DBT})_3](\text{ClO}_4)_2$  (dashed curve) on the same ITO electrode. Unfortunately, addition of  $[\text{Co}(\text{DBT})_3](\text{ClO}_4)_2$  produced a current decrease instead of an increase. Meanwhile, the solution turned orange from yellow. The negative amplification effect and the solution color change be explained by the formation of  $[\text{Co}(\text{DBT})_3][\text{Ru}(\text{bipy})(\text{CN})_4]$ . Because both the cationic  $[\text{Co}(\text{DBT})_3]^{2+}$  and anionic  $[\text{Ru}(\text{bipy})(\text{CN})_4]^{2-}$  are big in size, they might associate to form the neutral compound  $[\text{Co}(\text{DBT})_3][\text{Ru}(\text{bipy})(\text{CN})_4]$ , and this new compound could happen to be redox inert on the ITO electrode.

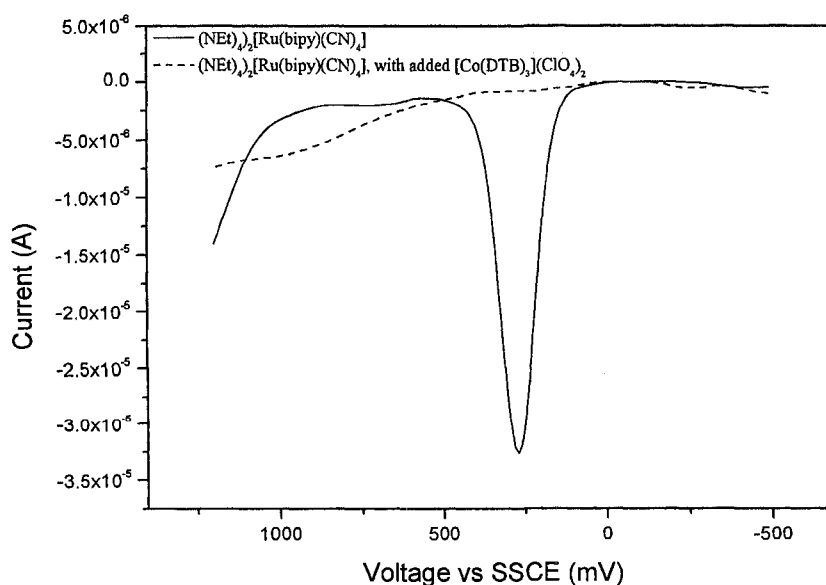


**Figure 2.36.** DPVs of  $(\text{NEt}_4)_2[\text{Ru}(\text{bipy})(\text{CN})_4]$  and  $[\text{Co}(\text{DTB})_3](\text{ClO}_4)_2$  in 100 mM TMAPF<sub>6</sub>/ACN electrolyte solutions. W.E., ITO (0.5 cm<sup>2</sup>); R.E., SSCE; C.E., Pt; 100 mV/s.

2) Catalytic oxidation of  $[\text{Co}(\text{DBT})_3](\text{ClO}_4)_2$  by 4-(10H-phenothiazin-10-yl)butane-1-sulfonate (LBS)

The results of catalytic oxidation of  $[\text{Co}(\text{DBT})_3](\text{ClO}_4)_2$  by LBS on the ITO electrode are shown in Figure 2.37 and Figure 2.38. As can be observed in Figure 2.37, the DPV peak current increased upon addition of  $[\text{Co}(\text{DBT})_3](\text{ClO}_4)_2$  and kept on increasing with the increase of the  $[\text{Co}(\text{DBT})_3](\text{ClO}_4)_2$  concentration up to 4.7 mM. Further improving the  $[\text{Co}(\text{DBT})_3](\text{ClO}_4)_2$  concentration to 6.7 mM resulted in a decrease of the DPV peak current. The insertion in Figure 2.37 shows the DPV peak current vs the concentration of  $[\text{Co}(\text{DTB})_3](\text{ClO}_4)_2$ . The DPV peak current observed at 4.7 mM  $[\text{Co}(\text{DBT})_3](\text{ClO}_4)_2$  is five times that of the LBS alone.

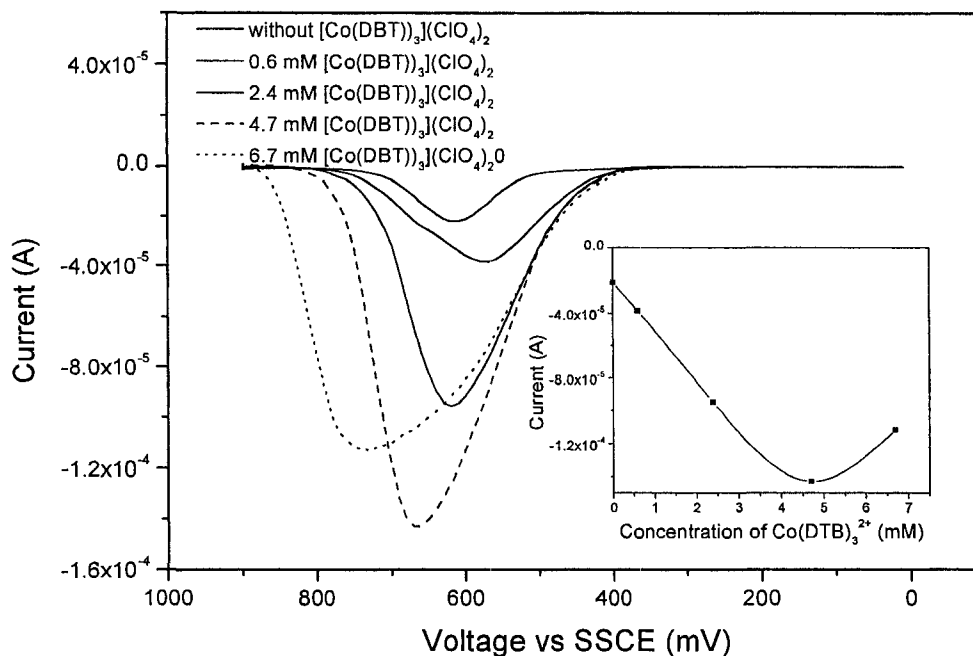


**Figure 2.37.** DPVs of LBS in the presence of different amount of  $[\text{Co}(\text{DTB})_3](\text{ClO}_4)_2$  in 100 mM TMAPF<sub>6</sub>/ACN. W.E., (0.5 cm<sup>2</sup>); R.E., SSCE; C.E., Pt; S.R. = 50 mV/sec; Sample Width = 17 msec; Pulse Amplitude = 50 mV; Pulse Width = 100 msec; Pulse Period = 200 msec. The insertion on the right lower corner shows the DPV peak current vs the concentration of  $[\text{Co}(\text{DTB})_3](\text{ClO}_4)_2$ .

CVs of the solution mixed with 4.7 mM and 6.7 mM  $[\text{Co}(\text{DBT})_3](\text{ClO}_4)_2$  were also taken, and are shown in Figure 2.38. Contrarily, the CV peak current increased upon increasing the  $[\text{Co}(\text{DBT})_3](\text{ClO}_4)_2$  concentration from 4.7 mM to 6.7 mM. Meanwhile, the peak potential positively shifted and the oxidation voltammogram broadened.

Such differences between CV and DPV are a good demonstration of their mathematical relationship. With a series of regular voltage pulses superimposed on the potential linear sweep, the DPV current is measured immediately before each potential change, and the current difference is plotted as a function of potential. Therefore, DPV can be considered approximately as a first-order derivative of CV.<sup>29</sup> From Figure 2.38, it can be seen that at the same potential, the oxidation voltammogram at 4.7 mM exhibits a bigger slope than that at 6.7 mM, i.e., the derivative of the former voltammogram is higher than that of the latter. This mathematically explains the corresponding DPV peak current and voltage change.

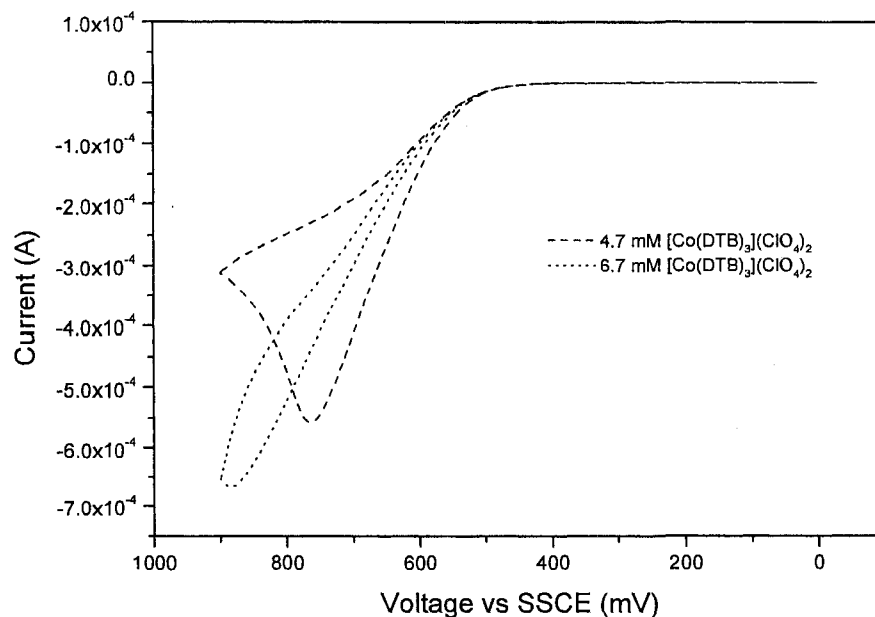


**Figure 2.38.** CVs of LBS with the presence of 4.7 mM and 6.7 mM  $[\text{Co}(\text{DTB})_3](\text{ClO}_4)_2$  in 100 mM TMAPF<sub>6</sub>/ACN electrolyte solutions. W.E., ITO (0.5 cm<sup>2</sup>); R.E., SSCE; C.E., Pt; 100 mV/s.

### 3) Catalytic oxidation of $[\text{Co}(\text{DTB})_3](\text{ClO}_4)_2$ by thioridazine

Figure 2.39 shows the results of catalytic oxidation of  $[\text{Co}(\text{DTB})_3](\text{ClO}_4)_2$  by thioridazine on the ITO electrode. The solid curve is the CV of thioridazine alone in 100 mM TMAPF<sub>6</sub> solution. The insertion on the right lower corner displays its zoom-in view. It has two oxidation peaks, with peak potentials  $E_p^1$  at 680 mV and  $E_p^2$  at 1030 mV. The dashed curve and the dotted curve are the CVs of the thioridazine solution mixed with 0.8 mM and 3.9 mM  $[\text{Co}(\text{DTB})_3](\text{ClO}_4)_2$ , respectively. These electrochemical results demonstrated an evident current amplification effect. With 3.9 mM  $\text{Co}(\text{DTB})_3^{2+}$  added, the peak current observed is 33 times that of the thioridazine alone. Meanwhile, the oxidation peak is shifted to a potential higher than  $E_p^1$  of thioridazine, but matching its  $E_p^2$ , which is unfortunately detrimental to DNA. This means that the first oxidation process of thioridazine wasn't be able to intercept all the Co(II) present in the diffusion layer, and the second oxidation process was required to participate.<sup>30</sup>

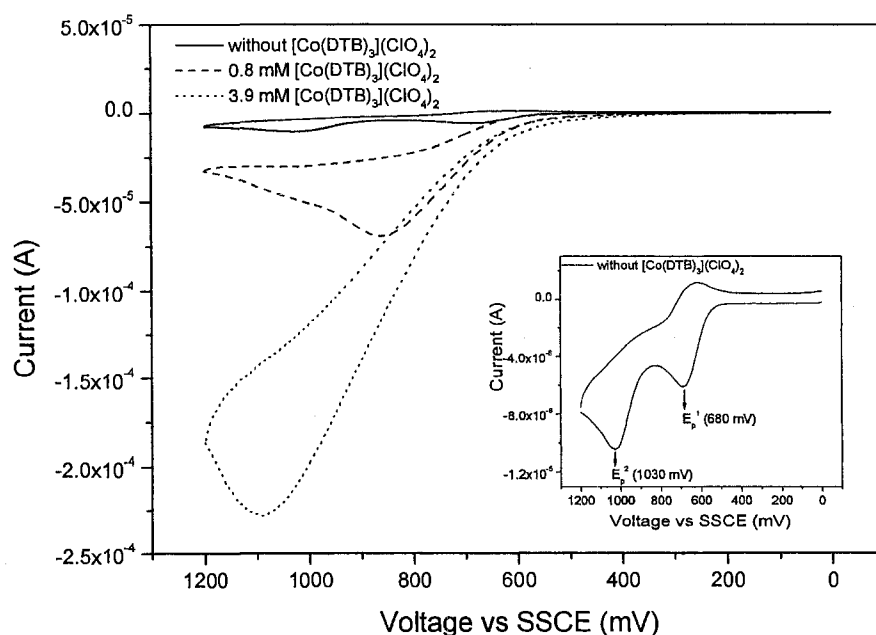


**Figure 2.39.** CVs of thioridazine in the presence of different amount of  $[\text{Co}(\text{DTB})_3](\text{ClO}_4)_2$  in 100 mM TMAPF<sub>6</sub>/ACN. W.E., (0.5 cm<sup>2</sup>); R.E., SSCE; C.E., Pt; S.R. = 100 mV/sec. The insertion on the right lower corner shows the zoom-in view of the CV of thioridazine without  $[\text{Co}(\text{DTB})_3](\text{ClO}_4)_2$ .

#### 4) Catalytic oxidation of $[\text{Co}(\text{DTB})_3](\text{ClO}_4)_2$ by phenothiazine

Figure 2.40 shows the DPVs of phenothiazine in the absence (solid curve) or presence of 0.7 mM  $[\text{Co}(\text{DTB})_3](\text{ClO}_4)_2$  (dashed curve) on the ITO electrode. The current decreased upon addition of  $[\text{Co}(\text{DTB})_3](\text{ClO}_4)_2$ . Like  $(\text{NEt}_4)_2[\text{Ru}(\text{bipy})(\text{CN})_4]$ , unsubstituted phenothiazine is not a good catalyst for oxidation of  $[\text{Co}(\text{DTB})_3]^{2+}$  for similar reasons.

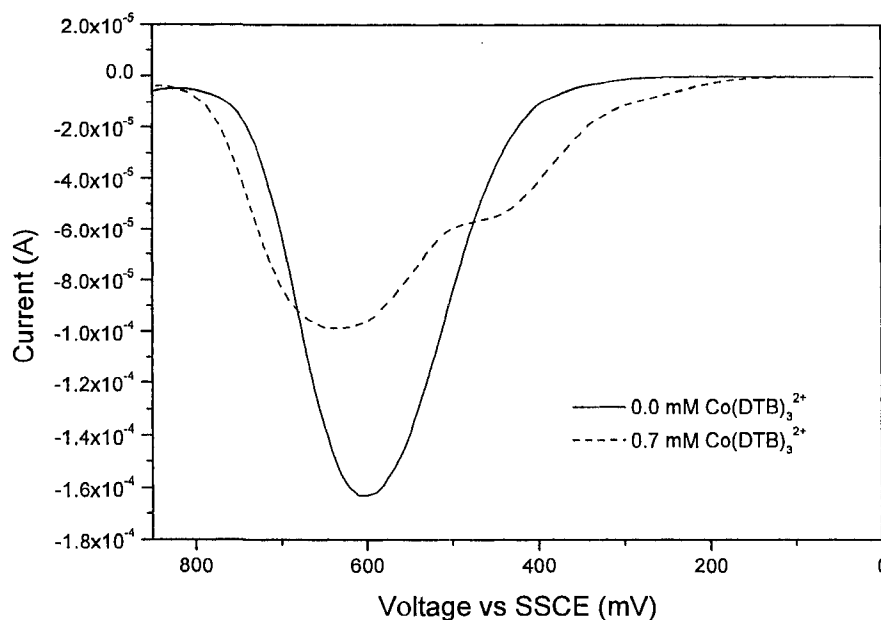


**Figure 2.40.** DPVs of phenothiazine and  $[\text{Co}(\text{DTB})_3](\text{ClO}_4)_2$  in 100 mM TMAPF<sub>6</sub>/ACN electrolyte solutions. W.E., ITO (0.5 cm<sup>2</sup>); R.E., SSCE; C.E., Pt; S.R. = 50 mV/sec; Sample Width = 17 msec; Pulse Amplitude = 50 mV; Pulse Width = 100 msec; Pulse Period = 200 msec.

#### 5) Catalytic oxidation of $[\text{Co}(\text{DTB})_3](\text{ClO}_4)_2$ by N,N,N',N'-tetramethyl-p-phenylene-diamine (TPA)

Figure 2.41 A shows the DPVs obtain on the ITO electrode in solutions containing TPA and various concentrations of  $[\text{Co}(\text{DTB})_3](\text{ClO}_4)_2$  ranging from 0.0 to 16.5 mM. The DPV of TPA alone (solid curve) exhibits two oxidation processes. The first one shows up at 77 mV and the second one at 660 mV, corresponding to oxidation of TPA to TPA<sup>+</sup> and

oxidation of  $\text{TPA}^+$  to  $\text{TPA}^{2+}$ , respectively.<sup>31</sup> Upon addition of  $[\text{Co}(\text{DTB})_3](\text{ClO}_4)_2$ , the first oxidation peak positively shifted without much changing in its current magnitude; meanwhile, the current of the second oxidation process increased and became 8.0 times its original value when the concentration of  $[\text{Co}(\text{DTB})_3](\text{ClO}_4)_2$  reached 16.5 mM.

Figure 2.41 B shows DPVs of  $[\text{Co}(\text{DTB})_3](\text{ClO}_4)_2$  on GC. The peak potential for  $\text{Co}^{2+}$  oxidation is at around 160 mV, which is higher than the first DPV peak potential of TPA on ITO (77 mV). This suggests that  $\text{TPA}^+$  doesn't have enough thermodynamic driving force to oxidize the mediator.

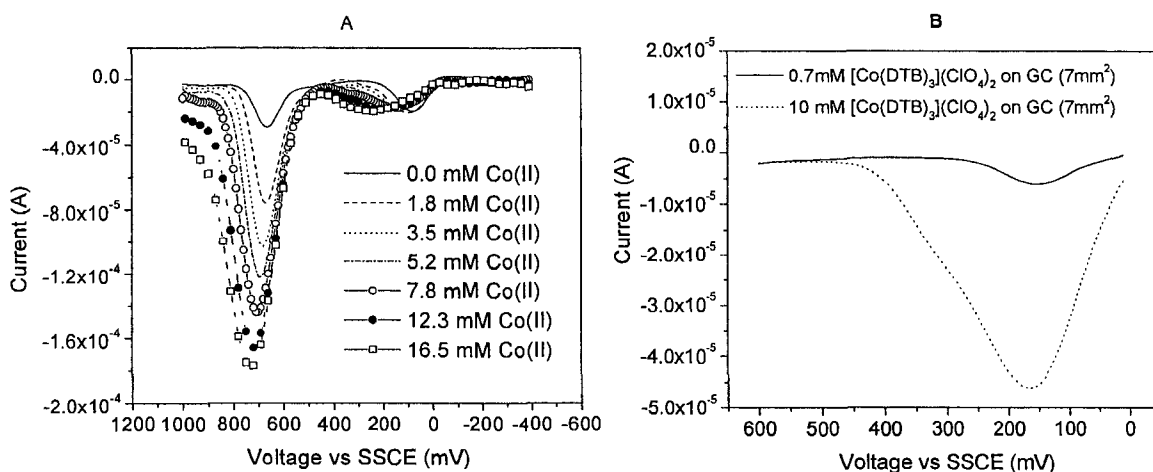


**Figure 2.41.** A) DPVs of TPA and  $[\text{Co}(\text{DTB})_3](\text{ClO}_4)_2$  in 100 mM  $\text{TMAPF}_6/\text{ACN}$  electrolyte solutions. W.E., ITO ( $0.5 \text{ cm}^2$ ); R.E., SSCE; C.E., Pt; S.R. = 50 mV/sec; Sample Width = 17 msec; Pulse Amplitude = 50 mV; Pulse Width = 100 msec; Pulse Period = 200 msec. B) DPVs of  $[\text{Co}(\text{DTB})_3](\text{ClO}_4)_2$  on GC ( $7 \text{ mm}^2$ ). DPV conditions is the same as A).

#### 6) Catalytic oxidation of $[\text{Co}(\text{DTB})_3](\text{ClO}_4)_2$ by quinizarin

Figure 2.42 A shows the CV of quinizarin obtained on the ITO electrode. At this scan rate (100 mV/s), quinizarin displays a broad oxidation peak from 400 to 900 mV and no evident reduction peak, implying extremely slow electron transfer rate between the redox couple and the ITO electrode surface. Basically, catalytic oxidation of  $\text{Co}(\text{II})$  on the ITO electrode involved one electrochemical process and one chemical process.

The electrochemical process is the electrochemical oxidation of the catalyst by the ITO electrode. Once the catalyst is oxidized, the chemical process, oxidation of Co(II) by the oxidized catalyst, can proceed and at the same time, the catalyst was reduced back to its original oxidation state. Both these processes are crucial to the overall catalytic efficiency. The slow electrochemical process displayed by quinizarin is not attractive for catalytic oxidation of Co(II).

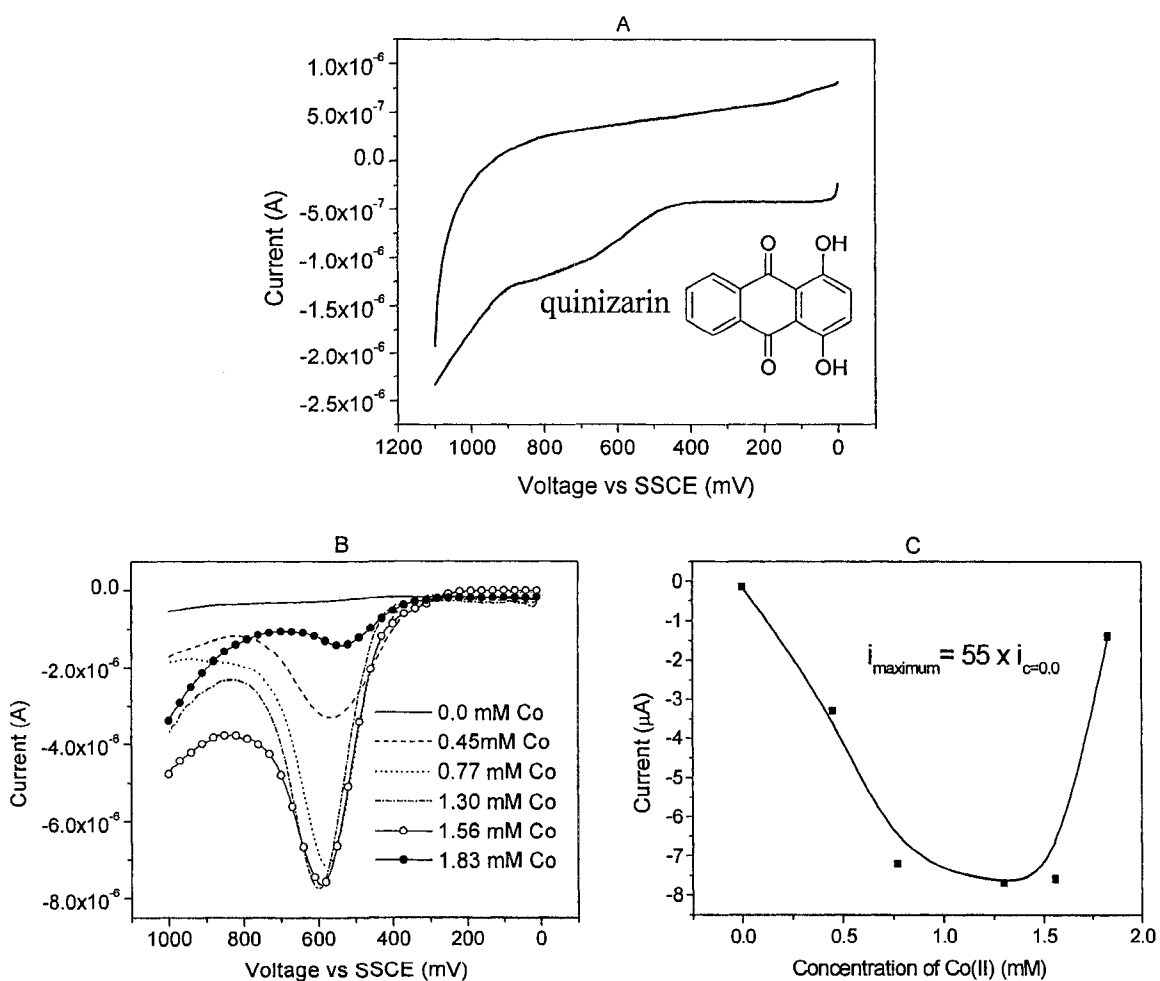


**Figure 2.42.** A) CV of TPA alone in 100 mM TMAPF<sub>6</sub>/ACN electrolyte solutions, W.E., ITO (0.5 cm<sup>2</sup>); R.E., SSCE; C.E., Pt; 100 mV/s. B) DPVs of quinizarin and  $[\text{Co}(\text{DTB})_3](\text{ClO}_4)_2$  in 100 mM TMAPF<sub>6</sub>/ACN electrolyte solutions. S.R. = 50 mV/sec; Sample Width = 17 msec; Pulse Amplitude = 50 mV; Pulse Width = 100 msec; Pulse Period = 200 msec. C) DPV peak current plotted vs. the concentration of  $[\text{Co}(\text{DTB})_3](\text{ClO}_4)_2$ .

Nevertheless, addition of  $[\text{Co}(\text{DBT})_3](\text{ClO}_4)_2$  into the quinizarin solution created a synergy effect. Figure 2.41 B and C show a significant current amplification. The DPV peak current was amplified by an impressive factor of 55 when the concentration of  $[\text{Co}(\text{DBT})_3](\text{ClO}_4)_2$  reached 1.30 mM. Explanation of this synergy effect at a molecular level required further investigation. The significant observation here, however, is that the oxidation of  $\text{Co}(\text{DTB})_3^{2+}$  is efficiently catalyzed on the ITO electrode by an organic compound possessing a slow heterogeneous electron transfer rate.

#### 7) Catalytic oxidation of $[\text{Co}(\text{DBT})_3](\text{ClO}_4)_2$ by $\text{Fe}(\text{BPB})_2(\text{CN})_2$

Dicyano-, tricyano-, and tetracyano-polyimine-iron(II) complexes have been of considerable research interests due to their specific electrochemical, solvchromic and piezochromic properties.<sup>23, 24, 32-36</sup> According to Toma et al.,<sup>36</sup>  $\text{Fe}(\text{CN})_2(\text{bipy})_2$  and  $[\text{Fe}(\text{CN})_4(\text{bipy})]^{2-}$  are redox reversible on Pt electrode with  $\text{Fe}^{3+/2+}$  redox potentials around 0.6 and -0.3 V vs SHE. Basically, the redox potentials depend on the relative stability constants of the oxidized and reduced species in solution.<sup>36</sup> Increasing the number of electron-donor cyanide ligand lead to the stabilization of the highest oxidation state and to a decrease of redox potential. Thus, the redox potential for tricyano- complex  $[\text{Fe}(\text{terpy})(\text{CN})_3]^-$  should be higher than that of its tetracyano- analog  $[\text{Fe}(\text{CN})_4(\text{bipy})]^{2-}$ , but lower than that of its dicyano- analog  $\text{Fe}(\text{CN})_2(\text{bipy})_2$ .

In this study, both  $\text{Fe}(\text{DMB})_2(\text{CN})_2$  and  $\text{KFe}(\text{terpy})(\text{CN})_3$  were synthesized and their electrochemical properties on ITO electrodes were examined and shown in Table 2.2. In a solution of 100 mM TMAPF<sub>6</sub>/acetonitrile, these two complexes exhibit  $E_{1/2}$  at 0.34 V and 0.25 V vs SSCE and  $\Delta E_p$  75 mV and 62 mV on the ITO electrode. Based on

these observations, their intercalative analogs,  $\text{Fe}(\text{BPB})_2(\text{CN})_2$  and  $\text{K}[\text{Fe}(\text{TTT})(\text{CN})_3]$ , were subsequently prepared as reporter catalysts to be used in DNA hybridization detection, assuming substitutions on the polyimine ligands won't significantly affect the electrochemical properties of the complexes. As shown in Table 2.2, the prepared  $\text{Fe}(\text{BPB})_2(\text{CN})_2$  and  $\text{K}[\text{Fe}(\text{TTT})(\text{CN})_3]$  have  $E_{1/2}$  at 0.44 V and 0.24 V vs SSCE, and  $\Delta E_p$  73 mV and 69 mV on the ITO electrode, consistent with the prediction.

Efficiency for catalytic oxidation of  $[\text{Co}(\text{DBT})_3](\text{ClO}_4)_2$  by these intercalative complexes on the ITO electrode was then evaluated. Figure 2.43 shows the results obtained for  $\text{Fe}(\text{BPB})_2(\text{CN})_2$ . The solid curve in Figure 2.43 is the DPV of  $\text{Fe}(\text{BPB})_2(\text{CN})_2$  alone. Peaks at 440 and 800 mV are due to  $\text{Fe}^{2+}$  oxidation and PTZ oxidation, respectively. Addition of 0.7 mM and 1.8 mM  $[\text{Co}(\text{DBT})_3](\text{ClO}_4)_2$  produced a current amplification near the  $\text{Fe}^{2+}$ -centered oxidation. Meanwhile, the PTZ-centered oxidation was only marginally amplified. However, when the concentration of  $\text{Co}(\text{DTB})_3^{2+}$  approached 2.9 mM, the  $\text{Fe}^{2+}$  centered peak current started decreasing; and a current amplification was observed near the PTZ-centered oxidation, meaning that, the  $\text{Fe}^{2+}$  centered electrode process was overloaded at this concentration, and the PTZ-centered electrode process began to play its role in the catalysis process.<sup>30</sup>

Unfortunately, the PTZ-center catalysis is not practical for actual DNA sensing because of its high potential. The meaningful catalysis will be only around the  $\text{Fe}^{2+}$  centered oxidation. The insert on the right lower corner of Figure 2.43 shows the peak current of metal centered oxidation vs the concentration of mediator  $[\text{Co}(\text{DTB})_3](\text{ClO}_4)_2$ . The maximum current enlarging factor for the metal centered oxidation is 3.7.

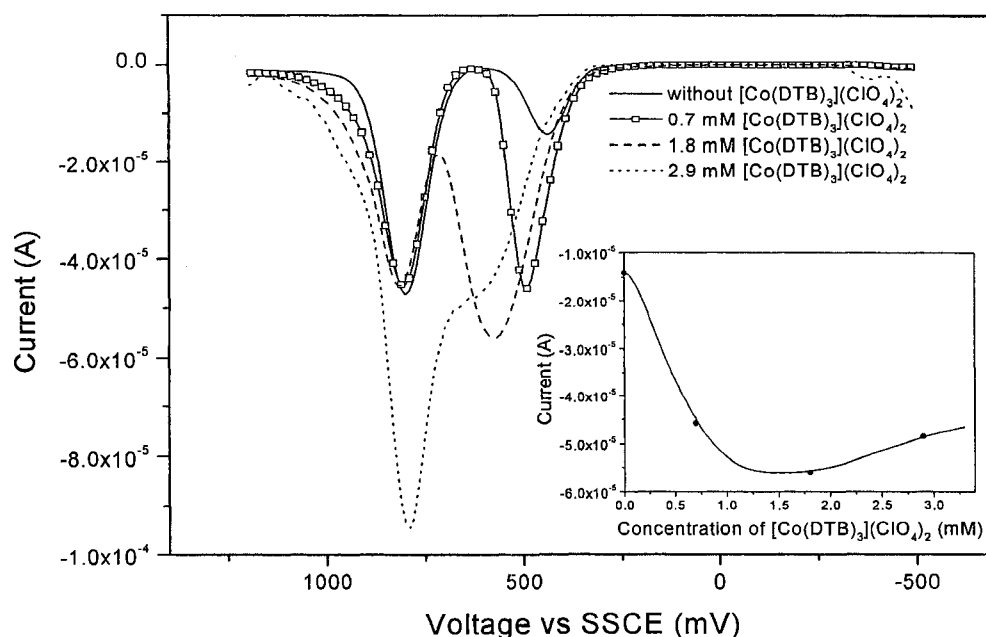


**Figure 2.43.** DPVs of  $\text{Fe}(\text{BPB})_2(\text{CN})_2$  in the presence of different amount of  $[\text{Co}(\text{DTB})_3](\text{ClO}_4)_2$  in 100 mM  $\text{TMAPF}_6/\text{ACN}$ . W.E.,  $(0.5 \text{ cm}^2)$ ; R.E., SSCE; C.E., Pt; S.R. = 50 mV/sec; Sample Width = 17 msec; Pulse Amplitude = 50 mV; Pulse Width = 100 msec; Pulse Period = 200 msec. The insertion on the right lower corner shows the DPV peak current vs the concentration of  $[\text{Co}(\text{DTB})_3](\text{ClO}_4)_2$ .

#### 8) Catalytic oxidation of $[\text{Co}(\text{DBT})_3](\text{ClO}_4)_2$ by $\text{KFe}(\text{TTT})(\text{CN})_3$

Figure 2.44 demonstrates the catalytic efficiency of  $\text{K}[\text{Fe}(\text{TTT})(\text{CN})_3]$  for oxidation of  $[\text{Co}(\text{DBT})_3](\text{ClO}_4)_2$  on the ITO electrode. Two major oxidations are observed in the DPV of  $\text{K}[\text{Fe}(\text{TTT})(\text{CN})_3]$  alone (solid curve). The peak at 230 mV is due to the oxidation of  $\text{Fe}^{2+}$  and the peak at 790 mV is due to the oxidation of PTZ. The small surface wave around 430 mV might be the result of an impurity produced from the solvent-ligand exchange reaction.<sup>1</sup> Addition of  $[\text{Co}(\text{DBT})_3](\text{ClO}_4)_2$  produced a current amplification effect, which was near the metal centered oxidation processes when the concentration of  $[\text{Co}(\text{DBT})_3](\text{ClO}_4)_2$  was low and moved to the PTZ centered oxidation process when the concentration of  $[\text{Co}(\text{DBT})_3](\text{ClO}_4)_2$  was high. At the concentration of

1.3 mM  $[\text{Co}(\text{DTB})_3](\text{ClO}_4)_2$ , the metal center oxidation peak current was amplified by a factor of 3.6.

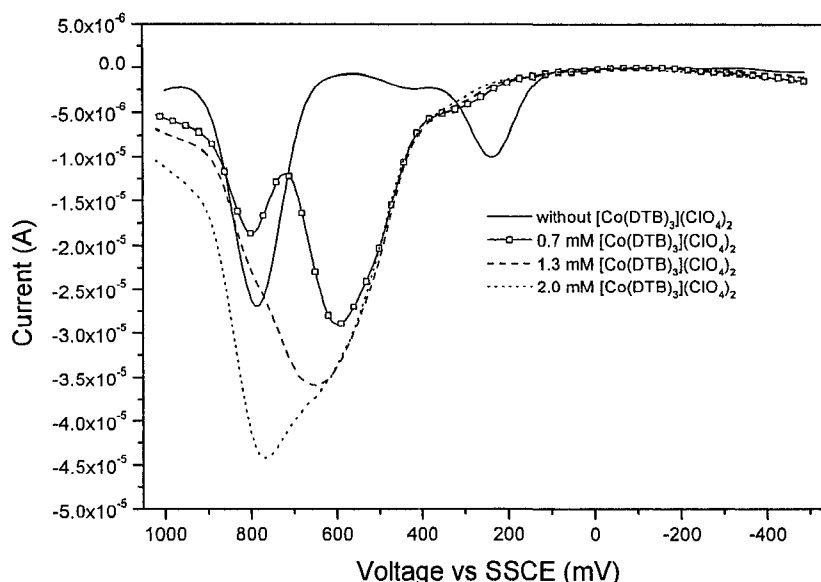


**Figure 2.44.** DPVs of  $\text{K}[\text{Fe}(\text{TTT})(\text{CN})_3]$  in the presence of different amount of  $[\text{Co}(\text{DTB})_3](\text{ClO}_4)_2$  in 100 mM TMAPF<sub>6</sub>/ACN. W.E., (0.5 cm<sup>2</sup>); R.E., SSCE; C.E., Pt; S.R. = 50 mV/sec; Sample Width = 17 msec; Pulse Amplitude = 50 mV; Pulse Width = 100 msec; Pulse Period = 200 msec.

#### 9) Catalytic oxidation of $[\text{Co}(\text{DBT})_3](\text{ClO}_4)_2$ by $\text{Ru}(\text{44POZ})_2\text{Cl}_2$

The solid curve in Figure 2.45 is the DPV of  $\text{Ru}(\text{44POZ})_2\text{Cl}_2$  alone on the ITO electrode. The peak at 650 mV is due to  $\text{Ru}^{2+}$  oxidation. The peak current increased upon addition of  $[\text{Co}(\text{DBT})_3](\text{ClO}_4)_2$ . The insert on the right lower corner of Figure 2.45 shows the DPV peak current vs the concentration of  $[\text{Co}(\text{DTB})_3](\text{ClO}_4)_2$ . At 21 mM of  $[\text{Co}(\text{DBT})_3](\text{ClO}_4)_2$ , the DPV peak current reached a maximum value which was 7.4 times of its un-amplified value. Further increasing of the concentration of  $[\text{Co}(\text{DBT})_3](\text{ClO}_4)_2$  made the oxidation peak positively shift to ~ 800 mV.

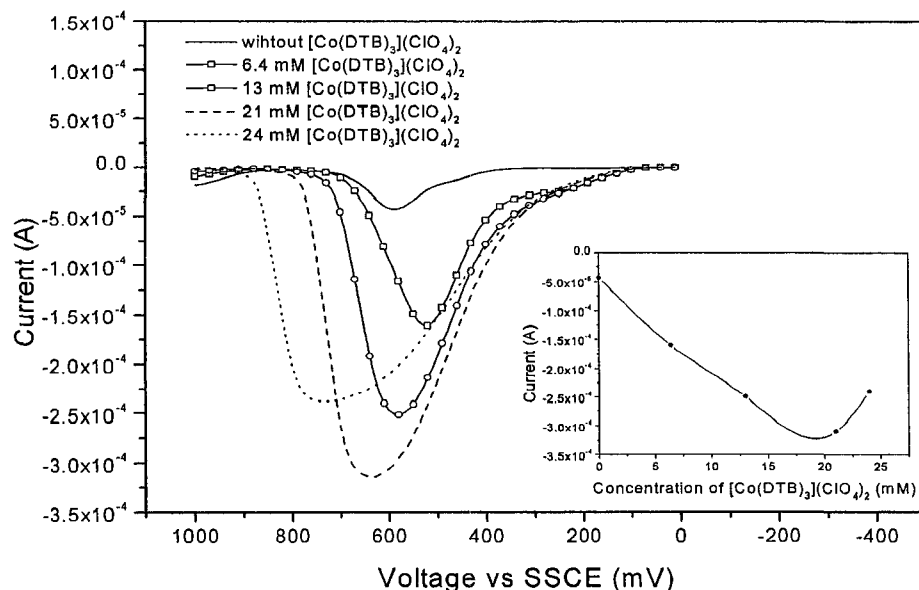


**Figure 4.25.** DPVs of Ru(44POZ)<sub>2</sub>Cl<sub>2</sub> in the presence of different amount of [Co(DTB)<sub>3</sub>](ClO<sub>4</sub>)<sub>2</sub> in 100 mM TMAPF<sub>6</sub>/ACN. W.E., (0.5 cm<sup>2</sup>); R.E., SSCE; C.E., Pt; S.R. = 50 mV/sec; Sample Width = 17 msec; Pulse Amplitude = 50 mV; Pulse Width = 100 msec; Pulse Period = 200 msec. The insertion on the right lower corner shows the DPV peak current vs the concentration of [Co(DTB)<sub>3</sub>](ClO<sub>4</sub>)<sub>2</sub>.

#### 10) Catalytic oxidation of [Co(DBT)<sub>3</sub>](ClO<sub>4</sub>)<sub>2</sub> by Ru(46PTZ)<sub>2</sub>Cl<sub>2</sub>

DPVs of Ru(46PTZ)<sub>2</sub>Cl<sub>2</sub> in the presence of different amount of [Co(DTB)<sub>3</sub>](ClO<sub>4</sub>)<sub>2</sub> on ITO are shown in Figure 2.46. The solid curve depicts the DPV of Ru(46PTZ)<sub>2</sub>Cl<sub>2</sub> alone. The Ru<sup>2+</sup> oxidation peak shows up at 165 mV vs SSCE. From Figure 2.46, it can be seen that the peak current increased upon addition of [Co(DBT)<sub>3</sub>](ClO<sub>4</sub>)<sub>2</sub> and became 6.2 time bigger when the concentration of [Co(DBT)<sub>3</sub>](ClO<sub>4</sub>)<sub>2</sub> increased to 0.6 mM. Moreover, an additional increase of the [Co(DBT)<sub>3</sub>](ClO<sub>4</sub>)<sub>2</sub> concentration yielded a peak current decrease. The insert of Figure 2.46 shows how the DPV peak current changed with the concentration of [Co(DTB)<sub>3</sub>](ClO<sub>4</sub>)<sub>2</sub>.

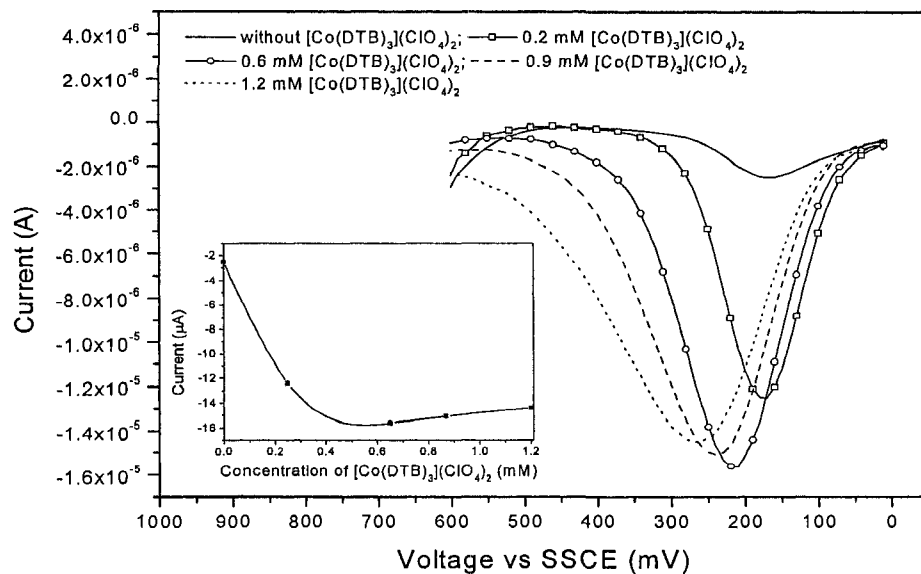


**Figure 2.46.** DPVs of  $\text{Ru}(46\text{PTZ})_2\text{Cl}_2$  in the presence of different amount of  $[\text{Co}(\text{DTB})_3](\text{ClO}_4)_2$  in 100 mM  $\text{TMAPF}_6/\text{ACN}$ . W.E.,  $(0.5 \text{ cm}^2)$ ; R.E., SSCE; C.E., Pt; S.R. = 50 mV/sec; Sample Width = 17 msec; Pulse Amplitude = 50 mV; Pulse Width = 100 msec; Pulse Period = 200 msec. The insertion on the left lower corner shows the DPV peak current vs the concentration of  $[\text{Co}(\text{DTB})_3](\text{ClO}_4)_2$ .

#### 11) Catalytic oxidation of $[\text{Co}(\text{DBT})_3](\text{ClO}_4)_2$ by $\text{Ru}(\text{MPB})_2(\text{Cl})_2$

Figure 2.47 shows the catalytic performance of  $\text{Ru}(\text{MPB})_2\text{Cl}_2$  for oxidation of  $[\text{Co}(\text{DBT})_3](\text{ClO}_4)_2$  on the ITO electrode. In the absence of  $[\text{Co}(\text{DBT})_3](\text{ClO}_4)_2$ , the DPV of  $\text{Ru}(\text{MPB})_2\text{Cl}_2$  (solid curve) shows a  $\text{Ru}^{2+}$  oxidation peak at 210 mV vs SSCE. The peak current increased upon addition of the mediator  $[\text{Co}(\text{DBT})_3](\text{ClO}_4)_2$ . The insertion on the left lower corner of Figure 2.47 shows how the DPV peak current changes with the concentration of  $[\text{Co}(\text{DTB})_3](\text{ClO}_4)_2$ . After being mixed with 10 mM  $[\text{Co}(\text{DBT})_3](\text{ClO}_4)_2$ , the solutions gave the highest peak current that was 39 times of its initial value. Adding more of the cobalt mediator causes a decline in the DPV peak current. In comparison with  $\text{Ru}(46\text{PTZ})_2\text{Cl}_2$ ,  $\text{Ru}(\text{MPB})_2(\text{Cl})_2$  is proven to be a better catalyst.

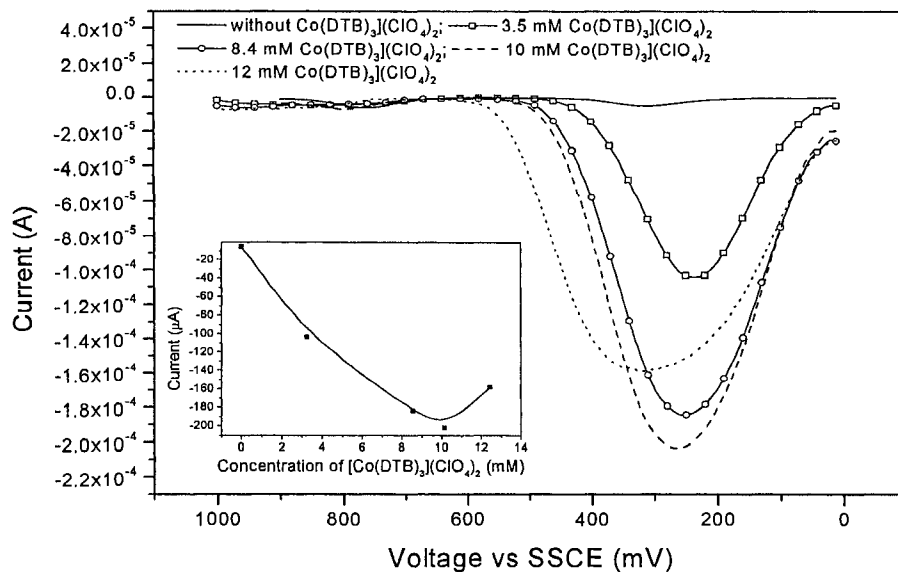


**Figure 2.47.** DPVs of  $\text{Ru}(\text{MPB})_2\text{Cl}_2$  in the presence of different amount of  $[\text{Co}(\text{DTB})_3](\text{ClO}_4)_2$  in 100 mM TMAPF<sub>6</sub>/ACN. W.E., (0.5 cm<sup>2</sup>); R.E., SSCE; C.E., Pt; S.R. = 50 mV/sec; Sample Width = 17 msec; Pulse Amplitude = 50 mV; Pulse Width = 100 msec; Pulse Period = 200 msec. The insertion on the left lower corner shows the DPV peak current vs the concentration of  $[\text{Co}(\text{DTB})_3](\text{ClO}_4)_2$ .

## 12) Catalytic oxidation of $[\text{Co}(\text{DBT})_3](\text{ClO}_4)_2$ by $\text{Ru}(\text{BPB})_2\text{Cl}_2$

The results of catalytic oxidation of  $[\text{Co}(\text{DBT})_3](\text{ClO}_4)_2$  by another ruthenium complex,  $\text{Ru}(\text{BPB})_2\text{Cl}_2$ , are shown in Figure 2.48. The solid curve is the DPV of  $\text{Ru}(\text{BPB})_2\text{Cl}_2$  alone obtained on the ITO electrode. The peaks at 300 mV and 800 mV are due to  $\text{Ru}^{2+}$  oxidation and PTZ oxidation, respectively. Addition of 1.1 mM to 5.9 mM  $[\text{Co}(\text{DBT})_3](\text{ClO}_4)_2$  into the catalyst solution produced a current amplification near the  $\text{Ru}^{2+}$  centered oxidation process. The insertion of Figure 2.48 depicts the  $\text{Ru}^{2+}$  centered DPV peak current vs the concentration of  $[\text{Co}(\text{DBT})_3](\text{ClO}_4)_2$ . The plot gradually became more leveled as the concentration of  $[\text{Co}(\text{DBT})_3](\text{ClO}_4)_2$  increased, suggesting that the catalytic efficiency declined as more mediator was added. Despite all

this, an amplification factor up to 55 was achieved at the highest concentration 5.9 mM, which is way above the maximum amplification factors displayed by either Ru(MPB)<sub>2</sub>Cl<sub>2</sub> or Ru(46PTZ)<sub>2</sub>Cl<sub>2</sub>.

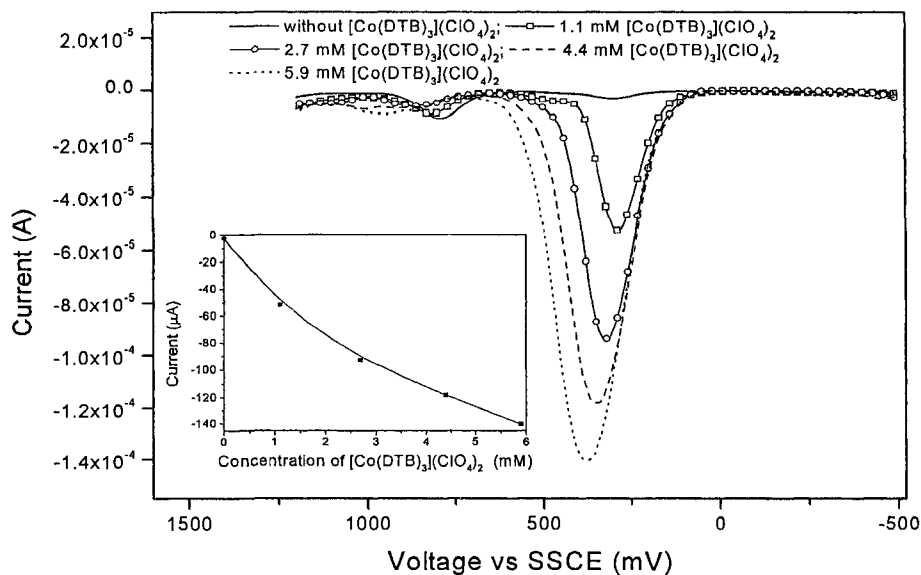


**Figure 2.48.** DPVs of Ru(BPB)<sub>2</sub>Cl<sub>2</sub> in the presence of different amount of [Co(DTB)<sub>3</sub>](ClO<sub>4</sub>)<sub>2</sub> in 100 mM TMAPF<sub>6</sub>/ACN. W.E., (0.5 cm<sup>2</sup>); R.E., SSCE; C.E., Pt; S.R. = 50 mV/sec; Sample Width = 17 msec; Pulse Amplitude = 50 mV; Pulse Width = 100 msec; Pulse Period = 200 msec. The insertion on the left lower corner shows the DPV peak current vs the concentration of [Co(DTB)<sub>3</sub>](ClO<sub>4</sub>)<sub>2</sub>.

### 13) Summary

In this study, twelve catalysts, either transition metal complexes or organic compounds, were tested for catalytic oxidation of [Co(DTB)<sub>3</sub>](ClO<sub>4</sub>)<sub>2</sub> on the ITO electrode. The results are summarized in Table 2.3, including the catalysts' maximum amplification factors (M.A.F.s) and the working potentials at which the catalysts display their M.A.F.s.

In general, the catalyst's electrochemical and chemical properties dominate its catalytic performance. Its oxidation potential on ITO must not be too low; but a high

oxidation potential of the catalyst does not guarantee an efficient catalysis. For example, due to its low potential, the oxidation process of TPA to TPA<sup>+</sup> will not catalyze the oxidation of Co(DTB)<sub>3</sub><sup>2+</sup> on ITO; on the other hand, even though (NEt<sub>4</sub>)<sub>2</sub>[Ru(bipy)(CN)<sub>4</sub>] demonstrates a high Ru<sup>2+</sup> oxidation potential on ITO, instead of activating the redox chemistry of the mediator [Co(DTB)<sub>3</sub>](ClO<sub>4</sub>)<sub>2</sub> on ITO, it is actually deactivated upon the addition of the mediator.

There isn't a necessary correlation between the heterogeneous electron transfer rate and the catalyst's performance either, considering the fact that the redox sluggish quinizarin displays an impressive amplification factor of 55.

**Table 2.3.** Maximum amplification factor (M.A.F.) of catalysts and the working potentials at which the catalysts display their M.A.F.s. For transition metal complex catalysts, the data are for the metal centered oxidation process.

Catalyst	M.A.F.	Peak Potential of M.A.F. vs SSCE
(NEt <sub>4</sub> ) <sub>2</sub> [Ru(bipy)(CN) <sub>4</sub> ]	<1	/
LBS	5	670 mV (DPV) 890 mV (CV)
thioridazine	33	1100 mV (DPV)
phenothiazine	<1	/
TPA	>8.1	720 mV (DPV)
quinizarin	55	600 mV (DPV)
Fe(BPB) <sub>2</sub> (CN) <sub>2</sub>	3.4	580 mV (DPV)
KFe(TPT)(CN) <sub>3</sub>	3.6	650 mV (DPV)
Ru(44POZ) <sub>2</sub> Cl <sub>2</sub>	7.4	650 mV (DPV)
Ru(46PTZ) <sub>2</sub> Cl <sub>2</sub>	6.2	215 mV (DPV)
Ru(MPB) <sub>2</sub> Cl <sub>2</sub>	39	265 mV (DPV)
Ru(BPB) <sub>2</sub> Cl <sub>2</sub>	>55	375 mV (DPV)

Three intercalative ruthenium(II) complexes, Ru(46PTZ)<sub>2</sub>Cl<sub>2</sub>, Ru(MPB)<sub>2</sub>Cl<sub>2</sub> and Ru(BPB)<sub>2</sub>Cl<sub>2</sub>, were prepared and studied during this research. Molecular structures of

their substituted bipyridine ligands are shown in Figure 2.49. For the bipyridine ligands of  $\text{Ru}(\text{MPB})_2\text{Cl}_2$  and  $\text{Ru}(\text{BPB})_2\text{Cl}_2$ , the alkyl chain that bridges the coordinating moiety to the intercalative PTZ moiety is short, suggesting a short intramolecular distance between the metal center and the PTZ moieties.  $\text{Ru}(\text{MPB})_2\text{Cl}_2$  and  $\text{Ru}(46\text{PTZ})_2\text{Cl}_2$  carry two PTZ groups while  $\text{Ru}(\text{BPB})_2\text{Cl}_2$  carries four. Compared with  $\text{Ru}(46\text{PTZ})_2\text{Cl}_2$ ,  $\text{Ru}(\text{MPB})_2\text{Cl}_2$  is found to be more effective for catalytic oxidation of  $[\text{Co}(\text{DTB})_3](\text{ClO}_4)_2$  on ITO, and  $\text{Ru}(\text{BPB})_2\text{Cl}_2$  is the most effective one. This might imply a possible promoting effect of the PTZ moieties.

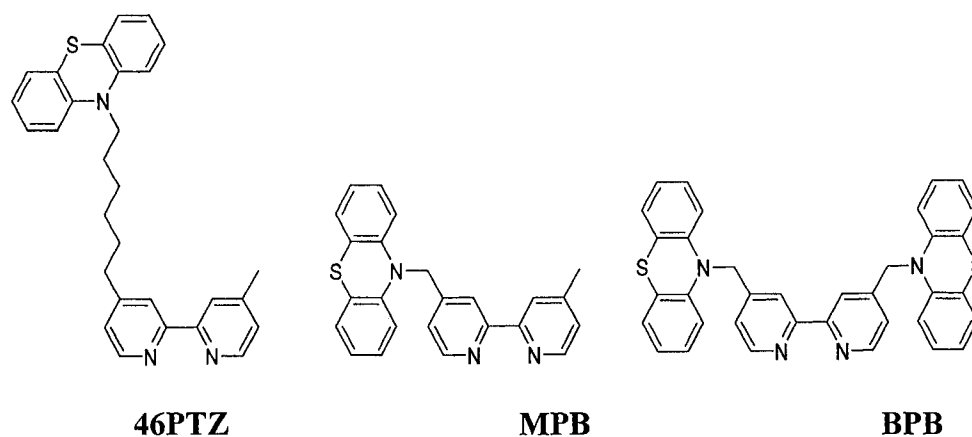


**Figure 2.49.** Molecular structure of 46PTZ, MPB and BPB.

Furthermore, the  $\text{Ru}(\text{BPB})_2\text{Cl}_2$  mediated catalysis is metal-centered, it consequently has low working potential (less than 600 mV), which is a prerequisite for un-damaging DNA hybridization detection and excludes the necessity to strictly control the electrochemical experimental conditions. Unless otherwise stated, for the following DNA hybridization sensing experiments in the next chapter,  $\text{Ru}(\text{BPB})_2\text{Cl}_2$  is used as the redox active catalyst.

1. Elliott, C. M.; Caramori, S.; Bignozzi, C. A., Indium Tin Oxide Electrodes Modified with Tris(2,2'-bipyridine-4,4'-dicarboxylic acid)iron(II) and the Catalytic Oxidation of Tris(4,4'-di-tert-butyl-2,2'-bipyridine)cobalt(II). *Langmuir* **2005**, 21, (7), 3022-3027.
2. Scott, M. J.; Nelson, J. J.; Caramori, S.; Bignozzi, C. A.; Elliott, C. M., Cis-Dichloro-bis(4,4'-dicarboxy-2,2'-bipyridine)osmium(II)-Modified Optically Transparent Electrodes: Application as Cathodes in Stacked Dye-Sensitized Solar Cells. *Inorganic Chemistry* **2007**, 46, (24), 10071-10078.
3. Sapp, S. A.; Elliott, C. M.; Contado, C.; Caramori, S.; Bignozzi, C. A., Substituted Polypyridine Complexes of Cobalt(II/III) as Efficient Electron-Transfer Mediators in Dye-Sensitized Solar Cells. *Journal of the American Chemical Society* **2002**, 124, (37), 11215-11222.
4. Elliott, C. M.; Sapp, S. A.; Bignozzi, C. A.; Contado, C.; Caramori, S. *PCT Int. Appl.* **2003**.
5. Cazzanti, S.; Caramori, S.; Argazzi, R.; Elliott, C. M.; Bignozzi, C. A., Efficient Non-corrosive Electron-Transfer Mediator Mixtures for Dye-Sensitized Solar Cells. *Journal of the American Chemical Society* **2006**, 128, (31), 9996-9997.
6. Bignozzi, C. A.; Caramori, S.; Silvia, C.; Elliott, C. M., Efficient non corrosive mixture of electron mediators for dye sensitized solar cells. *PMSE Preprints* **2006**, 95, 293.
7. Thorp, H. H., Electrocatalytic DNA oxidation. *Topics in Current Chemistry* **2004**, 237, (Long-Range Charge Transfer in DNA II), 159-181.
8. Meric, B.; Kerman, K.; Ozkan, D.; Kara, P.; Erdem, A.; Kucukoglu, O.; Erciyas, E.; Ozsoz, M., Electrochemical biosensor for the interaction of DNA with the alkylating agent 4,4'-dihydroxy chalcone based on guanine and adenine signals. *Journal of Pharmaceutical and Biomedical Analysis* **2002**, 30, (4), 1339-1346.
9. Kerman, K.; Kobayashi, M.; Tamiya, E., Recent trends in electrochemical DNA biosensor technology. *Measurement Science and Technology* **2004**, 15, (2), R1-R11.
10. de-los-Santos-Alvarez, P.; Lobo-Castanon, M. J.; Miranda-Ordieres, A. J.; Tunon-Blanco, P., Current strategies for electrochemical detection of DNA with solid electrodes. *Analytical and Bioanalytical Chemistry* **2004**, 378, (1), 104-118.
11. Wang, J., Electrochemical biosensors: Towards point-of-care cancer diagnostics. *Biosensors & Bioelectronics* **2006**, 21, (10), 1887-1892.
12. Wang, J., Nanoparticle-based electrochemical DNA detection. *Analytica Chimica Acta* **2003**, 500, (1-2), 247-257.
13. Drummond, T. G.; Hill, M. G.; Barton, J. K., Electrochemical DNA sensors. *Nature Biotechnology* **2003**, 21, (10), 1192-1199.
14. [http://www.accessexcellence.org/AE/AEC/CC/images/DNA\\_views.gif](http://www.accessexcellence.org/AE/AEC/CC/images/DNA_views.gif), Access Excellence Classic Collection.
15. Wang, J.; Rivas, G.; Cai, X.; Shiraishi, H.; Fariasp, P. A. M.; Dontha, N.; Luo, D., Accumulation and trace measurements of phenothiazine drugs at DNA-modified electrodes. *Analytica Chimica Acta* **1996**, 332, (2-3), 139-144.
16. Vanickova, M.; Buckova, M.; Labuda, J., Voltammetric determination of azepine and phenothiazine drugs with DNA biosensors. *Chemia Analytyczna (Warsaw)* **2000**, 45, (1), 125-133.

17. Zhong, J.; Qi, Z.; Dai, H.; Fan, C.; Li, G.; Matsuda, N., Sensing phenothiazine drugs at a gold electrode co-modified with DNA and gold nanoparticles. *Analytical Sciences* **2003**, *19*, (5), 653-657.
18. Chandramouli, K. H.; Thimmaiah, K. N.; Chandrashekar, A.; D'Souza, C. J. M., Interaction of 2-Chloro-N10-Substituted Phenoxazine with DNA and Effect on DNA Melting. *Nucleosides, Nucleotides & Nucleic Acids* **2004**, *23*, (10), 1639-1656.
19. Cai, H.; Cao, X.; Jiang, Y.; He, P.; Fang, Y., Carbon nanotube-enhanced electrochemical DNA biosensor for DNA hybridization detection. *Analytical and Bioanalytical Chemistry* **2003**, *375*, (2), 287-293.
20. Smith, A. P.; Lamba, J. J. S.; Fraser, C. L.; Yamane, M.; Narasaka, K., Efficient synthesis of halomethyl-2, 2'-bipyridines: 4, 4'-bis (chloromethyl)-2, 2'-bipyridine(2, 2'-bipyridine, 4, 4'-bis (chloromethyl)-). *Organic Syntheses* **2002**, *78*, 82-90.
21. Della Ciana, L.; Hamachi, I.; Meyer, T. J., Synthesis of side-chain derivatives of 2,2'-bipyridine. *Journal of Organic Chemistry* **1989**, *54*, (7), 1731-5.
22. Feldheim, D. L.; Baldy, C. J.; Sebring, P.; Hendrickson, S. M.; Elliott, C. M., Synthesis and catalytic activity of transition metal polymers containing alkane-linked bipyridine and terpyridine ligands. *Journal of the Electrochemical Society* **1995**, *142*, (10), 3366-72.
23. Gameiro, P.; Pereira, E.; Garcia, P.; Breia, S.; Burgess, J.; de Castro, B., Derivatives of bis(2,2'-bipyridyl)dicyanoiron(II) with long alkyl chains - versatile solvatochromic probes that form metalloaggregates in water-rich media. *European Journal of Inorganic Chemistry* **2001**, (11), 2755-2761.
24. Schilt, A. A., Mixed ligand complexes of iron(II) and (III) with cyanide and aromatic di-imines. *Journal of the American Chemical Society* **1960**, *82*, 3000-5.
25. Larson, S. L.; Elliott, C. M.; Kelley, D. F., Charge Separation in Donor-Chromophore-Acceptor Assemblies: Linkage and Driving Force Dependence of Photoinduced Electron Transfers. *Journal of Physical Chemistry* **1995**, *99*, (17), 6530-9.
26. Andreades, S.; Zahnow, E. W., Anodic cyanations of aromatic compounds. *Journal of the American Chemical Society* **1969**, *91*, (15), 4181-4190.
27. Kato, M.; Yamauchi, S.; Hirota, N., Excited-state properties of a (2, 2'-bipyridine) ruthenium (II) complex, [Ru (CN) 4 (bpy)] 2-, a model of localized excitation. *The Journal of Physical Chemistry* **1989**, *93*, (9), 3422-3425.
28. Krause, R. A., *Inorg. Chim. Acta* **1977**, *22*, 209.
29. [http://en.wikipedia.org/wiki/Differential\\_pulse\\_voltammetry](http://en.wikipedia.org/wiki/Differential_pulse_voltammetry).
30. Elliott, C. M.; Bignozzi, C. A.; Xue, D.; Grainger, D. W.; Caramori, S.; Dissette, V. Electrochemical detection of complex formation using probes immobilized on electrode surfaces, U.S. Pat. Appl. Publ. (2008), . 2006-536478, 2008081329, 20060928, 2008.
31. Yao, T.; Musha, S.; Munemori, M., Anodic voltammetry and ESR studies of p-phenylenediamine and some of its derivatives in acetonitrile. *Chemistry Letters* **1974**, (8), 939-44.
32. Alousy, A.; Blundell, N. J.; Burgess, J.; Hubbard, C. D.; Van Eldik, R., Solvatochromism and piezochromism of dicyano-, tricyano-, and tetracyano-

- diimine-iron(II) complexes. *Transition Metal Chemistry (Dordrecht, Netherlands)* **2002**, 27, (3), 244-252.
33. Burgess, J.; Chambers, J. G.; Haines, R. I., Solvatochromic behavior of intramolecular charge-transfer spectra of inorganic diimine complexes. *Transition Metal Chemistry (Dordrecht, Netherlands)* **1981**, 6, (3), 145-51.
  34. Burgess, J.; Twigg, M. V., Kinetics of aquation of bis(2,2':6',2''-terpyridyl)iron(II) in acidic media and its reactions with cyanide ion. *Journal of the Chemical Society, Dalton Transactions: Inorganic Chemistry (1972-1999)* **1974**, (19), 2032-6.
  35. Toma, H. E.; Malin, J. M., Properties and reactivity of some pentacyanoferrate(II) complexes of aromatic nitrogen heterocycles. *Inorganic Chemistry* **1973**, 12, (5), 1039-45.
  36. Toma, H. E.; Takasugi, M. S., Preferential solvation effects in the electrochemistry and charge-transfer spectra of cyanoiron(II) complexes. *Journal of Solution Chemistry* **1989**, 18, (6), 575-83.

## Chapter 3: Probe ss-DNA Attachment on ITO Electrodes

### INTRODUCTION

Biosensors and biochips that are selective to nucleic acid targets usually use immobilized ss-DNA oligonucleotide probes.<sup>1-10</sup> Silane,<sup>2, 5, 8</sup>  $\alpha,\omega$ -dicarboxylic acid<sup>4, 7, 9</sup> and  $\omega$ -phosphonoalkyl carboxylic acid<sup>3, 6, 10</sup> have been previously used for immobilization of ss-DNA onto ITO surfaces. In this study, we employed an extensive collection of strategies to functionalize ITO surfaces with terminal carboxylic groups to enable covalent attachment of the DNA probe, 5'-CTGAACGGTAGCATCTTGAC-(CH<sub>2</sub>)<sub>6</sub>-NH<sub>2</sub>. Amino functional groups were covalently attached onto ITO surfaces utilizing silane chemistries; subsequent treatment of the surfaces with succinic anhydride introduced carboxylic groups. We also grew sebacic acid monolayers on ITO surfaces by modifying the procedures utilized by Napier et al.<sup>7</sup> and Hedges et al.<sup>4</sup> to grow 1,12-dodecanedicarboxylic acid monolayers. In addition, functionalizing the ITO electrodes with a wide variety of  $\omega$ -phosphonoalkyl carboxylic acid were done following Eckhardt and coworkers.<sup>3</sup> The functionalized ITO electrodes were subject to electrochemical analysis and XPS characterization.

The DNA probe was immobilized onto the ITO electrodes through activation of the terminal -COOH groups on the ITO surface with ethylenedicarbodiimide (EDC) and *N*-hydroxysuccinimide (NHS), followed by nucleophilic reaction of the NHS-ester with the terminal primary amine on the DNA probe to form stable amide bonds.

## BACKGROUND

### Non-specific Attachment of Catalyst onto ITO Surfaces

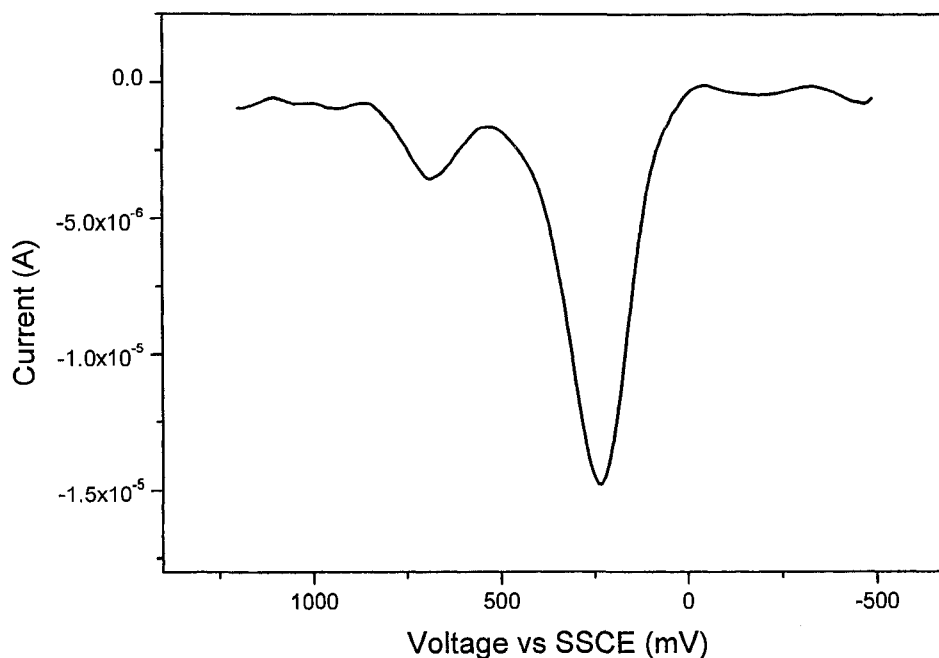


**Figure 3.1.** DPV of the ITO electrode ( $0.5 \text{ cm}^2$ ) treated with  $\text{Ru}(\text{MPB})_2\text{Cl}_2$  in the acetonitrile solution containing  $0.4 \text{ mM}$   $[\text{Co}(\text{DTB})_3](\text{ClO}_4)_2$  and  $100 \text{ mM}$   $\text{TMAPF}_6$  R.E., SSCE; C.E., Pt; S.R. =  $50 \text{ mV/sec}$ ; Sample Width =  $17 \text{ msec}$ ; Pulse Amplitude =  $50 \text{ mV}$ ; Pulse Width =  $100 \text{ msec}$ ; Pulse Period =  $200 \text{ msec}$ .

As previously mentioned in Chapter 2, the DNA detection strategy employed in our research relies on selective intercalation of the catalyst into ds-DNA to transduce hybridization events into electrochemical signals. Therefore, non-specific attachment of the catalyst to the electrode surface introduces false positive signals. Figure 3.1 demonstrates an evident current amplification effect, where the ITO electrode was first vigorously cleaned and dried, then soaked in an acetonitrile solution of  $\text{Ru}(\text{MPB})_2\text{Cl}_2$   $10^{-5}$  M for 15 minutes; after a thorough rinse with acetonitrile, the electrode was subject to the electrochemical analysis. As it can be seen from Figure 3.1, the  $\text{Ru}^{2+}$  oxidation current

was significantly amplified in the solution of 0.4mM [Co(DTB)<sub>3</sub>](ClO<sub>4</sub>)<sub>2</sub>. Even after three hours' soaking of the electrode in the electrolyte solution, the electrode still showed similar amounts of current, demonstrating strong absorbance of the ruthenium catalyst to the unmodified ITO surface.

### **Immobilization of DNA Probe onto ITO Electrodes**

DNA attachment onto conductive and transparent ITO substrates has attracted considerable interest in the area of DNA diagnosis,<sup>1, 3, 7-17</sup> medicine analysis<sup>18-25</sup> and electrochemical molecular recognition of chemicals.<sup>26</sup> Briefly, methods for immobilization of DNA to ITO surfaces fall into the following four categories:

- i) physical absorption of DNA onto bare ITO surfaces,
- ii) one step incorporation of both DNA and functional molecules onto the ITO surfaces,
- iii) functionalization the ITO surface with reactive functional groups, followed by physical absorption of DNA onto functionalized ITO surfaces,
- iv) functionalization the ITO surface with reactive functional groups, follow by the reaction of the surface functional groups with the terminal functional groups on the DNA probe to form stable covalent bonds.

The first method suffers from low DNA packing density. It is not suitable for this study due to possible catalyst attachment to the uncovered ITO surfaces. The second method usually involves complicated procedures to modify the DNA probe with the same functional group as that in the functional molecule. Diagnostic DNA detection mainly utilized the last method due to its reliability and repeatability, compared with the third

method. In addition, the covalent bonding between the surface terminal functional groups with the DNA terminal functional groups allows the DNA probes more flexibility, which is beneficial for recruiting the complementary DNA targets.

This study explores modification of ITO electrodes with a bifunctional silane, aliphatic  $\alpha,\omega$ -dicarboxylic acid or  $\omega$ -phosphonoalkyl carboxylic acid and immobilization of DNA probe to the organic monolayer using well-established amide coupling chemistry. To fabricate a highly sensitive and selective biosensor, the electrochemically inert organic monolayer has to be stable enough to withstand the hybridization conditions, meanwhile, a complete coverage of the ITO surface is imperative to block catalysts from nonspecifically attaching.

## EXPERIMENTAL

### Chemicals and Materials

The HPLC-purified probe DNA oligonucleotide 5'-CTGAACGGTAGCATCTTG-AC-(CH<sub>2</sub>)<sub>6</sub>-NH<sub>2</sub> was purchased from TriLink Biotechnologies (San Diego, CA). Such a sequence is selected because it forms a stable duplex with its complementary pair at room temperature, with minimal interference due to self-complementarity or secondary structure.<sup>27-30</sup> Hydrochloric acid of analytical grade was obtained from Mallinckrodt. Acetone, methanol, ethanol, 2-propanol, and sodium hydroxide were all ACS grade purchased from Fisher. Methanol used for electrode functionalization was distilled over Mg/I<sub>2</sub>. Optima grade ACN from Fisher was used for the electrochemical studies. 18 M $\Omega$  water was obtained from a MILLI-Q<sup>TM</sup> water purification system. 1-Ethyl-3-(3-

dimethylaminopropyl)-carbodiimide (EDC) and N-hydroxysuccinimide (NHS) were from ACROS ORGANICS. Other Chemicals were purchased from Aldrich.

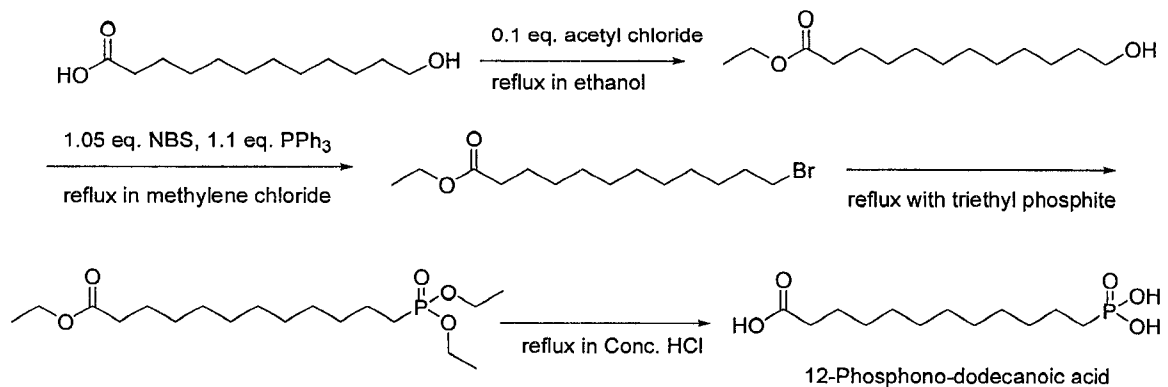
### **XPS Apparatus**

XPS studies of electrode surfaces were carried out on a Physical Electronics PHI 5800 spectrometer equipped with a concentric hemispherical analyzer. The average pressure in the high vacuum chamber during the analysis was of the order of  $5 \times 10^{-9}$  Torr. Aluminum monochromatic  $K\alpha$  radiation (1486.6 eV) was used as the excitation source. Unless otherwise stated, the photoelectrons were collected at a  $15^\circ$  take-off angle. Physical Electronics PC ACCESS and MULTIPAK resident softwares controlled data acquisition and processing. Full survey scans were performed setting a pass energy of 187.85 eV with an eV/step of 0.800, while an acquisition time of 2 min was generally used. Utility scans were carried out with a pass energy of 117.4 eV and an eV/step of 0.5, acquiring C(1s) and N(1s) signals for 10 min. Finally, high-resolution acquisitions of the N(1s) and C(1s) peaks were performed employing 23.5 eV of pass energy and 0.1 eV/step for 15 min. Voigt profile fitting of the XPS spectra was achieved by means of the XPS PEAK 4.1 program.

### **Synthesis**

#### 1) 12-phosphono-dodecanoic acid (PDA)

PDA was prepared according to the Pawsey et al.'s methods.<sup>31</sup> The synthesis procedure is shown below. It starts with the compound 12-hydroxy-dodecanoic acid purchased from Sigma-Aldrich.



a) 12-hydroxy-dodecanoic acid ethyl ester

Catalytic amount of acetyl chloride (7.0 $\mu$ l, 0.10 mMol) was added by syringe into the solution of 12-Hydroxy-dodecanoic acid (0.21 g, 0.94 mMol) in 15 ml dry ethanol. The solution was refluxed under nitrogen for 2 hours. Volatiles were removed under reduced pressure. The residue was purified through a silica column (10g SiO<sub>2</sub>) with 1: 4 ethyl acetate / hexane as the eluent, resulting in 0.23 g white solid (yield 100 %). Figure 3.2 shows its <sup>1</sup>H NMR spectrum in CDCl<sub>3</sub>.

b) 12-bromo-dodecanoic acid ethyl ester

Under nitrogen, 15ml dry methylene chloride was added into the solid mixture consisting of triphenylphosphine (0.27g, 1.0 mMol), 12-hydroxy-dodecanoic acid ethyl ester (0.23g, 0.94 mMol) and N-bromosuccinimide (0.19g, 1.0 mMol) and was stirred. The solution was refluxed for 36 hours and cooled to room temperature. Volatiles were evaporated under reduced pressure. The residue was purified through a silica column (10g SiO<sub>2</sub>) with gradient ether/hexane (1:100 to 3:100) as the eluent, giving a colorless oil (yield 0.24g, 82 %). Figure 3.3 shows its <sup>1</sup>H NMR spectrum in CDCl<sub>3</sub>.

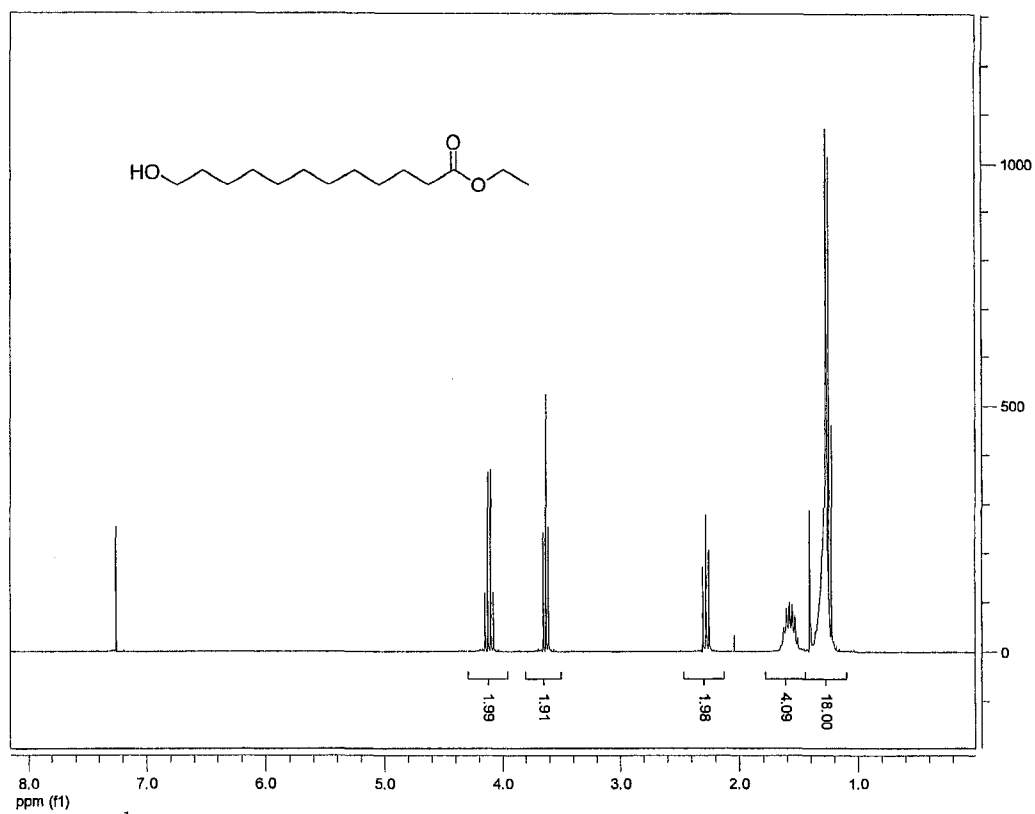


**Figure 3.2.**  $^1\text{H}$  NMR spectrum of 12-hydroxydodecanoic acid ethyl ester in  $\text{CD}_3\text{Cl}$ .

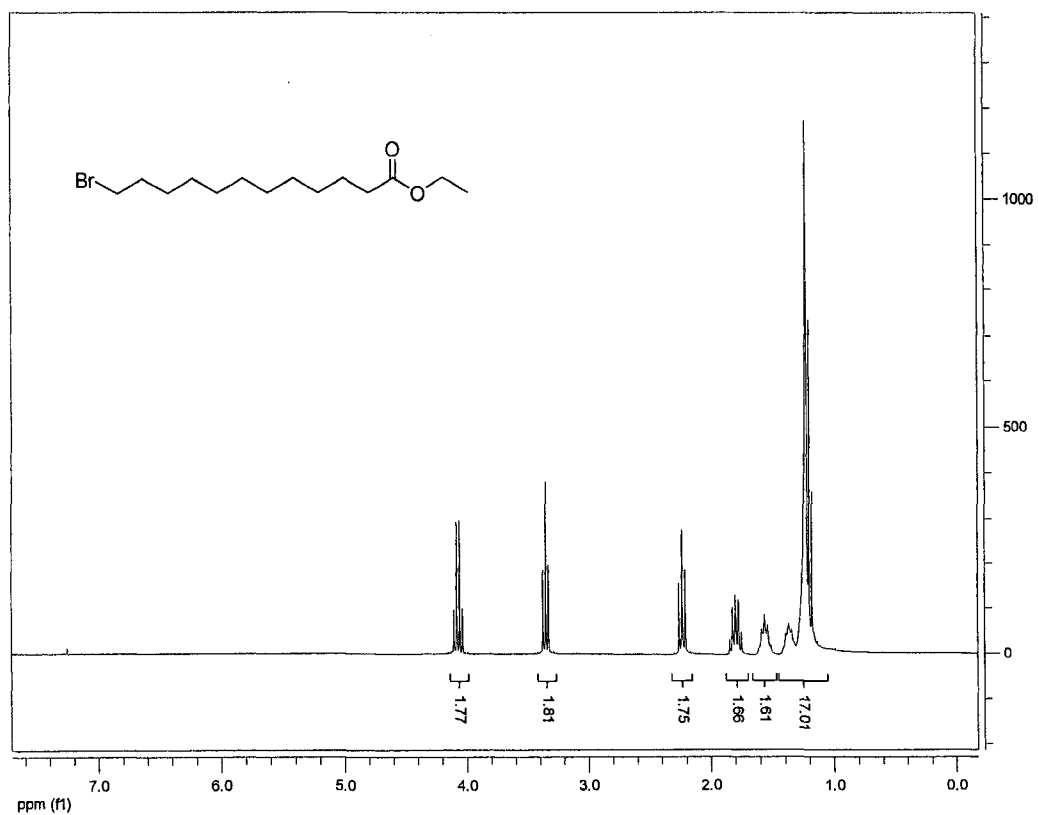


**Figure 3.3.**  $^1\text{H}$  NMR spectrum of 12-bromododecanoic acid ethyl ester in  $\text{CD}_3\text{Cl}$ .

c) 12-phosphono-dodecanoic acid

Under nitrogen, 12-bromo-dodecanoic acid ethyl ester (0.24 g, 0.77 mMol) was dissolved in 0.70 ml triethyl phosphate (4.1 mMol). The solution was degassed and refluxed under nitrogen for 5 hours. After cooling to room temperature, the mixture containing produced 12-(diethyl-phosphono)-dodecanoic acid ethyl ester and excess triethyl phosphate was added with 3 ml concentrated HCl solution and was refluxed for another 21 hours. 2 ml water was then added upon which white crystals formed. The solid was collected by filtering, washed thoroughly with water and dried at 40°C in vacuum overnight. The dry product weighed 0.17 g (yield 79 %). Its  $^1\text{H}$  NMR and  $^{13}\text{C}$  NMR spectrum in  $\text{CD}_3\text{OD}$  are shown in Figure 3.4 and Figure 3.5, respectively .

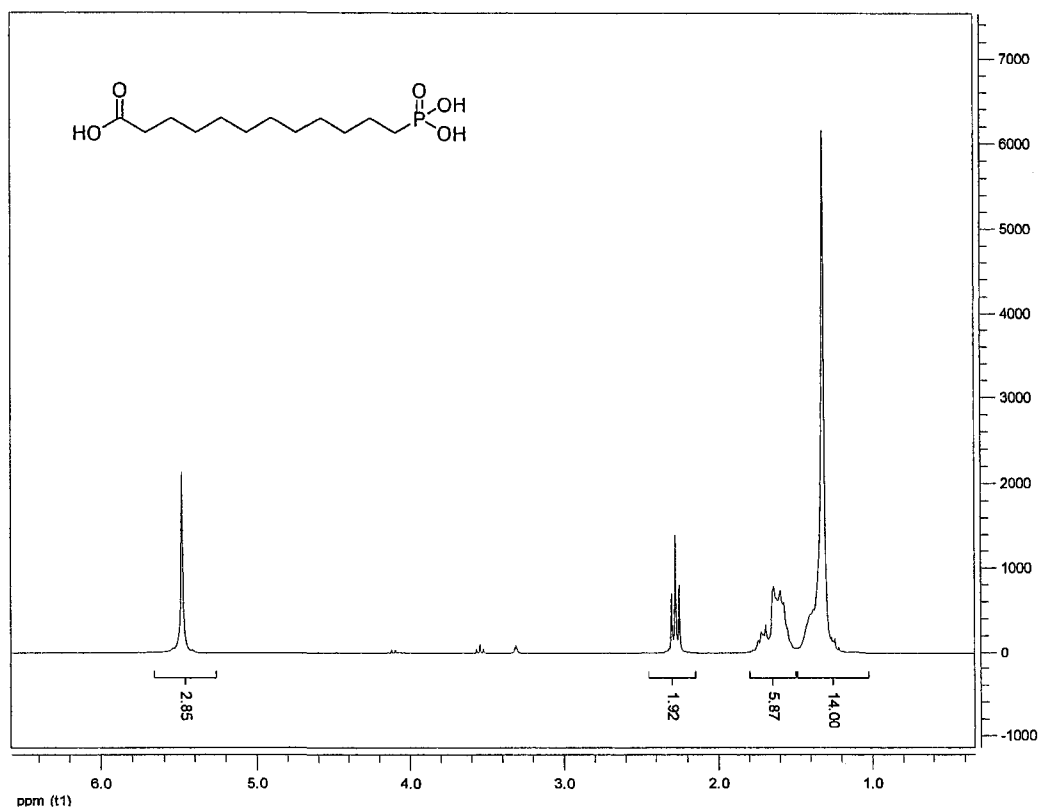


**Figure 3. 4.**  $^1\text{H}$  NMR spectrum of 12-phosphonododecanoic acid in  $\text{CD}_3\text{OD}$ .

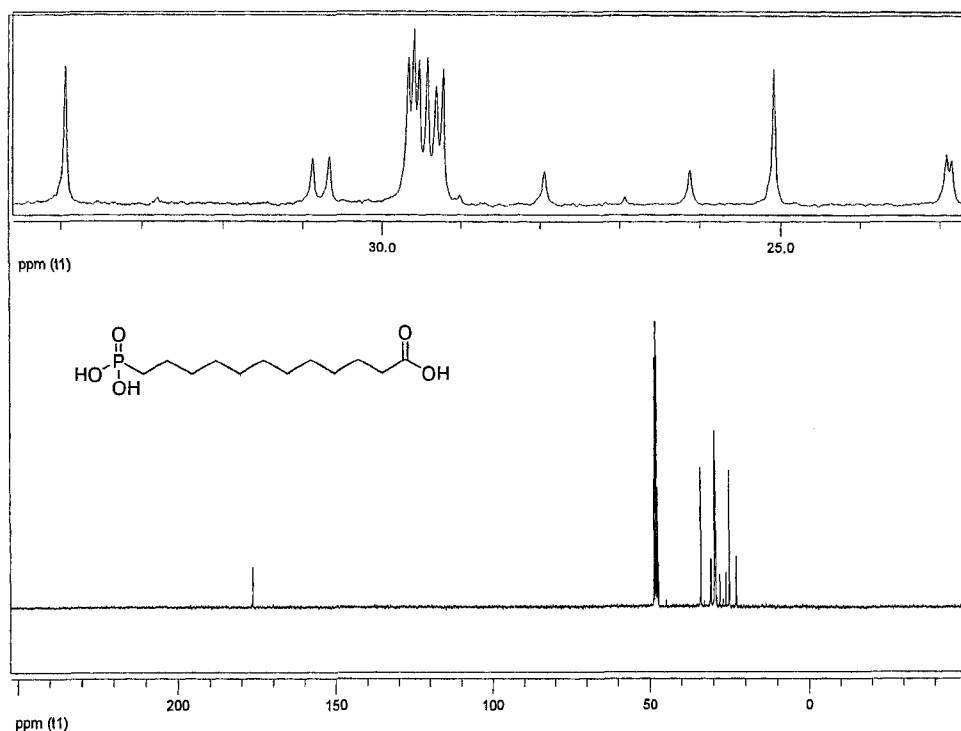
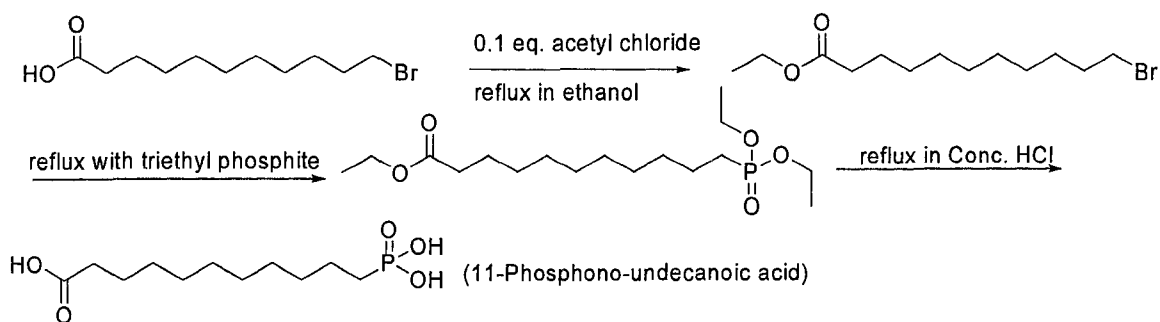


**Figure 3.5.**  $^{13}\text{C}$  NMR spectrum of 12-phosphonododecanoic acid in  $\text{CD}_3\text{OD}$ .

## 2) 11-phosphono-undecanoic acid (PUA)



### a) 11-bromo-undecanoic acid ethyl ester

Catalytic amount of (0.15 ml) acetyl chloride was added under nitrogen into the solution of 11-bromo-undecanoic acid (2.6g, 0.021Mol) in 200 ml dry ethanol. The solution was refluxed under nitrogen for 2 hours. Volatiles were removed under reduced pressure and the residue was purified through a silica column (30g) with gradient ether / hexane (1:100 to 3:100) as the eluent, resulting in 6.1 g colorless oil (yield 100 %). Its  $^1\text{H}$  NMR and  $^{13}\text{C}$  NMR spectra are shown below.

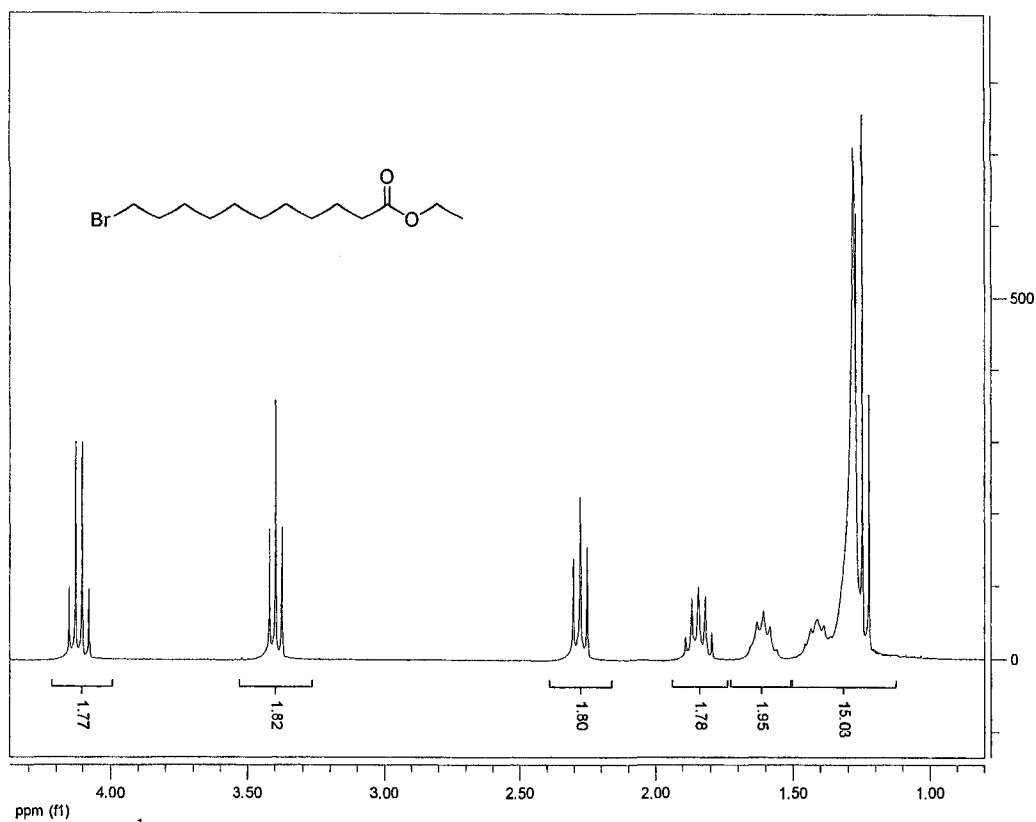


**Figure 3.6.**  $^1\text{H}$  NMR spectrum of 11-bromoundecanoic acid ethyl ester in  $\text{CDCl}_3$ .

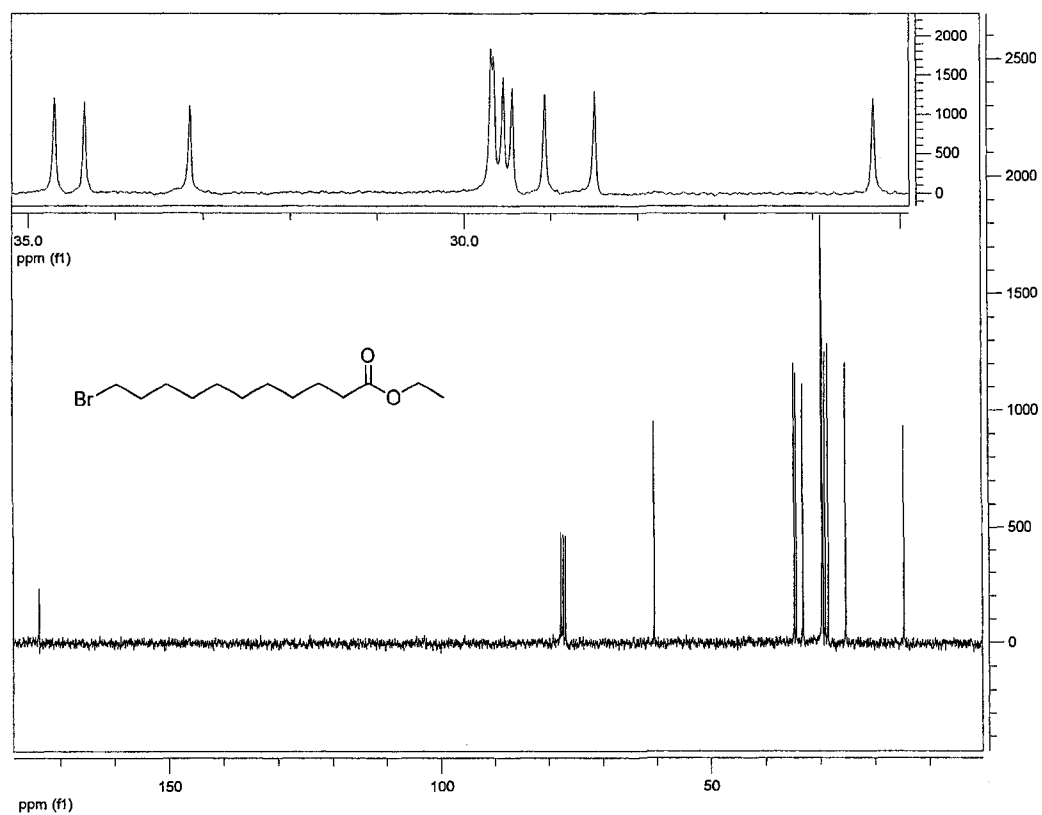


**Figure 3.7.**  $^{13}\text{C}$  NMR spectrum of 11-bromoundecanoic acid ethyl ester in  $\text{CDCl}_3$ .

b) 11-(diethyl-phosphono)-undecanoic acid ethyl ester

11-Bromo-undecanoic acid ethyl ester (6.2g 0.021 Mol) was added into 19 ml triethyl phosphite (0.110 Mol). The solution was refluxed under nitrogen for 5 hours, cooled to room temperature. To remove excess triethyl phosphate, the product was run through a silica column with 1:3 ethyl acetate/hexane as the eluent (yield 6.7g, 92%).

c) 11-phosphono-undecanoic acid

11-(Diethoxy-phosphoryl)-undecanoic acid ethyl ester (5.6g, 0.016Mol) was mixed with 65ml concentrated HCl. The mixture was refluxed for 38 hours, cooled to room temperature within 3 hours. The white crystalline product was collected by filtering, rinsed thoroughly with water and ether, and air dried (2.7g yield 64%). Its  $^1\text{H}$  and  $^{13}\text{C}$  NMR spectra are shown in Figure 3.8 and Figure 3.9, respectively.

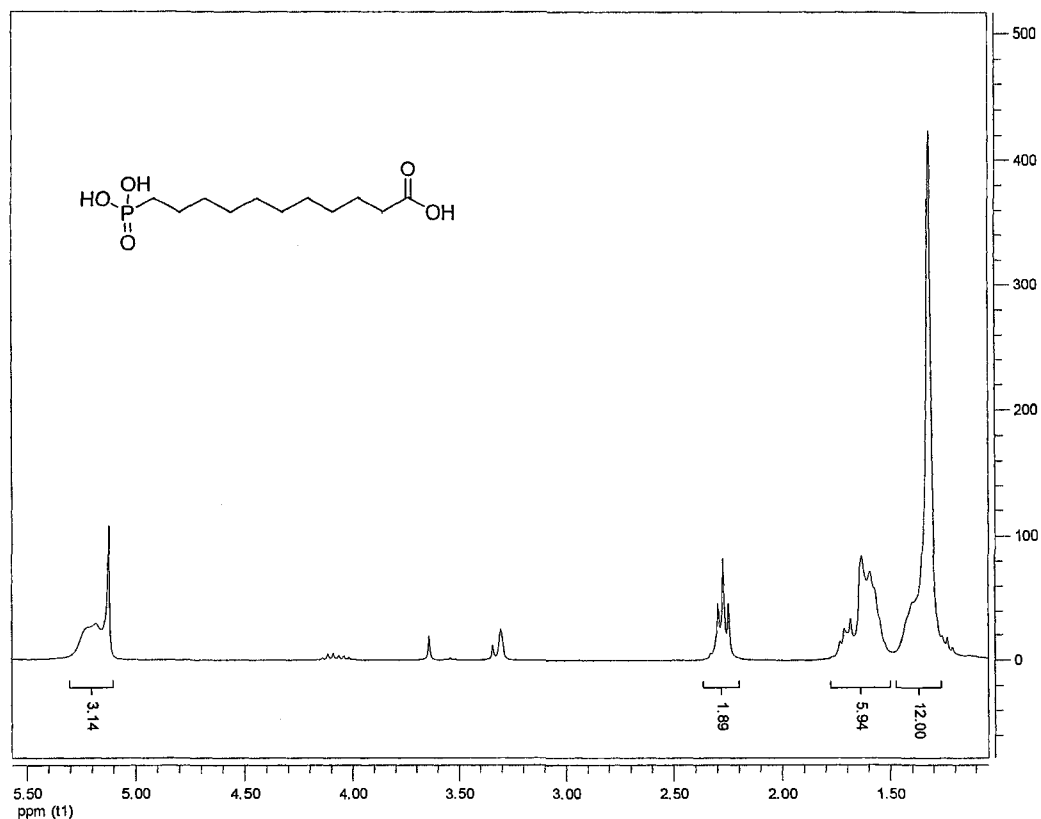


**Figure 3.8.**  $^1\text{H}$  NMR spectrum of 11-phosphonoundecanoic acid in  $\text{CD}_3\text{OD}$ .

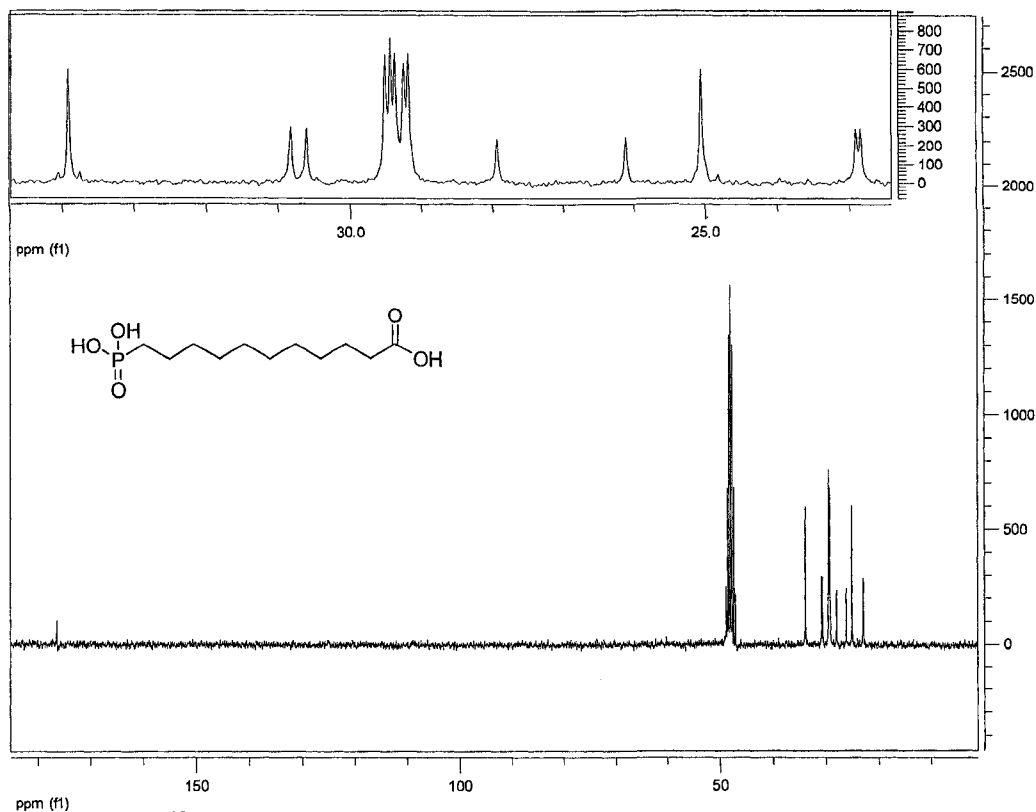
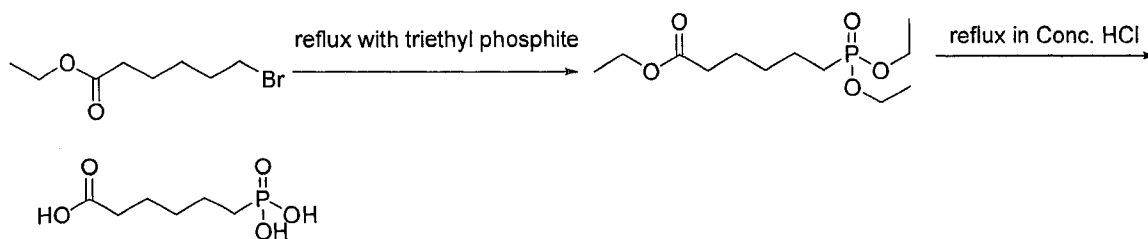


**Figure 3.9.**  $^{13}\text{C}$  NMR spectrum of 11-phosphonoundeconoic acid in  $\text{CD}_3\text{OD}$ .

### 3) 6-phosphono-hexanoic acid (PHA)



#### a) 6-(diethyl-phosphono)-hexanoic acid ethyl ester

Under  $\text{N}_2$ , the mixture of ethyl 6-bromohexanoate (3.1ml, 0.018Mol) and triethylphosphine (9.2ml, 0.054Mol) was refluxed for 5 hours. To hydrolyze excess triethylphosphine, 15ml water was added and the mixture was refluxed for another 3 minutes. After that, the solution was cooled to room temperature and 35ml water was added. The product was extract into benzene 50ml x 2. The benzene solution was dried

over  $\text{Na}_2\text{SO}_4$  and evaporated under reduced pressure. The residue was purified by silica column with gradient methanol/methylene chloride (1:100 to 4:100) as the eluent. Figure 3.10 shows the  $^1\text{H}$  NMR spectrum of the product in  $\text{CD}_3\text{CN}$ .

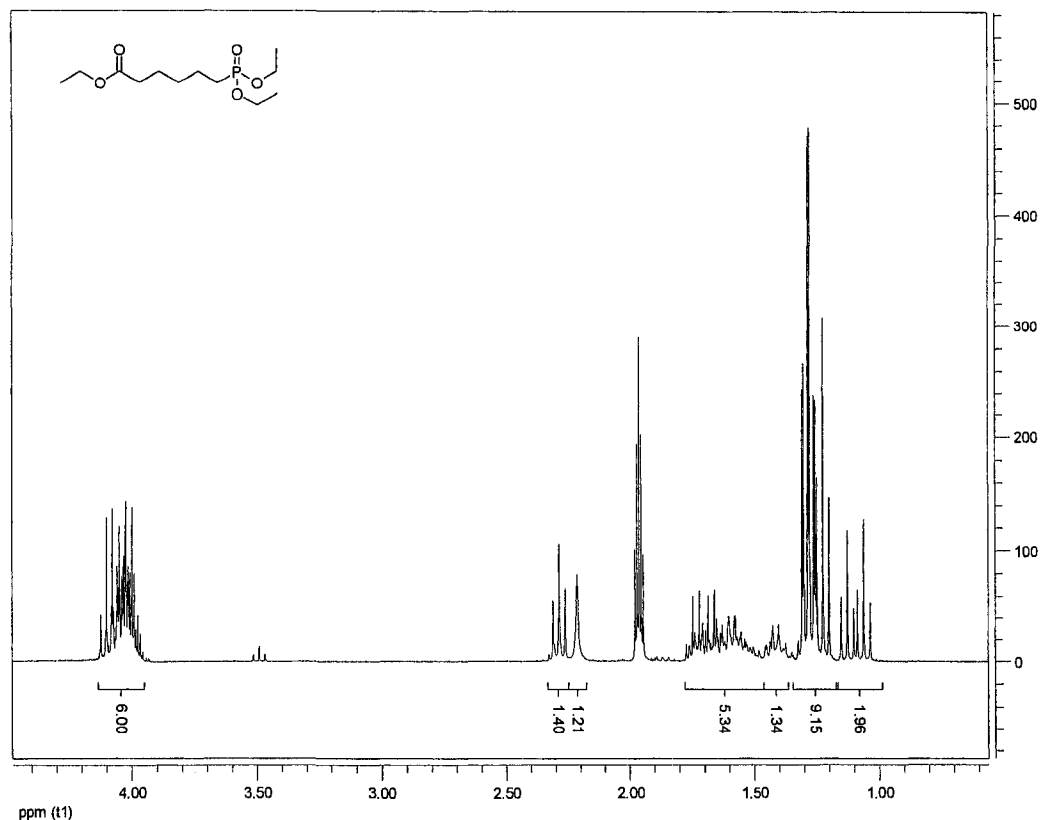


**Figure 3.10.**  $^1\text{H}$  NMR spectrum of 6-(diethylphosphono)-hexanoic acid ethyl ester in  $\text{CD}_3\text{CN}$ .

#### b) 6-phosphono-hexanoic acid (PHA)

The mixture of concentrated  $\text{HCl}$  (65 ml) and 6-(diethyl-phosphono)-hexanoic acid ethyl ester (4.5g, 0.016Mol) was refluxed for 24 hours. After cooling to room temperature, the mixture was extracted with ethyl acetate (50ml x 3) to remove unhydrolyzed ester. Then the aqueous solution was evaporated under reduced pressure and the residue was further dried at  $40^\circ\text{C}$  in vacuum overnight (yield 1.9g, 60%).  $^1\text{H}$  NMR and MS spectra of the product are shown in Figure 3.11 and Figure 3.12.

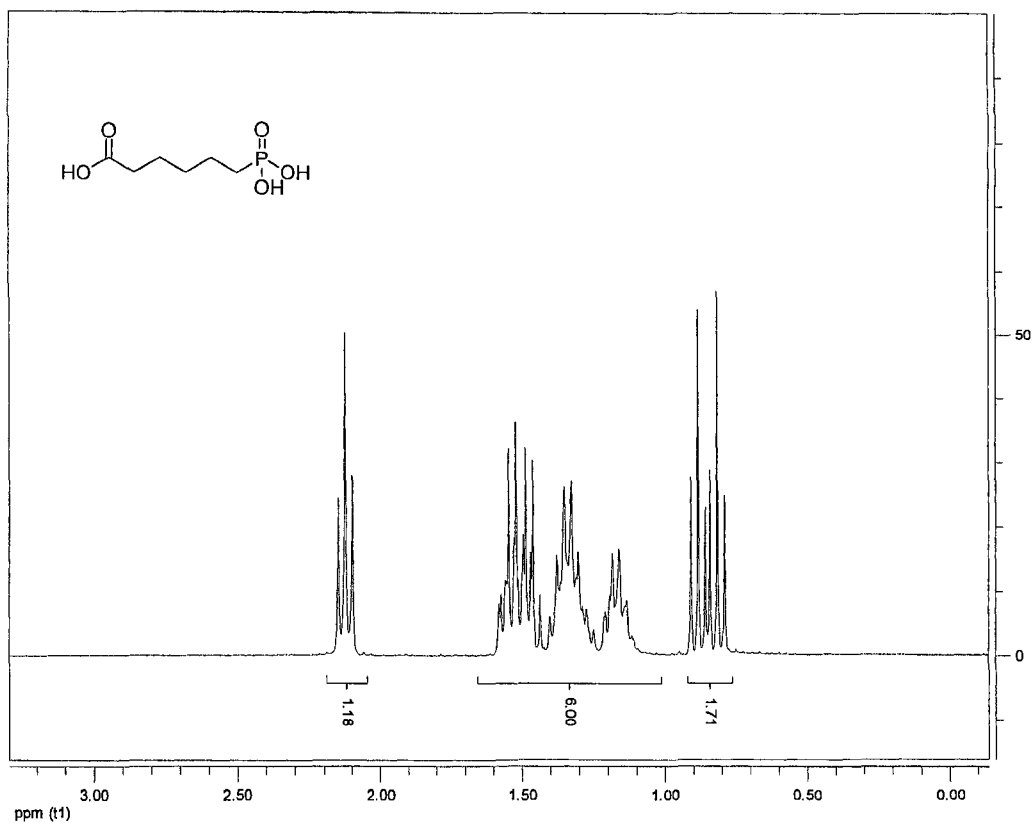


Figure 3.11.  $^1\text{H}$  NMR of 6-phosphono-hexanoic acid in  $\text{D}_2\text{O}$ .

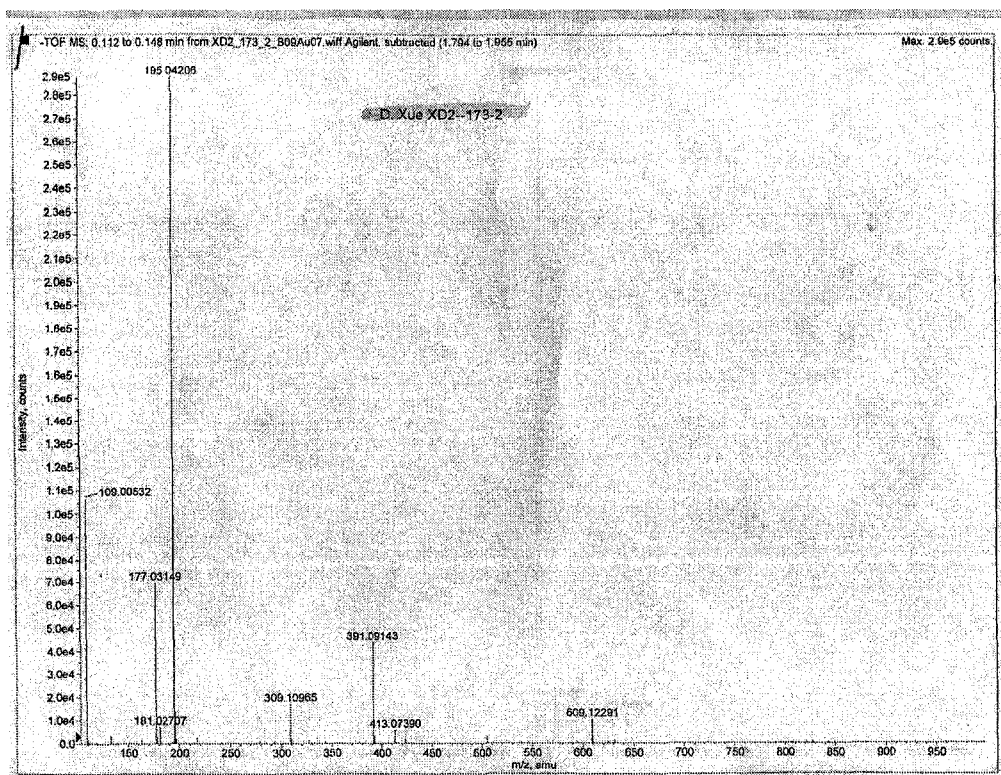
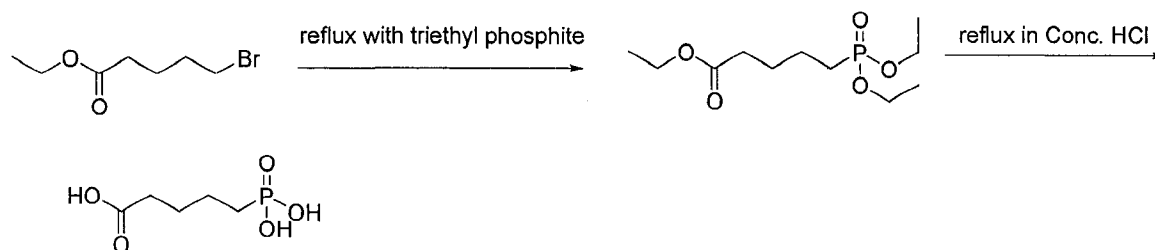


Figure 3.12. TOF MS of 6-phosphono-hexanoic acid.

4) 5-phosphono-pentanoic acid (PPEA)



a) 5-(diethyl-phosphono)-pentanoic acid ethyl ester

5-(diethyl-phosphono)-pentanoic acid ethyl ester was prepared following the procedure to prepare 6-(diethyl-phosphono)-hexanoic acid ethyl ester except that ethyl 5-bromopentanoate was used as the starting material instead of ethyl 6-bromohexanoate. Figure 3.13 shows the  $^1\text{H}$  NMR spectrum of 5-(diethyl-phosphono)-pentanoic acid ethyl ester in  $\text{CDCl}_3$ .

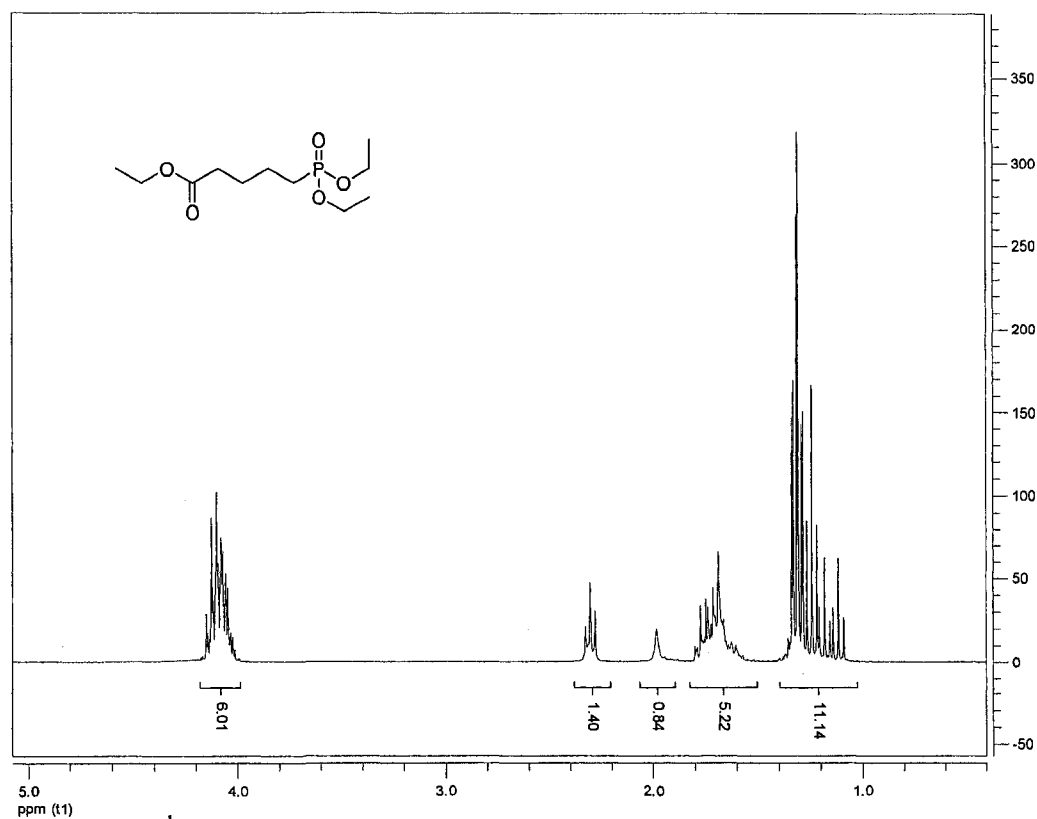


**Figure 3.13.**  $^1\text{H}$  NMR spectrum of 5-(diethylphosphono)-pentanoic acid ethyl ester in  $\text{CDCl}_3$ .

b) 5-phosphono-pentanoic acid (PPEA)

The mixture of concentrated HCl (45 ml) and 5-(diethyl-phosphono)-pentanoic acid ethyl ester (2.3g, 8.4 mMol) was refluxed for 24 hours and cooled to room temperature. After thorough extracting with ethyl acetate (50ml x 3) to remove unreacted ester, the aqueous solution was dried at 50°C under reduced pressure. The oily residue solidified upon drying in vacuum overnight, weighed 0.92 g (yield 60%). <sup>1</sup>H NMR and TOF MS spectra of the product are shown in Figure 3.14 and 3.15, respectively.

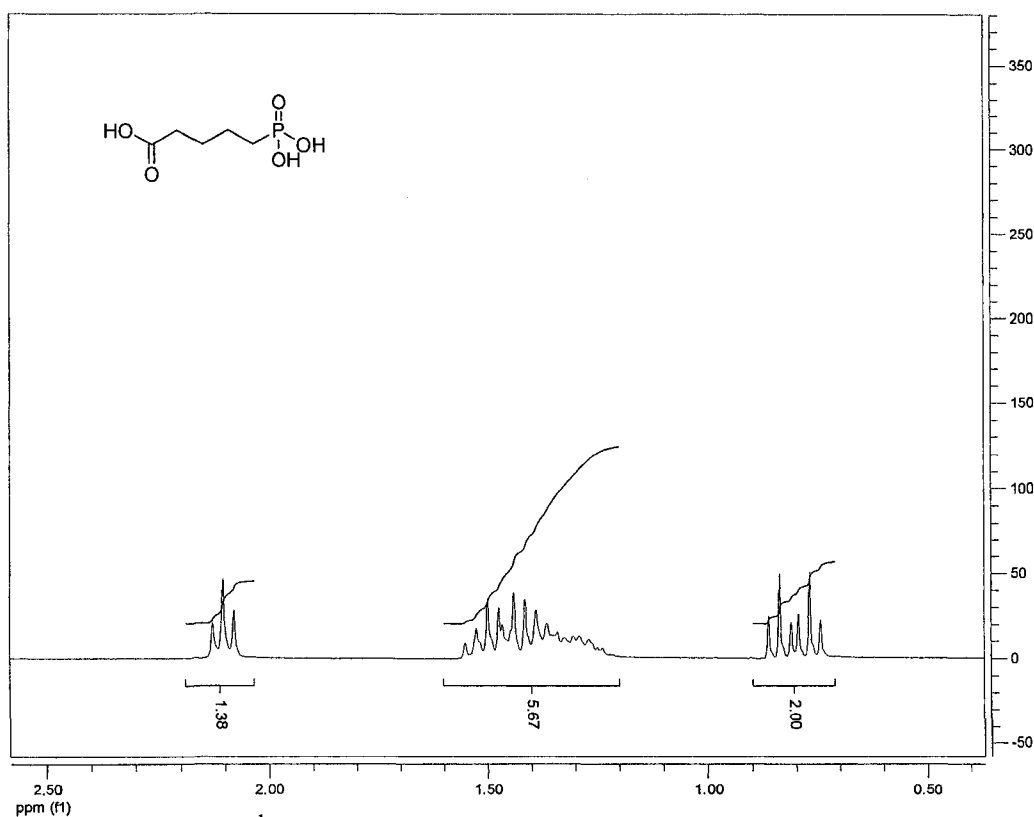


**Figure 3.14.** <sup>1</sup>H NMR spectrum of 5-phosphono-pentanoic acid in D<sub>2</sub>O.

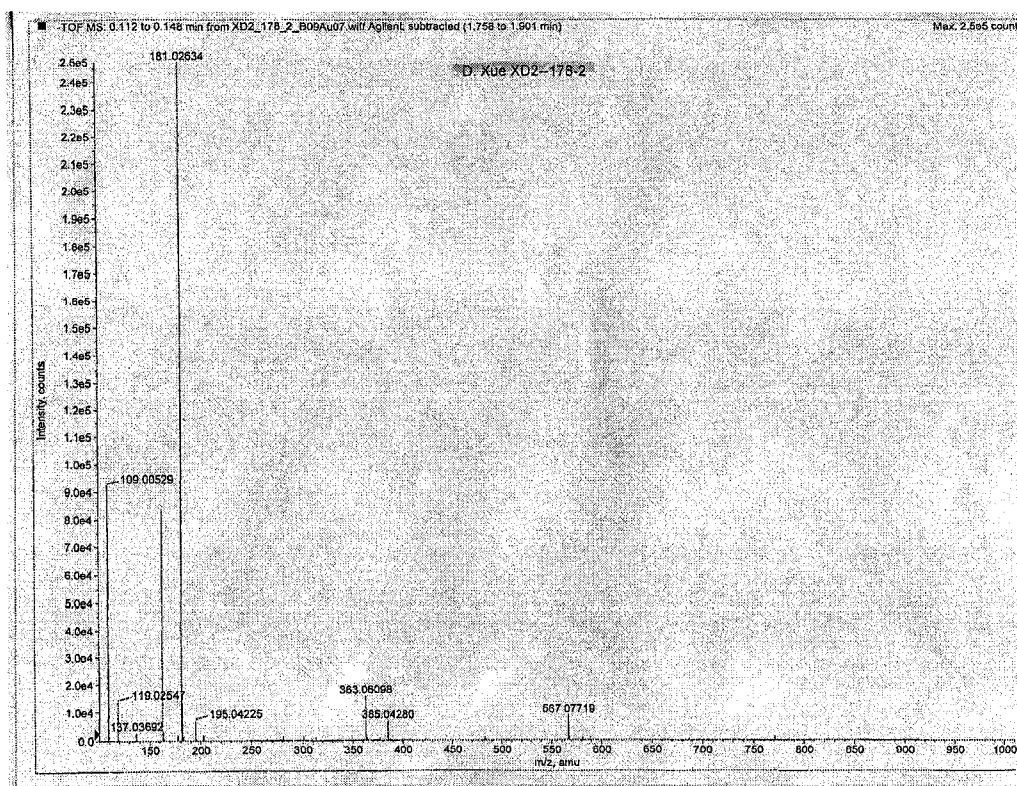


**Figure 3.15.** TOF MS of 5-phosphono-pentanoic acid.

## Functionalization of the ITO Electrodes

### 1) Electrode pretreatment

Each electrode was carefully cleaned by sonication in an Alconox/deionized (DI) water solution (approximately 1/2 tbsp in 100 mL) for 15 min, rinsed with 18 M $\Omega$  water and i-propanol, sonicated in i-propanol for 15 min, rinsed again with i-propanol, and sonicated in 18 M $\Omega$  water twice for 15 min each time and dried at 115 $^{\circ}$ C. Finally, the surfaces were cleaned using a Harrick PDC3XG air plasma cleaner for 35 min prior to surface functionalization.

## 2) Functionalization of ITO with (3-aminopropyl) trimethoxysilane

Method a): derivatization of the ITO surface with liquid silane dissolved in toluene.

The freshly cleaned ITO electrodes were soaked in 2M NaOH aqueous solution for 24 hours. After sonicating the surface with 18 M $\Omega$  water for 15 minutes and air-drying, adsorbed water was removed by drying at 115 °C for 4 h. The silanization reaction was carried out according to the procedure described by Vianello et al.<sup>32</sup> Under nitrogen, electrodes were treated overnight in a refluxing toluene solution containing 10% v/v (3-aminopropyl)trimethoxysilane. After amination, the electrodes were rinsed with toluene, iso-propanol followed by 18 M $\Omega$  water and cured at 115°C for 4 hours.

Method b): vapor deposition of (3-aminopropyl)trimethoxysilane on ITO surface

Figure 3.16 shows the experimental setup for vapor deposition of (3-aminopropyl)trimethoxysilane on the electrode surface. The high-temperature silane vapor (210°C at 1 atm) is very corrosive to ordinary metals, therefore a bottomless glass container and a Pt wire were used to hold the ITO electrode. The ITO electrode and its holders were vigorously cleaned. Meanwhile, the liquid (3-aminopropyl)trimethoxysilane contained in a round bottom double-neck flask was heated to boil and refluxed under N<sub>2</sub>. The freshly cleaned ITO electrode was quickly put into the flask while sitting in its glass holder. The ITO electrode was positioned above the liquid silane but underneath the reflux ring. The vapor deposition went on for 30 minutes. After cooling to room temperature, the electrode was taken out and quickly soaked in iso-propanol. Physically absorbed silane was removed by sonicating the electrode in iso-propanol for 15 minutes and then sonicating in 18 M $\Omega$  water for 15 minutes. The electrode was then blown dry with N<sub>2</sub>.

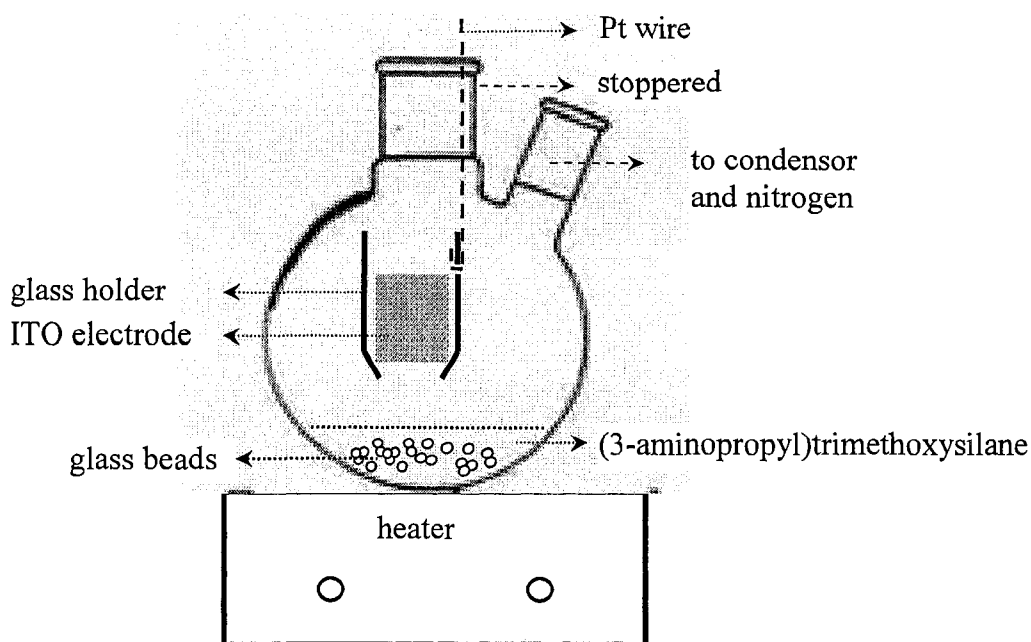


**Figure 3.16.** Experimental setup for vapor deposition of (3-aminopropyl)trimethoxysilane on the ITO electrode surface.

### 3) Succinylation of the silanized ITO surface.

Following Vianello's strategy,<sup>32</sup> the succinylation was performed under nitrogen, in anhydrous diethyl ether containing 10% v/v pyridine and 30 mM succinic anhydride. Each slide was immersed in the reacting solution in a closed 20-mL glass scintillation vials and left in an end-over-end stirrer overnight at room temperature. The slides, after rinsing with anhydrous diethylether were washed with ethylenediaminetetraacetic acid (EDTA) aqueous solutions, 18 MΩ water and air dried.

### 4) Functionalization of ITO with an $\alpha,\omega$ -dicarboxylic acid, sebacic acid

Functionalization of ITO with sebacic acid was done by following the procedures utilized by Napier et al.<sup>7</sup> and Hedges et al.<sup>4</sup> to grow 1,12-dodecanedicarboxylic acid monolayers on ITO surfaces. Carboxylic acid monolayers were physically bound by

immersion of the pretreated ITO substrates in 10 mM sebacic acid solution in acetonitrile for 24 hours. The functionalized substrates were thoroughly rinsed in acetonitrile and ethanol to remove weakly bound species.

## 5) Functionalization of ITO with $\omega$ -phosphonoalkyl carboxylic acid

### a) Functionalization of the ITO Electrodes with PDA

Following Eckhardt et al.,<sup>3</sup> the freshly cleaned ITO electrodes were soaked in 4 mM PDA solution in methanol for times ranging from 30 minutes to 24 hours. The unattached PDA was rinsed off the ITO electrodes with a gentle wash of water and the electrodes allowed to dry. To enhance the stability of the monolayer,<sup>33</sup> the functionalized electrode was cured at 115°C for 20 hs.

### b) Functionalization of the ITO Electrodes with PUA

The cleaned and dried ITO electrodes were soaked in a 5ml methanol solution of 10 mM PUA in a covered Petri dish of 5cm diameter, and were allowed to incubate for 20 hours with a gentle rocking motion of 25rpm at a 6° angle delivered by a Lab-Line Maxi rotator. The electrodes were rinsed with water, dried at room temperature and cured at 115°C for 20 hours. The rinsing procedure is very critical to maintain the monomer layer. Vigorous rinsing caused the monolayer to peel off. On the other hand, insufficient rinsing resulted in a thick PUA layer which acted as a barrier to electron transfer. Also, an excess of carboxy-alkyl phosphonate monolayer can lead to electrostatic inhibition of oligonucleotide probe binding and target hybridization.<sup>3</sup>

6) Functionalization of ITO with  $\omega$ -phosphonoalkyl carboxylic acid via  $ZrO_2$  coupling

Following the literature procedures<sup>1, 26</sup>, ITO electrodes was modified with  $ZrO_2$  followed by attachment of  $\omega$ -phosphonoalkyl carboxylic acid.

Step 1. Modification of ITO with  $ZrO_2$

Method a):<sup>26</sup> Clean ITO substrates were immersed in a 1mM zirconyl chloride aqueous solution at 55°C overnight, sonicated in water for 15 minutes, rinsed with water, cured at 100°C for 4 hours and subject to surface analysis.

Method b):<sup>1</sup> Solid  $Na_2SO_4$  50 mg was added into the solution of 100 ml water containing 1 mM zirconyl chloride, upon which white solid formed. The precipitate was removed by centrifuge filtration.  $Zr(IV)$  was coupled to the ITO surface by immersing the pretreated substrates in the supernatant at 55°C overnight. The electrodes were removed from solution, sonicated in water for 15 minutes and dried at room temperature. Water residues on the ITO surface was removed by heating the electrodes at 100°C for 4 hours.

Step 2. Functionalization of  $ZrO_2$  modified ITO with  $\omega$ -phosphonoalkyl carboxylic acid

**Table 3.1** the experimental conditions for treatment of ITO with different  $\omega$ -phosphonoalkyl carboxylic acids.

Derivatizing Solution in Methanol	ITO	ITO modified with $ZrO_2$
10 mM PUA	D1	Z1
10 mM PUA , 30 mM $NEt_3$	D2	Z2
10 mM PHA, 30 mM $NEt_3$	D3	Z3
10 mM PPEA, 30 mM $NEt_3$	D4	Z4
5 mM PUA, 5 mM PHA, 30 mM $NEt_3$	D5	Z5
5 mM PUA, 5 mM PPEA, 30 mM $NEt_3$	D6	Z6

Table 3.1 shows the experimental conditions to immobilize  $\omega$ -phosphonoalkyl carboxylic acid onto the ITO surface via  $ZrO_2$  coupling. For comparison purposes, the experiments also include ITO electrodes which are not pretreated with  $ZrO_2$ . Preliminary results showed that heat treatment of the PHA or PPEA functionalized ITO electrodes resulted in etching of the ITO thin films. Thus, triethyl amine was added into the solution to neutralize the acids. Derivatization of the ITO surface with the selected acid was done by immersing the substrates in the corresponding solution for 24 hours. Weakly bonded acids were removed by a gentle wash of methanol. The electrodes were then cured at  $110^\circ\text{C}$  for 20 hours and cooled to room temperature. To ensure a stable platform for DNA hybridization, the ITO electrodes were treated with the hybridization buffer by applying a drop of 2xSSC buffer onto the ITO surface. The electrodes were subsequently incubated in 100% humidity overnight, rinsed with  $18\text{ M } \Omega$  water, air dried and stored in a desiccator before use.

#### 7) Functionalization of ITO with $TiO_2$ and tantalum-doped conducting $TiO_2$

##### a) ITO modification with $TiO_2$

15 ml of absolute ethanol was equally divided into two cleaned and dried vials and was cooled to  $-30^\circ\text{C}$ . With brisk stirring,  $200\ \mu\text{l}$  of  $Ti(\text{isopropoxide})_4$  and  $40\ \mu\text{l}$  of 1M HCl were added individually into these cold ethanol vials. The two solutions were then mixed and stirred at room temperature for three days. A 1:5 dilution of the resultant solution with absolute ethanol followed by a filtration through a  $0.2\ \mu\text{m}$  syringe filter gave the coating solution.

A cleaned ITO substrate was spin-coated with the solution at 1600 rpm. The gel films were heat-treated in air at 450°C for one hour and then rinsed in ethanol.

b) ITO modification with conducting TiO<sub>2</sub>

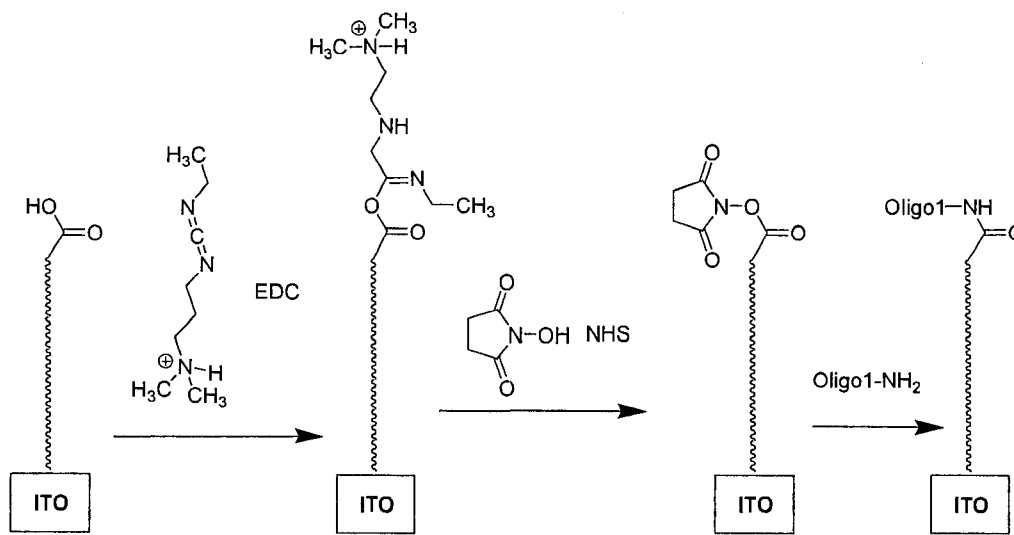
A solution of 45mg TaCl<sub>5</sub> in 2.0 ml absolute ethanol was filtered through a 0.2 μm syringe filter and cooled to 0°C. The solution became cloudy after an addition of 2.1 ml of Ti(isopropoxide)<sub>4</sub> and became clear again following an addition of 1.5 ml of -30°C absolute ethanol containing 1.0 mmole of HCl and 7.3 mmole of H<sub>2</sub>O. After being stirred at 0°C for 10 minutes and at 40°C for 1 hour, the solution was filtered through 0.2 μm syringe filter.

The solution prepared above was spin-coated onto a clean ITO electrode at 1600 rpm and heated at 700°C in air for one hour. After cooling to room temperature, glassy particles were found on the ITO surface and were gently removed with Kimwipe.

8) Electrochemical analysis of functionalized ITO surfaces

Preliminary results show that the catalyst Ru(BPB)<sub>2</sub>Cl<sub>2</sub> tends to strongly absorbed onto the bare ITO surface and exhibits catalytic activity toward oxidation of Co(DTB)<sub>3</sub><sup>2+</sup>. But a complete organic monolayer prevents this non-specific attachment from occurring. To tell whether all the active sites on surface were protected against the catalyst absorption, the electrodes were soaked in an acetonitrile solution of the catalyst for 15 minutes and then rinsed with acetonitrile to remove weakly bonded catalyst; after that, the electrodes were put in an acetonitrile solution of Co(DTB)<sub>3</sub>](ClO<sub>4</sub>)<sub>2</sub> with 100 mM TMAPF<sub>6</sub> and scanned to obtain current-to-voltage responses.

### Probe DNA Attachment on Functionalized ITO Electrodes



**Scheme 3.1.** Activation of the surface -COOH by EDC/ NHS and followed by covalent bonding of the DNA probe oligo1-NH<sub>2</sub> onto the ITO surface. Oligo1-NH<sub>2</sub> = 5'-CTGAACGGTAGCATCTTGAC-(CH<sub>2</sub>)<sub>6</sub>-NH<sub>2</sub>-3'.

As shown in Scheme 3.1, the terminal -COOH groups on the ITO surface were sequentially activated by ethylenediacarbodiimide (EDC); *N*-hydroxysuccinimide (NHS). The produced NHS-ester intermediate was then attacked by the terminal amine of the 3' modified probe to form an amide bond.

To realize the covalent coupling of the probe to the -COOH monolayer, the solution containing the probe (oligo1-NH<sub>2</sub>, 20  $\mu$ M) and the coupling agent (EDC 60 mM and NHS 15 mM) in MES buffer (pH=6.0, 0.1M MES with 0.25 M NaCl) was carefully applied to the ITO electrode (50  $\mu$ l solution for each single ITO electrode, 10  $\mu$ l for each ITO spot for the array electrode or 0.5  $\mu$ l for the microarray electrode) and was allowed to incubate in 75% humidity at room temperature for 14 hours. The electrode was rinsed with water and dried in the air. The probe modified ITO electrodes were stored in a desiccator before use.

## RESULTS AND DISCUSSION

### Functionalization of ITO with (3-Aminopropyl)-trimethoxysilane

Both a chemical solution deposition method, noted as method a), and a vapor deposition method, noted as method b), were used to derivatize ITO substrates with (3-aminopropyl)-trimethoxysilane (vide infra). Surfaces of the silanized ITO electrodes were characterized by X-ray Photoelectron Spectroscopy (XPS).

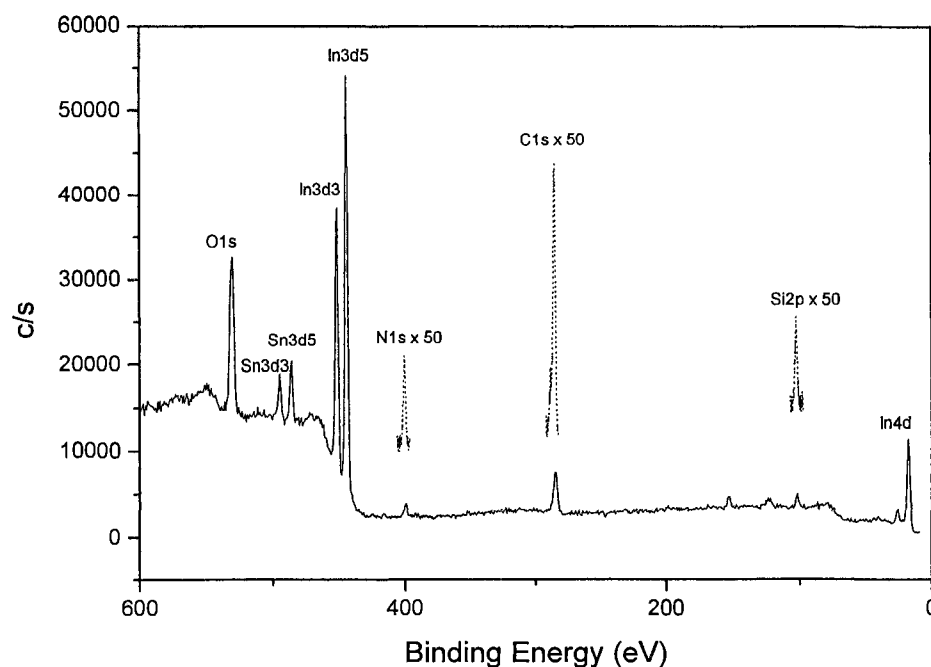


**Figure 3.17.** XPS spectrum of ITO functionalized with (3-aminopropyl) trimethoxysilane via method a), a survey scan along with high resolution scans (x 50) of N1s, C1s and Si2p (dotted curves).

XPS spectra (Figure 3.17 and Figure 3.18) show the presence of silicon, carbon, and nitrogen on the ITO surfaces. Substrates functionalized via method a) showed increases in silicon and nitrogen signals and a decrease in carbon, compared to those functionalized via method b), suggesting that method b) delivered a lower surface density of silane but a higher carbon contamination. During functionalization of ITO substrates using method b), refluxing of an unknown liquid (b.p.  $\sim 150^{\circ}\text{C}$ ) in the vapor-deposition flask was

observed before reaching the boiling point of (3-aminopropyl) trimethoxysilane ((b.p. 210°C). This heat-generated impurity might contaminate the ITO surface, preventing dense deposition of (3-aminopropyl) trimethoxysilane. Thus, electrodes functionalized with method a) instead of method b) were used for further reactions as follows.

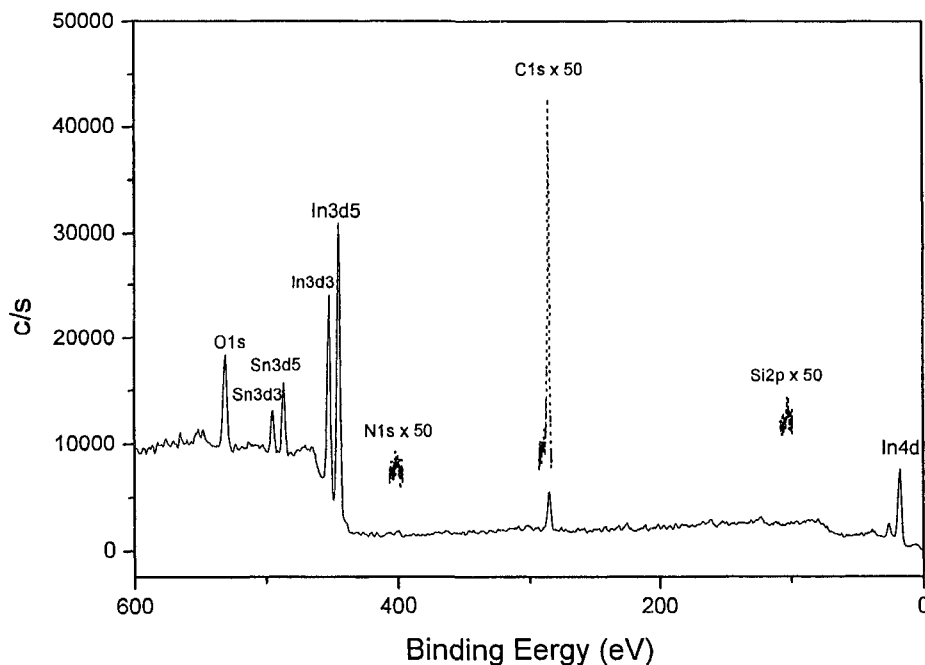


**Figure 3.18.** XPS spectrum of ITO functionalized with (3-aminopropyl) trimethoxysilane via method b), a survey scan along with high resolution scans (x 50) of N1s, C1s and Si2p (dotted curves).

### Acylation of Silanized ITO Surfaces

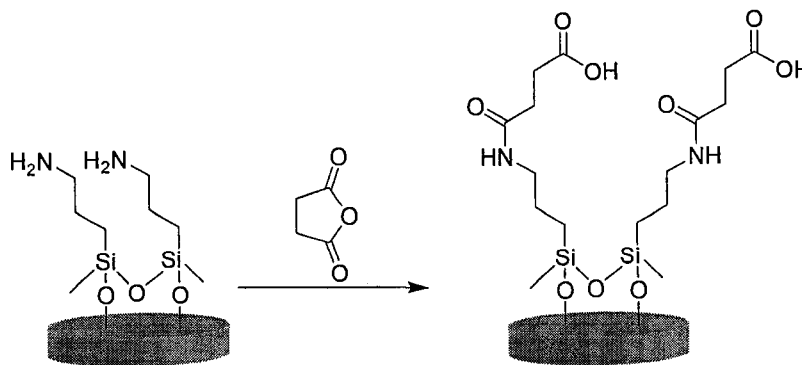


**Figure 3.19.** Schematic illustration of surface acylation of silane functionalized ITO electrode.

The  $\text{-COOH}$  groups were introduced on the ITO surface by treating the silanized surfaces with succinic anhydride,<sup>32</sup> as shown in Figure 3.19. The acylating reaction were confirmed by XPS analysis. As can be observed in Figure 3.20, the intensity of high-resolution Si2p signal decreased by a factor of 0.7 after acylation, indicating a 30% silane loss on the ITO surface. Consequently, the C1s signal after acylation is normalized by a factor of  $1/0.7$  for easy comparison with that before acylation (Figure 3.21).

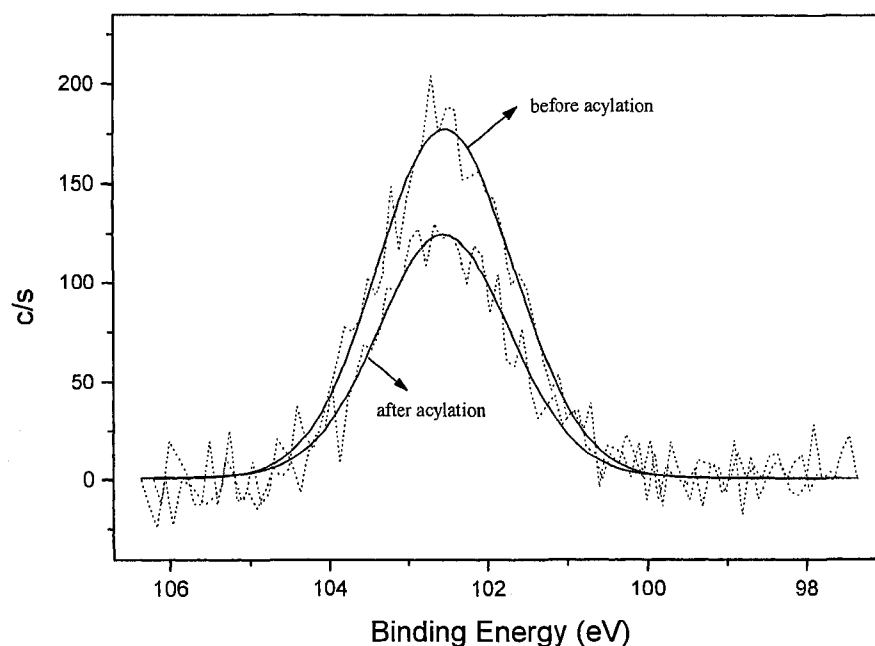


**Figure 3.20.** XPS spectra of high resolution Si2p for (3-aminopropyl) trimethoxysilane modified ITO surface (via method a)) before and after succinic anhydride treatment.

While precise assignment of each signal to particular carbon atoms cannot be certain, the spectrum provides evidence for acylation of the terminal amines on the ITO surface. Specifically, the appearance and increase in C1s peaks at binding energies of 288.0 eV and 284.6 eV arise from electron-deficient carbon atoms adjacent to

electronegative atoms (e.g., nitrogen and oxygen) and aliphatic carbon atoms, as one would expect from simple qualitative considerations of the surface acylation reaction (Figure 3.18).

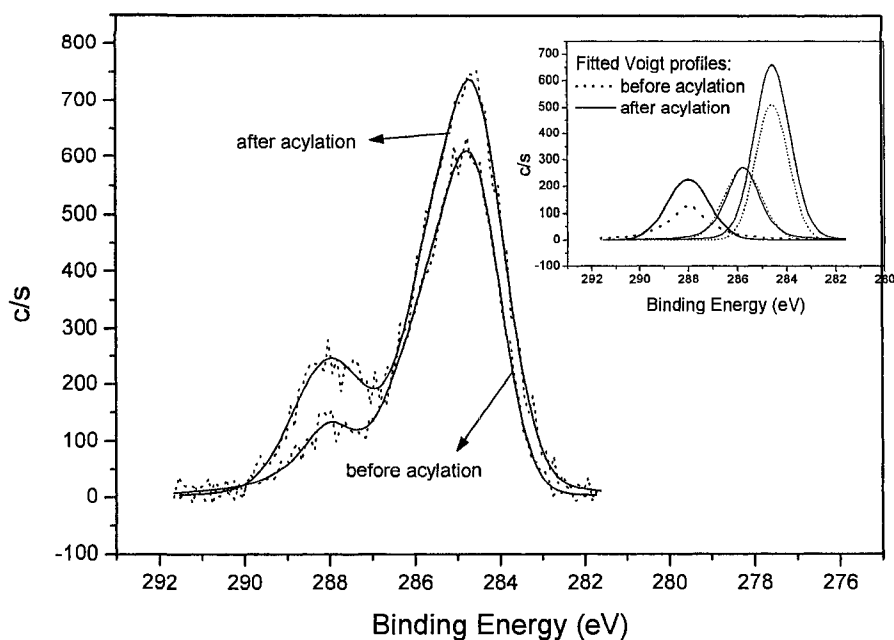


**Figure 3.21.** XPS spectra of high resolution C1s for (3-aminopropyl) trimethoxysilane modified ITO surface (via method a)) before and after succinic anhydride treatment. The insertion shows the fitted Voigt profiles.

After acylation, the electrodes were treated with the catalyst  $\text{Ru}(\text{BPB})_2\text{Cl}_2$  and electrochemically analyzed in a solution of 0.3 mM  $[\text{Co}(\text{DTB})_3](\text{ClO}_4)_2$ , the data are shown in Figure 3.22. Upon catalyst treatment, the electrode gave rise to a significant catalysis toward  $\text{Co}(\text{DTB})_3^{2+}$  oxidation, suggesting that not all the active sites on the ITO surface were covered by the monolayer and the catalyst was non-specifically absorbed onto the exposed ITO surface. Zeng et al.<sup>1</sup> also reported an incomplete coverage of the ITO surface by silane.

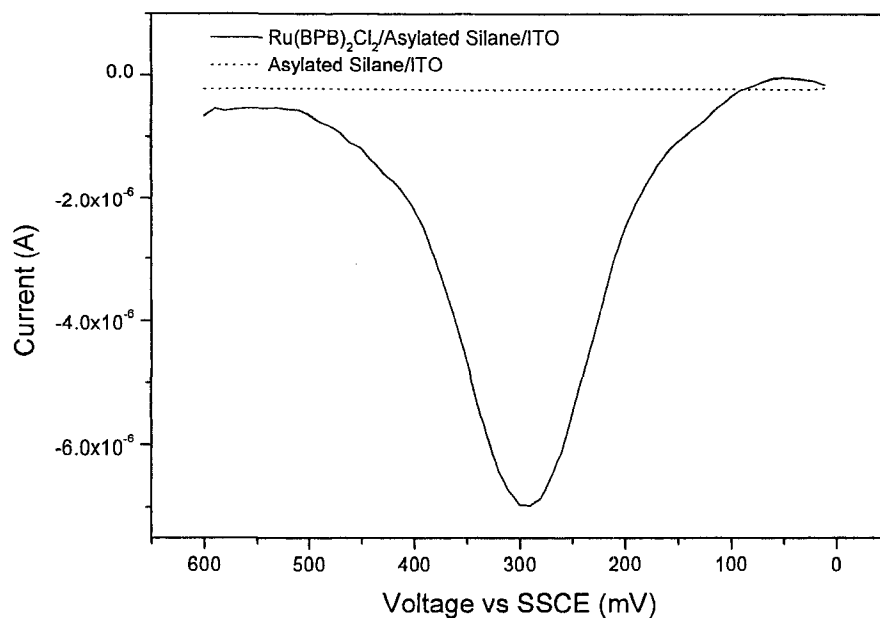


**Figure 3.22.** DPVs of ITO electrodes with and without treatment with  $\text{Ru}(\text{BPB})_2\text{Cl}_2$  in an acetonitrile solution containing 0.3 mM  $[\text{Co}(\text{DTB})_3](\text{ClO}_4)_2$  and 100 mM TMAPF<sub>6</sub>. The electrodes were pre-functionalized with (3-aminopropyl) trimethoxysilane via method a), followed by acylation with succinic anhydride.

### Functionalization of ITO with Sebacic Acid

Figure 3.23 shows the XPS C1s signal for a clean ITO electrode and a sebacic acid-derivatized ITO electrode. In 24 hours, a sebacic acid monolayer was formed as shown from comparison before and after treatment with sebacic acid solutions. The sebacic acid molecules are believed to attach onto the ITO surface via one of the carboxylic acid groups, while the nonpolar interaction along the carbon chains and the hydrogen bonding among the other carboxylic acid ends help the formation of the self assembled monolayer.<sup>4, 7</sup>

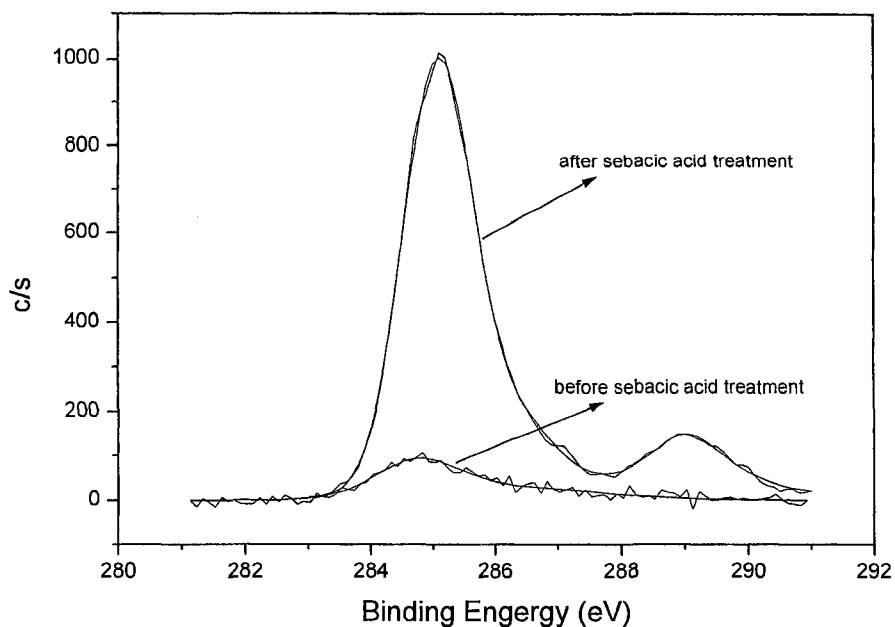


**Figure 3.23.** XPS C1s high resolution spectra (sample depth 2 nm, 15° takeoff angle) of clean ITO and sebacic acid-derivatized ITO electrodes.

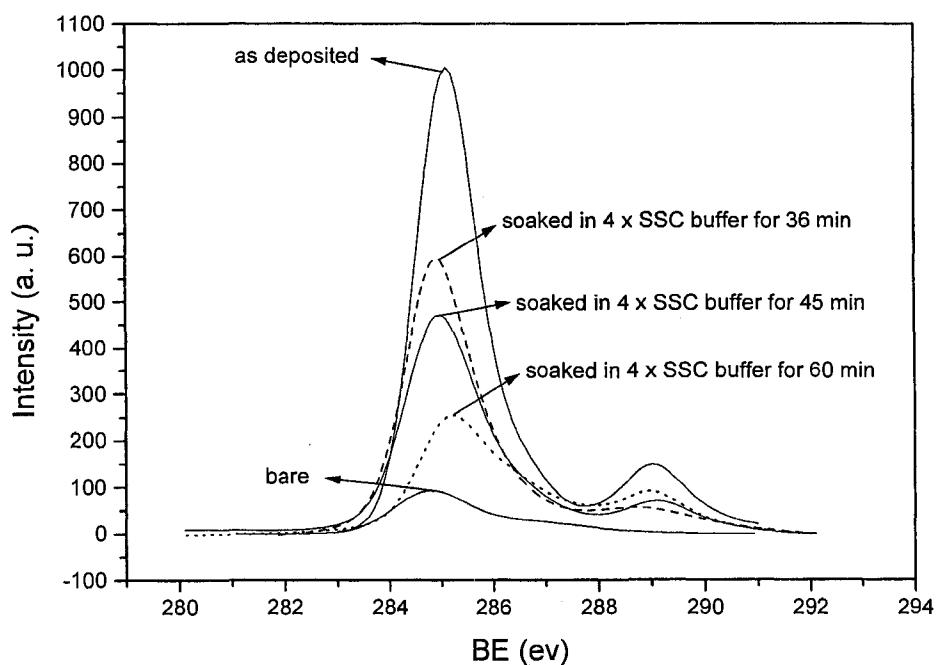


**Figure 3.24.** XPS C1s high resolution spectra (sample depth 2 nm, 15° take off angle) of bare ITO and sebacic acid-derivatized ITO electrodes after soaking in 4 x SSC buffer (pH=7.0) for a certain amount of time. For easy comparison purposes, only fitted Voigt profiles are shown.

Stability of the obtained monolayer against hybridization buffer was tested. The as-deposited films were immersed in a hybridization buffer 4 x SSC of pH=7.0. After specified amounts of time, the electrodes were removed from solution, rinsed with water and air dried. XPS analysis of the electrode were carried out to determine the surface composition. The results are shown in Figure 3.24 on the previous page. Upon soaking the film, the C1s XPS signal started decreasing. Within 60 minutes, the XPS intensity decreased to a level close to that for a vigorously cleaned bare ITO surface, indicating that most of the sebacic acid molecules have left the surface. The poor stability of this sebacic acid monolayer might account for its bad repeatability encountered earlier in this study.

### Functionalization of ITO $\omega$ -Phosphonoalkyl Carboxylic Acid

#### a) Functionalization of the ITO Electrodes with PDA

A monolayer of PDA was formed through selective binding of the phosphonate groups onto the surface of ITO<sup>3,6</sup> and the pendent carboxylic acid groups were left for the attachment of the probe DNA modified with terminal amine groups. XPS analysis of the PDA modified ITO surfaces is shown in Figure 3.25.

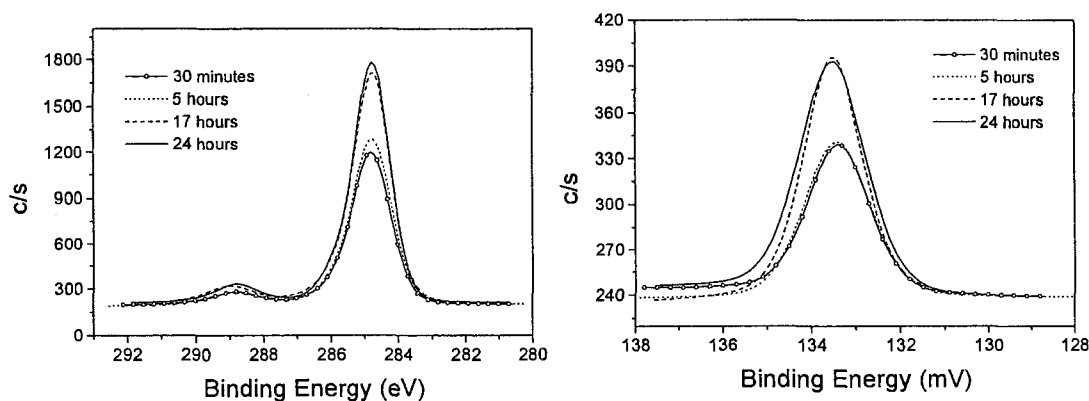


**Figure 3.25.** XPS C1s (on the left) and P2p (on the right) high resolution spectra of ITO after soaking in the PDA/methanol solution for the specified time.

It can be seen that the C1s and P2p XPS signals of the ITO surface increased as the soaking duration extended from 30 minutes to 17 hours. Further extension to 20 hours didn't alter the XPS intensity, suggesting that the absorption and formation of the PDA layer was complete within 17 hours of soaking. Compositional calculation shows that the atomic % of C1s is 12 times of that of P2p, which is in accordance with PDA's molecular formula  $C_{12}H_{25}O_5P$ .

#### b) Functionalization of the ITO Electrodes with PUA

As previously mentioned, preparation of PUA started from 11-bromoundecanoic acid. It took three steps (esterification, phosphonation and acid hydrolysis) to finish the synthesis. Due to the limitation of starting materials availability, preparation of PDA started from 12-hydroxydodecanoic acid and it was a four-steps (esterification, bromination, phosphonation and acid hydrolysis) synthesis. Moreover, the starting material for PDA costs 26 times more than that for PUA (Aldrich price). Thus optimizing the PUA modification process is of great economic importance.

Our research found that incubation of the ITO electrodes for 20 hours in the 10 mM PUA solution with gentle swirling at 25rpm through a  $6^\circ$  angle gave the best results. The depth of the PUA solution above the ITO surface without swirling was optimized to be 2.5 mm. Under these conditions, the electrode stays in solution most of the time but alternately goes in and out of the solution, which allows two potential ways for building the PUA monolayer: self assembling of the PUA molecules at the electrode/solution interface and Langmuir-Blodgett transfer of the PUA film from the air/solution interface to the electrode/solution interface.<sup>34</sup> The as-deposited PUA films were meticulously

rinsed with water, dried at room temperature and cured at 115°C for 20 hours. Figure 3.26 show a XPS survey scan and C1s and P2p elemental scans of the PUA modified ITO surface. The presence of the P2p peak on the spectrum confirmed a PUA adlayer on the ITO surface. Electrochemical analysis of the surface coverage of the PUA film and its stability toward hybridization buffer will be discussed later in section 6.

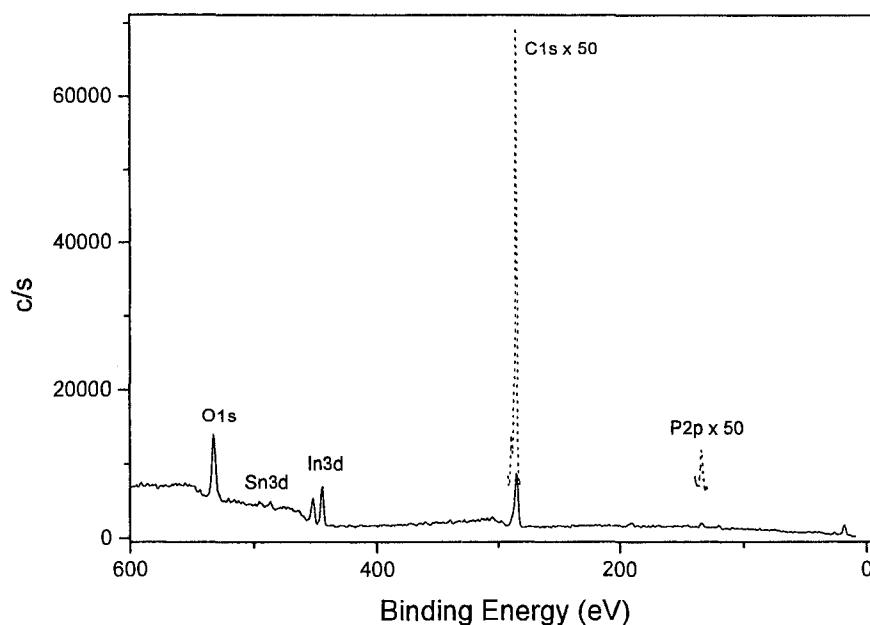


**Figure 3.26.** XPS spectrum of ITO functionalized with PUA, a survey scan along with high resolution scans (x 50) of C1s, and P2p.

### Modification of ITO with $ZrO_2$

Zr(IV) has been reported to have a strong tendency to react with ITO.<sup>35</sup> In addition, Zr(IV)-phosphonate linkage has previously been used to produce well defined multilayers of zirconium bisphosphonates<sup>36</sup> and provide for a monolayer of aldehyde groups for DNA attachment.<sup>1</sup> During this research, the ITO surfaces were activated by the aqueous solution of zirconyl chloride with (noted as method a) or without (noted as method b)

Na<sub>2</sub>SO<sub>4</sub>. XPS analysis shows the presence of Zr on the activated surfaces. As can be seen from comparison of Figure 3.27 with Figure 3.28, method b) produced a surface of higher Zr(IV) density. According to Zeng et al.,<sup>1</sup> addition of a weak base Na<sub>2</sub>SO<sub>4</sub> into the acidic solution of zirconyl chloride caused slow hydrolysis of the Zr(IV) salt, which was beneficial for Zr(IV) deposition on the ITO surface.

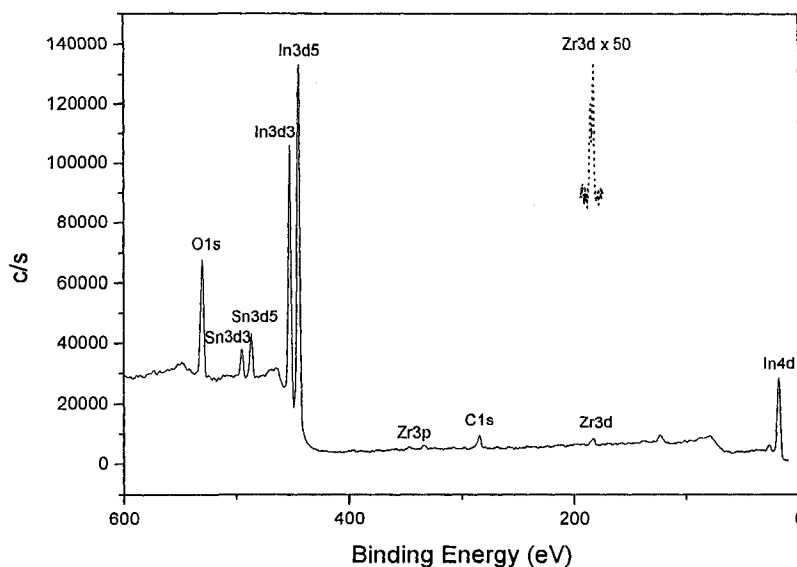


**Figure 3.27.** XPS spectrum of ITO after functionalization with zirconyl chloride via method a), a survey scan along with a utility scan (x 50) of Zr3d.

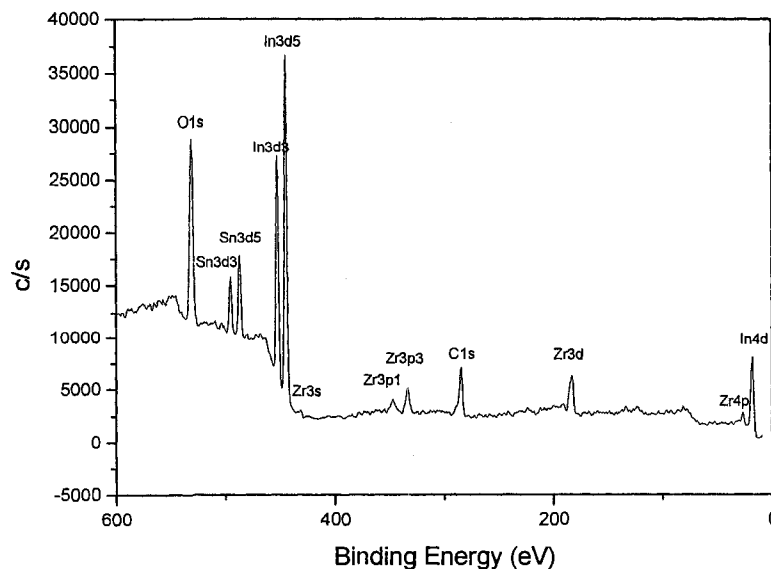


**Figure 3.28.** XPS survey scan of ITO functionalized with Zr(IV) via method b).

## Functionalization of ITO with $\omega$ -Phosphonoalkyl Carboxylic Acid via $ZrO_2$ Coupling

ITO electrodes activated with Zr(IV) via method b) and those that were not activated at all were simultaneously functionalized with selected  $\omega$ -phosphonoalkyl carboxylic acid (PUA, PHA or PPEA). Preliminary results showed that the acids PHA or PPEA tended to etch the ITO films during thermal curing of the acid treated electrodes, which was done to enhance the stability of the acid monolayer.<sup>33</sup> As such, triethyl amine ( $NEt_3$ ) was added into the coating solution to neutralize the acids. Since PUA was not corrosive to ITO even at elevated temperatures, functionalization of ITO with both neutralized PUA and un-neutralized PUA was done to investigate the amine effect.

After removal of excess acids by overnight hybridization buffer treatment, the electrodes were challenged with a solution of  $Ru(BPB)_2Cl_2$  and subject to electrochemical analysis in 1 mM  $Co(DTB)_3](ClO_4)_2$  solution. The electrochemical data are shown in Figure 3.28.

As the electrochemical results suggested, unfortunately, Zr(IV) pre-treatment of the ITO surface did not help significantly in suppressing non-specific attachment of the catalyst. This might be due to the fact that deposition of the  $ZrO_2$  was not optimized during this research and the literature didn't provide for a detailed and accurate procedure description. More efforts have to be made to make this strategy to work, for example, morphology control of the  $ZrO_2$  layer through optimizing the sol-gol formation conditions and the coating conditions.

From comparison of Figure 3.28 B and Figure 3.26 C, it can be seen that the modification performance of PUA was not significantly affected by neutralization of acid with  $NEt_3$ , which is consistent with Schuler's discovery<sup>37</sup> that self-assembled monolayers

on smooth  $\text{TiO}_2$  produced in aqueous solutions of ammonium salt of dodecyl phosphonic acid were similar in quality as the ones produced in organic solvents of the free acid.

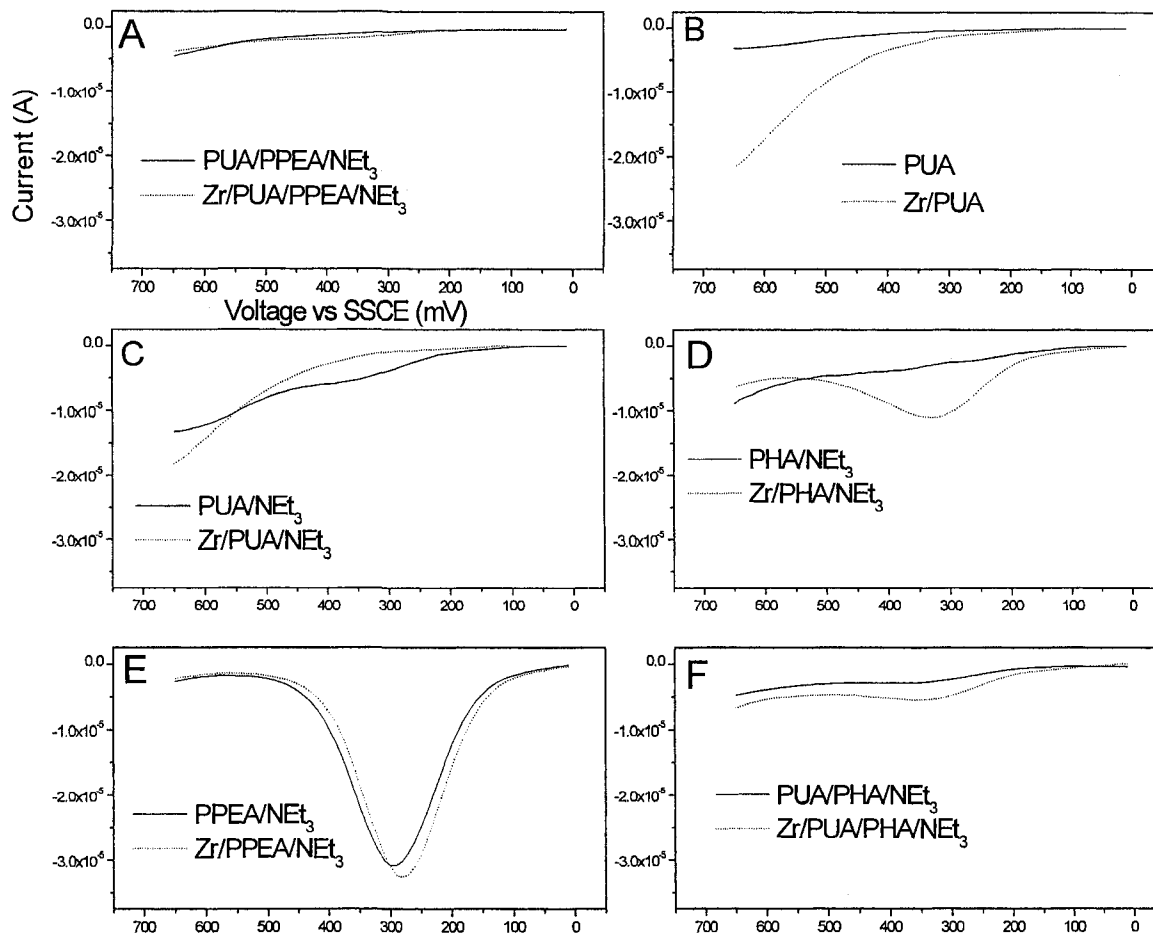


**Figure 3.28.** DPVs of  $\text{Ru}(\text{BPB})_2\text{Cl}_2$  treated ITO electrodes in the acetonitrile solution of 1 mM  $\text{Co}(\text{DTB})_3(\text{ClO}_4)_2$  and 100 mM  $\text{TMAPF}_6$ . The solid curve is for electrodes that were not pre-treated with Zr(IV) prior to the acid treatment; the dashed curve is for electrodes treated with selected acid via Zr(IV) coupling. A) ITO electrodes treated with neutralized 1:1 PUA/PPEA; B) ITO electrodes treated with un-neutralized PUA; C) ITO electrodes treated with neutralized PUA; D) ITO electrodes treated with neutralized PHA; E) ITO electrodes treated with neutralized PPEA; F) ITO electrodes treated with neutralized 1:1 PUA/PHA.

The results also lead to the discovery that the PUA and 1:1 PPEA/PUA functionalized ITO surfaces were free of non-specific binding of the catalyst even though the surfaces were pre-treated with the hybridization buffer overnight, suggesting a

complete surface coverage and a stable organic layer. Another advantage of the mixed acid PPEA/PUA monolayer is the easy electron transfer through the PPEA “defects” from DNA to the ITO surface, as shown in Figure 3.29.

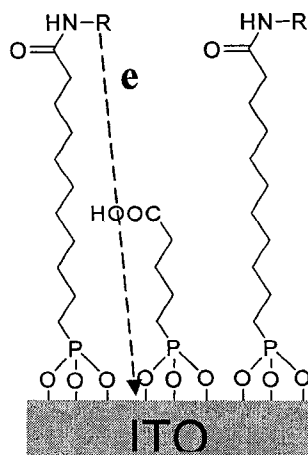


**Figure 3.29.** Schematic illustration of electron transfers from DNA to the ITO surface through PPEA centered “defects”. R represents the ds-DNA.

### Functionalization of ITO with $\text{TiO}_2$ and Tantalum-Doped Conducting $\text{TiO}_2$

Modification of transparent metal oxide electrodes with  $\text{TiO}_2$  has been extensively studied for solar cell applications.<sup>38-44</sup> Besides, the procedure to grow alkanephosphonic acids monolayers on the native oxide surface of titanium was also well established.<sup>45</sup> Taking advantage of the ample literature results, functionalization of ITO surfaces with  $\text{TiO}_2$  or tantalum-doped conducting  $\text{TiO}_2$  films was carried out and the modified surfaces were characterized by XPS and electrochemical methods.

The XPS analysis results are shown in Figure 3.30 and Figure 3.31. The presence of  $\text{Ti}2p$  and  $\text{Ti}3p$  peaks indicate a  $\text{TiO}_2$  film on the ITO surface. XPS compositional calculation shows that the two films have similar  $\text{Ti}/\text{In}$  ratio (Table 3.2). Nevertheless, it

is hard to tell whether Ta was present by the XPS results since the Ta4f peaks overlaps with the Sn4d peaks and the Ta4p peaks overlaps with the Ti2p3 peak.

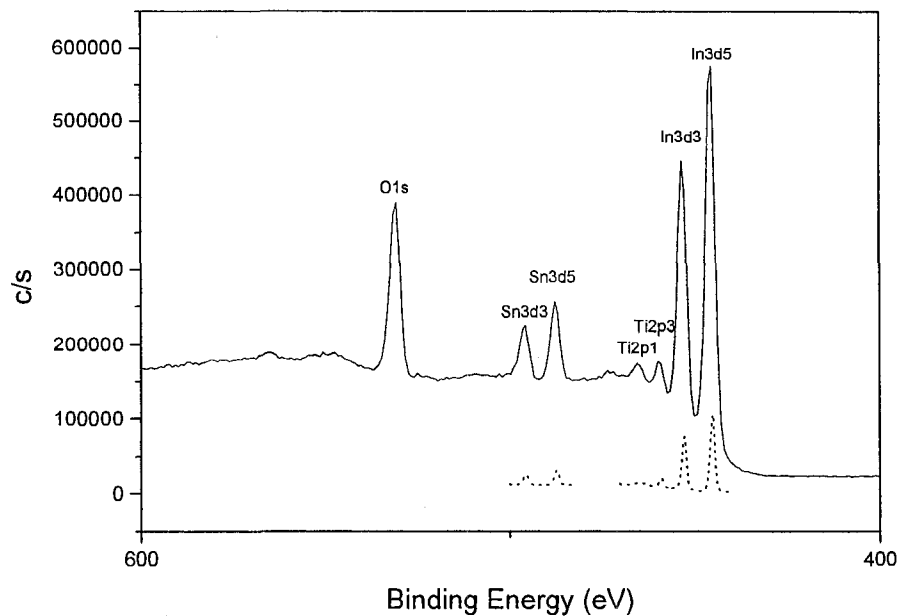


**Figure 3.30.** XPS of TiO<sub>2</sub> modified ITO surface, a survey scan (the solid curve) and high resolution scans of Sn3d, Ti2p, and In3d (dashed curves). 45° take off angle.

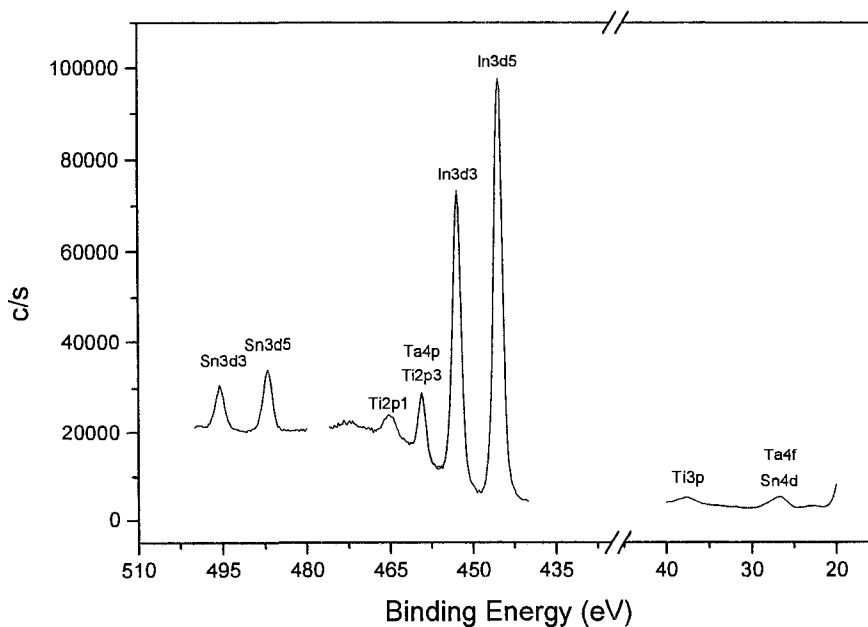


**Figure 3.31.** XPS analysis of the Ta-doped-TiO<sub>2</sub> modified ITO surface, high resolution scans of Sn3d, Ti2p, In3d and Ta4p and Ta4f. 45° take off angle.

**Table 3.2.** XPS elemental composition analysis of ITO surfaces modified with TiO<sub>2</sub> and conducting TiO<sub>2</sub>

ITO surface	Atomic % of Ti	Atomic % of In
Modified with TiO <sub>2</sub>	32.9	57.1
Modified with conducting TiO <sub>2</sub>	35.7	54.3

The results of electrochemical analysis of the modified ITO electrodes are shown in Figure 3.32 and Figure 3.33. CVs of the electrodes were obtained in the solution of [Co(DTB)<sub>3</sub>](ClO<sub>4</sub>)<sub>2</sub> and Ru(BPB)<sub>2</sub>Cl<sub>2</sub>. Figure 3.32 reveals that Ru(BPB)<sub>2</sub>Cl<sub>2</sub> was redox sluggish on the ITO electrode modified with TiO<sub>2</sub>, suggesting a thick TiO<sub>2</sub> layer. However, doping the TiO<sub>2</sub> film with tantalum increased its electronic conductivity so that Ru(BPB)<sub>2</sub>Cl<sub>2</sub> exhibited catalytic activity on the electrode surface toward [Co(DTB)<sub>3</sub>](ClO<sub>4</sub>)<sub>2</sub> oxidation, as shown in Figure 3.33. Therefore, derivatizing the conducting TiO<sub>2</sub> treated ITO surfaces with carboxylic acid for DNA attachment purposes is a challenging task worth the efforts.

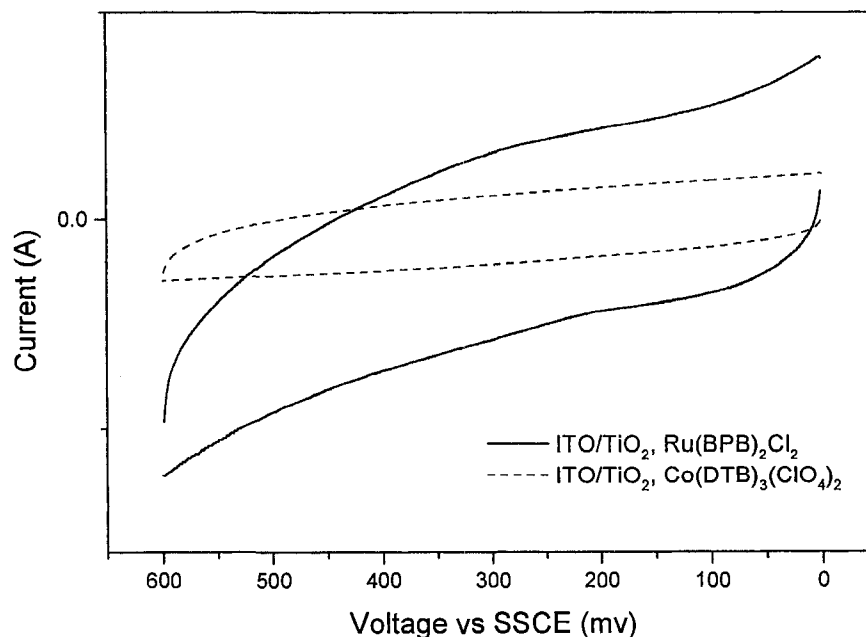


**Figure 3.32.** CVs of [Co(DTB)<sub>3</sub>](ClO<sub>4</sub>)<sub>2</sub> (dashed line) and Ru(BPB)<sub>2</sub>Cl<sub>2</sub> (solid line) on TiO<sub>2</sub> modified ITO electrodes. 100 mM TMAPF<sub>6</sub>/ACN; R.E., SSCE; C.E., Pt; 100 mV/s.

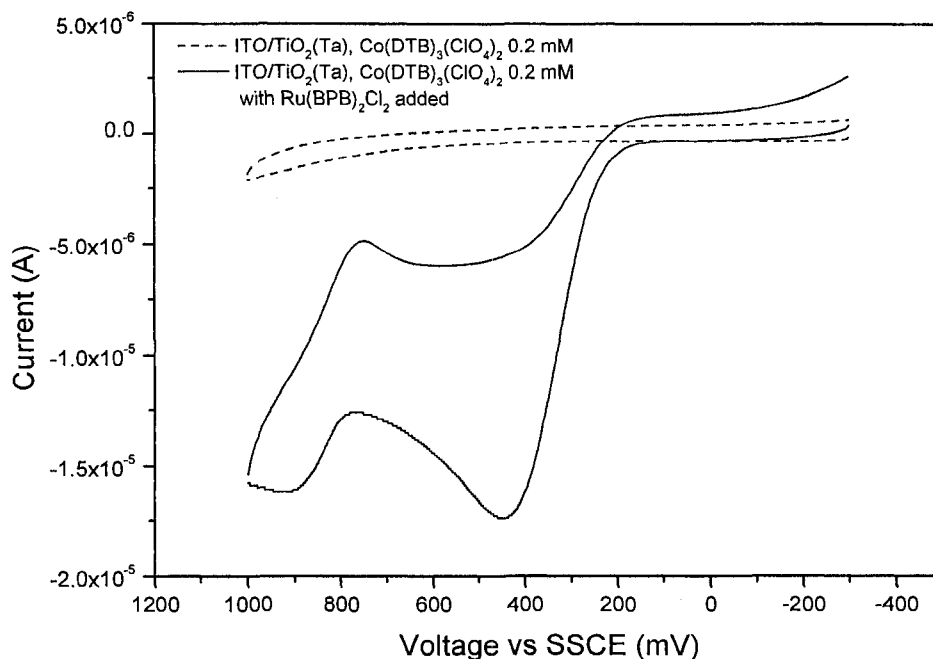


**Figure 3.31.** CVs of  $[\text{Co}(\text{DTB})_3](\text{ClO}_4)_2$  with (solid line) and without (dashed line)  $\text{Ru}(\text{BPB})_2\text{Cl}_2$  on the ITO electrode modified with conducting  $\text{TiO}_2$ . 100 mM  $\text{TMAPF}_6/\text{ACN}$ ; R.E., SSCE; C.E., Pt; 100 mV/s.

### Probe DNA Attachment on Functionalized ITO Electrodes

XPS, traditionally a materials science analytical technique, has been shown to be an efficient, label-free method for studying DNA on a surface.<sup>14, 30, 46, 47</sup> In this study, substantial amounts of phosphorous (4-6 at. %) from functional phosphonic acid layer precluded efficient use of phosphorous for XPS study of DNA immobilization, leaving nitrogen as the only unique characteristic element. Table 3.3 shows typical XPS data for the probe DNA attachment onto functionalized ITO surfaces. It lists XPS high resolution N1s peak area comparing immobilization of DNA probes with (positive control) and without (negative control 4) terminal aminoalkyl groups. The table also lists the results for a vigorously cleaned bare ITO surface (negative control 1). Besides, activation of the

surface  $\text{-COOH}$  groups with coupling agents ethylenedicarbodiimide (EDC) and *N*-hydroxysuccinimide (NHS) (negative control 2) as well as immobilization of the probe oligo1-( $\text{CH}_2$ )<sub>6</sub>- $\text{NH}_2$  in the absence of EDC and NHS (negative control 3) are also examined.

According to Hermanson,<sup>48</sup> amine-derivatization after DNA oligomer probe synthesis is a convenient synthetic strategy to enable microarray probe immobilization: nucleophilic amine functional groups readily covalently react with NHS active esters to create covalent amide linkages. Oligonucleotides lacking amine functional groups can also attach to surfaces via either physisorption (e.g., combinations of hydrogen bonding, acid-base, hydrophobic, electrostatic interactions) or possibly (though unlikely due to poor nucleophilicity at printing  $\text{pH} < 11$ ) covalent attachment through pyrimidine or purine amine groups pendant on nucleotide bases.<sup>49-52</sup> As shown in Table 3.3, EDC/NHS-treated substrate surface displayed a N1s peak of area 104, which can be attributed to activation of hydrolyzed carboxylic acid moieties to form NHS ester functional groups.<sup>29</sup> Grafting of the probe Oligo1-( $\text{CH}_2$ )<sub>6</sub>- $\text{NH}_2$  onto the substrate surface via EDC/NHS coupling gave a notable increase in the XPS N1s intensity ( $280-104=176$ ); comparatively, retention of probe Oligo1, which lacks the reactive terminal amine groups, gave much less N1s signal ( $158-104=54$ ), suggesting that immobilization of the probe was dominated by covalent bonding rather than physisorption. In addition, challenging the surface with a solution containing Oligo1-( $\text{CH}_2$ )<sub>6</sub>- $\text{NH}_2$  but not the coupling agents gave a small N1s peak of area 35, indicating a small amount of physically attached probes.

Table 3.3 XPS N 1s peak areas

Experiments	Positive Control	Negative Control 1	Negative Control 2	Negative Control 3	Negative Control 4
EDC 60 mM NHS 15 mM	✓	✗	✓	✗	✓
oligo1-(CH <sub>2</sub> ) <sub>6</sub> -NH <sub>2</sub> 20 μM	✓	✗	✗	✓	✗
oligo1 20 μM	✗	✗	✗	✗	✓
XPS N1s peak area	280	0	104	35	158

### Summary

Carboxylic functional groups have been introduced onto ITO surfaces utilizing silane chemistries, aliphatic  $\alpha,\omega$ -dicarboxylic acid modification as well as  $\omega$ -phosphonoalkyl carboxylic acid modification. Electrochemical analysis of the functionalized surfaces shows an incomplete surface coverage by the silane layer and the XPS results suggest poor stability of the sebacic acid monolayer, leaving  $\omega$ -phosphonoalkyl carboxylic acid modification as the best choice.

In this study, functionalization of ITO surfaces was optimized by selecting the best modifier among a number of  $\omega$ -phosphonoalkyl carboxylic acids. PUA was chosen over PDA due to ease of synthesis and starting material availability at low price. Both PUA and 1:1 PPEA/PUA modified ITO surfaces are free of non-specific catalyst attachment, suggested by the electrochemical results. PUA modified surfaces have been successfully used for DNA hybridization detection (see the following chapter). Moreover, insertion of PPEA molecules (HO)<sub>2</sub>OP-(CH<sub>2</sub>)<sub>4</sub>-COOH into the PUA (HO)<sub>2</sub>OP-(CH<sub>2</sub>)<sub>10</sub>-COOH] layer

is expected to facilitate heterogeneous electron transfers owing to the shorter tunneling distance through PPEA. DNA hybridization detection using 1:1 PPEA/PUA modified ITO electrodes will be discussed in the next Chapter.

Attempts to enhance stability of the  $\omega$ -phosphonoalkyl carboxylic acid monolayer by activation of the substrate surface with Zr(IV) failed, possibly due to the poor quality of the ZrO<sub>2</sub> thin film, which demands more work in the future. There is no doubt that an optimized Zr(IV) coupling will increase the stability and repeatability of the monolayer to endure harsh hybridization conditions, for example, high temperature or high pH detections. Additionally, ITO electrodes treated with conducting TiO<sub>2</sub> films exhibited promising catalytic activity toward Co(DBT)<sub>3</sub><sup>2+</sup> oxidation and might provide for an interesting platform for DNA hybridization sensing.

1. Zeng, J.; Krull, U. J., *ChimicaOggi/ChemistryToday* **2003**, 48-52.
2. Diehl, F.; Grahlmann, S.; Beier, M.; Hoheisel, J. D., *Nucleic Acids Research* **2001**, 29(7), e38.
3. Eckhardt, A. E.; Mikulecky, J. C.; Napier, M. E.; Thomas, R. S.; Thorp, H. H. Monolayer and electrode for detecting a label-bearing target and method of use thereof *U.S.* **2002**.
4. Hedges, D. H. P.; Richardson, D. J.; Russell, D. A., *Langmuir* **2004**, 20, (5), 1901-1908.
5. Li, J.; Wang, H.; Zhao, Y.; Cheng, L.; He, N.; Lu, Z., *Sensors* **2001**, 1, 53-59.
6. Lowe, L. B.; Brewer, S. H.; Kraemer, S.; Fuierer, R. R.; Qian, G.; Agbasi-Porter, C. O.; Moses, S.; Franzen, S.; Feldheim, D. L., *Journal of the American Chemical Society* **2003**, 125, (47), 14258-14259.
7. Napier, M. E.; Thorp, H. H., *Langmuir* **1997**, 13, (23), 6342-6344.
8. Xu, J.; Zhu, J.-J.; Zhu, Y.; Gu, K.; Hong-YuanChen, *ANALYTICAL LETTERS* **2001**, 34(4), 503-512.
9. Cerruti, M. G.; Sauthier, M.; Leonard, D.; Liu, D.; Duscher, G.; Feldheim, D. L.; Franzen, S., *Analytical Chemistry* **2006**, 78, (10), 3282-3288.
10. Moses, S.; Brewer, S. H.; Kraemer, S.; Fuierer, R. R.; Lowe, L. B.; Agbasi, C.; Sauthier, M.; Franzen, S., *Sensors and Actuators, B: Chemical* **2007**, B125, (2), 574-580.
11. Armistead, P. M.; Thorp, H. H., *Analytical Chemistry* **2001**, 73, (3), 558-564.
12. Armistead, P. M.; Thorp, H. H., *Bioconjugate Chemistry* **2002**, 13, (2), 172-176.
13. Johnston, D. H.; Cheng, C.-C.; Campbell, K. J.; Thorp, H. H., *Inorganic Chemistry* **1994**, 33, (26), 6388-90.
14. Petrovykh, D. Y.; Kimura-Suda, H.; Tarlov, M. J.; Whitman, L. J., *Langmuir* **2004**, 20, 429.
15. Yang, I. V.; Ropp, P. A.; Thorp, H. H., *Analytical Chemistry* **2002**, 74, (2), 347-354.
16. Wei, H.; Wang, E., *Chemistry Letters* **2007**, 36, (2), 210-211.
17. Wei, M.-Y.; Guo, L.-H.; Chen, H., *Microchimica Acta* **2006**, 155, (3-4), 409-414.
18. Arora, K.; Chaubey, A.; Singhal, R.; Singh, R. P.; Pandey, M. K.; Samanta, S. B.; Malhotra, B. D.; Chand, S., *Biosensors & Bioelectronics* **2006**, 21, (9), 1777-1783.
19. Prabhakar, N.; Arora, K.; Singh, S. P.; Pandey, M. K.; Singh, H.; Malhotra, B. D., *Analytica Chimica Acta* **2007**, 589, (1), 6-13.
20. Prabhakar, N.; Arora, K.; Singh, S. P.; Singh, H.; Malhotra, B. D., *Analytical Biochemistry* **2007**, 366, (1), 71-79.
21. Prabhakar, N.; Sumana, G.; Arora, K.; Singh, H.; Malhotra, B. D., *Electrochimica Acta* **2008**, 53, (12), 4344-4350.
22. Wang, L.-R.; Qu, N.; Guo, L.-H., *Analytical Chemistry (Washington, DC, United States)* **2008**, 80, (10), 3910-3914.
23. Vanickova, M.; Buckova, M.; Labuda, J., *Chemia Analityczna (Warsaw)* **2000**, 45, (1), 125-133.
24. Zhong, J.; Qi, Z.; Dai, H.; Fan, C.; Li, G.; Matsuda, N., *Analytical Sciences* **2003**, 19, (5), 653-657.

25. Wang, J.; Rivas, G.; Cai, X.; Shiraishi, H.; Fariasp, P. A. M.; Dontha, N.; Luo, D., *Analytica Chimica Acta* **1996**, 332, (2-3), 139-144.
26. Hong, H. G.; Kim, Y., *Journal of Electroanalytical Chemistry* **2000**, 489, (1-2), 106-110.
27. Mazzola, L. T.; Frank, C. W.; Fodor, S. P. A.; Mosher, C.; Lartius, R.; Henderson, E., *Biophys. J.* **1999**, 76, 2922.
28. Forman, J. E.; Walton, I. D.; Stern, D.; Rava, R. P.; Trulson, M. O., *ACS Symp. Ser.* **1998**, 682, 206.
29. Gong, P.; Grainger, D. W., *Surface Science* **2004**, 570, (1-2), 67-77.
30. Gong, P.; Harbers, G. M.; Grainger, D. W., *Analytical Chemistry* **2006**, 78, (7), 2342-2351.
31. Pawsey, S.; McCormick, M.; De Paul, S.; Graf, R.; Lee, Y. S.; Reven, L.; Spiess, H. W., *Journal of the American Chemical Society* **2003**, 125, (14), 4174-4184.
32. Vianello, F.; Zennaro, L.; Di Paolo, M. L.; Rigo, A.; Malacarne, C.; Scarpa, M., *Biotechnology and Bioengineering* **2000**, 68, (5), 488-495.
33. Hanson, E. L.; Schwartz, J.; Nickel, B.; Koch, N.; Danisman, M. F., *Journal of the American Chemical Society* **2003**, 125, (51), 16074-16080.
34. XU, J.; ., H.-L. L., *Journal of Colloid and Interface Science* **1995**, 176, (1), 138-149.
35. Schwartz, J.; Bernasek, S. L., *Catalysis Today* **2001**, 66, (1), 3-13.
36. Stockhause, S.; Neumann, P.; Schrader, S.; Kant, M.; Brehmer, L., *Synthetic Metals* **2002**, 127, (1-3), 295-298.
37. Schuler, M.; Tosatti, S.; Gruner, P.; Garg, R.; Textor, M. Stability of Self-Assembled Alkane phosphate/-phosphonate Monolayers on Smooth Titanium Oxide. Semester Thesis, Swiss Federal Institute of Technology, CH-8092 Zurich, Switzerland 2002.
38. Elliott, C. M.; Sapp, S. A.; Bignozzi, C. A.; Contado, C.; Caramori, S. *PCT Int. Appl.* **2003**.
39. Sapp, S. A.; Elliott, C. M.; Contado, C.; Caramori, S.; Bignozzi, C. A., *Journal of the American Chemical Society* **2002**, 124, (37), 11215-11222.
40. Hart, J. N.; Cheng, Y.-B.; Simon, G. P.; Spiccia, L., *Journal of Nanoscience and Nanotechnology* **2008**, 8, (5), 2230-2248.
41. Li, J.; Huang, Q., *Taiyangneng Xuebao* **2008**, 29, (2), 139-144.
42. Kitamura, T.; Matsui, H.; Okada, K., *Hyomen Gijutsu* **2008**, 59, (3), 172-176.
43. Kawaraya, M., *Seramikkusu* **2008**, 43, (3), 170-176.
44. Prezhdo, O. V.; Duncan, W. R.; Prezhdo, V. V., *Accounts of Chemical Research* **2008**, 41, (2), 339-348.
45. Gawalt, E. S.; Avaltroni, M. J.; Koch, N.; Schwartz, J., *Langmuir* **2001**, 17, (19), 5736-5738.
46. Leavitt, A. J.; Wenzler, L. A.; Williams, J. M.; Thomas, J.; Beebe, P., *J. Phys. Chem.* **1994**, 98, 8742.
47. Saprigin, A. V.; Thomas, C. W.; Dulcey, C. S.; Patterson, C. H.; Spector, M. S., *Surf. Interface Anal.* **2004**, 36, 24.
48. Hermanson, G. T., *Bioconjugate Techniques*, Academic Press (1995).
49. Sehgal, D.; Vijay, I. K., *Anal. Biochem.* **1994**, 218, 87.
50. Huang, E.; Zhou, F.; Deng, L., *Langmuir* **2000**, 16, 3272.

51. Millan, K. M.; Mikkelsen, S. R., *Anal. Chem.* **1993**, 65, 2317.
52. Millan, K. M.; Saraullo, A.; Mikkelsen, S. R., *Anal. Chem.* **1994**, 66, 2943.

## Chapter 4: DNA Hybridization Detection Based on Catalytic Oxidation of $\text{Co}(\text{DTB})_3^{2+}$

### INTRODUCTION

This chapter focuses on electrochemical sensing of DNA hybridization events in solution. Sensors fabricated through silane monolayers, sebacic acid monolayers, PDA monolayers, PUA monolayers as well as mixed acid PUA/PPEA monolayers were used. The results for detection of target DNA (complementary or mismatched) at various concentrations ranging from micromolar to picomolar and even subpicomolar are reported. Detections of micromolar targets were performed at various concentrations of  $\text{Co}(\text{DTB})_3^{2+}$ . The used sensing platforms varied in size from 7 mm to  $100\mu\text{m}$ , including single electrodes of 7 mm diameter, 7x8 array electrodes of 3 mm diameter and 1x 8 microarray electrodes of 1 mm x 0.1 mm.

In addition, this study also explores detection of a synthetic target DNA in a dilute blood serum matrix. Stability of the functional organic monolayer toward the serum solution of different pH was investigated. Serum treatments of the sensor surface at different stages during target DNA sensing were made to study the serum effect on the detecting performance of the biosensor. Finally, sensing of complementary target DNA in the presence of serum was carried out.

Parallel to the electrochemical measurements, XPS and fluorescence microscope imaging were also used to investigate the surface hybridization chemistry.

Based on previous findings, this part concludes the overall study of indirect electrochemical sensing of DNA hybridization based on catalytic oxidation of  $\text{Co}(\text{DTB})_3^{2+}$  on ITO and proposes what should be done in the near future.

## EXPERIMENTAL

### Materials

*Table 4.1.* Oligonucleotide sequences and modifications

	5' modification	oligonucleotide sequence	3' modification
A	Oligo1-(CH <sub>2</sub> ) <sub>6</sub> -NH <sub>2</sub>	CTGAACGGTAGCATCTTGAC	-(CH <sub>2</sub> ) <sub>6</sub> -NH <sub>2</sub>
B	Oligo2	GTCAAGATGCTACCGTTCAG	
C	Oligo1	CTGAACGGTAGCATCTTGAC	
D	Cy5-Oligo2	Cy5	GTCAAGATGCTACCGTTCAG
E	Cy3-Oligo1	Cy3	CTGAACGGTAGCATCTTGAC

The DNA oligonucleotides were purchased from TriLink Biotechnologies. Table 4.1 lists all the sequences and modifications of the oligonucleotides used for this work. As previously mentioned, Oligo A was used as the probe. Oligo B was the complementary target and Oligo C the mis-matched target. Oligos D and E were used as the dye-labeled complementary and mis-match target, respectively. They were used for fluorescence imaging. Serum was prepared from human blood with high speed centrifuge (performed in the Hartshorn Health Center lab at Colorado State University) and stored at -30°C when not in use.

### Sensor Fabrication

Description of sensor fabrication were previously detailed in Chapter 2. Briefly, a monolayer with terminal carboxylic acid was formed on the ITO surface (cleaned 35 minutes with a Harrick PDC3XG air plasma cleaner) and then the 3'-modified probe Oligo1-(CH<sub>2</sub>)<sub>6</sub>-NH<sub>2</sub> was covalently attached to the carboxylic acid terminated monolayer via EDC/NHS coupling. Example coupling conditions are 20 μM probe, 60 mM EDC

and 15 mM NHS for 14 hours in 75% humidity in a 0.1M MES buffer at pH 6.0 with 0.25 M NaCl.

### **Hybridization of Single ITO Biosensors with Target DNA**

#### a) Micromolar target

Hybridization of the probe DNA mobilized on single ITO sensors (0.5 cm<sup>2</sup>) with target DNA was performed in 2 x SSC buffer (pH=7.0). A 50 µl solution containing 2 µM target (the complementary target oligo2 or mismatched target oligo1) was carefully spread onto the sensor surface with an Eppendorf pipette and the electrode was incubated at room temperature in 100 % humidity for 10 hours. After rinsing with 2 x SSC and then with cold 0.2 x SSC, the sensor was blown dry with nitrogen.

#### b) Nanomolar target

The sensors modified with probe ss-DNA were soaked with gentle rocking for 10 hours in a 5mL 2 x SSC buffer solution containing 3 nM complementary target oligo2 or mismatched target oligo1, rinsed with 2 x SSC followed with cold 0.2 x SSC, and blown dry with nitrogen. The gentle rocking stir of the hybridization solution was delivered by a Lab-Line Maxi rotator at 25 rpm through a 6° rotation.

#### c) Picomolar target

The sensors were soaked with gentle rocking in a 25mL 2 x SSC buffer solution containing 4 pM complementary target oligo2 for 24 hours. The electrodes were then rinsed with 2 x SSC buffer followed with cold 0.2 x SSC, and blown dry with nitrogen.

### **Hybridization of Array ITO Biosensors with Target DNA**

The array electrode used here consists of 7 x 8 ITO spots with an active area of 7 mm<sup>2</sup> for each spot. Initially, all the ITO spots were identically modified to attach probe ss-DNA. Then half of the spots in alternate positions on the array were challenged with a 10 µL 2 x SSC buffer solution containing 2 µM complementary target Oligo2. The array was incubated at room temperature in 100% humidity for 10 hours, and the solution was carefully removed with a capillary pipette. Then, 15 µl of 2 x SSC buffer was added to each target treated spot with an Eppendorf pipette, incubated for a few minutes, and was removed with a separate capillary pipette. This washing procedure was repeated two more times, and the array was rinsed with a cold 0.2 x SSC wash bottle, blown dry with nitrogen.

### **Hybridization of Micoarray ITO Biosensors with Target DNA**

Fabrication of the ITO microarray was mentioned in Chapter 2. Each array contains eight individual microelectrodes. Prior to probe immobilization, areas of the microelectrodes were electrochemically calibrated by comparing the current response of an acetonitrile solution containing 1mM Fe(DMB)<sub>2</sub>(CN)<sub>2</sub> and 100 mM TMAPF<sub>6</sub>, using a single ITO electrode (0.5 cm<sup>2</sup>) as the standard. The results for micorarray #1, micorarray #2 and micorarray #3 are shown in Table 4.2, Table 4.3 and Table 4.4, respectively. These three microarrays provide for 24 microelectrodes which were all identically modified with PUA monolayer to attach probe ss-DNA. Hybridization with complementary target DNA was carried out in 2 x SSC buffer at four different concentrations, 3nM, 30pM, 3pM, and 0.3pM, with each concentration assigned with six microelectrodes. Each electrodes was challenged with a 0.5µl Oligo2 solutions and

allowed to incubate at room temperature in 100% humidity overnight. Excess target DNA was removed by rinsing the microarray with 2 x SSC buffer followed with cold 0.2 x SSC. After air drying, the electrodes were stored in a desiccator before use.

**Table 4.2.** Microelectrode area and hybridization conditions for microarray #1

<b>Microarray #1</b>	<b>Area mm<sup>2</sup></b>	<b>Oligo2 (0.5µl)</b>
No.1	0.19	3 nM
No.2	0.08	3 nM
No.3	0.08	3 pM
No.4	0.07	3 pM
No.5	0.08	0.3 pM
No.6	0.08	0.3 pM
No.7	0.10	30 pM
No.8	0.11	30 pM

**Table 4.3.** Microelectrode area and hybridization conditions for microarray #2

<b>Microarray #2</b>	<b>Area mm<sup>2</sup></b>	<b>Oligo2 (0.5µl)</b>
No.1	0.07	3 pM
No.2	0.09	3 pM
No.3	0.09	30 pM
No.4	0.06	0.3 pM
No.5	0.09	30 pM
No.6	0.10	3 nM
No.7	0.04	0.3 pM
No.8	0.09	3 nM

**Table 4.4.** Microelectrode area and hybridization conditions for microarray #3

<b>Microarray #3</b>	<b>Area mm<sup>2</sup></b>	<b>Oligo2 (0.5µl)</b>
No.1	0.13	30 pM
No.2	0.11	30 pM
No.3	0.09	0.3 pM
No.4	0.06	0.3 pM
No.5	0.10	3 pM
No.6	0.10	3 pM
No.7	0.18	3 nM
No.8	0.18	3 nM

### **Fluorescence Microscope Imaging**

For fluorescence imaging, the single-electrode sensors were treated with Cy5-Oligo2 or Cy3-Oligo1 target solutions at 2  $\mu\text{M}$ . Fluorescent images were captured on a CoolSnap cf CCD camera (Roper Scientific Photometrics) mounted on a Nikon Diaphot 300 fluorescent microscope (Nikon, Tokyo, Japan) driven by MetaMorph imaging software (Universal Imaging, Downingtown, PA). Images were saved as JPEG files and opened in Adobe Photoshop 6.0 (Adobe Systems, San Jose, CA), where overall brightness was increased for final production. A Cy5 filter and a Cy3 filter were selected for the Cy5- and Cy3-labeled experiments, respectively.

### **DNA Labeling with Catalysts**

Catalyst labeling was performed at room temperature in optimal grade acetonitrile. Electrodes were soaked with gentle rocking in the  $10^{-6}$ - $10^{-5}$  M catalyst solution for 15 minutes and washed with the pure acetonitrile to remove the non-selectively absorbed catalyst. The catalyst labeled electrodes were stored dry in desiccator before electrochemical measurement.

### **Electrochemical Experiments**

Cyclic voltammograms (CVs) were scanned initially from -500mv (vs SSCE) at 100 mv/s; differential pulsed voltammograms (DPVs) were scanned from 0 to 600 mv (vs SSCE) at 100 mv/s with the following conditions: sample width 17 ms, pulse amplitude 50 mV, pulse width 50 ms, pulse period 200 ms. All the electrochemistry was run in a one-compartment electrochemical cell. The counter electrode was a large-area platinum

coil, and a sodium saturated calomel electrode (SSCE) or a silver wire was used as the reference electrode or quasi-reference electrode. In all cases 0.1 M TMAPF<sub>6</sub> in ACN was employed as the supporting electrolyte.

### **Serum Experiments**

#### a) Serum treatment of PUA/PPEA modified ITO surfaces

Blood serum was diluted (10%) with buffers to control pH. The buffers used to dilute it were 0.2M MES with 0.5M NaCl (pH 6.0), 2 x SSC (pH 7.0) and 0.1M NaHCO<sub>3</sub> with 0.5M NaCl (pH 8.0). A 50  $\mu$ l dilute serum solution was applied to the 2:1 PUA/PPEA treated ITO surface (0.5 cm<sup>2</sup>) with an Eppendorf pipette and incubated at room temperature in 100% humidity for 4 hours. The electrodes were rinsed with the corresponding buffer followed with cold dilute buffer (10%), blown dry with nitrogen and stored in a desiccator overnight. To test the stability of these serum treated surfaces toward catalyst attack, the electrodes were subsequently soaked in a ca. 10<sup>-5</sup> M Ru(BPB)<sub>2</sub>Cl<sub>2</sub>/acetonitrile solution for 15 minutes, rinsed with acetonitrile and air dried. Electrochemical analysis was done in an acetonitrile solution of 1 mM [Co(DTB)<sub>3</sub>](ClO<sub>4</sub>)<sub>2</sub> and 100 mM TMAPF<sub>6</sub>

#### b) Serum treatment of sensor surfaces during the process of sensing target DNA

As previously described, our approach for electrochemical detection of DNA hybridization follow the sequence: ITO sensor fabrication → hybridization with target DNA → labeling the surface DNA duplex with redox active catalyst → electrochemical analysis of the electrode in a [Co(DTB)<sub>3</sub>](ClO<sub>4</sub>)<sub>2</sub>/acetonitrile solution. Here, serum

treatment of the ITO sensor ( $0.5 \text{ cm}^2$ ) was carried out alternately between each two adjacent steps listed above, to investigate the effect that serum exerts on the performance of the biosensors. In general,  $50 \mu\text{l}$  of the dilute serum (10% in 2 x SSC) was applied to the electrode surface and incubated at room temperature in 100% humidity for 4 hours. After rinsing with 2 x SSC followed with cold 0.2 x SSC, the electrodes were blown dry with nitrogen.

c) Electrochemical detection of target DNA in the presence of serum

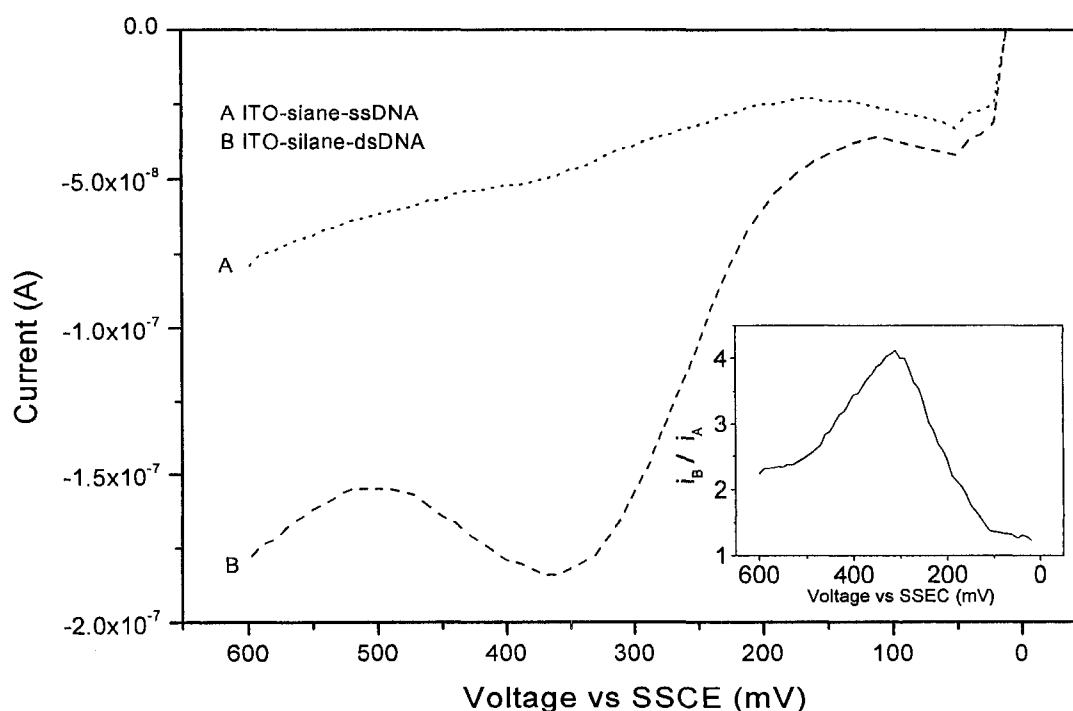
A  $50 \mu\text{l}$  2 x SSC buffer solution containing  $2 \mu\text{M}$  Oligo2 and 10% serum was applied to the probe-modified sensor surface ( $0.5 \text{ cm}^2$ ) and incubated at room temperature in 100% humidity overnight. After rinsing with 2 x SSC followed with cold 0.2 x SSC, the electrodes were blown dry with nitrogen. Electrochemical measurements were performed in an acetonitrile solution of  $1 \text{ mM}$   $[\text{Co}(\text{DTB})_3](\text{ClO}_4)_2$  and  $100 \text{ mM}$  TMAPF<sub>6</sub>.

## RESULTS AND DISCUSSION

### Detection on silane-functionalized ITO surface

Figure 4.1 shows the results of electrochemical sensing of the complementary target performed at silane-functionalized ITO single electrodes ( $0.5 \text{ cm}^2$ ). Initially, both electrodes were identically modified with (3-aminopropyl) trimethoxysilane and succinic anhydride followed with probe ss-DNA. The electrode B was then challenged with a  $2 \mu\text{M}$  complementary target solution and both electrodes were simultaneously treated with the catalyst  $\text{Ru}(\text{BPB})_2\text{Cl}_2$ . As was mentioned in Chapter 3, silane devirated ITO

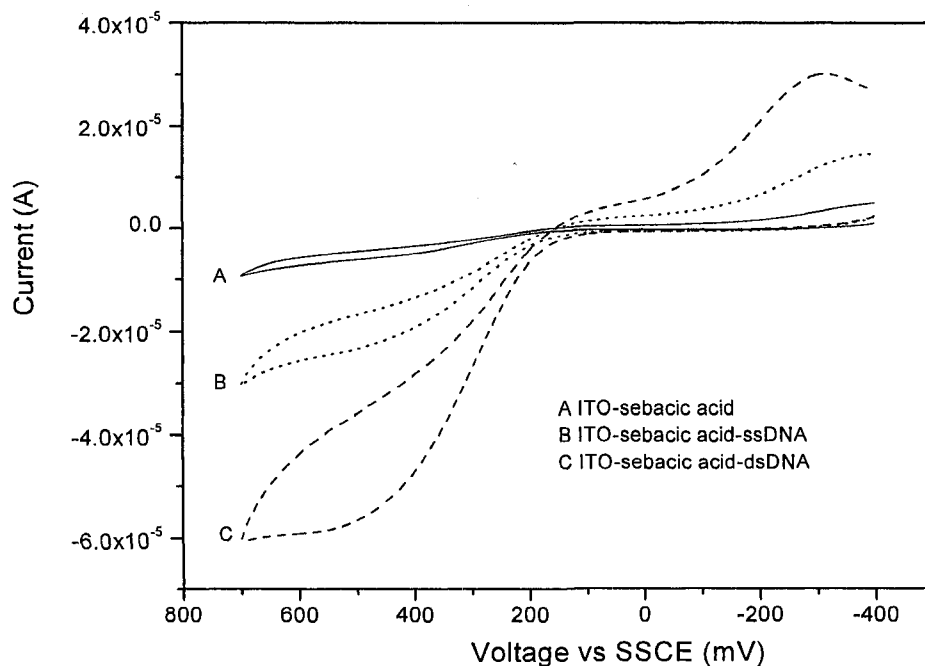
surfaces are vulnerable to catalyst attack. Therefore after the catalyst treatment, the electrodes were subject to a thorough wash of acetonitrile followed by a brief wash of 1:1 2 x SSC / acetonitrile. DPVs were measured in a solution of 0.35 mM  $[\text{Co}(\text{DBT})_3](\text{ClO}_4)_2$  and 100 mM TMAPF<sub>6</sub>. Figure 4.1 shows that the target/probe duplex has formed on electrode B and successfully recruited the catalyst, whereas less catalyst activity is apparent on electrode A containing only the ss-DNA probe. The small current signal on electrode A is caused by non-specific attachment of the catalyst on the sensor surface. The insert of Figure 4.x shows the current ratio of the two electrodes vs the applied potential. At 310 mV vs SSCE, a maximum signal to background of 4 is observed.



**Figure 4.1.** DPVs of the silane-modified electrode (A) and DNA probe-modified sensors which were treated (C) or not treated (B) in the  $2\mu\text{M}$  complementary target solution. Both electrodes were treated the same way with catalyst  $\text{Ru}(\text{BPB})_2\text{Cl}_2$  before the measurements.

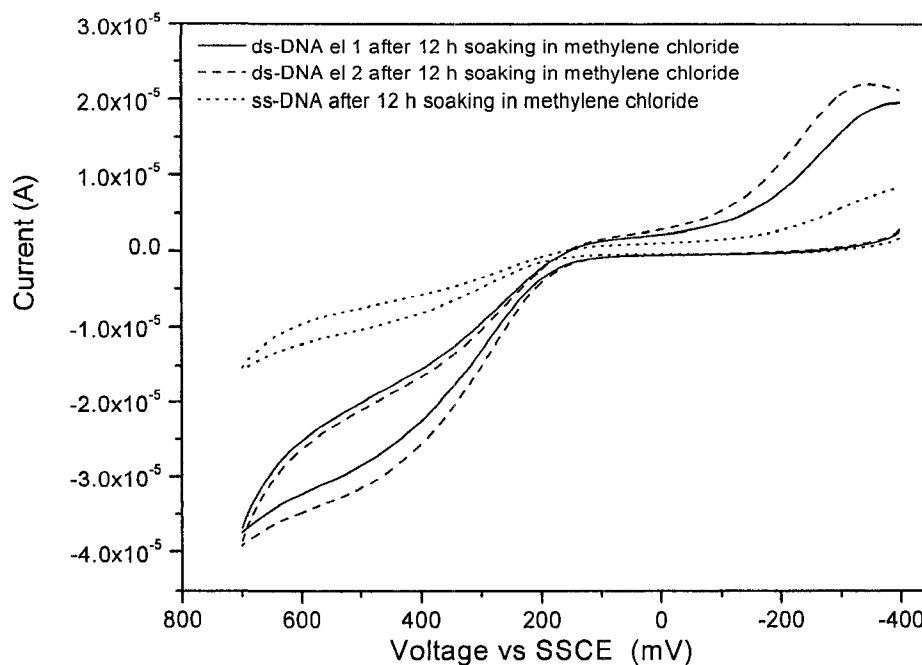
### Detection on sebacic acid-functionalized ITO surface<sup>1</sup>

Figure 4.2 shows the results of electrochemical sensing of the complementary target performed at sebacic acid-functionalized ITO single electrodes ( $0.5 \text{ cm}^2$ ). ITO electrodes modified with ss-DNA alone and modified with ss-DNA which was subsequently hybridized with its complement from solution were both exposed to a solution of  $\text{Ru}(\text{MPB})_2\text{Cl}_2$ . After soaking these electrodes in pure solvent to remove physisorbed catalyst, the electrodes were placed into a solution containing  $\text{Co}(\text{DTB})_3^{2+}$  and their potential cycled. Figure 4.2 reveals a significant catalytic current on both the ds-DNA and ss-DNA modified ITO surfaces, but the current for the ds-DNA is 5 to 7 times larger than for the ss-DNA. Small amount of current was also observed on the surface modified with just sebacic acid, indicative of non-specific catalyst attachment.



**Figure 4.2** Hybridization detection on sebacic acid functionalized ITO electrodes: CVs of the sebacic acid -modified electrode (A) and DNA probe-modified sensors which were treated (C) or not treated (B) in the  $2 \mu\text{M}$  complementary target solution. All three electrodes were treated the same way with catalyst  $\text{Ru}(\text{MPB})_2\text{Cl}_2$  before the measurements. Reprinted from Reference 1.

The stability of the association between the ds-DNA and the redox marker (i.e., catalyst) is demonstrated by the CVs reported in Figure 4.3. After 12 hours of soaking the electrodes in methylene chloride, it was still possible to distinguish ds-DNA from ss-DNA, despite an overall decrease in absolute current intensity: the ratio between current obtained from the presumably catalyst intercalated ds-DNA and ss-DNA was in fact substantially unchanged.



**Figure 4.3.** CVs of two Ru(MPB)<sub>2</sub>Cl<sub>2</sub>-labeled ds-DNA (solid line and dashed line) and one Ru(MPB)<sub>2</sub>Cl<sub>2</sub>-labeled ss-DNA (dotted line). All the electrodes were soaked in methylene chloride for 12 h after catalyst treatment. Reprinted from Reference 1.

### Detection on PDA-functionalized ITO surface

Figure 4.4 shows the effect of thermal treatment of the PDA functional monolayer on the sensor's detecting performance. PDA functionalized ITO electrodes were heated at 110°C for a specified time and probe ss-DNA was attached. The sensors were then

challenged with Oligo2 at 2  $\mu\text{M}$  and labeled with  $\text{Ru}(\text{MPB})_2\text{Cl}_2$  from acetonitrile solution. Electrochemical measurement was performed in an acetonitrile solution containing 1 mM  $[\text{Co}(\text{DTB})_3](\text{ClO}_4)_2$  and 100 mM TMAPF<sub>6</sub>.

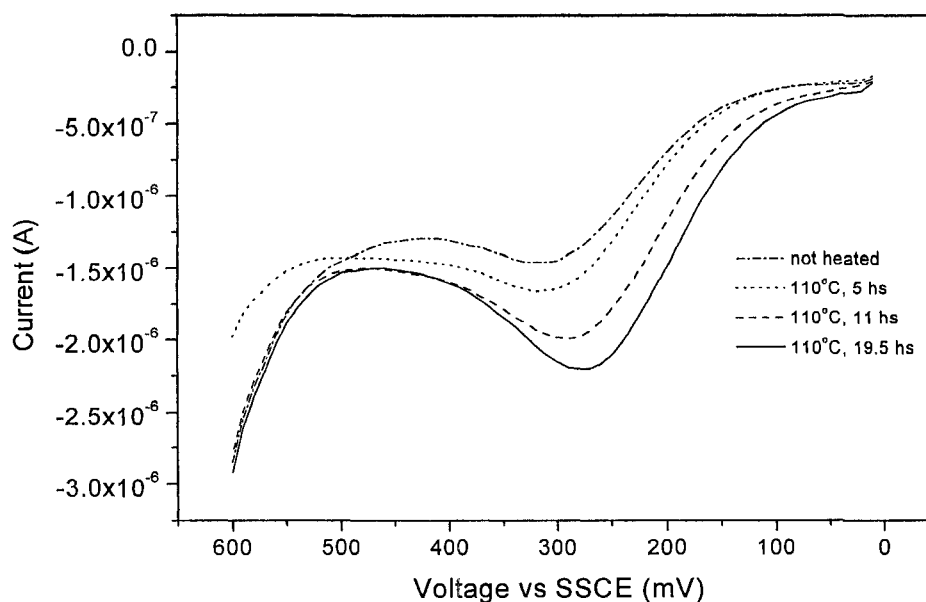


**Figure 4.4.** DPVs in 1 mM  $[\text{Co}(\text{DTB})_3](\text{ClO}_4)_2$  for DNA sensors which were challenged with complementary Target DNA (2  $\mu\text{M}$ ) and labeled with  $\text{Ru}(\text{MPB})_2\text{Cl}_2$ . These sensors were fabricated the same way except the duration for thermal treatment of the self assembled PDA layer.

As shown in Figure 4.4, the PDV current increased as the heating duration extended up to 19.5 hours. The higher current results from a more effective Co(II) catalytic oxidation, which can be rationalized by higher surface concentrations of the formed DNA duplex and hence the intercalated Ru complex. Gawalt and coworkers<sup>2</sup> reported an outstanding stability enhancement of the self-assembled alkanephosphonic acid monolayer on the native oxide surface of titanium upon thermal treatment. For this research, a more complete organic monolayer plays a dual role in improving sensor performance. On one hand, it suppresses noise by blocking non-specific catalyst

adsorption; on the other hand, it increases positive signals by binding more DNA probes to the sensor surface. Heating treatment at higher temperatures for a longer time however, could cause decarboxylation of the carboxylic acid. We subsequently use 110<sup>0</sup>C for 20 hours.

### **Detection on PUA-functionalized ITO surface**

Experiments utilizing DPA derivatized ITO surfaces yield encouraging results. Unfortunately, the prepared PDA was quickly used up. Instead of making more PDA, we prepared its analog, PUA, for the sake of easy synthesis and reasonable cost. Application of PUA functionalized ITO electrodes for target DNA sensing is shown as follows.

#### a) Detection of 2 $\mu$ M complementary target Oligo2 using single ITO biosensors<sup>3</sup>

Figure 4.5 shows results of the hybridization detection of 2  $\mu$ M complementary target at PUA-functionalized ITO electrodes (0.5 cm<sup>2</sup>). For probe ss-DNA modified sensors, the current remains around zero no matter how the mediator concentration changes, indicating an absence of the catalyst on the ITO surface. The sensor challenged with complementary target Oligo2 produced a significant amount of catalytic current; and the current increased as the concentration of Co(DTB)<sub>3</sub>](ClO<sub>4</sub>)<sub>2</sub> increased up to 5.75 mM, consistent with the phenomena observed for catalytic oxidation of Co(DTB)<sub>3</sub>](ClO<sub>4</sub>)<sub>2</sub> by Ru(MPB)<sub>2</sub>Cl<sub>2</sub> from solution (in Chapter 2), suggesting a high surface concentration of the intercalated Ru complex. At 5.75 mM Co(DTB)<sub>3</sub>](ClO<sub>4</sub>)<sub>2</sub>, the electrodes modified with the ds-DNA gave rise to catalytic currents that were ~200 times larger than for the ss-DNA.

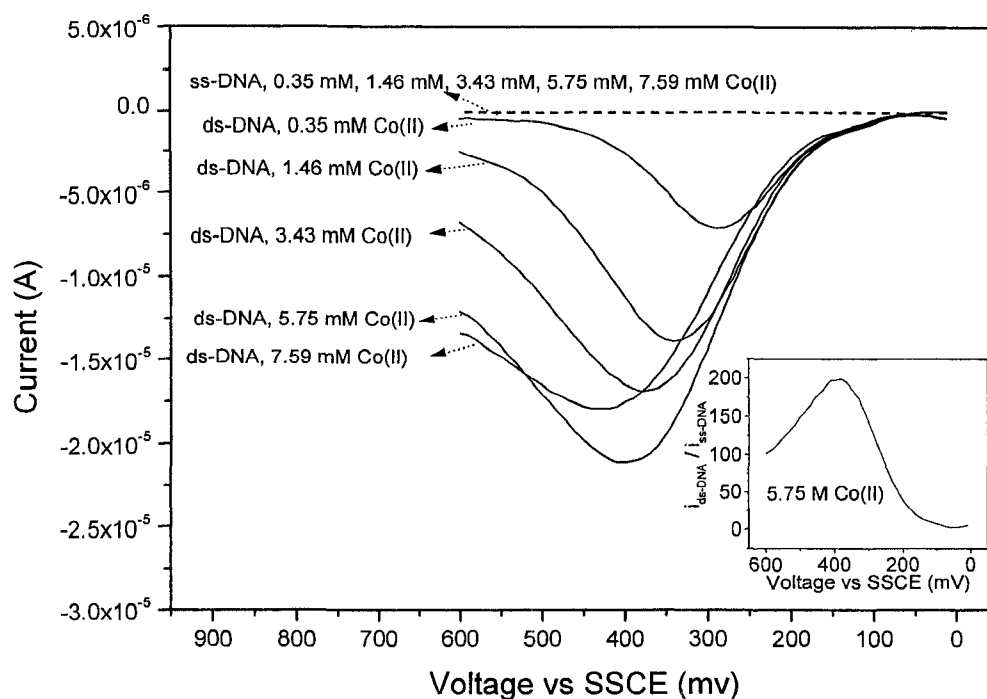


**Figure 4.5.** Hybridization detection on PUA functionalized ITO electrodes: DPVs of the probe-modified sensors which were treated (solid curves) or not treated (dashed curves) in the  $2\mu\text{M}$  complementary target solution. All were treated the same way with catalyst  $\text{Ru}(\text{BPB})_2\text{Cl}_2$  before the measurements in  $[\text{Co}(\text{DTB})_3](\text{ClO}_4)_2$  solution.

b) Detection of  $2\mu\text{M}$  complementary target Oligo2 using array ITO biosensors

As shown in Figure 4.6 a), half of the 56 ITO sensing spots (the dark circles, 33 mm diameter) were challenged with  $2\mu\text{M}$  Oligo2 so that duplex formed on their surfaces. The array was then labeled with catalyst  $\text{Ru}(\text{BPB})_2\text{Cl}_2$ . Using a platinum coil as the counter electrode and a silver wire as the quasi-reference electrode, electrochemical measurements were performed in an acetonitrile solution of  $0.4\text{ mM } [\text{Co}(\text{DTB})_3](\text{ClO}_4)_2$  and  $100\text{ mM TMAPF}_6$ . The electronic contact of the ITO spot with the potentiostat was established through a micro-GC electrode. A DPV was obtained for each ITO spot by scanning the GC electrode from spot to spot. And the DPV peak currents vs the position of the ITO spot was plotted in Figure 4.8 b).

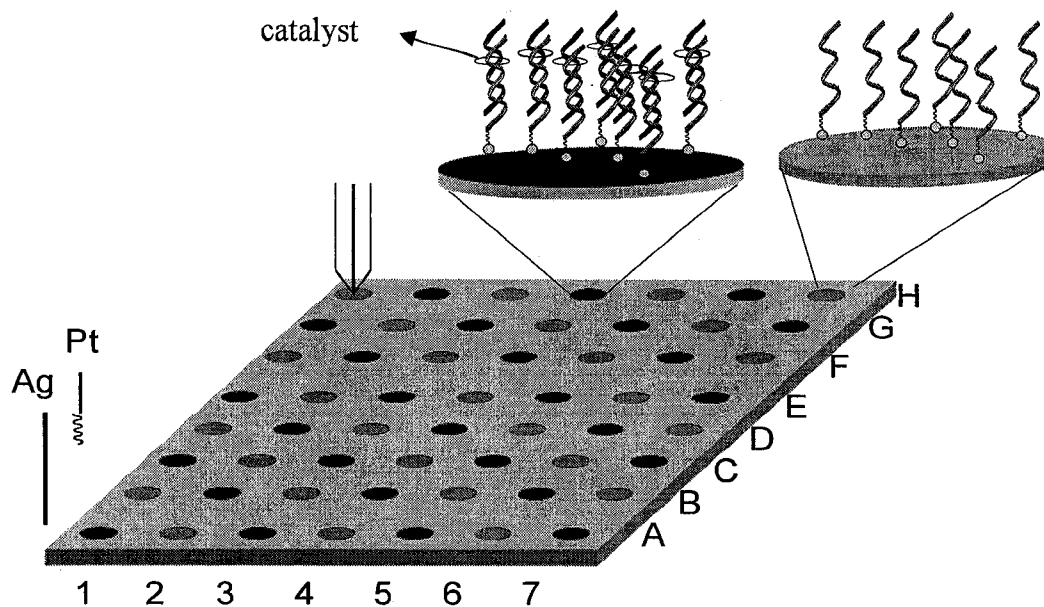


**Figure 4.6 a.** Schematic illustration of DNA hybridization detection on ITO array electrode and the electrochemical cell configuration.

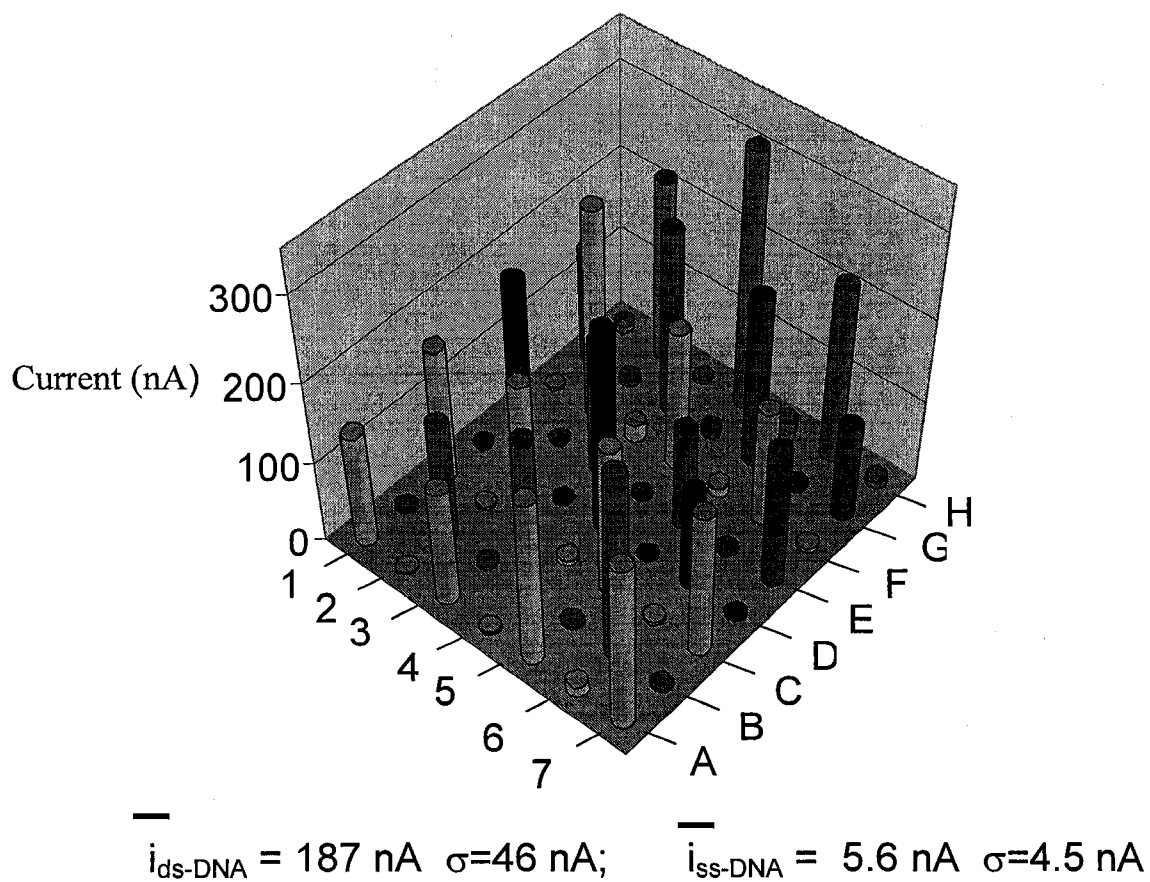


**Figure 4.6 b.** Array detection of 2  $\mu$ M complementary target: DPV peak current vs. ITO spot position.

The ds-DNA modified spots produced significant catalytic currents with an average of 187 nA and a standard deviation of 46 nA; while the ss-DNA modified spots produced an average current of 5.6 nA and a standard deviation of 4.5 nA. The overall signal-to-noise is 33. Due to the hydrophobism of the PUA layer, it took efforts to keep the liquid drops of target solution from running onto adjacent electrodes. Accidental contamination of the target solution resulted in a small current on some of the ss-DNA spots.

c) Discrimination of 2  $\mu\text{M}$  complimentary target from mis-matched target<sup>3</sup>

Figure 4.7 shows the sensor's ability to discriminate between complimentary target DNA and mis-matched. Three identically fabricated single ITO biosensors ( $0.5 \text{ cm}^2$ ) were used. Sensor B was challenged with 2  $\mu\text{M}$  mismatched target Oligo1 while Sensor C with 2  $\mu\text{M}$  complementary target Oligo2. And Sensor A provides background measurements.

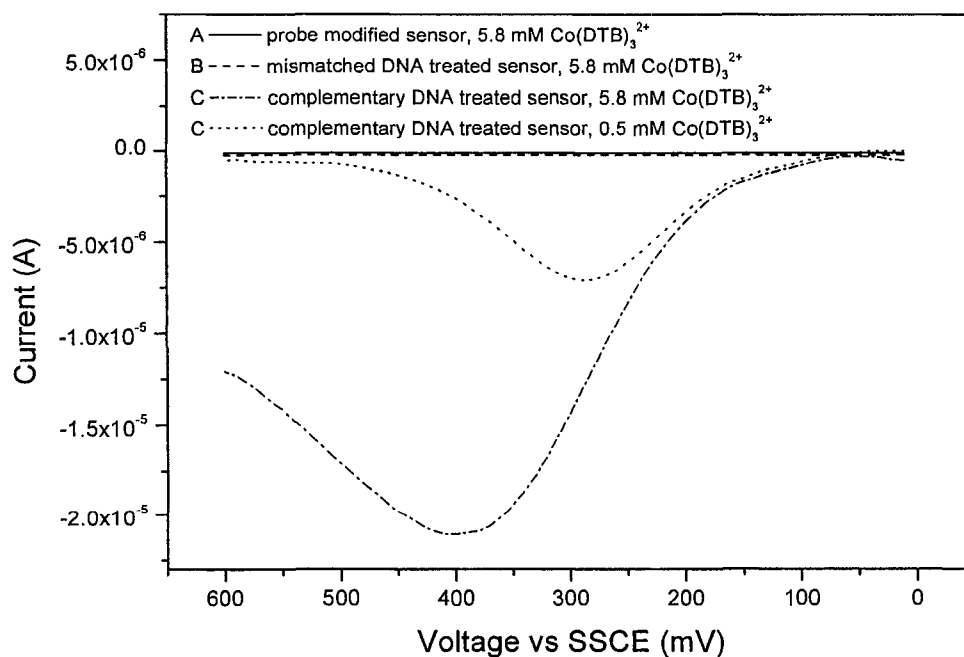


**Figure 4.7.** DPVs of the sensors treated with no target solution (A) or with the 2  $\mu\text{M}$  mismatched Oligo1 (B) and the 2  $\mu\text{M}$  complementary target Oligo2 (C and D). Measurements for the electrode A, B and C were made at 5.8 mM  $[\text{Co}(\text{DTB})_3](\text{ClO}_4)_2$ , while D at 0.5 mM  $[\text{Co}(\text{DTB})_3](\text{ClO}_4)_2$ . Reprinted from Reference 3.

Negligible current results for the electrode challenged with mismatched ss-DNA target; while significant current is observed from the electrode challenged with complementary ss-DNA target. As the concentration of  $[\text{Co}(\text{DTB})_3](\text{ClO}_4)_2$  is increased from 0.5 to 5.8 mM, the peak current increases nonlinearly and shifts to more positive potentials. The non-linear response and the peak shift are both consistent with a combination of uncompensated resistance and slow electron-transfer kinetics becoming significant at the higher concentration.

#### d) Fluorescence imaging<sup>3</sup>

Figure 4.8 shows fluorescent microscope images. The sensors were treated with Cy5-Oligo2 or Cy3-Oligo1 target solutions at  $2\mu\text{M}$  and subjected to fluorescence microscope observations. To provide contrast, both electrodes were intentionally and carefully scratched prior to examination. The left-hand image (4x) is of a ss-DNA probe-modified ITO electrode that was challenged with fluorescently-tagged complimentary target (cy5-Oligo2). The dark scratch is clearly visible in the grey background. Fortuitously, material scratched from the surface of this electrode lodged at the end of the scratch trough producing a clear, bright fluorescence spot in the image. In contrast, the right-hand image (40x) is from an identical ss-DNA probe-modified ITO electrode that was challenged with a fully mismatched (to the ss-DNA probe) labeled target (cy3-Oligo1). This surface shows no contrast from the scratch and no evidence of fluorescence, confirming the electrochemical results that fully mismatched target DNA won't hybridize the surface probe DNA.

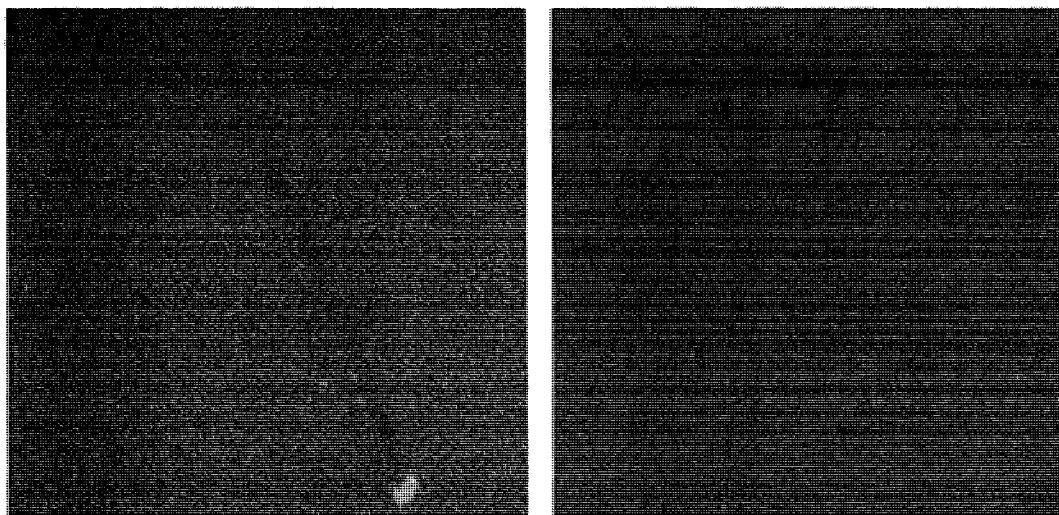


**Figure 4.8.** Fluorescent images of sensors treated with complementary target Cy5-Oligo2 (left) and fully mis-matched target Cy3-Oligo1 (right). Both samples were scratched across their faces in order to provide image contrast. Reprinted from Reference 3.

e) Detection of 3 nM target

Figure 4.9 shows results of the hybridization detection of the 3 nM complementary target and 3 nM fully mismatched target using single ITO biosensors ( $0.5 \text{ cm}^2$ ) fabricated employing PUA monolayers. Electrochemical measurements were performed in an acetonitrile solution of 0.5 mM  $[\text{Co}(\text{DTB})_3](\text{ClO}_4)_2$  and 100 mM TMAPF<sub>6</sub>. As it can be seen from Figure 4.9, the electrodes challenged with mismatched ss-DNA target exhibit negligible catalytic current (curve B and curve C); while significant current is observed from the electrode challenged with complementary ss-DNA target (curve D), implying the occurrence of DNA duplex formation and hence catalyst intercalation on the ITO surface. Deviation of curves A, B and C from the zero current line are possibly due to background charging current from the instrument or the electrochemical cell. The

sensor's signal-to noise for detecting 3 nM complementary target over mismatched target is  $> 1000$  after correction of the measured currents relative to the background.

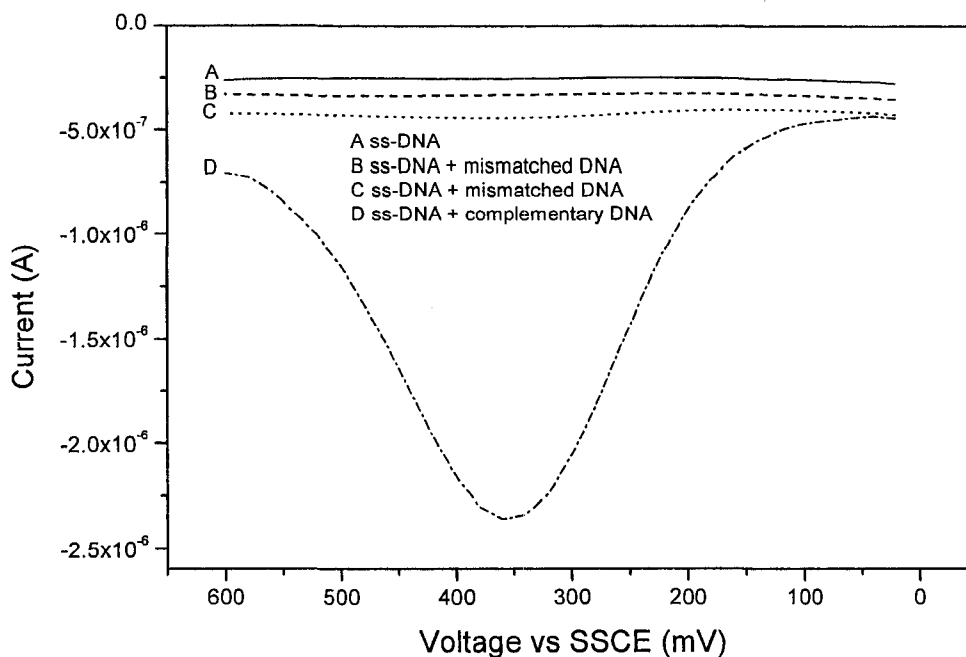


**Figure 4.9.** DPVs of the sensors treated with no target solution (A) or with 3nM mis-matched Oligo1 (B and C) or with 3nM complementary target Oligo2 (D). Measurements for the electrode A, B and C were made in the acetonitrile solution of 0.5 mM  $[\text{Co}(\text{DTB})_3](\text{ClO}_4)_2$  and 100 TMAPF<sub>6</sub>.

#### f) Detection of 4 pM target

Figure 4.10 shows typical, representative differential pulse voltammograms for two single ITO electrodes ( $0.5 \text{ cm}^2$ ), each measured in the same 0.10 mM solution of  $\text{Co}(\text{DTB})_3^{2+}$ . The sensors A and B differed only in that the former was stirred with gentle rocking for 24 hrs in 25 mL of a 4 pM solution of the complimentary target DNA. It is apparent that on electrode A the target/probe duplex has formed and successfully

recruited the catalyst whereas no catalyst is present on electrode B containing only the ss-DNA probe. The current curves also display deviation from the zero current line.

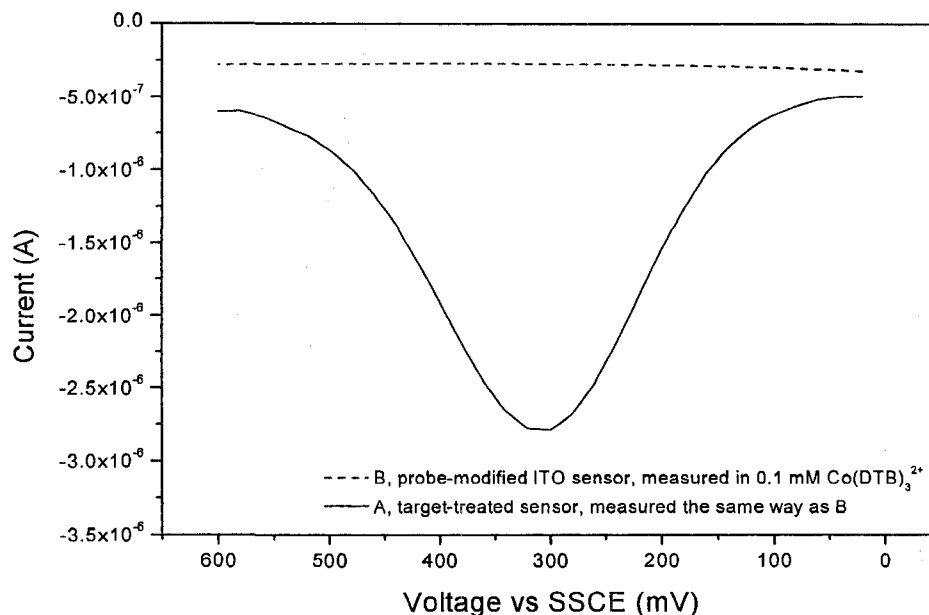


**Figure 4.10.** DPVs of the probe-modified sensors with (sensor A, solid curve) and without (sensor B, dashed curve) treatment in the 4 pM target solution. Both were treated the same way with catalyst Ru(BPB)<sub>2</sub>Cl<sub>2</sub> before the measurements.

#### g) Detection of DNA target using microarray electrodes

Microarray detections use much less samples. Assuming a probe packing density of  $10^{12}$  molecules/cm<sup>2</sup> and a hybridization efficiency ~100%,<sup>4</sup> 0.5 μL of the 3nM target solution ( $\sim 9 \times 10^8$  molecules) would hybridize all the probes immobilized on a microarray electrode of 0.1 mm<sup>2</sup> area ( $\sim 6 \times 10^8$  molecules). On the basis of the signal-to-noise and background from data in Figure 4.5 to Figure 4.10, sensing such a target solution using a microelectrode would yield a current response of nano to tens of nano amperes, still measurable by conventional electrochemical instruments.

Unfortunately, with our current experimental conditions, the small-volume solution (0.5 $\mu$ l) used to attach the probe DNA or hybridize the target DNA quickly evaporates (sometimes dries up) before the humidity chamber is closed. This caused precipitation of EDC/NHS and DNA nucleotides to ITO surfaces, constituting a possible problem for microarray detection.

As shown in Figure 4.11A, the current responses from microarray detection of 3 nM target is short of a well defined oxidation peak. Additionally, it exhibits evident inconsistency among the six microarrays. Four of sensors gave rise to false negative signals. The other two yielded true positive signals but the currents were considerably different, despite the fact that these two sensors had almost the same area (0.19 mm<sup>2</sup> compared with 0.18 mm<sup>2</sup>). The absence of a well-defined diffusional-shaped peak is indicative of kinetic control over the overall redox process.

Detections of target at 30 pM, 3pM and 0.3 pM displayed the same nonconclusive results, as can be seen from Figure 4.11B, C and D. It is possible that these detections suffered from insufficient target and hence a poor hybridization ratio on the sensor surfaces. The current responses of 0.3 pM solutions are extremely small, on the order of 10<sup>-10</sup> amperes, beyond the instrument's measurement range, and therefore are fairly noisy too.

Apparently, these small scale experiments differ considerably from those large scale ones. Optimizing the microarray technique demands more consistent and systematic work, including microarray preparation, probe immobilization and hybridization condition improvements.

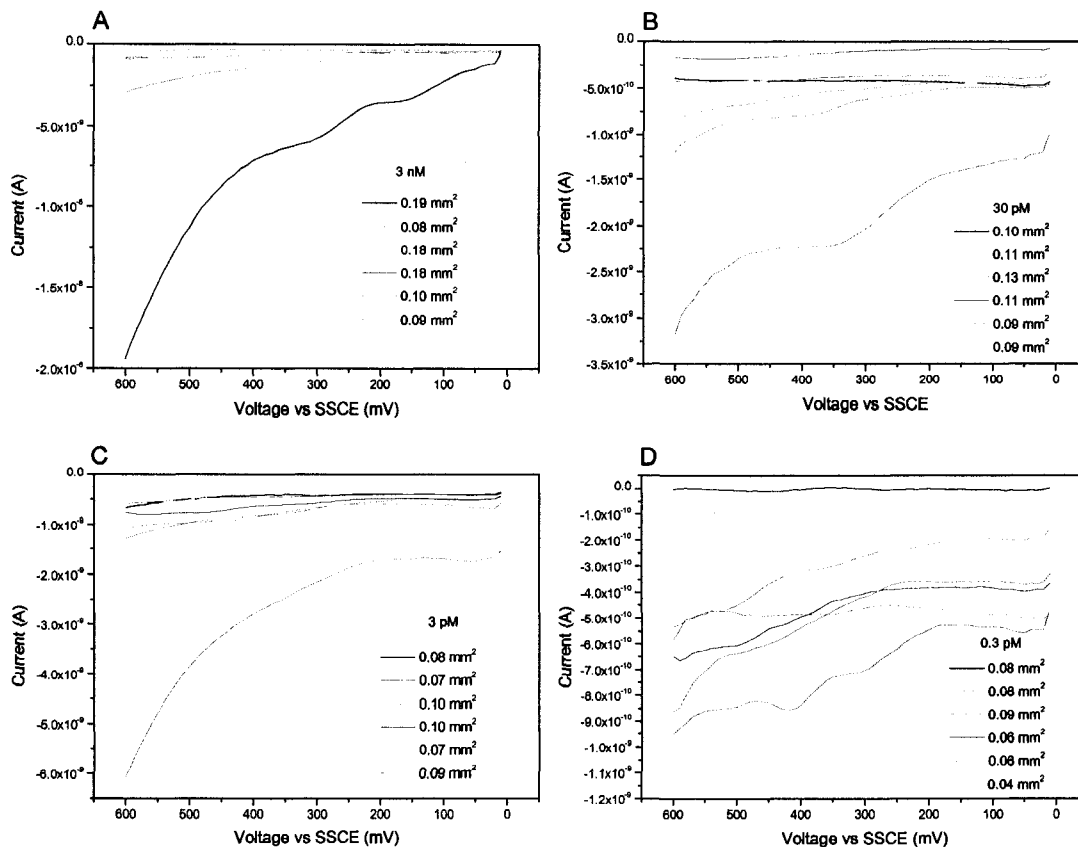


**Figure 4.11.** DNA hybridization detection of complementary target using microarrays. A) DPVs of microarrays challenged with 0.5  $\mu\text{L}$  of the 3nM Oligo2 solution, B) DPVs of microarrays challenged with 0.5  $\mu\text{L}$  of the 30pM Oligo2 solution, C) DPVs of microarrays challenged with 0.5  $\mu\text{L}$  of the 3pM Oligo2 solution, D) DPVs of microarrays challenged with 0.5  $\mu\text{L}$  of the 0.3pM Oligo2 solution. All measurements were taken in an acetonitrile solution containing 0.18 mM  $[\text{Co}(\text{DTB})_3](\text{ClO}_4)_2$  and 100 mM TMAPF<sub>6</sub>.

### Detection of Target DNA in the Presence of Serum Proteins

#### a) Serum treatment of PUA/PPEA functionalized ITO surfaces

As shown in Figure 4.12, a significant catalytic current was observed on the electrode treated with serum at pH 8.0, indicative of non-specific catalyst attachment to the ITO surface. The basic buffer might cause deprotonation of the acids, and hence decrease the monolayer stability. No current was detected on the electrode treated with

serum at pH 7.0. As such, 2 x SSC buffer of pH 7.0 was selected as the hybridization solution for the following detections.

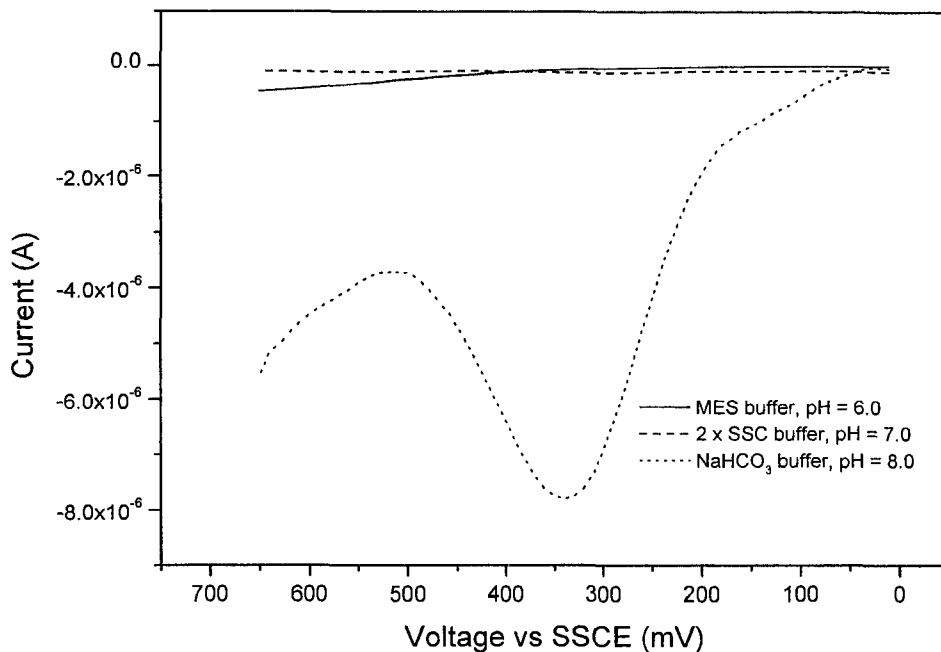


**Figure 4.12.** DPVs of ITO electrodes treated with PUA/PPEA/NEt<sub>3</sub> and followed by diluted serum. . All were treated the same way with catalyst I before the measurements in 1 mM [Co(DTB)<sub>3</sub>](ClO<sub>4</sub>)<sub>2</sub> acetonitrile solution.

b) Serum treatment of ITO surfaces during the process of sensing target DNA

Figure 4.13 shows the effect of serum treatment on the performance of the ITO biosensors. The sensors were fabricated by covalently attaching probe ss-DNA to PUA/PPEA functionalized surfaces. Upon challenging with complementary target Oligo2, the sensor gave rise to an evident catalytic current, consistent with previous findings from PUA functionalized sensors, demonstrating the effectiveness of the PUA/PPEA sensing platforms. However, the current signals were significantly suppressed whenever serum proteins were introduced into the system (curves No.1, No2,

and No3).

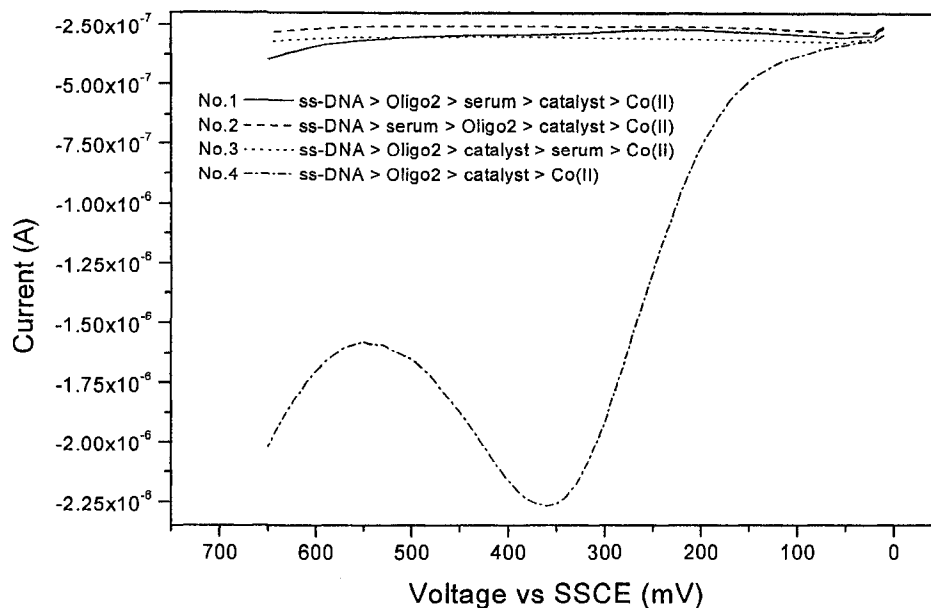


**Figure 4.13.** Serum effects on ITO sensors. All the ITO electrodes were treated the same way with a layer of 2:1:6 PUA/PPEA/NET<sub>3</sub>, followed by attachment of ss-DNA probes. No.4 is a control experiment without serum treatment. First the sensor was treated with the complementary target 2 $\mu$ M Oligo2, then with the catalyst Ru(BPB)<sub>2</sub>Cl<sub>2</sub> before being analyzed by DPV in Co(II) solution. No.1, No.2 and No.3 were experiments done with serum treatments (10% diluted). For No.1, serum was applied after hybridization and before catalyst treatment, while No.2 before hybridization, No.3 after catalyst treatment.

### c) Electrochemical detection of target DNA in the presence of serum

Figure 4.14 compares the results of sensing complementary target Oligo2 from solution with and without serum. Without serum, the sensor gave rise to a positive signal in the form of a significant catalytic current (curve C). On the other hand, without Oligo2, the sensor B yielded a decent noise level which is perfect for sensitive DNA detection (curve B). Sadly, upon addition of serum to the target solution, the sensor yielded no current, which is apparently a false negative signal (curve A).

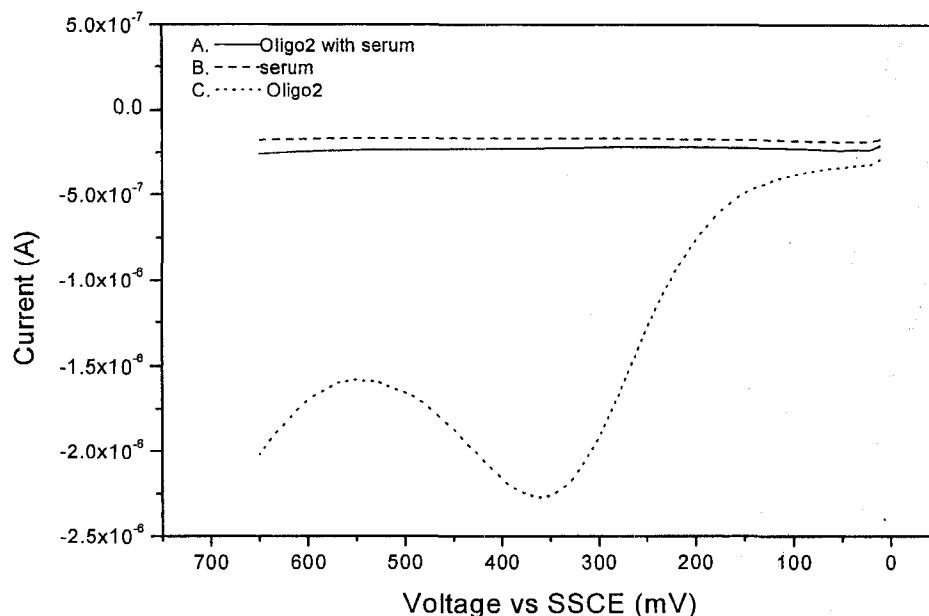


**Figure 4.14.** Serum effects on ITO sensors. All the ITO electrodes were treated the same way with a layer of 2:1:6 PUA/PPEA/NEt<sub>3</sub>, followed by attachment of ss-DNA probes. First the sensor was treated with the complementary target 2 $\mu$ M Oligo2 with (A) or without serum (C) or serum without Oligo2 (B), then treated with the catalyst Ru(BPB)<sub>2</sub>Cl<sub>2</sub> before being analyzed by DPV in Co(II) solution.

After electrochemical measurements, the electrodes were rinsed with acetonitrile and analyzed with XPS. The XPS results are shown in Figure 4.15. The XPS spectrum of Sensor C, which was challenged with Oligo2 alone, displays a small N1s peak due to the presence of oligonucleotides on the sensor surface, while Sensor A, challenged with both Oligo2 and serum, exhibits a much higher N1s signal. The increase of N1s intensity must arise from addition of serum protein since all the other treating conditions were the same for these two electrodes. Considerable N1s signal was also observed on the XPS spectrum of Sensor B, which was treated with serum alone, implying presence of a serum adlayer on its surface. The thickness of the serum layers on A and B was deduced to be

high based on the fact that the indium signal (compare the In3d intensity of A and B with C) of these electrodes were greatly attenuated.

These XPS observations explain or at least partially explain the degraded performance of biosensors. Upon immersing the sensor into a solution containing serum, a thick protein layer forms on the electrode surface. The serum layer was so thick that the sensor loses its ability for electrochemical DNA sensing, likely by blocking of  $\text{Co(DTB)}_3^{2+}$  access to the electrode surface (and the catalyst on it).

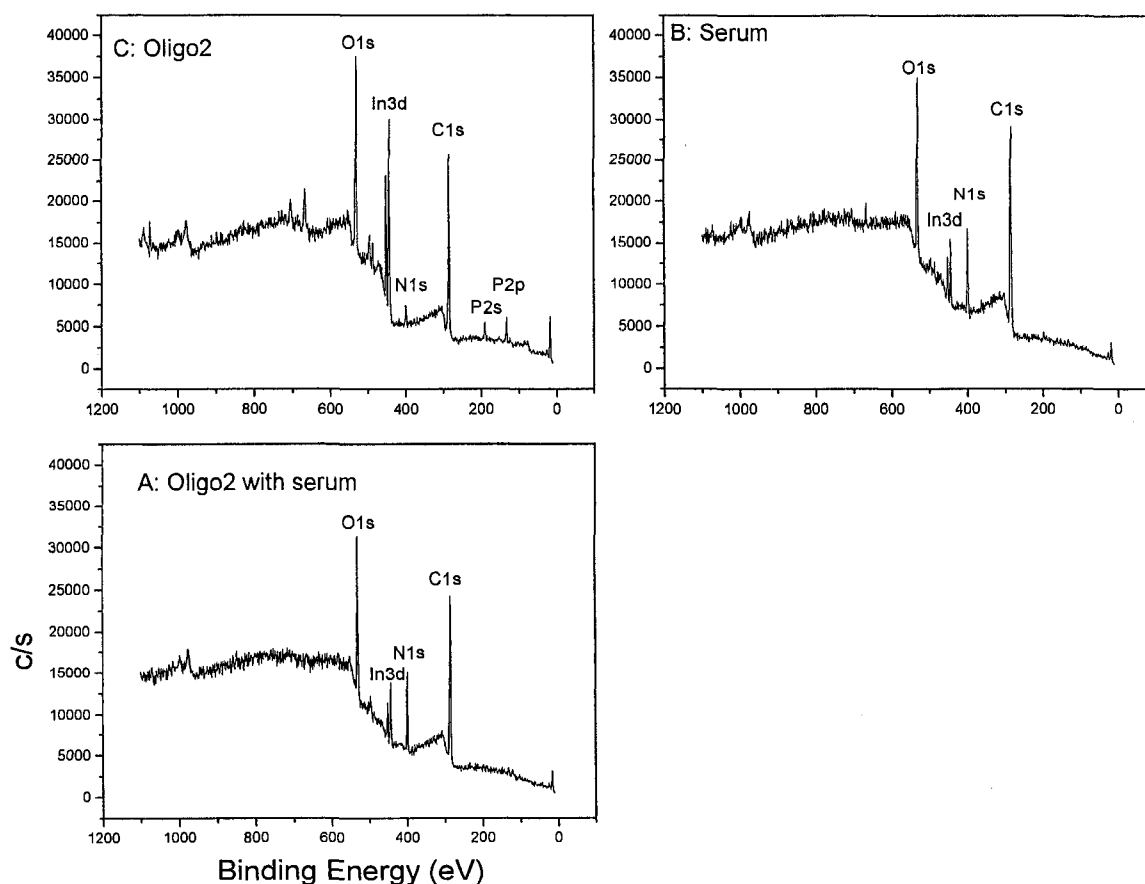


**Figure 4.15.** XPS analysis of sensors A, B and C shown in Figure 4.15. After DPV experiments, the sensors were carefully rinsed with acetonitrile, dried in the air and analyzed by XPS.

## SUMMARY

Table 4.5 lists the results of DNA detection using single ITO sensors ( $0.5 \text{ cm}^2$ ) fabricated through different functional monolayers.  $\omega$ -Phosphoalkyl carboxylic acid, in this case, PUA, was found to give the best result. As was discussed in Chapter 3, silane and sebacic acid monolayers were either not complete or not stable, thus the ITO electrodes experiences non-specific catalyst attachment, which increased the background / noise level.

**Table 4.5.** DNA detection using single ITO sensors ( $0.5 \text{ cm}^2$ ) fabricated through different functional monolayers.

Monolayers through which sensors are fabricated	Target concentrations	DNA sensing signal-to noise <sup>a</sup>
Silane	2 $\mu\text{M}$	4
Sebacic acid	2 $\mu\text{M}$	5-7
PUA	2 $\mu\text{M}$	200

a. Here “signal-to-noise” is defined as the ration of DPV at  $i_p$  to the current at the same potential for the corresponding ss-DNA modified electrodes.

Using single ITO sensors fabricated through PUA monolayers, the detection limit was pushed down to picomolars. Owing to the current amplification mechanism, we achieved excellent signal-to-noise.

Efforts were made to decrease the sample amount by utilizing microelectrodes. The results were discouraging but the micorarray techniques have not been optimized. Attempts to carry out DNA sensing in the presence of serum proteins also failed to produce encouraging data.

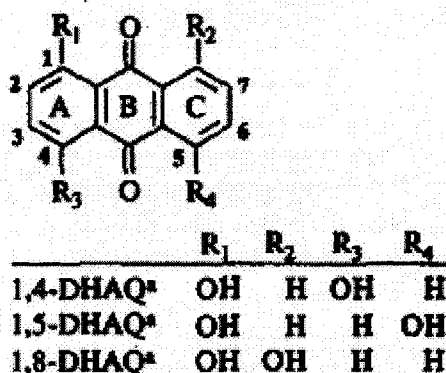
The following lists some suggested future directions for study :

i) Development of new catalysts.

To avoid non-specific catalyst attachment to the electrode surface, more stable catalysts are desirable for DNA labeling, for example, water soluble complex  $\text{Ru}(\text{bpy})_2(\text{DHAQ})_x$ , ( $x= 0, 1, \text{ or } 2$ ), where bpy stands for 2,2'-bipyridine, DHAQ stands for dihydroxyanthraquinone (deprotonated, see Scheme 4.1)

**Scheme 4.1.**

Reprinted from Reference 5.



\*Ruthenium coordination assumed at the  $\text{OH}_1$  (deprotonated) and adjacent quinone O.

According to Gooden et al.,<sup>5</sup> these ruthenium complex display reversible  $\text{Ru}^{3+/2+}$  redox chemistries on Pt. Table 4.6 list their electrochemical properties. Particularly, the complexes exhibit proper redox potentials suitable for DNA detection, interestingly in aqueous solutions (values in parentheses), too. If these ruthenium complexes were used as DNA labels, it is possible to combine the two following steps, target sensing and ds-DNA labeling, into an integrated step during DNA hybridization detection. Figure 4.16A shows the molecular structure of  $[\text{Ru}(\text{bpy})_2(1,5\text{-DHAQ})]\text{PF}_6$ . It carries one positive

charge. Deprotonation of  $[\text{Ru}(\text{bpy})_2(1,5\text{-DHAQ})]\text{PF}_6$  is expected to produce its neutral analog,  $\text{Ru}(\text{bpy})_2(1,5\text{-DHAQ})$ , as shown in Figure 4.16B.

**Table 4.6.** Electrochemical data for the dihydroxyanthraquinone complexes with  $\text{Ru}(\text{bpy})_2$  in acetonitrile. Reprinted from Reference 5.

Electrochemical data for the dihydroxyanthraquinone complexes with $\text{Ru}(\text{bpy})_2$ in acetonitrile <sup>a,b</sup>					
Complex	Oxidations <sup>c</sup> (V)		Reductions (V)		
	$E_{1/2}(1)$	$E_{1/2}(2)$	$E'_{1/2}(1)$	$E'_{1/2}(2)$	$E'_{1/2}(3)$
$(\text{Ru}(\text{bpy})_2)_x1,4\text{-DHAQ}$					
$x=0$			-0.58	-1.13	
$x=1$	+0.70		-0.78	-1.28	-1.71
$x=2$	+0.55 (+0.41)	+0.81 (+0.62)	-0.95	-1.35	-1.69
$(\text{Ru}(\text{bpy})_2)_x1,5\text{-DHAQ}$					
$x=0$			-0.54	-1.00	
$x=1$	+0.69		-0.69	-1.14	-1.69
$x=2$	+0.66 (+0.55)	+0.79 (+0.64)	-0.75	-1.23	-1.68
$(\text{Ru}(\text{bpy})_2)_x1,8\text{-DHAQ}$					
$x=0$			-0.56	-1.16	
$x=1$	+0.73 (+0.63)		-0.68	-1.19	-1.63

<sup>a</sup> Potential measurements were at a Pt electrode and referenced to a saturated calomel electrode (SCE) in 0.1 M TEAP- $\text{CH}_3\text{CN}$  at  $25 \pm 1^\circ\text{C}$ . Potentials are uncorrected. 0.45 V was obtained for the  $\text{Fc}^+/\text{Fc}$  couple (Fc = ferrocene).

<sup>b</sup> Values in parentheses are for aqueous solution.

<sup>c</sup> For the dimers:  $[3,2] + e^- \rightarrow [2,2]$   $E_{1/2}(1)$ ;  $[3,3] + e^- \rightarrow [3,2]$   $E_{1/2}(2)$ .

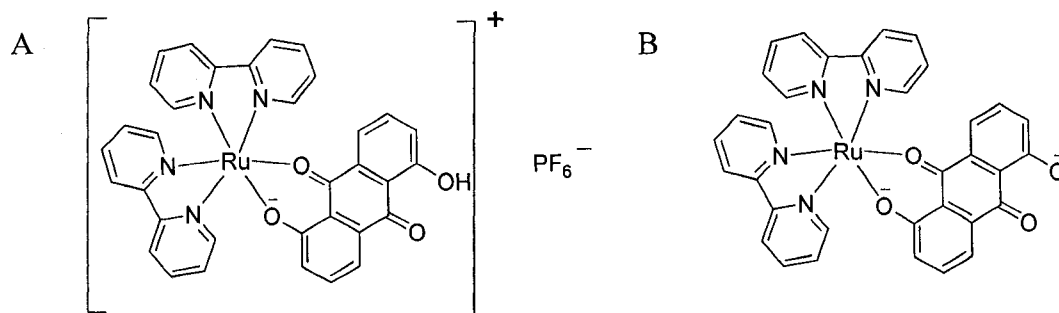


**Figure 4.16.** Molecular structures of  $[\text{Ru}(\text{bpy})_2(1,5\text{-DHAQ})]\text{PF}_6$  (A) and its neutral analog,  $\text{Ru}(\text{bpy})_2(1,5\text{-DHAQ})$  (B).

ii) Optimization of the process of ITO modification with via Zr(IV) and Ti(IV).

Due to the fact that Zr(IV) has a strong tendency to react with ITO<sup>6</sup> as well as phosphonate groups,<sup>7,8</sup> There is no doubt that an optimized Zr(IV) coupling will increase

the stability and repeatability of the  $\omega$ -phosphonoalkyl carboxylic acid monolayer formation and ability to endure harsh hybridization conditions, for example, high temperature or high pH detections and enhance the chances to reuse the biosensors. Additionally, ITO electrodes treated with conducting TiO<sub>2</sub> films exhibited promising catalytic activity toward Co(DBT)<sub>3</sub><sup>2+</sup> oxidation and might provide for an interesting platform for DNA hybridization sensing.

iii) Systematic study on the packing density of the functional organic monolayer and the DNA probe.

As can be seen from previous discussions, quantitative knowledge of the surface concentration of the probe is imperative to predict current response and help with microelectrode design and hybridization condition control (for example, selecting reasonable target concentration and volume). By controlling the concentration of probe DNA employed during fabrication,<sup>4,9</sup> the surface coverage of the ss-DNA probe can be tuned. At optimized surface concentration, higher target hybridization efficiency results.<sup>4</sup> Knowing the surface monolayer coverage of the electrode helps to understand its electrochemistry.

Traditional electrochemical methods,<sup>9,10</sup> fluorescence imaging and <sup>32</sup>P-radiometric assay<sup>4</sup> could be used to quantify the surface functional molecules and the DNA probes.

iv) Continuous investigation of microarray detections.

Once a stable and selective catalyst is found, Efforts at microarray detection should be expanded. In the absence of non-specific catalyst attachment to the ITO surface, the

completeness of the functional organic monolayer is no longer critical (which is required otherwise to exclude catalyst adsorbance). In that case, thus, a shorter modifier, for example, 4-(phosphonomethyl)-benzoic acid,<sup>11, 12</sup> could be used to functionalize the ITO surface via Zr(IV) coupling.<sup>8</sup> Thinner organic layers usually means faster heterogeneous electron tunneling. With this approach, better current responses from the microarray sensors might be realized. Also, microarray printing techniques<sup>4</sup> to spot DNA could prevent evaporation of solution.

v) Optimization of the electrochemical biosensors for detecting DNA in blood serum.

Poly(ethylene oxide) (PEO), also called poly(ethylene glycol) (PEG), has been praised for minimal interaction with Proteins.<sup>13, 14</sup> Medical devices, once surface-modified with PEO/PEG segments, exhibit a smaller protein adsorption and cell adhesion than their corresponding naked analogs.<sup>14, 15</sup> Presumably, ITO surfaces modified with a monolayer of  $\text{HOOC}-(\text{CH}_2\text{-O-CH}_2)_n\text{-PO(OH)}_2$  ( $n=2-4$ ) might be more protein repulsive, providing a better and more reliable platform to sense DNA in protein-containing solutions such as serum. blood serum. Preparation of  $\text{HOOC-CH}_2\text{-O-CH}_2\text{-PO(OH)}_2$  has been previously reported,<sup>16</sup> providing a starting place to synthesize its long-chain analogs.

1. Elliott, C. M.; Bignozzi, C. A.; Xue, D.; Grainger, D. W.; Caramori, S.; Dissette, V. Electrochemical detection of complex formation using probes immobilized on electrode surfaces, U.S. Pat. Appl. Publ. (2008), . 2006-536478, 2008081329, 20060928, 2008.
2. Gawalt, E. S.; Avaltroni, M. J.; Koch, N.; Schwartz, J., Self-Assembly and Bonding of Alkanephosphonic Acids on the Native Oxide Surface of Titanium. *Langmuir* **2001**, 17, (19), 5736-5738.
3. Xue, D.; Elliott, C. M.; Gong, P.; Grainger, D. W.; Bignozzi, C. A.; Caramori, S., Indirect Electrochemical Sensing of DNA Hybridization Based on the Catalytic Oxidation of Cobalt (II). *Journal of the American Chemical Society* **2007**, 129, 1854-1855.
4. Gong, P.; Harbers, G. M.; Grainger, D. W., Multi-technique Comparison of Immobilized and Hybridized Oligonucleotide Surface Density on Commercial Amine-Reactive Microarray Slides. *Analytical Chemistry* **2006**, 78, (7), 2342-2351.
5. Gooden, V. M.; Cai, H.; Dasgupta, T. P.; Rowan Gordon, N.; Hughes, L. J.; Sadler, G. G., The synthesis and characterization of monomeric complexes of Ru (bpy) 2 with dihydroxyanthraquinones. *Inorganica Chimica Acta* **1997**, 255, (1), 105-110.
6. Schwartz, J.; Bernasek, S. L., Organometallic chemistry at the interface with materials science. *Catalysis Today* **2001**, 66, (1), 3-13.
7. Stockhause, S.; Neumann, P.; Schrader, S.; Kant, M.; Brehmer, L., Structural and optical properties of self-assembled multilayers based on organic zirconium bisphosphonates. *Synthetic Metals* **2002**, 127, (1-3), 295-298.
8. Zeng, J.; Krull, U. J., Immobilization of oligonucleotides on indium tin oxide surfaces using zirconium coupling. *Chimica Oggi/Chemistry Today* **2003**, 48-52.
9. Xiao, Y.; Qu, X.; Plaxco Kevin, W.; Heeger Alan, J., Label-free electrochemical detection of DNA in blood serum via target-induced resolution of an electrode-bound DNA pseudoknot. *Journal of the American Chemical Society* **2007**, 129, (39), 11896-7.
10. Willner, I.; Riklin, A., *Anal. Chem.* **1994**, 66, 1535-1539.
11. Chaplais, G.; Le Bideau, J.; Leclercq, D.; Vioux, A., Polarized-Dependent IR ATR Study for the Structural Characterization of Solid-State Phosphonates: Case of Aluminum (4-Carboxyphenyl)methylphosphonate. *Chemistry of Materials* **2003**, 15, (10), 1950-1956.
12. Kitazume, T.; Lin, J. T.; Takeda, M.; Yamazaki, T., Stereoselective synthesis of fluorinated materials catalyzed by an antibody. *Journal of the American Chemical Society* **1991**, 113, (6), 2123-6.
13. Irvine, D. J.; Mayes, A. M.; Satija, S. K.; Barker, J. G.; Sofia-Allgor, S. J.; Griffith, L. G., *J. Biomed. Mater. Res.* **1998**, 40, 498.
14. Vert, M.; Domurado, D., Poly(ethylene glycol): protein-repulsive or albumin-compatible? *Journal of biomaterials science. Polymer edition* **2000**, 11, (12), 1307-17.
15. Gombotz, W. R.; Guanghui, W.; Horbett, T. A.; Hoffman, A. S., *J. Biomed. Mater. Res.* **1991**, 25, 1547.

16. Maier, L.; Crutchfield, M. M., Organic phosphorus compounds. 70. Preparation and properties of new phosphorus containing chelating agents for calcium and magnesium ions. *Phosphorus and Sulfur and the Related Elements* **1978**, 5, (1), 45-51.

## ***Part II: Redox Conducting Polymers (Chapter 5)***

### **Chapter 5: Redox Conducting Polymers Containing Locked Concentration Gradient: Preparation and Study**

#### **INTRODUCTION**

This part of our study mainly concerns redox polymer films containing permanently locked concentration gradient, including preparation of these polymer films and study of their electrochemical properties. Physically “locked” concentration gradients in redox conducting films have been previously reported in a few groups<sup>1-6</sup>. In those reports, redox concentration gradients were immobilized by drying and/or cooling the film so that ion transportation in the films was thermally suppressed. Unfortunately, this preservation of the gradients was not permanent and was subject to a limited range of operational conditions. Finite ionic motion and the subsequent degradation of the gradients could be induced over time.

Our work has been aimed to permanently locking the redox gradients by chemically attaching counterions to the polymer backbone while maintaining the concentration gradients. Thus, limitations of the cooling/drying approach may be overcome.

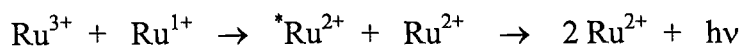
#### **BACKGROUND**

The widespread interest in redox polymers has been spurred by their applicability in the area of chemically modified electrodes<sup>1-17</sup>. For example, the electrocatalytic reduction

of O<sub>2</sub> on redox polymer modified electrodes has been of particular interest<sup>12-15</sup> for fuel cell applications. Redox polymers are characterized by the presence of spatially and electrostatically isolated electroactive sites. Typically, a redox polymer consists of a system where a redox-active transition metal based pendant group is covalently bound to some sort of polymer backbone which may or may not be electroactive<sup>17</sup>. Electrodes can be coated with redox polymers in several microstructural formats called sandwich, array, bilayer, and micro- electrodes<sup>16</sup>. Redox concentration gradients have been created using these microstructures<sup>1-6</sup>. Results of investigations of electron / ion transport through these gradient containing microstructures have been reported, which is essential for understanding the conductivity properties of these chemical materials. These microstructures also exhibit potentially useful electrical and optical responses, including current rectification and electroluminescence<sup>1-3,5,6</sup>.

Maness et al.<sup>2,3</sup> and Terrill et al.<sup>5,6</sup> utilized two distinct systems, Ru(bpy)<sub>3</sub>-based and viologen-based films, to study the gradient containing redox films. Both systems demonstrated interesting electronic properties due to the redox concentration gradients. In addition, the Ru(bpy)<sub>3</sub>-based films were capable of exhibiting electrochemically generated luminescence (ECL) when they possessed a serial gradient configuration. Moreover the ECL quantum yields match the efficiency of the best organic-polymer-based light-emitting devices<sup>1</sup>.

The light emission is a result of the following reaction:



Light emission occurred from the junction of the two gradients as shown in Figure 5.1. Degradation of the gradient results in loss of light production. Thus, the preservation

of the redox concentration gradients formed in these ECL films is integral to the development of practical light emitting devices employing these materials.

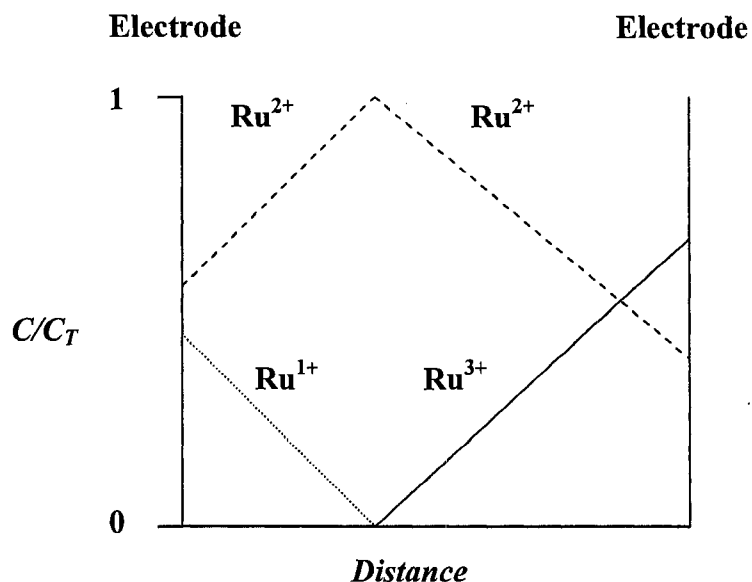


**Figure 5.1.** The diagrams depict the concentration gradients of the redox states in a polymer film between two electrodes.  $C/C_T$  is the relative concentration of the oxidized states. The lines represent the concentration of the species with distance.

The literature approaches to “freeze” the concentration gradient involved cooling and/or drying the film while maintaining the bias. Drying the film could significantly reduce ionic transport rate through the film. Further suppression of the ionic conductivity was achieved by modestly reducing the temperature of the film (ca.  $-30^{\circ}C$ , depending on the film employed). Preservation of the gradients by drying and cooling the films was however, not permanent. Finite ionic motion and the subsequent degradation of the gradients could be induced in  $Ru(bpy)_3$ -based films operating under reverse bias for prolonged times (ca. 10 mins). The resulting change in the electronic behavior of these films was consistent with gradient relaxation.

Our approach to locking the redox concentration gradients utilized pendant acrylate groups on the polymer chain. The monomers used in our study contain more than one acrylate group per molecule. Monomer films spin-coated on working electrodes are dried and thermally polymerized. In previous studies<sup>11</sup>, it was found that only 25% of the acrylate groups of the monomer participated in thermal polymerization at 150°C, leaving a significant portion of the pendant acrylate groups available for polymerization with incorporated polymerizable counterions.

By cycling the redox state of the polymer in a solution containing polymerizable electrolyte, polymerizable counterions would be electrochemically exchanged into the films. Then, redox concentration gradients would be formed by applying a potential bias to the polymer film using a bipotentiostat. After that, the film is removed from solution and allowed to dry, during which time the gradients in the film would be maintained by application of a potential bias. The film would then be heated a second time to graft the incorporated counterions to the polymer as well as further polymerize the film itself. The grafted counterions would then permanently lock the redox concentration gradient in the film. This gradient should be stable regardless of exposure to solvents, temperature variations and a wide range of voltage biases.

The counterions chosen for use possess pendant acrylate moieties. Figure 5.2(a) shows the structure of the electrolyte (2-acryloyloxy-ethyl)-tributyl-ammonium 3-acryloyloxy-propane-1-sulfonate,  $\text{ATA}^+\text{APS}^-$ . Both the cation  $\text{ATA}^+$  and anion  $\text{APS}^-$  are modified with polymerizable acrylate groups. These functional groups should thermally polymerize with the acrylate groups on the polymer at temperature that should not have any deleterious affect on the films.

The redox active monomers used in this study are shown in Figure 5.2(b). All are heteroleptic complexes of iron with cyano and bipyridine-based ligands. They were chosen primarily for three reasons: i) As can be seen from Table 5.1,  $\text{Fe}(\text{CN})_2(\text{bipy})_2$  and  $[\text{Fe}(\text{CN})_4(\text{bipy})]^{2-}$  have  $\text{Fe}^{3+/2+}$  redox activities at potentials around zero (vs SCE), which allows for easy operation since strict exclusion of water and air from the electrochemical cell is not necessary at those potentials, ii) they exhibit fast electrochemical rates (see Table 5.1), suggesting facile redox gradient formation across their polymer films and iii) the redox potentials of  $\text{Fe}(\text{CN})_2(\text{bipy})_2$  and  $[\text{Fe}(\text{CN})_4(\text{bipy})]^{2-}$  are in the region where the polymerizable electrolyte,  $\text{ATA}^+\text{APS}^-$ , is essentially electrochemically inactive.

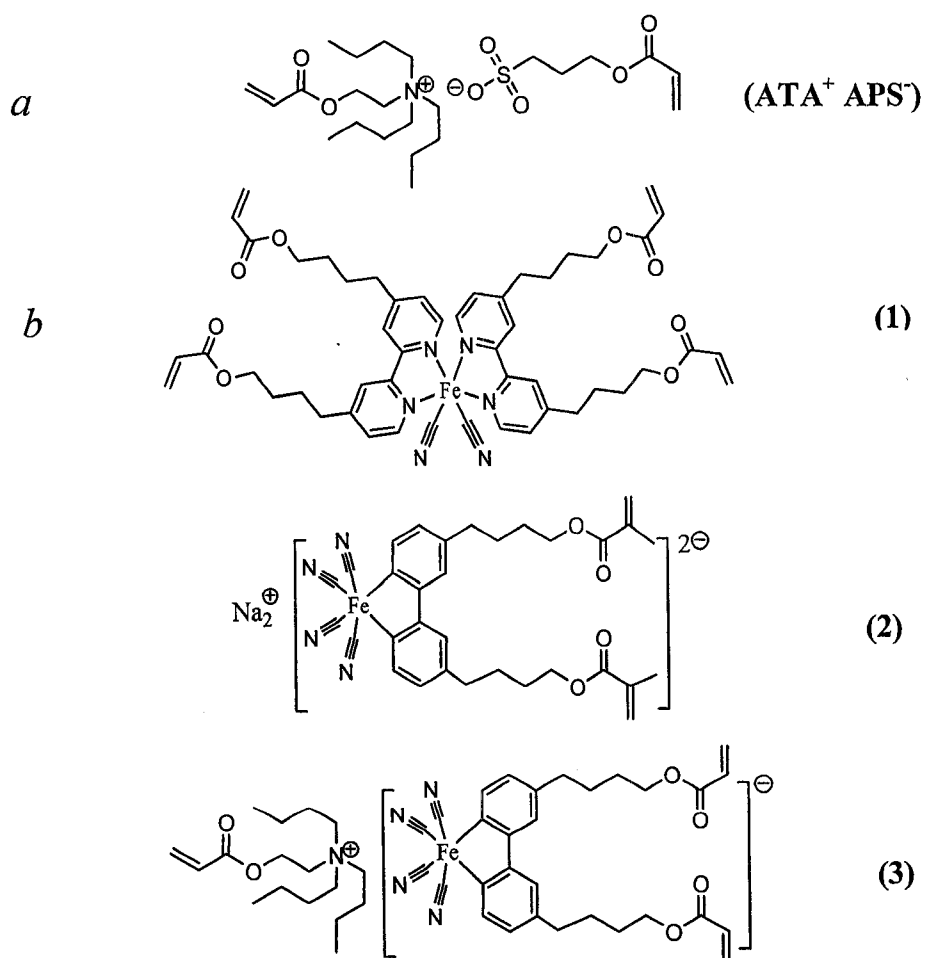


**Figure 5.2.** (a) molecular Structures of polymerizable electrolyte  $\text{ATA}^+\text{APS}^-$  and (b) molecular Structures of monomers 1, 2 and 3.

**Table 5.1.** Electrochemical properties of iron complexes.  $E^{\circ}$ : formal redox potential;  $(k_{s,h})_{obs}$ : apparent electrochemical rate constant.

	$Fe[B(pz)_4]_2^a$	$Fe[HB(pz)_3]_2^a$	$Fe(CN)_2(bipy)_2^b$		$[Fe(CN)_4(bipy)]^{2-}^b$
Solvent	1:1 acetone /THF	1:1 acetone /THF	water	DMF	water
$E^{\circ}$ , V vs SCE	0.06	-0.04	0.53	0.47	0.31
$(k_{s,h})_{obs}$ /cm s <sup>-1</sup>	1.5	2.2	0.63	0.41	0.43

a: data are obtained from Reference<sup>18</sup>

b: data are obtained from Reference<sup>19</sup>

Monomer **1** is a neutral iron(II) complex with 4 acrylate groups. The overall oxidation state of monomer **1** is zero, there are no associated counterions and polymerizable anions  $APS^-$  would be incorporated during the gradient forming process. Monomer **2** is an anionic iron(II) complexes with two acrylate groups. The complex has a 2- overall charge and is associated with two  $Na^+$  ions for purpose of charge neutrality. The  $Na^+$  ions can be electrochemically replaced by polymerizable cations  $ATA^+$  prior to establishing the concentration gradient. Monomer **3** is an anionic iron(III) complexes with two acrylate groups. It has one negative charge and is associated with one charge-compensating cation  $ATA^+$ , which will be fixed in the film via crosslinking with the monomer.

As can be seen from Table 5.1, Iron complexes with polypyrazolyborate  $[Fe(pzb)_2]^{+0}$  ( $pzb^- = \text{hydrotris(pyrazol-1-yl)borate } [HB(pz)_3]^-$  or tetrakis(pyrazol-1-yl)borate  $[B(pz)_4]^-$ ) also exhibit<sup>18</sup> ~zero redox potentials (vs SCE) and fast electrochemical rates. Attempts were made to prepare their polymerizable analogs (see below). But in the end, those efforts were abandoned, and all further efforts focused on the heteroleptic CN/bipy systems.

# EXPERIMENTAL

## Chemicals and Equipment

A Bioanalytical System BAS 100 B Potentiostat-Galvanostat controlled by BAS 100 W software resident on an IBM-compatible personal computer, was used for electrochemical studies of electrolytes and redox active monomers. A Pine Instruments RDE4 bipotentiostat, modified to provide a potential range of  $\pm 5$  V, was utilized for both film voltammetry and gradient formation. A Keithley 178 digital multimeter was used in conjunction with the RDE4 to closely monitor the potentials applied to the films. Voltammetry of gradient-locked films was achieved using an EG&G Princeton Applied Research Model 173 potentiostat/ galvanostat. Temperature controlled polymerization experiments were performed with a LAB-LINE Duo Vac Oven in conjunction with a Welch Duo Seal oil pump to maintain the pressure inside the oven (3 mmHg).

All chemicals used were purchased from Aldrich unless otherwise stated. All solvents were A. C. S. grade or better. Optima grade acetonitrile was purchased from Fisher Scientific.

## Electrodes and Cells

For all electrochemical experiments, a single compartment cell was used with a sodium saturated calomel (SSCE) electrode as the reference electrode and a platinum wire as the counter electrode. The interdigitated array (IDA) electrodes were purchased from Abtech Scientific, Inc. Two types of IDA electrodes were used in this study, Pt 1025.5 and Pt 0550.3. Both of them had two "combs" of Pt array microelectrodes (digits) sputter-deposited onto an insulating glass chip. Figure 5.3 shows a schematic diagram depicting the IDA structure. Pt 1025.5 has 25 digit pairs. Each digit has width 10 $\mu$ m,

digit length 5mm and interdigit space 10 $\mu$ m. Pt 0550.3 IDA has 50 pairs of digits with width 5 $\mu$ m, length 3mm and interdigit space 5 $\mu$ m. A clip produced in our lab accomplishes electrical contact to the IDAs.

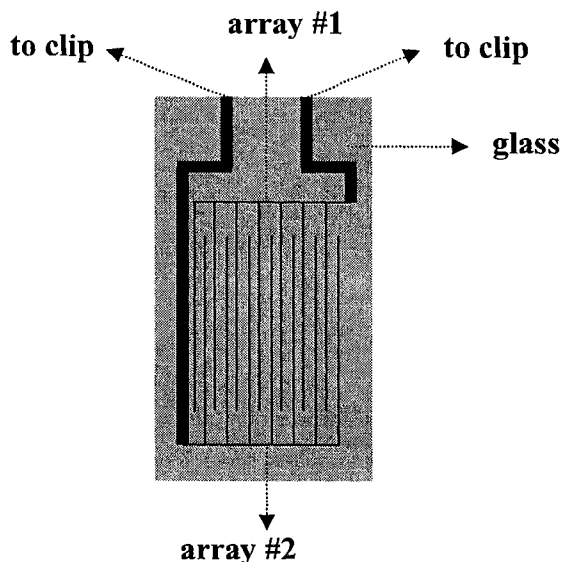


**Figure 5.3.** Schematic diagram of IDA electrode consisting of two interdigitated arrays. This diagram does not depict the realistic digit numbers.

### Synthesis of Polymerizable Electrolytes

The electrolyte with polymerizable cation and polymerizable anion (2-acryloyloxy-ethyl)-tributyl-ammonium 3-acryloyloxy-propane-1-sulfonate,  $\text{ATA}^+\text{APS}^-$ , was prepared step-by-step as follows:

#### *A. (2-hydroxy-ethyl)-tributylammonium bromide*

(2-Hydroxy-ethyl)-tributylammonium bromide was prepared by modification of the literature procedure.<sup>20</sup> Equal molar amounts of tributylamine (6.5g, 35 mMol) and 2-bromoethanol (4.6 g, 35 mMol) were stirred at 70 °C under nitrogen for two days. The mixture was cooled to room temperature and dissolved in 50 ml water. The resultant

aqueous solution was thoroughly washed with ether to remove unreacted tributylamine and 2-bromoethanol. Evaporation of the aqueous layer under reduced pressure afforded the crude product as thick oil. Methylene chloride 100 ml was used to dissolve the product. The methylene chloride solution was dried with sodium sulfate and evaporated under reduced pressure. The residue weighed 9.80 g (yield 91%) and was used for preparation of (2-acryloyloxy-ethyl)-tributyl-ammonium bromide without further purification. <sup>1</sup>H NMR spectrum in CDCl<sub>3</sub> is shown in Figure 5.4.

*B. (2-acryloyloxy-ethyl)- tributyl-ammonium bromide*

(2-acryloyloxy-ethyl)- tributyl-ammonium bromide was prepared by modification of the literature procedure utilized by Fuerstner et al. to prepare (R)-acrylic acid 1-methyl-hex-5-enyl ester<sup>21</sup>. Under nitrogen, a solution of acrylate chloride (7.7 ml, 98 mMol) in 10 ml dry methylene chloride was added via cannula into the solution of 150 ml dry methylene chloride containing (2-hydroxy-ethyl)-tributyl-ammonium bromide (9.8 g, 32 mMol) and triethylamine (13 ml, 95 mMol), during which time the temperature of the reaction was maintained at 0 °C using ice/water bath. The mixture was then stirred under nitrogen from 0 °C to room temperature overnight. Solids formed when the solution was cooled back to 0 °C. The formed solids were removed by filtering. The filtrate was extracted with brine and dried with sodium sulfate. Volatiles were removed by rotatory evaporation. The residue was purified by column separation (silica, deactivated by 1% triethylamine/ hexane, as discussed in Chapter 2) with gradient methanol/methylene chloride as eluent; weighed 2.0 g (yield 18 %).

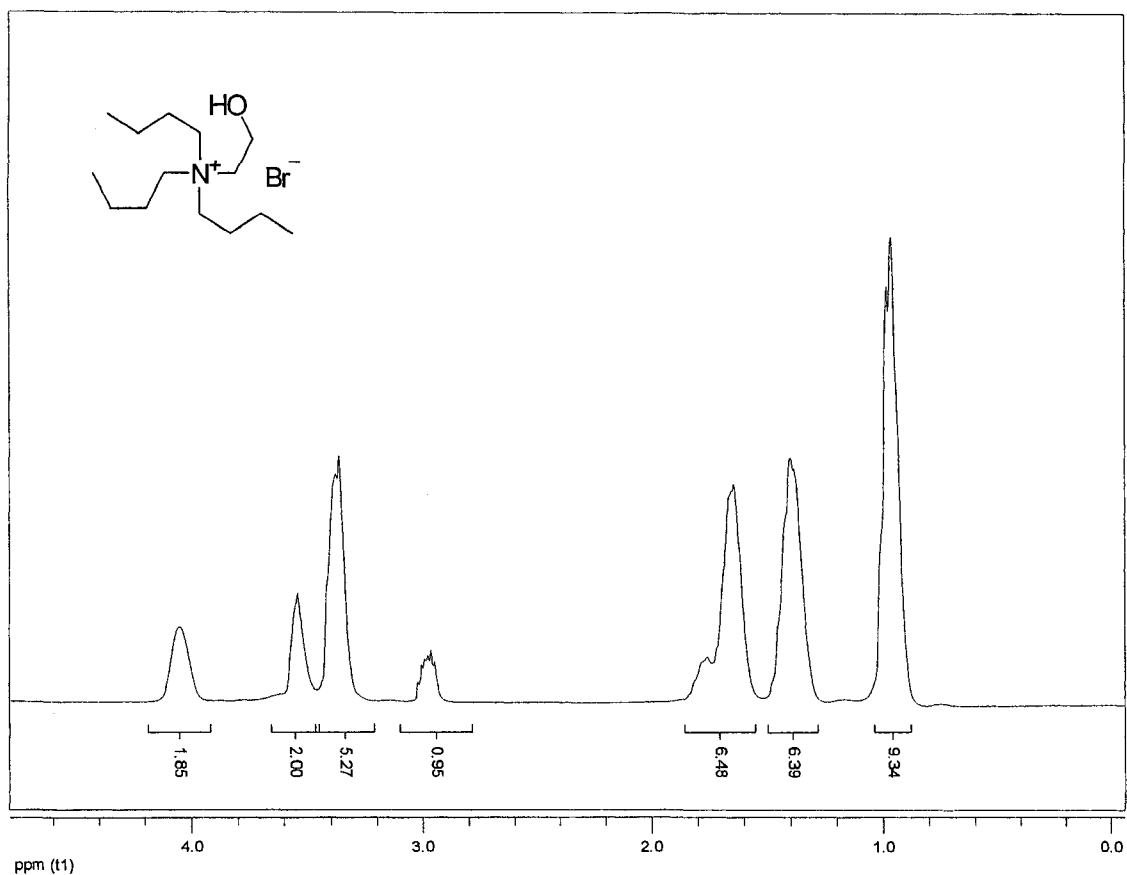


**Figure 5.4.** <sup>1</sup>H NMR spectra of (2-hydroxy-ethyl)-tributyl-ammonium bromide in CDCl<sub>3</sub>.

*C. (2-acryloyloxy-ethyl)- tributyl-ammonium 3-acryloyloxy-propane-1-sulfonate*

A solution of (2-acryloyloxy-ethyl)-tributyl-ammonium bromide (2.0g, 5.8 mMol) in 30 ml methylene chloride was slowly added into a solution of potassium 3-acryloyloxy-propane-1-sulfonate (2.7 g, 12 mMol) in 30 ml deionized water. After one hour's vigorous stirring, the mixture was transferred to a separatory funnel. The lower organic layer was collected and dried with sodium sulfate. Removal of the volatiles by rotatory evaporation resulted in crude product as thick oil. The product was purified by column separation (silica, deactivated by 1% triethylamine/ hexane) with gradient methanol/methylene chloride as eluent. Voltammograms of the product in methylene chloride are shown in Figure 5.5

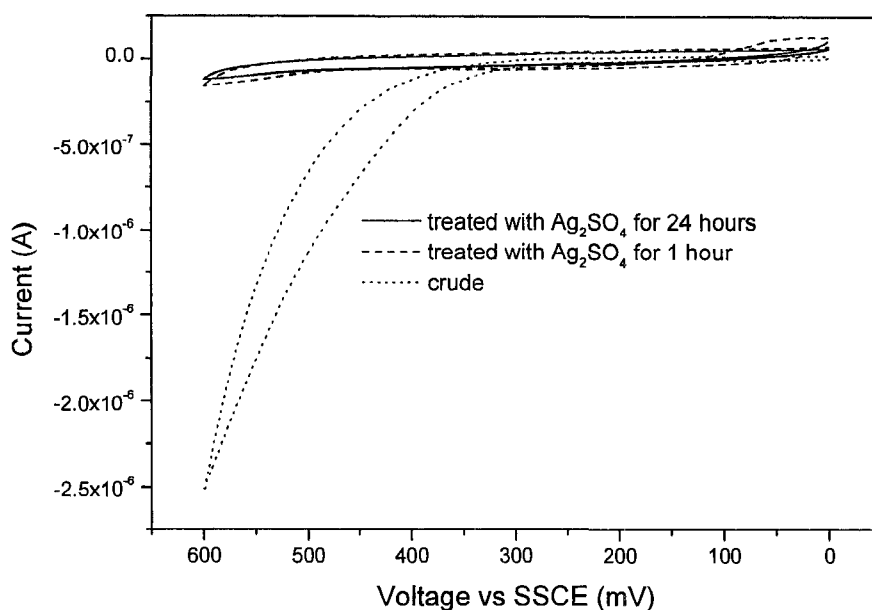


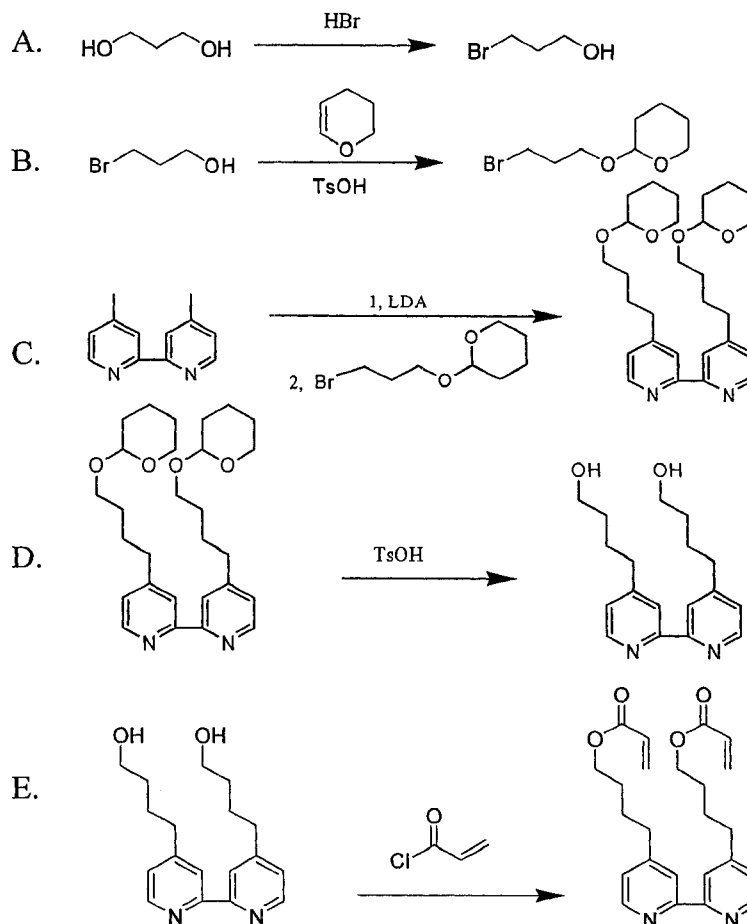
**Figure 5.5.** CVs of  $\text{ATA}^+\text{APS}^-$  on a Au (1 mm diameter) electrode in methylene chloride. Scan rate, 100 mV/s; R.E., SSCE; C.E., Pt wire.

As can be seen from the dotted curve in Figure 5.5, the product collected from column separation still contains electroactive impurity  $\text{Br}^-$ , which gave rise to a oxidation peak  $> 320$  mV vs SSCE. Since  $\text{Br}^-$  tends to absorb strongly onto the surface of solid silver sulfate, 2.0 g silver sulfate was then added in the methylene chloride solution (30 ml) of the product to remove the halogen contamination. Aliquots were taken out for electrochemical analysis while the mixture was stirred. As shown in Figure 5.5, the current dramatically decreased within one hour's  $\text{Ag}_2\text{SO}_4$ -treatment (dashed curve); and was further suppressed overnight (solid curve). The overall yield is 1.4 g (51%) after silver sulfate was removed by centrifuge and solvent was evaporated.

### Synthesis of the Coordinating Bipyridine Ligands

The strategy to synthesize the substituted bipyridine ligands is shown in Scheme 5.1.

*Scheme 5.1*



The following is preparation of all these compounds.

*A. 3-bromopropanol*

3-bromopropanol was prepared according to literature procedures<sup>22</sup>. To a solution of 1,3-propanediol (7.6 g, 0.10 mole) in 200 ml benzene was added hydrogen bromide (48% aqueous solution, 11 ml, 0.10 mole). The mixture was refluxed under nitrogen overnight while trapping water using a Dean-Stark water separator. After the reaction mixture was cooled to room temperature, benzene was removed under reduced pressure and the product was dissolved in 50 ml ether. The ether solution was washed with 20 ml 1M NaOH, 2 x 20 ml water and 20 ml brine, dried with sodium sulfate, and evaporated under reduced pressure, resulting in yellowish oil 8.8 g (yield 63 %).

*B. 2-(3-bromo-propoxy)-tetrahydropyran*

The literature procedure<sup>23</sup> was modified as follows: under nitrogen, a solution of 3-bromopropanol (28 g, 0.20 mol) and *p*-toluenesulfonic acid monohydrate (0.39g, 2.0 mmol) in 200 ml ether was cooled to 0 °C. 3,4-Dihydro-2*H*-pyran (31 ml, 0.32 mol) was added by cannula while stirring. The mixture was stirred from 0 °C to room temperature overnight. Then the solution was washed by 100 ml saturated sodium bicarbonate aqueous solution, 100 ml water, and 100 ml brine, dried with sodium sulfate. Ether was removed by rotatory evaporation. The residue was purified by vacuum distillation (3mm Hg, 84-90 °C), resulting in 39 g colorless liquid (yield 100 %).

*C. 4,4'-bis[(tetrahydropyran-2-yloxy)-butyl]-2,2'-bipyridine*

Preparation of 4,4'-bis[(tetrahydropyran-2-yloxy)-butyl]-2,2'-bipyridine was reported in literature<sup>24</sup>. A solution of butyl lithium (1.6M in hexane, 40ml, 61 mmol) was added dropwise into a solution of di-isopropylamine (8.5 ml, 61 mmol) in 40 ml dry THF under nitrogen, during which time the reaction temperature was maintained at 0 °C using a water/ice bath. The mixture was stirred at 0 °C for 50 mins. The resultant yellow solution was then added via cannula into a solution of 4,4'-dimethyl-2,2'-bipyridine (5.6 g, 30 mmol) in 210 ml dry THF, which was cooled to 0 °C. After the addition was done, the solution was stirred at 0 °C for one hour. A solution of 2-(3-bromo-propoxy)-tetrahydropyran (14g, 60 mmol) in 40 ml dry THF was then added via cannula. The mixture was stirred from 0 °C to room temperature overnight. 10 ml methanol was added to quench the reaction. Volatiles were removed under reduced pressure. The residue was dissolved in 100 ml methylene chloride. The methylene chloride solution was washed

with water and brine, dried with sodium sulfate and evaporated under reduced pressure, resulting in 15 g solid product (yield 100%).

*D. 4, 4'-bis(4-hydroxy-butyl)-2,2'-bipyridine*

4,4'-bis(4-hydroxy-butyl)-2,2'-bipyridine was synthesized from 4,4'-bis[(tetrahydropyran-2-yloxy)-butyl]-2,2'-bipyridine<sup>24</sup>. A solution of 4,4'-bis[(tetrahydropyran-2-yloxy)-butyl]-2,2'-bipyridine (5.6 g, 12 mmol) and *p*-toluenesulfonic acid monohydrate (0.65g, 3.4 mmol) in 150 ml absolute ethanol was refluxed under nitrogen overnight. Ethanol was removed with rotatory evaporation. The residue was dissolved in 100 ml methylene chloride. The methylene chloride solution was washed with saturated sodium bicarbonate, water and brine, dried with sodium sulfate and evaporated under reduced pressure. The obtained solid was purified by column separation (silica, deactivated by 1% triethylamine/ hexane) with gradient methanol/methylene chloride as eluent, weighed 3.3 g (yield 93%).

*E. 4,4'-bis(4-acryloyloxy-butyl)-2,2'-bipyridine (bab-bipy)*

Following the literature procedure<sup>21</sup>, a solution of acrylate chloride (1.21 ml, 14.2 mmol) in 15 ml dry methylene chloride was added via cannula into a solution of 4, 4'-bis(4-hydroxy-butyl)-2,2'-bipyridine (1.66g, 5.52 mmol) and triethylamine (4.47 ml, 31.8 mmol) in 50 ml dry methylene chloride, during which time the reaction temperature was maintained at 0°C with an ice-water bath. The solution was stirred from 0 °C to room temperature overnight. Volatiles were removed under reduced pressure. The residue was dissolved in 50 ml methylene chloride. The methylene chloride solution was washed with

saturated sodium bicarbonate, water and brine, dried with sodium sulfate and evaporated under reduced pressure. The crude product was purified by column separation (silica, deactivated by 1% triethylamine/ hexane) with gradient methanol/methylene chloride as eluent, weighed 1.85 g (yield 82%).  $^1\text{H}$  NMR spectrum is shown in Figure 5.6.

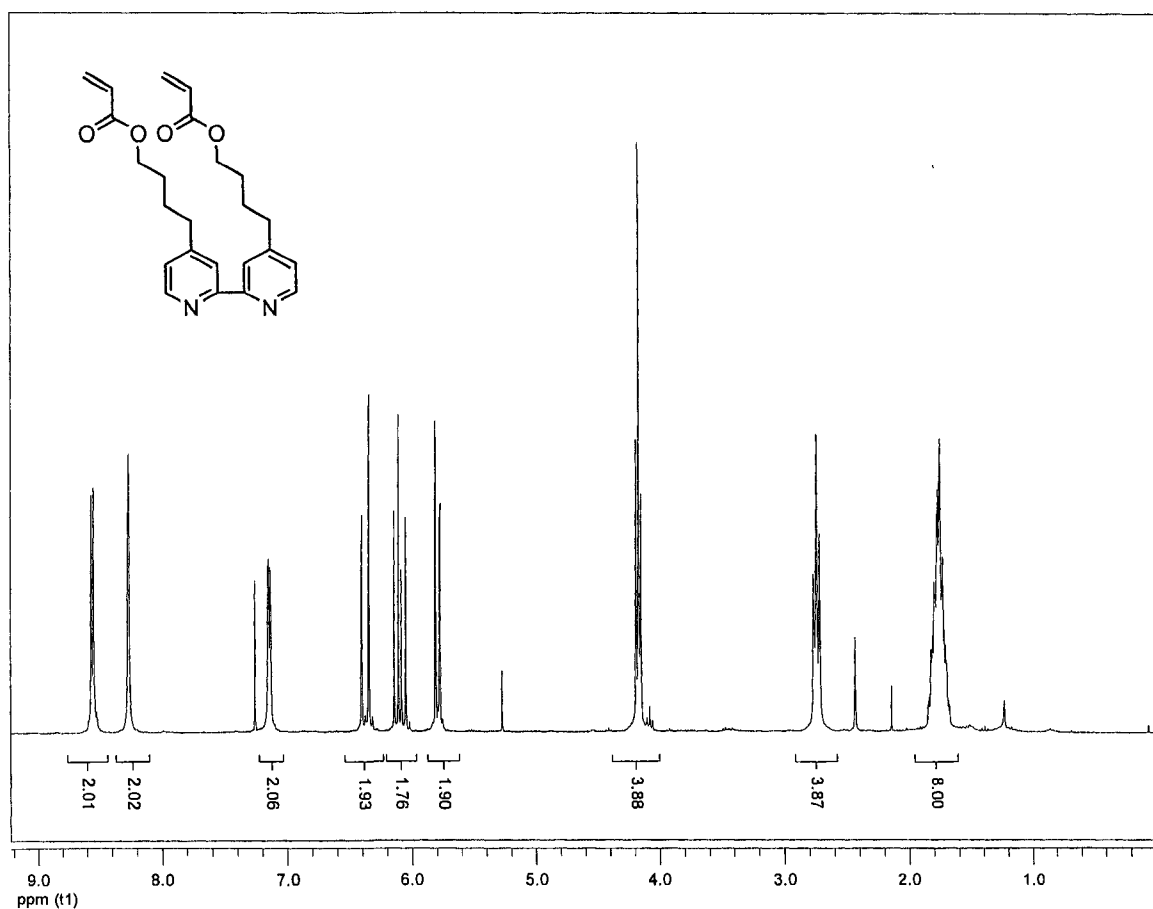


**Figure 5.6.**  $^1\text{H}$  NMR spectra of 4,4'-bis(4-acryloyloxybutyl)-2,2'-bipyridine in  $\text{CDCl}_3$ .

## Synthesis of Polypyrazolyborate Ligands

### A. 4-(3-Hydroxypropyl)pyrazole

*2-Ethoxy-3-tetrahydropyran* carboxaldehyde diethyl acetal is prepared in 100% yield by the method of Jones et al.<sup>25</sup> Dihydropyran (51 g, 0.56 mol) was added dropwise over a 2-h period to triethyl orthoformate (0.271, 1.6 mol) and  $\text{BF}_3 \cdot \text{Et}_2\text{O}$  (0.30 ml). The

reaction vessel was cooled periodically to maintain the temperature below 40 °C. After stirring overnight at room temperature, excess triethyl orthoformate was removed under reduced pressure and the product was distilled (3 mm Hg, 66°C) to give 122 g of clear, colorless liquid.

4-(3-Hydroxypropyl)pyrazole is prepared according to the method of Jones et al.<sup>25</sup> by adding the acetal (0.12 kg, 0.56 mol) in 90 ml of ethanol to hydrazine-dihydrochloride (62 g, 0.59 mol) in 170 ml of water. After heating overnight at 40-50 °C, the pH of the now homogeneous solution was adjusted to 13 with NaOH and volatile material was removed under reduced pressure. The residue was extracted with ethanol (3 X 100 ml) and the solvent was evaporated, yielding a yellow oil which was then distilled at 170~180°C under vacuum (3 mm Hg). The product (53 g) was isolated in 81% yield, its NMR spectra is shown in Figure 5.7.

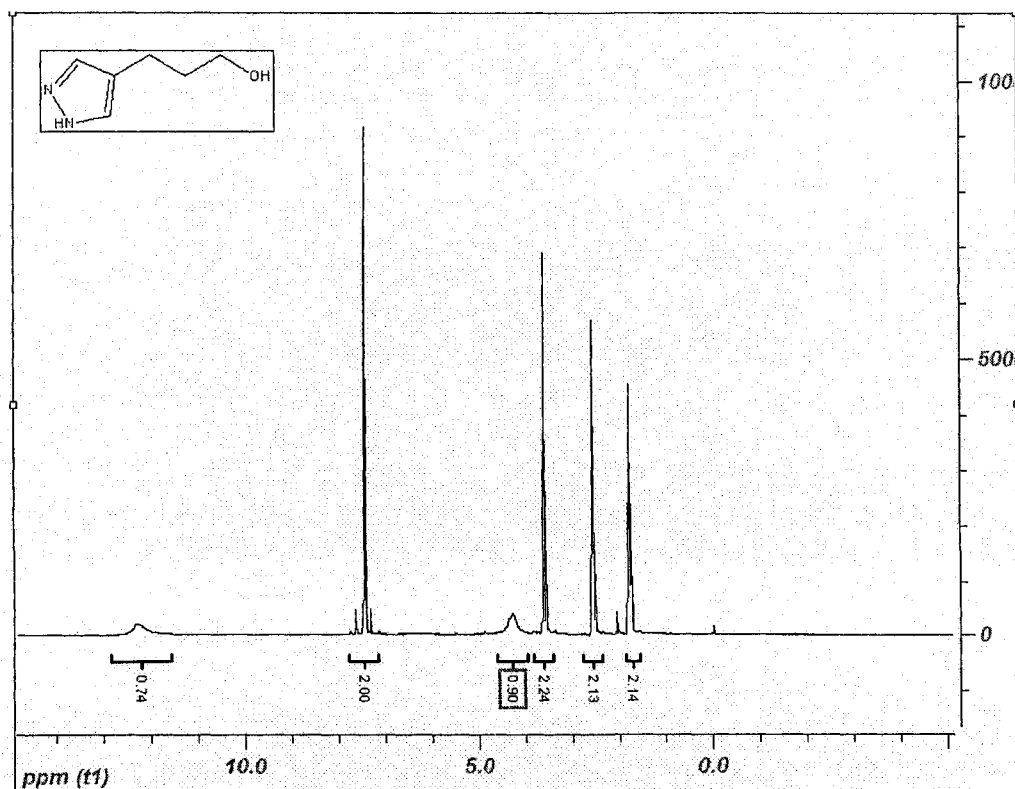


Figure 5.7. <sup>1</sup>H NMR spectra of 4-(3-Hydroxypropyl)pyrazole in CD<sub>3</sub>OD.

B. 4-(3-Aminopropyl)pyrazole

*4-(3-Chloropropyl)pyrazole~hydrochloride* was prepared by adding 4-(3-hydroxypropyl)pyrazole (8.7 g, 0.069 mol) to 34 ml of thionyl chloride, holding the temperature at 60 °C for 15 min, and removing the excess thionyl chloride at 70 °C under vacuum to leave a crystalline, yellow residue. This was then recrystallized from ethanol-ethyl ether to give a white solid, 11 g, yield 85%

*4-(3-Phthalimidopropyl)pyrazole* was made by adding sodium bicarbonate (6.6 g, 0.079 mol) at 25 °C to a solution containing 4-(3-chloropropyl)pyrazole~hydrochloride (11 g, 0.059 mol) and potassium phthalimide (11 g, 0.059 mol) in 75 ml of dimethylformamide. The mixture was refluxed for 30 minutes and 20 mg NaI was added and refluxed for another 30 minutes, cooled, filtered, and added to 200 ml of water to give a white precipitate. This was recrystallized from water to give a white solid of 9.7 g, in 67% yield.

*4-(3-Aminopropyl)pyrazole.dihydrochloride* was prepared by refluxing the phthalimide intermediate (9.7 g, 0.038 mol) in 90 ml of 6 N HCl overnight. The clear solution is cooled to 4 °C, phthalic acid is removed by filtration, and the filtrate was evaporated to dryness. The residue was recrystallized from ethanol-ethyl ether to give 5.9 g of a white solid, in 77% yield.

*4-(3-Aminopropyl)pyrazole* was prepared by titrating the ethanol solution of 4-(3-aminopropyl)pyrazole.dihydrochloride with saturated NaOH solution till the solution's pH reached 8~9. Solids were removed with filtering and the filtrate was evaporated to dryness under reduced pressure. The oil residue was distilled under vacuum (3 mm Hg); the fraction of 160°C was collected. The NMR spectrum in D<sub>2</sub>O is shown in Figure 5.8.

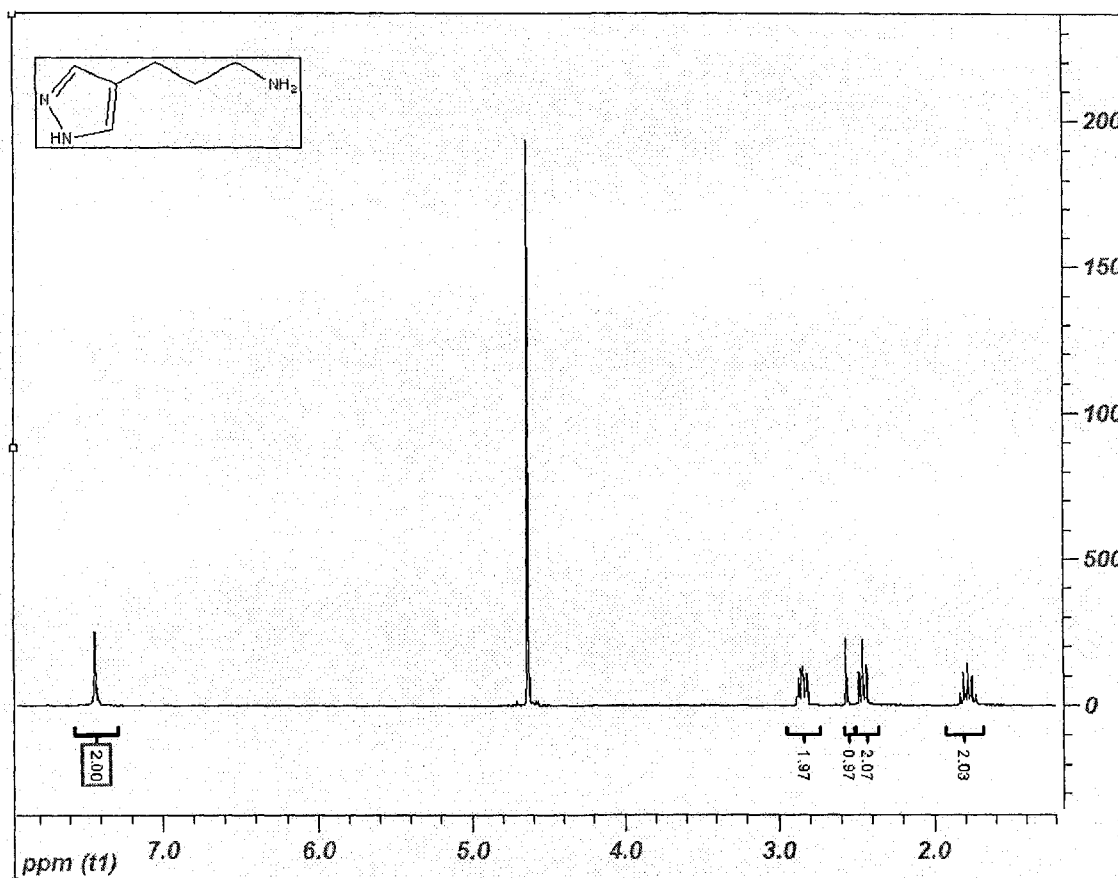


Figure 5.8. <sup>1</sup>H NMR spectra of 4-(3-aminopropyl)pyrazole in D<sub>2</sub>O.

C. Potassium hydrotris(4-R-pyrazolyl)borate, where R stands for -3-hydroxypropyl or -3-aminopropyl)

Preparations were attempted following Trofimenko's method.<sup>26</sup> A solid mixture of one equivalent of KBH<sub>4</sub> and four equivalents of 4-R-pyrazolyl was heated to a temperature ranging from 165 °C to 180 °C until 3 equivalents of hydrogen was produced (the volume of hydrogen was measured by water exclusion method). The mixture was cooled to room temperature and washed thoroughly with ether. The product was analyzed by NMR, IR and titration with Fe<sup>2+</sup> aqueous solution (see comments made after Scheme 5.5).

D. Triethylammonium p-phenylene-di-(trispirazolyborate)

*1,4-Bis(dibromoboryl)benzene* was prepared by the method of Haubold and coworkers.<sup>27</sup> Liquid BBr<sub>3</sub> was purified by vacuum distillation using Schlenk lines. Purified BBr<sub>3</sub> (4.0 ml, 42 mmol) was charged with stirring into a schlenk flask fitted with 1,4-bis(trimethylsilyl)benzene (4.4 g, 19 mmol). The solution was heated at 80°C under nitrogen for two days. Volatiles were removed by vacuum distillation, the solid residue was recrystallized in 1:1 pentane / methylene chloride at -70°C, giving a white crystalline solid, weighing 3.8 g (yield 48%). The NMR spectrum in CDCl<sub>3</sub> is shown in Figure 5.9.

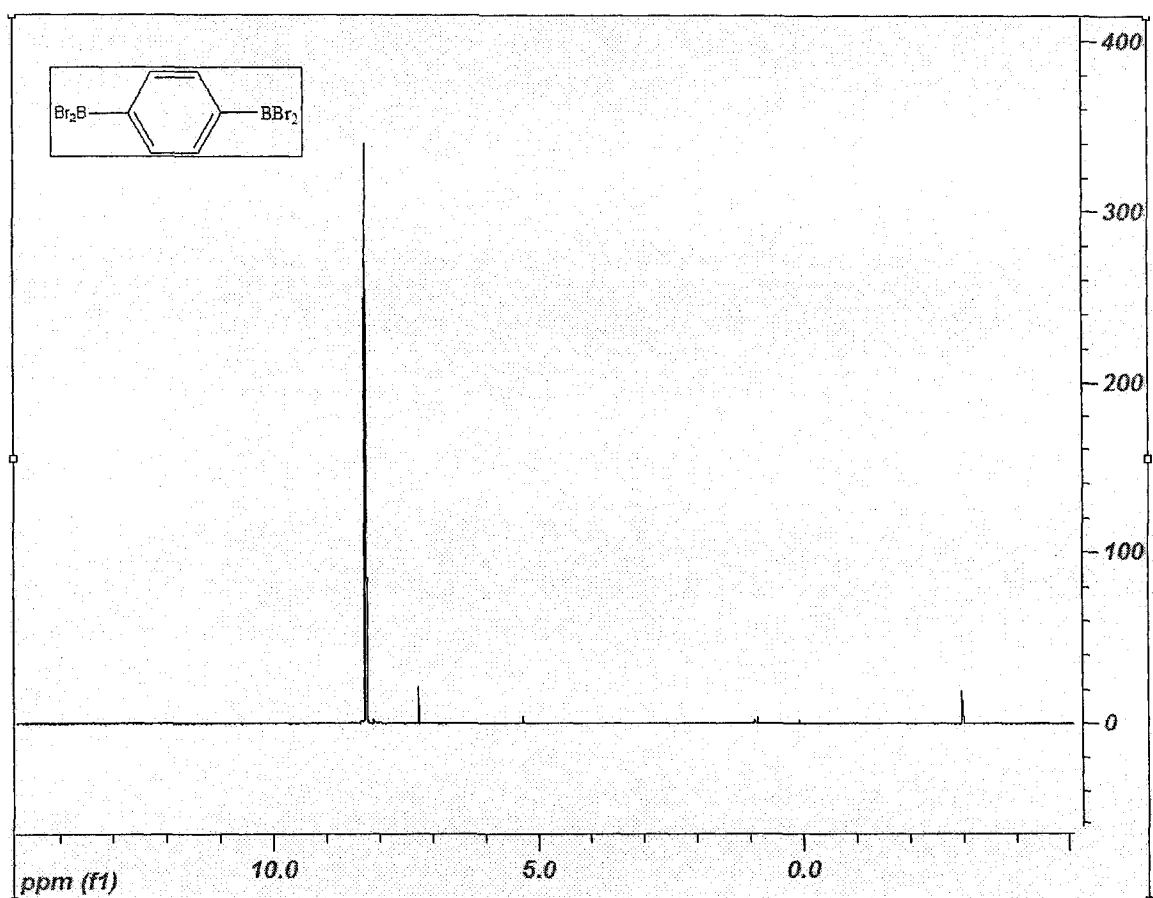


Figure 5.9. <sup>1</sup>H NMR spectra of *1,4-bis(dibromoboryl)benzene* in CDCl<sub>3</sub>.

Preparation of triethylammonium p-phenylene-di-(trispyrazolylborate) was attempted by modification of the literature method.<sup>28</sup> In a nitrogen glove box, 1,4-bis(dibromoboryl)benzene (0.19 g, 0.46 mmol) was dissolved in 30 ml acetonitrile, and a solution of pyrazole (0.19 g, 2.8 mmol) in 15 ml acetonitrile was added dropwise while stirring. Excess triethylamine (~1 ml) was added and the mixture was stirred overnight. Volatiles were removed under reduced pressure and the solid residue was dried in vacuum overnight (see comments made after Scheme 5.5).

### Preparation of Cyanoiron Bipyridine Complexes

*Dicyano-bis-[4,4'-di(4-acryloyloxy-butyl)-2,2'-bipyridine]Iron(II)* (**1**) was successfully prepared following Schilt's strategy<sup>29</sup> to prepare  $\text{Fe}(\text{CN})_2(\text{bipy})_2$ . A solution of 4,4'-bis(4-acryloyloxy-butyl)-2,2'-bipyridine (1.4g, 3.3 mmol) and ammonium iron(II) sulfate hexahydrate (0.44g, 1.1 mmol) in 45 ml water was heated to 90 °C, into which a freshly prepared solution of potassium cyanide (1.1 g, 17 mmol) in 3 ml water was added all at once. After brief stirring, the solution was left to cool at room temperature for a few hours. Methylene chloride 50 ml was added to extract the product from the aqueous mixture. The methylene chloride solution was separated, dried over sodium sulfate and evaporated under reduced pressure. The residue was purified by column separation (silica, deactivated by 1% triethyleamine/hexane) with gradient methanol /methylene chloride as eluent, weighed 1.9 g (yield 82%).

*Potassium Tetracyano-mono-[4,4'-di(4-hydroxyl-butyl)-2,2'-bipyridine] ferrate(II)* was prepared by following the Schilt's strategy to prepare  $\text{K}_2[\text{Fe}(\text{CN})_4(\text{bipy})]$  with minor

modification. A solution of 4,4'-di(4-hydroxyl-butyl)-2,2'-bipyridine (1.25g, 4.16 mmol) and ammonium iron(II) sulfate hexahydrate (0.543 g, 1.38 mmol) in 300 ml water was heated to 90 °C. A freshly prepared solution of potassium cyanide (20.0 g, 0.31mol) in 30 ml water was added all at once. The mixture was stirred at 90 °C overnight and was allowed to cool to room temperature. After being washed thoroughly with methylene chloride, the aqueous solution was concentrated in vacuum with mild heating to ca. 50 ml, upon which a red solid formed. The solid was collected by filtration, dried at 35 °C in vacuum overnight, weighed 1.07 g (yield 100%).

*Sodium tetracyano-mono-{4,4'-di[4-(2-methyl-acryloyloxy)-butyl]-2,2'-bipyridine} ferrate(II) (2)* was prepared as follows. A solution of methacryloyl chloride (0.10 ml, 0.99 mmol) in 10 ml dry methylene chloride was added dropwise via cannula into a suspension of red solid potassium tetracyano-mono-[4,4'-di(4-hydroxyl-butyl)-2,2'-bipyridine] ferrate(II) (0.044g, ca. 90 μmol) in 15 ml dry methylene chloride under nitrogen, during which time the reaction temperature was maintained at 0 °C. The mixture was stirred from 0 °C to room temperature overnight, resulting in a yellow solution with some white precipitate. Solids were removed by filtering. Methanol 1 ml was added into the filtrate to quench excess methacryloyl chloride. Volatiles were evaporated. The residue was dissolved in 5 ml methanol. Dry sodium carbonate was added into the methanol solution and stirred overnight. The solution slowly turned from yellow to red. Excess sodium carbonate was filtered off. Filtrate was evaporated under reduced pressure. The product was purified by passing through a silica column with 1:10 water/acetone as eluent.

*Potassium Tetracyano-mono-[4,4'-di(4-hydroxyl-butyl)-2,2'-bipyridine] ferrate(III)* was prepared by oxidation of its Fe(II) analog with bromine. Over three fold excess of liquid bromine was added with a glass Pasteur pipette into a solution of potassium tetracyano-mono-[4,4'-di(4-hydroxyl-butyl)-2,2'-bipyridine] ferrate(II) ( 0.15g) in 5 ml methanol. The mixture was stirred overnight. Volatiles were evaporated. The crude product was used to prepare (2-acryloyloxy-ethyl)-tributyl-ammonium tetracyano-mono-[4,4'-di(4-acryloyloxy- butyl)-2,2'-bipyridine] ferrate(III) without further purification.

*(2-Acryloyloxy-ethyl)-tributyl-ammonium tetracyano-mono-[4,4'-di(4-acryloyloxy-butyl)-2,2'-bipyridine] ferrate(III)* (**3**) was prepared as follows. A suspension of potassium tetracyano-mono-[4,4'-di(4-hydroxyl-butyl)-2,2'-bipyridine] ferrate(III) (ca. 0.28 mMol), (2-hydroxy-ethyl)-tributyl-ammonium bromide (0.085g, 0.27 mmol) and triethylamine (1.0 ml, 7.1 mmol) in 30 ml dry methylene chloride was carefully degassed. Acryloyl chloride (0.35 ml, 4.3 mmol) was added via syringe at 0 °C. The mixture was stirred from 0 °C to room temperature overnight, during which time the red solid potassium tetracyano-mono-[4,4'-di(4-hydroxyl-butyl)-2,2'-bipyridine] ferrate(III) disappeared and some white solid developed, which was removed by filtering. Excess acryloyl chloride in the filtrate was quenched with 3 ml methanol. The quenched filtrate was washed with 10 ml water and 5 ml brine, dried with sodium sulfate and evaporated under reduced pressure. The solid product was degassed in vacuum overnight, weighed 0.093g, yield 39%.

### **Monomer Film Formation and Initial Polymerization**

Monomer solutions (ca. 20  $\mu$ l) were spin-coated onto working electrodes (GC or IDA) at 1500 rpm. The solvent was allowed to evaporate at room temperature. Once dry,

a uniform thin film of monomer covered the electrode. Repeating the above process produced thicker films.

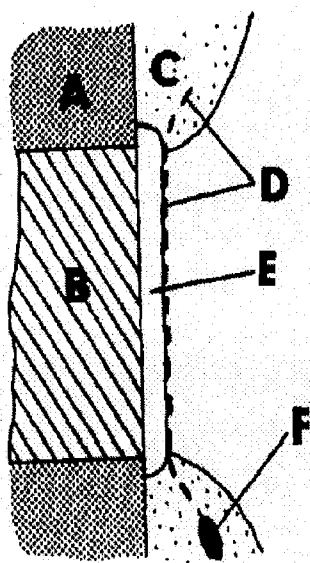
Monomer solutions were prepared by dissolving the monomer in an organic solvent. Methanol solutions of 20 mM **1** and **2** (20 mM) were prepared. A solution containing both **1** and **3** was prepared by adding a methylene chloride solution of **3** (~20 mM) dropwise into a methylene chloride solution of **1** (~20 mM), until the molar ratio of **3** to **1** reached unity. Contents of the mixture were determined electrochemically with cyclic voltammetry (CV) and square wave voltammetry (SWV).

Monomer films were thermally polymerized in vacuum (3mm Hg) at elevated temperature. Unpolymerized monomer was removed with solvent rinsing. Given the high number of acrylate groups on each monomer, crosslinked polymers should readily form. The degree of polymerization was crucial for film quality and concentration gradient formation. Insufficient polymerization produced unstable films, which would dissolve either during rinsing process or during attempts to perform electrochemistry. On the other hand, over-crosslinking hindered movement of counter ion within the film, which would make redox gradient formation difficult.

### **“Sandwich” Electrode Fabrication**

The construction of the “sandwich” electrode (shown in Figure 5.10) has been previously reported during our group’s earlier work<sup>7</sup>. A monomer film supported on a glassy carbon (GC) electrode (3 mm diameter) was thermally polymerized (100°C, 30 min.). A second very thin film (<< 1 μm) was then spin-coated over the first film and a piece of Au minigrid was pressed onto the surface. The assembly was heat-treated a second time (100°C, 5 min.) to bond the Au to the polymer surface. Electrical contact was

provided to the edge of gold electrode using a conducting silver paint. Finally, the GC/polymer/Au was masked with epoxy so as to expose only the Au surface to solution.



- A Pyrex mount
- B GC (0.07 cm<sup>2</sup>)
- C epoxy mask
- D porous gold minigrid electrode
- E polymer film
- F silver paint contact for Au electrode

*Figure 5.10.* "Sandwich" electrode construction. Reprinted from reference 7.

### Redox Gradient Formation and Locking

As shown in Figure 5.11, redox gradient formation was carried out using a bipotentiostat to control the potentials of the working electrodes (WE1 and WE2), which were coated with a redox film. In a solution of 50mM ATA<sup>+</sup>APS<sup>-</sup> in acetonitrile, the potential of WE1 is held at a fixed potential lower than the Fe<sup>2+/3+</sup> redox potential of the polymer film, and WE2 was slowly scanned to a potential higher than the redox potential and was held at that potential until the current decayed to a steady value. For sandwich electrodes, WE1 is the Au electrode and WE2 is the GC electrode. For IDA electrode, one of the combs is designated as WE1 and the other one as WE2. Application of a potential bias to the polymer film, a concentration gradient was developed in the film.

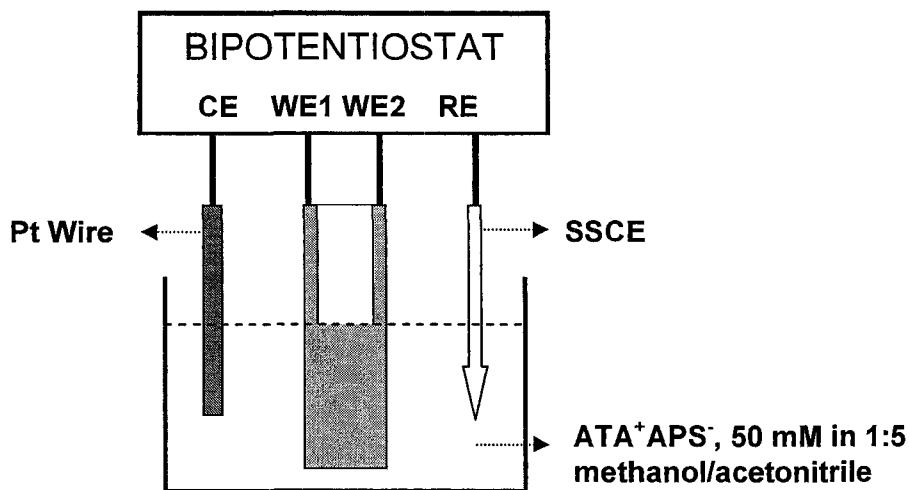


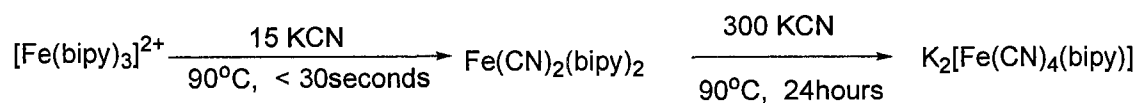
**Figure 5.11.** Electrochemical experiments to form a redox concentration gradient.

Then, the working electrodes were taken out of the electrolyte solution without being detached from the bipotentiostat. The film containing the redox gradient was rinsed with acetonitrile, dried in air and heated at elevated temperature (vide infra). A thin copper bus was used to maintain the electrical connection between the bipotentiostat and the electrodes throughout these rinsing, drying and heating processes.

## RESULTS AND DISCUSSION

### Synthesis of the Bipyridine-Based Monomers

*Scheme 5.2*



The above scheme was utilized by Schilt<sup>29</sup> to prepared mixed-ligand iron(II) complexes with cyanide (CN<sup>-</sup>) and 2,2'-bipyridine (bipy). The neutral iron complex

$\text{Fe}(\text{CN})_2(\text{bipy})_2$  formed almost instantly after mixing a solution of 15 equivalents of KCN with a hot solution of one equivalent  $[\text{Fe}(\text{bipy})_3]^{2+}$ . However, it took a lot more KCN (over 300 equivalents excess) and much longer reaction time (24 hours) for the anionic complex  $[\text{Fe}(\text{CN})_4(\text{bipy})]^{2-}$  to form.

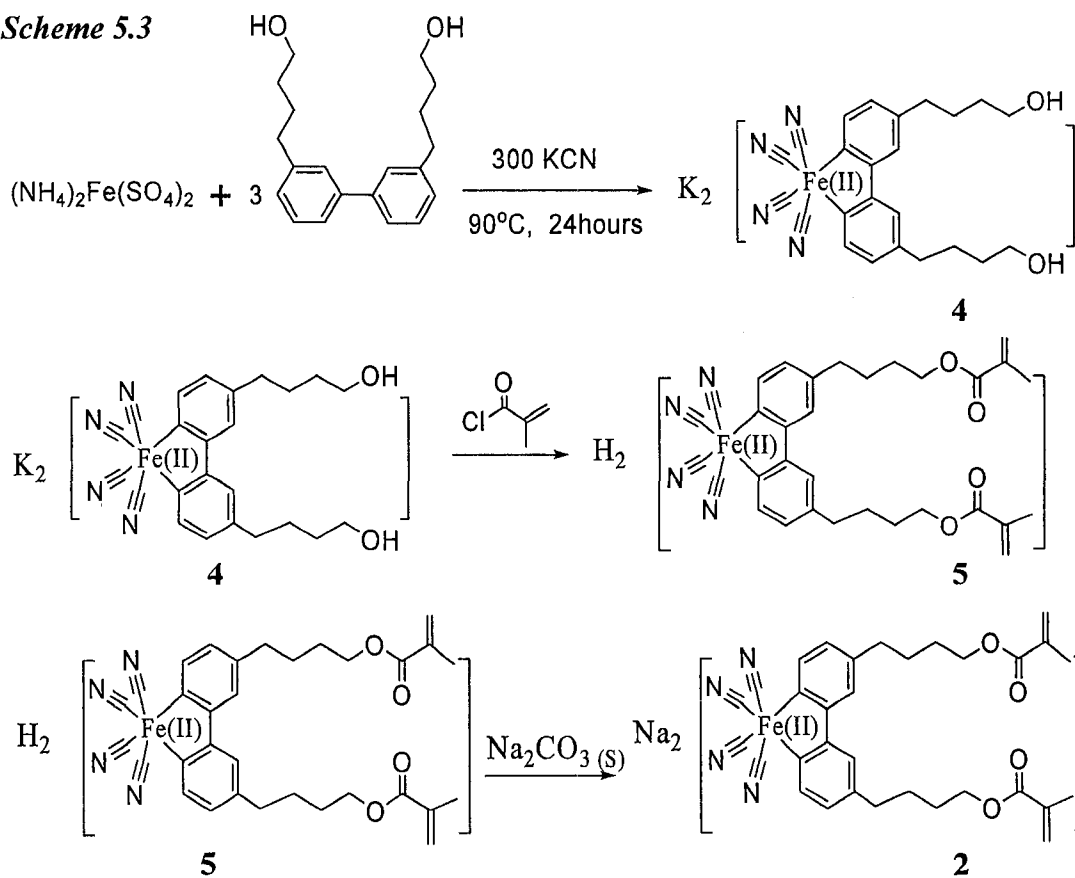
Synthesis of monomer **1** following Schilt's strategy was a success. It involved replacing one of the coordinating bipyridine ligands with two anionic cyano groups. One of the competing side reactions was hydrolysis of acrylate groups on the bipyridine ligands. The pKa of HCN is 9.1, thus aqueous solution of KCN are sufficiently basic to catalyze acrylate hydrolysis. Since the formation of **1** was quick (less than 30 seconds after mixing of the two reactants), ester hydrolysis had little chance to occur.

However, attempts to prepare  $[\text{Fe}(\text{CN})_4(\text{bab-bipy})]^{2-}$  via the Schilt route failed. No acrylate hydrogen was present in the  $^1\text{H}$  NMR spectrum of the product. According to Schilt, preparation of these anionic complexes required over 300 equivalents of KCN and 24 hours' heating. Under these reaction conditions, all the esters were hydrolyzed.

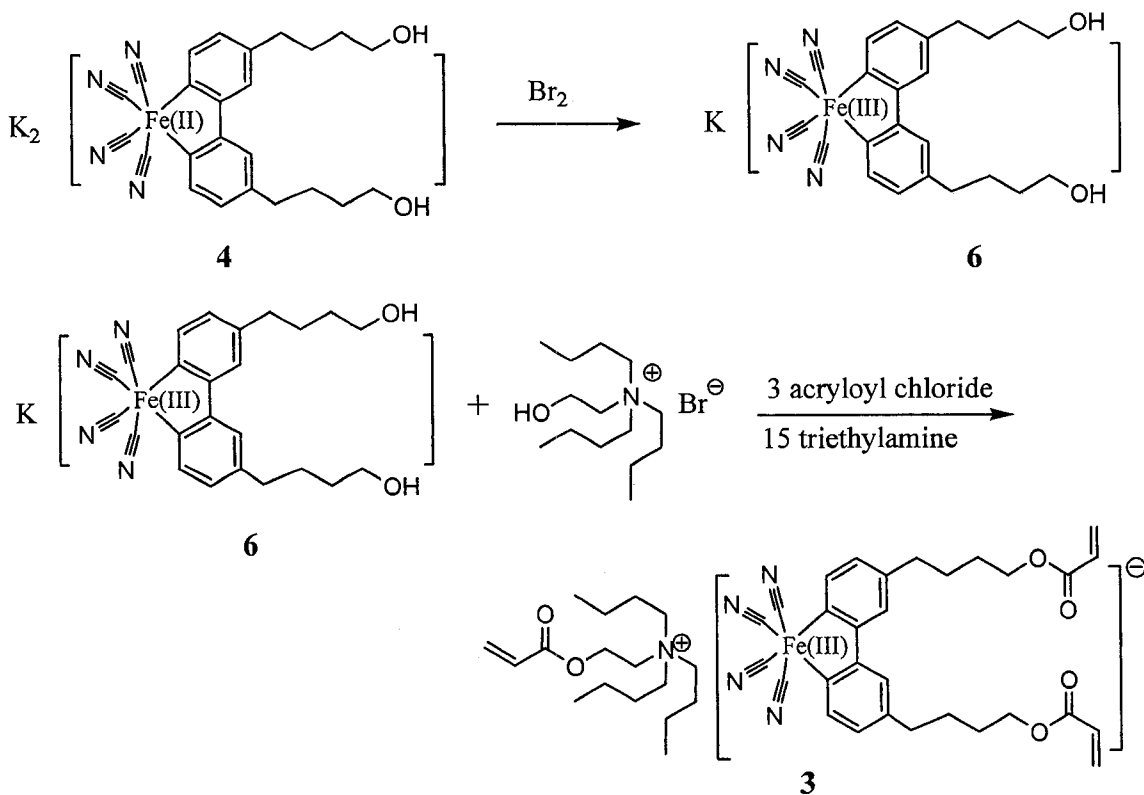
Thus, a different strategy (as shown in Scheme 5.3) was used to prepare the anionic iron complex. First, the precursor complex **4** was prepared following Schilt's procedure. Subsequent esterification of **4** with acryloyl chloride gave acid **5**<sup>29</sup>. The acid, **5**, was then neutralized with by stirring with solid  $\text{Na}_2\text{CO}_3$  to give monomer **2**.

Monomer **3** was prepared for its high solubility in organic solvents. As shown in Scheme 5.4, oxidizing precursor **4** with bromine afforded Fe(III) complex **6**. Treatment of a mixture of one equivalent **6** and one equivalent (2-hydroxy-ethyl)-tributyl-ammonium bromide with three equivalent acryloyl chloride and fifteen equivalent triethylamine gave polymerizable monomer **3**.

Scheme 5.3



Scheme 5.4



## Solvatochromic Behaviour of the Iron(II) Monomers

Mixed-ligand iron complexes with cyano and N-heterocyclic ligands are strongly colored, arising from metal-to-ligand charge-transfer bands in the visible region<sup>30</sup>. The visible color of monomers **1** and **2** is red/purple in methanol/ethanol, blue in acetonitrile and green in methylene chloride. The solvatochromic behavior of a large number of complexes has been previously reported<sup>19,31</sup>. The complexes prepared during this study provide a dramatic illustration of the solvent effects in the electronic spectra of the cyanoiron(II) complexes, as shown in Figure 5.12.

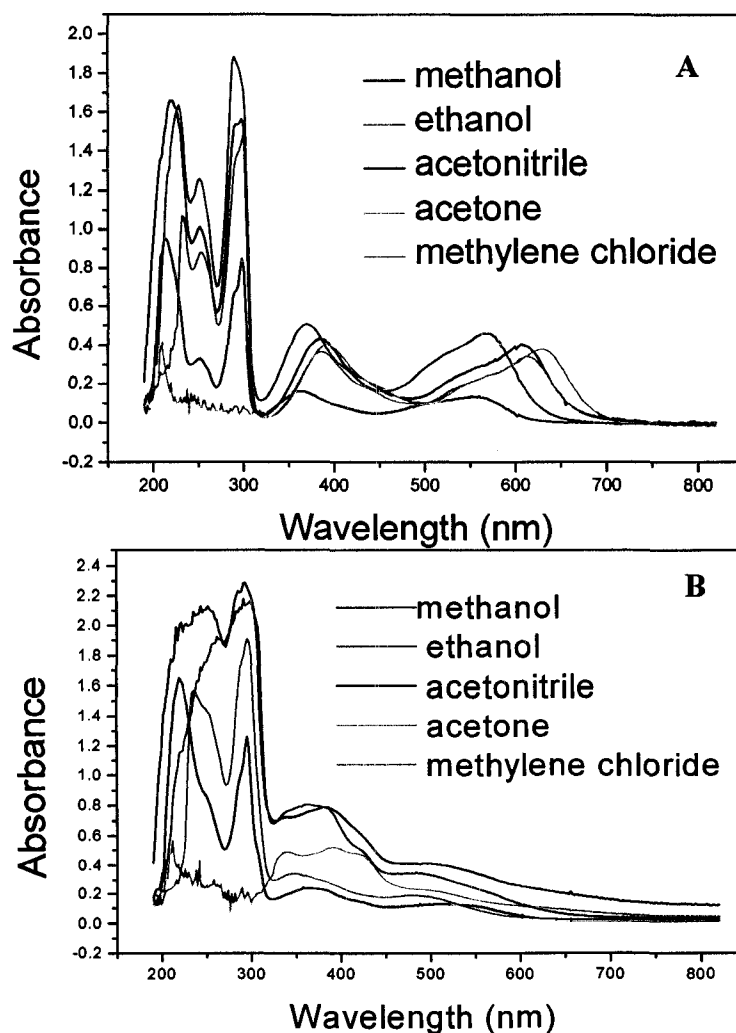
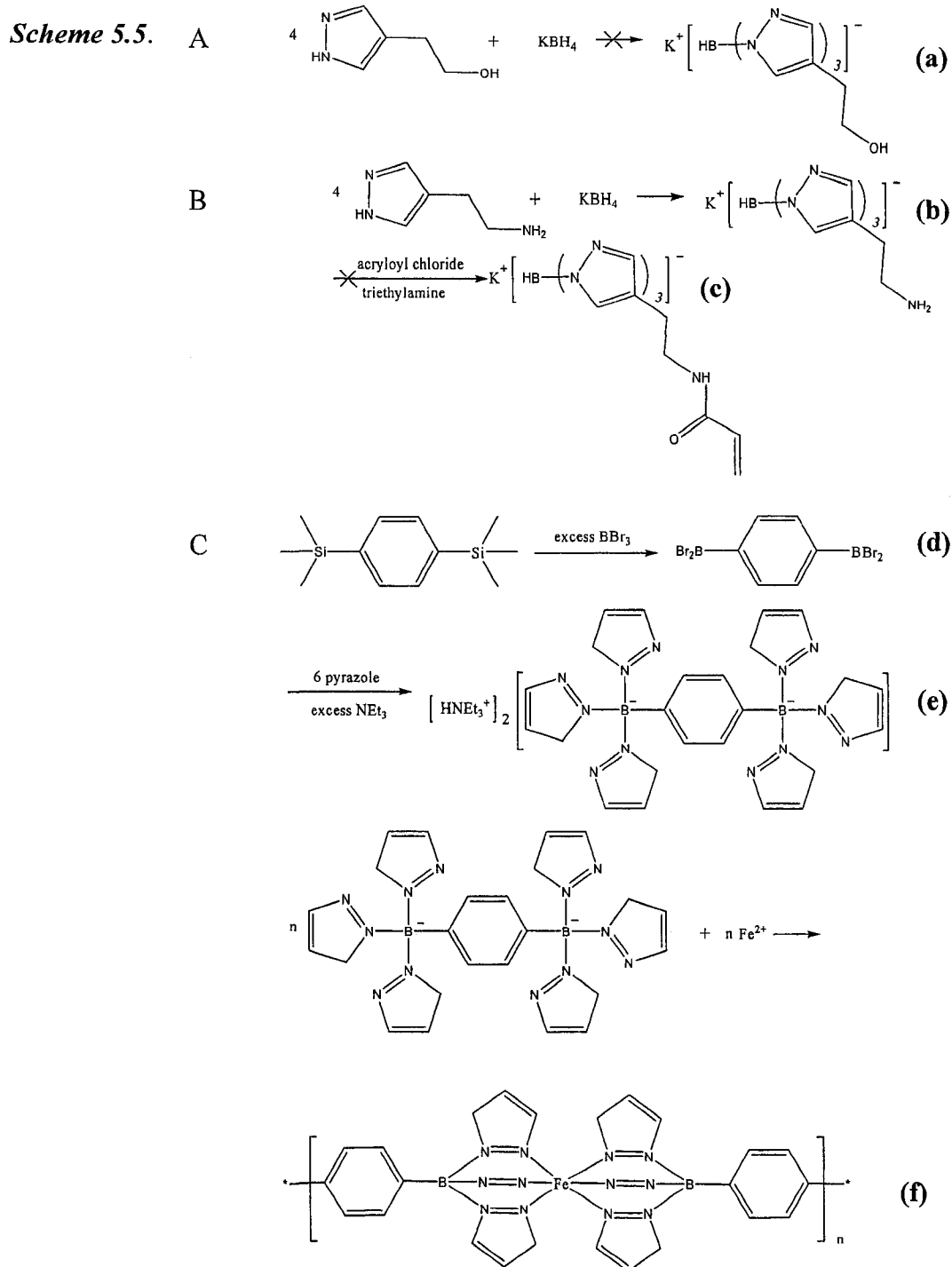


**Figure 5.12.** A. UV-Vis spectra of monomer **1** (A) and monomer **2** (B) (0.1 to 0.2 mM) in methanol (wine red), ethanol (red), acetonitrile (blue), acetone (cyan) and methylene chloride (green).

## Synthesis of the Polypyrazolyborate-Based Monomers and Polymers



As shown in Scheme 5.5, several strategies were attempted to prepare polypyrazolyborate-based ligands. Borates **a** and **b** contain terminal hydroxyl and amion

groups, respectively. Polymerizable acryloyl  $\text{CH}_2=\text{CH}-\text{CO}-$  moieties were expected to be introduced upon reacting with acryloyl chloride. According to Trofimenko,<sup>26,32-34</sup> the iron(II) complex with hydrotrispyrazolylborate exhibit a strong wine red color. Unfortunately, titrating the products of Reaction A and the second step of Reaction B with an aqueous solution of  $\text{Fe}^{2+}$  showed no red color, indicating that neither **a** nor **c** was present. Iron test with **b** showed a positive color change, but the red color disappeared a few minutes after the titration and a green solid formed. The amino functionalities apparently compete for coordination to the iron.

Since difficulties were encountered in making to make monomers **a-c**, a new strategy shown in Scheme 5.5 C was utilized in an attempt to prepare the polymer **f**, assuming that its redox concentration gradient could be fixed by polymerizing the incorporated electrolytes alone. The assumption is based on the fact the polymerizable electrolyte  $\text{ATA}^+\text{APS}^-$  contains two acrylate moieties, and will be subject to facile crosslinking upon thermal treatment and hence be locally immobilized. The NMR results confirmed the success in synthesizing the compound **d** (see Figure 5.9). Titration the crude product **e** with  $\text{Fe}^{2+}$  did produce a red solid; the solid however, turned white after a few day's storage in the glove box, suggesting a poor stability of the polymer. Thus, only cyanoiron complexes with polymerizable bipyridine were further studied (see below).

### Coating Solution Preparation

Coating solutions containing a single redox monomer were prepared by dissolving the monomer in an organic solvent, methanol. A coating solution containing two redox monomers **1** and **3** was prepared by mixing two individual monomer solutions while monitoring the content of the mixture with CV and SWV. Figure 5.13 and 5.14 show CV

and SWV of the final solution. For both voltammograms, the redox process at lower potential was due to the  $\text{Fe}^{2+/3+}$  couple of **3** on the electrode and the process at higher potential was due to the  $\text{Fe}^{2+/3+}$  couple of **1**. Thus the molar ratio of two monomers is equal to the current ratio of the two both redox processes. As can be observed from both CV and SWV, the coating solution has been adjusted to have monomer **1** and monomer **3** in a 1:1 ratio.

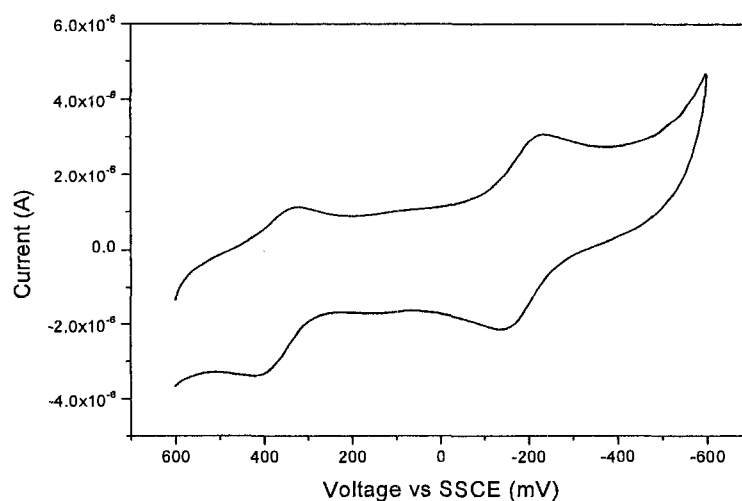


**Figure 5.13.** CV of the coating solution containing **1** and **3** with a molar ratio of unity. W.E., GC ( $0.5 \text{ cm}^2$ ); R.E., SSCE; C.E., Pt; Scan rate =  $100 \text{ mV/sec}$ ;  $50 \text{ mM TMAPF}_6/\text{CH}_2\text{Cl}_2$ .

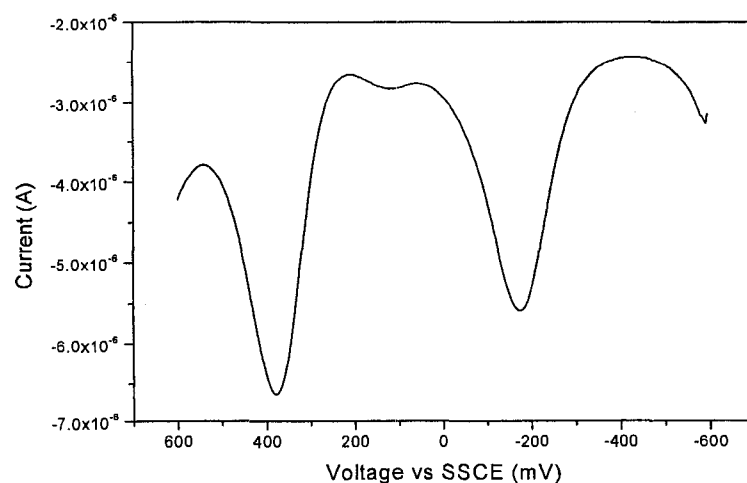


**Figure 5.14.** SWV of the coating solution containing both **1** and **3** in methylene chloride with a molar ratio of ca. unity. W.E., GC ( $0.5 \text{ cm}^2$ ); R.E., SSCE; C.E., Pt; Step E =  $4 \text{ mV}$ ; S.W. Amplitude =  $25 \text{ mV}$ ; Frequency =  $15 \text{ Hz}$ ; Samples per Point = 256;  $50 \text{ mM TMAPF}_6/\text{methylene chloride}$ . The small peak at ca.  $175 \text{ mV}$  (also visible in Figure 5.13) is an unknown impurity present at only a few percent.

## **Initial Film Polymerization**

The conditions employed for monomer polymerization were determined by trial and error. Attempts to perform polymerization in air at atmospheric pressure failed to produce usable films. Films polymerized in air at lower temperatures (90 to 150<sup>0</sup>C) were not sufficiently polymerized and dissolved during the rinsing process; while polymerization at higher temperatures >150<sup>0</sup>C damaged GC electrodes by cracking the silver paint used to make electrical contact between the GC plate and the conducting wire.

These obstacles were overcome by polymerization in vacuum. Under reduced pressure (3 mm Hg), the polymerization temperature was decreased to a reasonable level. Monomer **1** films were polymerized at 100<sup>0</sup>C (7 to 35 minutes, depending on the thickness of the film). And poly(**2**) films were achieved at 140<sup>0</sup>C. The higher temperature requirement in **2** is likely due to the fact that monomer **2** has only 2 acrylate groups, instead of 4. And the optimum temperature to produce poly(**1&3**) films was found to be 110<sup>0</sup>C.

After successful polymerization, the film was rinsed with solvent to remove unpolymerized monomers and soluble oligomers. Rinsed films were then air dried. Inspection of the dry films with microscope (10 -30 times) was very important as defects occasionally formed in the film. The films were considered usable for gradient formation as long as they were free of holes and cracks by microscope examination.

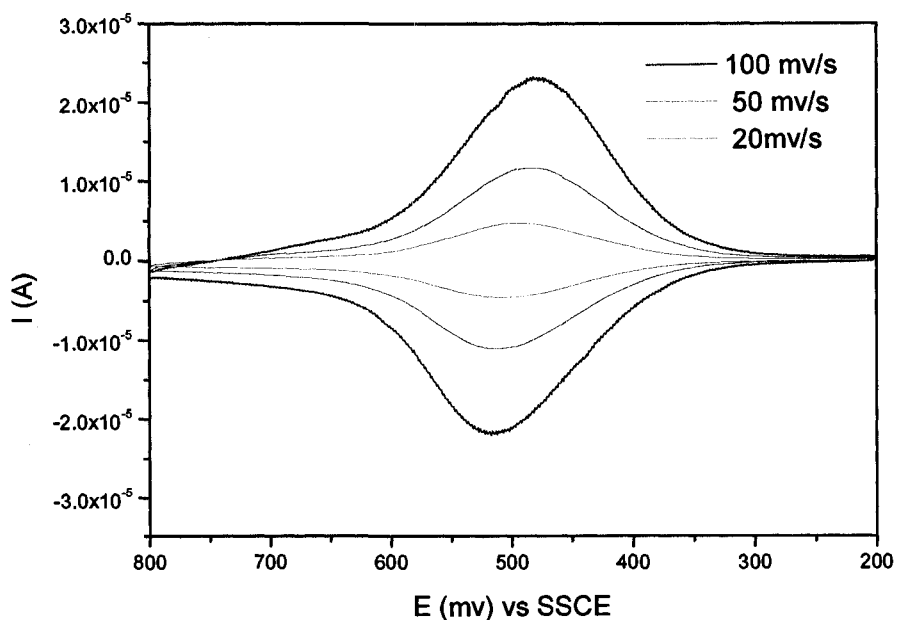
## **Cyclic Voltammeteries of Poly ( 1 )**

Figure 5.15 shows CVs of a poly ( **1** ) film, arising from polymerization of the corresponding monomer film supported on a GC electrode at 100<sup>0</sup>C under reduced

pressure for 7 minutes. The results are summarized in Table 5.1, including peak separation  $\Delta E_p$ , redox potential  $E_{1/2}$ , anodic peak current  $i_{pa}$ , cathodic peak current  $i_{pc}$  and anodic charge  $Q_a$ .  $Q_a$  was calculated by integration of the anodic current over time. As can be seen from Table 5.2, the  $i$  vs.  $E$  response is typical of a surface bound redox system (or finite linear diffusion)<sup>10,17</sup> with  $\Delta E_p \sim 0$  and  $i_p \propto v$ .

**Table 5.2:** Electrochemical properties of Poly ( 1 ) summarized from Figure 5.15. vs SSCE

$v$ (mV/s)	$\Delta E_p$ (mV)	$E_{1/2}$ (mV)	$i_{pa}$ ( $\mu A$ )	$i_{pc}$ ( $\mu A$ )	$Q_a$ ( $\mu C$ )
20	14	500	-4.5	4.8	-43
50	32	497	-11	12	-41
100	40	497	-22	23	-40



**Figure 5.15.** CVs of a poly ( 1 ) coated GC electrode in 1:5 methanol /acetone containing 50 mM TMAPF<sub>6</sub>. R.E., SSCE; C.E., Pt wire.

## Cyclic Voltammetries of Poly ( 2 )

CVs of a poly( 2 ) film coated GC electrode are shown in Figure 5.16 and Figure 5.17. The film was produced by polymerization of the corresponding monomer film at 140°C under reduced pressure for 30 minutes. The CV in Figure 5.16 was obtained in a methanol/acetonitrile (1:5) solution containing 50 mM TMAPF<sub>6</sub>; while those in Figure 5.17 were scanned in an aqueous solution of 100 mM NaCl. The poly( 2 ) film exhibited a broad *i* vs. *E* curve (especially in organic solution), which is typical of highly cross-linked films<sup>7</sup> (due to higher polymerization temperature and longer polymerization duration). Broadness of the *i* vs. *E* curve decreased in aqueous solution containing NaCl, owing possibly to the smaller size of NaCl than that of TMAPF<sub>6</sub> thus easier ion transportation in the highly crosslinked poly( 2 ) film and possibly better solvent swelling of the polymer. As can be seen from Table 5.2, the *i* vs. *E* behavior of poly ( 2 ) deviated from a finite linear diffusion system, suggesting an overall slow charge transfer in the poly( 2 ) film.

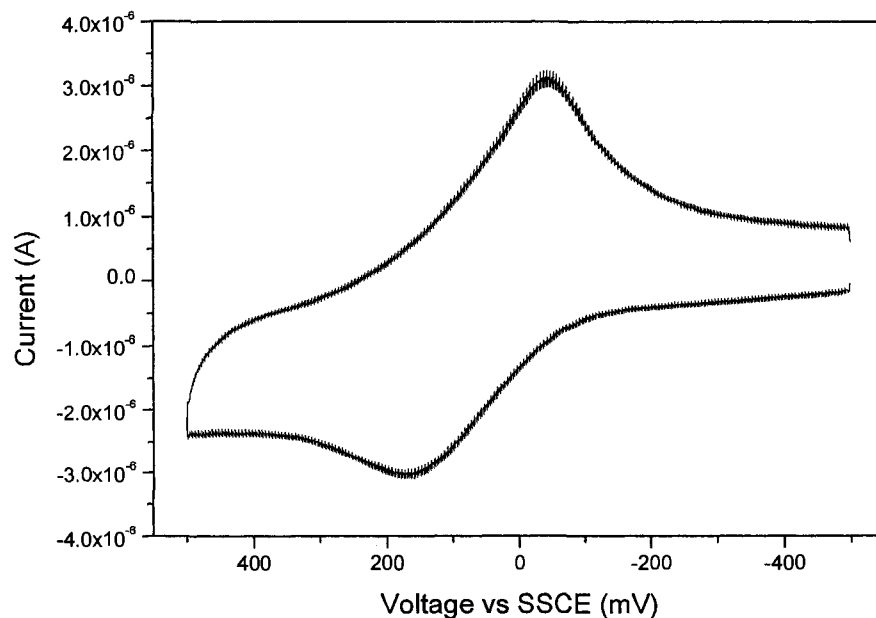


**Figure 5.16.** CVs of a poly ( 2 ) coated GC electrode in 1:5 methanol /acetonitrile containing 50 mM TMAPF<sub>6</sub>. Scan Rate, 100 mV/s; R.E., SSCE; C.E., Pt wire.

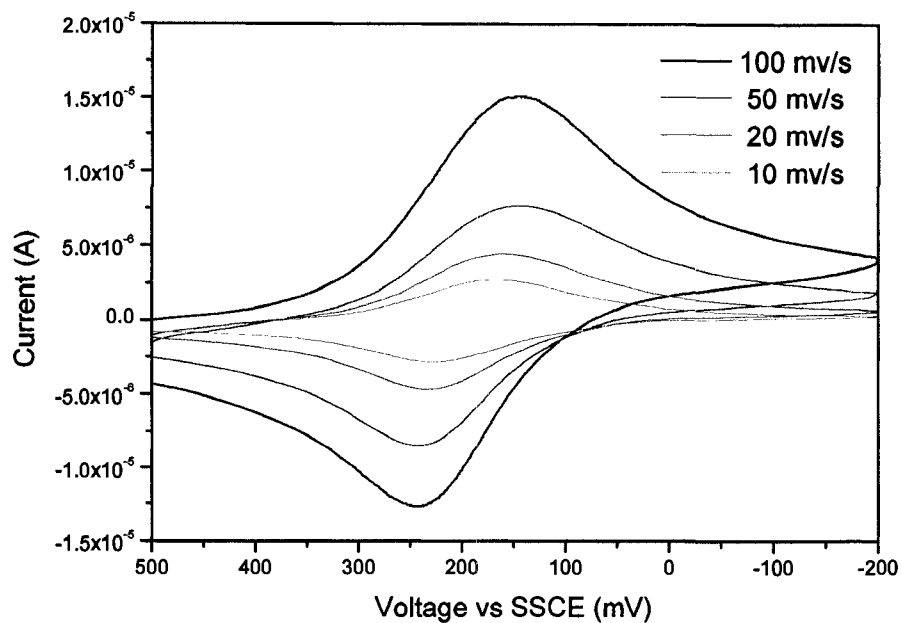


**Figure 5.17.** CVs of a poly ( 2 ) coated GC electrode in 100 mM NaCl aqueous solution. R.E., SSCE; C.E., Pt wire.

**Table 5.3.** Electrochemical properties of a Poly ( 2 ) film deduced from Figure 5.16 and Figure 5.17. \* vs SSCE.

Electrolyte	$\nu$ (mV/s)	$\Delta E_p$ (mV)	* $E_{1/2}$ (mV)	$i_{pa}$ ( $\mu$ A)	$i_{pc}$ ( $\mu$ A)	Qa ( $\mu$ C)
50mM TMAPF <sub>6</sub> in CH <sub>3</sub> OH/CH <sub>3</sub> CN (1:5)	100	212	64	-3.1	3.1	15
100 mM NaCl in Water	10	60	196	-2.8	2.7	60
	20	72	196	-4.7	4.5	55
	50	96	195	-8.4	7.7	42
	100	96	192	-13	15	46

### Dual Mode CVs of the Sandwich Electrode GC/Poly ( 1 )/Au

Typical dual mode CVs of the sandwich electrode GC/ Poly ( 1 )/Au in an acetonitrile solution of polymerizable electrolyte  $\text{ATA}^+\text{APS}^-$  50 (mM) are shown in Figure 5.18. Even though the potential of the Au electrode was maintained at 0 mV vs SSCE, a potential lower than the reduction peak potential of the polymer, it still recorded current of magnitude comparative to that on the GC electrode, suggesting that charge transport in the polymer film occurred, which was essential for the concentration gradient to form in the film.

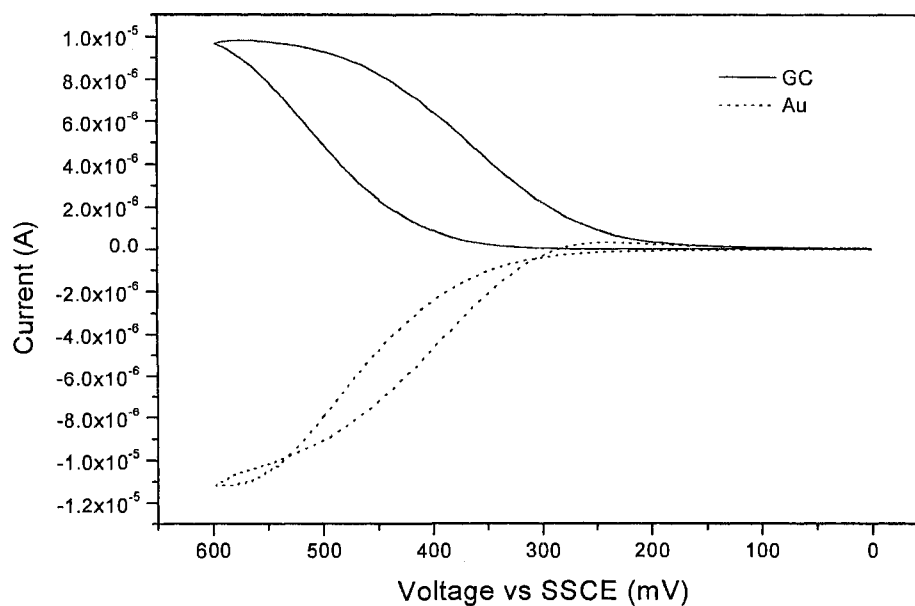


**Figure 5.18.** Dual mode CVs of Poly ( 1 ) sandwiched between GC and Au electrodes. GC was scanned while the potential of Au was held at 0 mV vs SSCE. The solid curve is the CV recorded on GC at 5mV/s, and the dotted curve is the current response of the Au electrode. R.E., SSCE; C.E., Pt wire; Electrolyte, 50 mM  $\text{ATA}^+\text{APS}^-$  in acetonitrile.

### Gradient Formation in Poly( 1 ) Films Sandwiched between GC and Au

Redox gradient was created in the film using a bipotentiostat. While maintaining the

potential of Au at 0mV vs SSCE, the GC electrode was scanned from 0 to 600 mV at 5mV/s and stayed at 600 mV, so that a potential bias of 600 mV was applied to the polymer film. At the moment when the GC electrode stopped scanning, the measured current magnitude instantly started decreasing and continued to decay until a ready state value was reached. It was typical for the films to give small steady state currents (ca. 0.1 to 0.01 $\mu$ A). These steady state currents varied among films (up to several hundreds of nA). These variations were likely due to the film thickness and degree of crosslinking.

Upon removing the redox-gradient containing films from the electrolyte solution, a sharp decrease of current occurred again and the current decayed to a value much less than the steady state current ( $<10^{-8}$ A).

### **Redox Gradient Formation in Poly( **1&3** ) Films Coated on IDA Electrodes**

Redox gradient formation in poly( **1&3** ) films was attempted on both Pt0550.3 and Pt1025.5 IDA electrodes. One of the combs (WE1) was held at -300mV vs SSCE, and the other (WE2) was scanned from zero to -300mV then back to 600mV and held at 600mV for 20 mins. Figure 5.19 shows the corresponding  $i$  vs  $v$  traces on a Pt0550.3 IDA electrode. On this electrode, the current magnitude of WE1 and WE2 are comparable to each other, meaning that charge transportation occurred across the polymer film. After 20 minutes, the system reached a steady state. At this steady state, both the film and the electrolyte reached stationary concentration profiles, there was not net ionic current and the current was entirely due to the electron transfer through the polymer film.<sup>35</sup> Thus, the apparent resistance of the film at steady state is equal to its electronic resistance, which was calculated to be  $6 \times 10^6 \Omega$ .

No measurable current was produced however, on the WE1 electrode when Pt1025.5 IDA electrodes were used. Our initial research lacked in precise control of the thickness of the monomer film and its polymerization degree, thus resulted in poor repeatability. The ploy ( **1&3** ) film on the Pt1025.5 IDA electrode could be overly crosslinked and hence highly resistive, making it hard for electrons to hop through the 10  $\mu\text{m}$  interdigit distance.

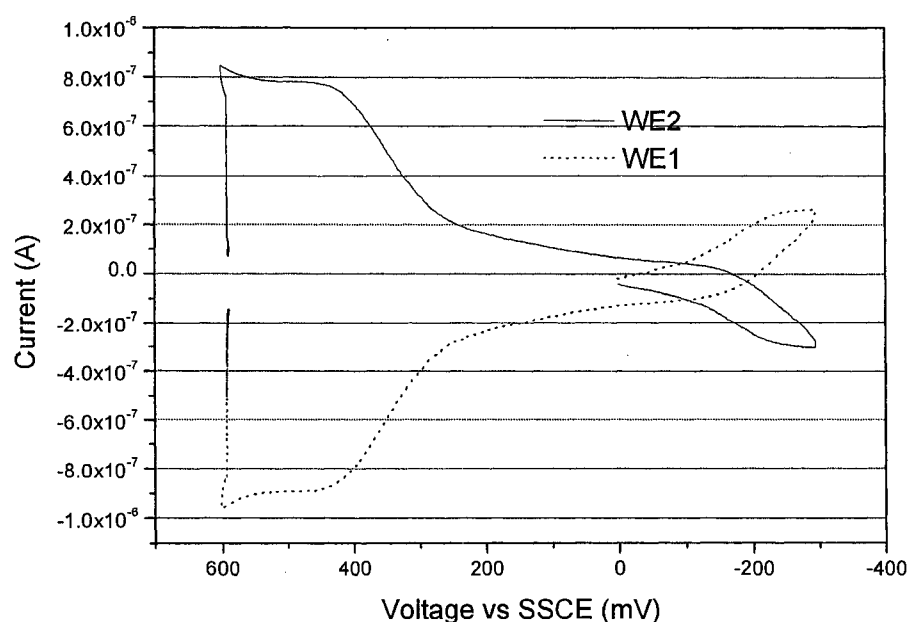


**Figure 5.19.** Dual mode Voltogram of a poly ( **1&3** ) coated IDA electrode Pt0550.3, recorded during concentration gradient formation in electrolyte solution of 50 mM  $\text{ATA}^+\text{APS}^-$  in acetonitrile. WE2 was scanned at 100mV/s from zero to -300 mV, then back to 600 mV and stopped at 600 mV for 20 minutes, while the potential of WE1 was kept at -300mV. The solid curve is recorded on WE2, and the dotted curve on WE1. R.E., SSCE; C.E., Pt wire.

After gradient formation, the Pt0550.3 IDA electrode was removed from solution, dried in the air and subject to inspection under microscope while maintaining the potential bias applied to it. No visible gradient was seen despite the color difference between the oxidized iron complex (red) and the reduced iron complex (purple).<sup>29</sup>

## Locking of the Redox Gradients in the Films

Films with redox gradients were placed in the vacuum oven at elevated temperature to attempt to permanently lock the gradients. Figure 5.20 shows the current response of a dry poly( **1&3** ) film containing ostensibly locked gradients to a scanning potential (2 V to -2 V) at 100 mV/s. The measured current was very low and noisy, suggesting a highly resistive film. All the films became more resistive ( $>1 \times 10^9 \Omega$ ) after the gradient was thermally locked, implying a slower electron hopping rate in the film of higher polymerization degree.

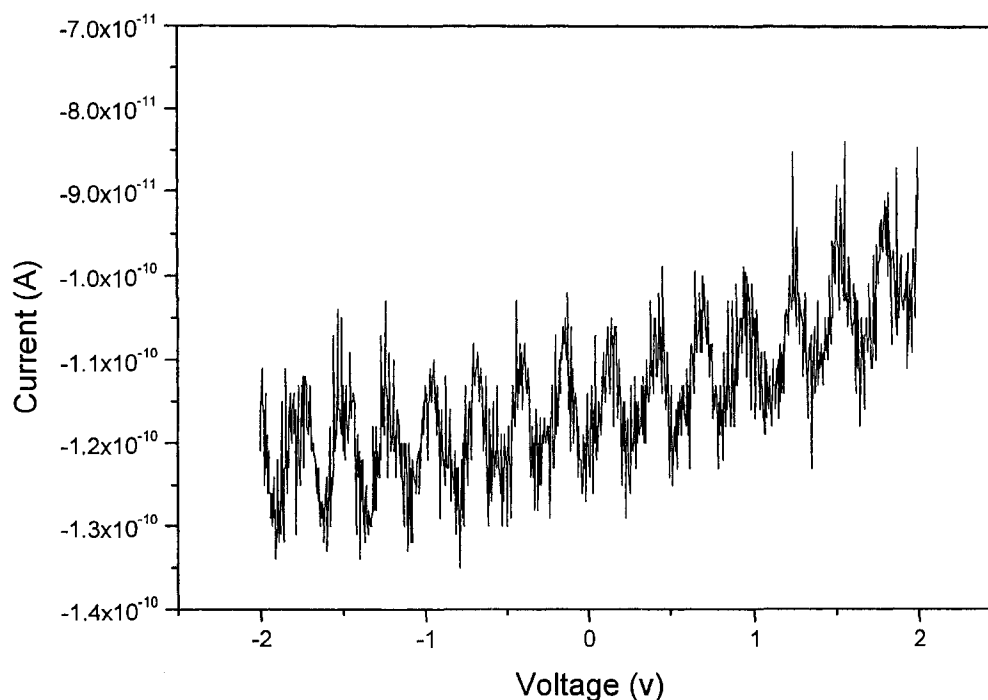


**Figure 5.20.** Current-Voltage responses of a dry, locked poly( **1&3** ) film coated on a Pt0550.3 IDA electrode. The gradient was formed in a 50 mM ATA<sup>+</sup>APS<sup>-</sup> / acetonitrile solution with a potential bias of 900 mV. The formed gradient was thermally locked at 110°C in vacuum for three hours

According to Kaufman<sup>8,9</sup>, solvent-induced pendent group motion could provide the necessary dynamic interactions to allow rapid electron transfer to occur through the

polymer. In addition, swelling of the film would facilitate finite ionic motion. Thus, a higher electrical conductivity was expected for films swollen by solvents. The black curve in Figure 5.21 shows the current response of the poly( **1&3** ) film after it was soaked in acetonitrile for 10 minutes. In comparison with the dry film (Figure 5.20), the swollen film gave a higher current. Meanwhile, a solid-diode behavior, i.e., the nonlinear current response, was also observed for the swollen film, only more pronounced.

Unfortunately, the blank test produced a similar current response (red curve in Figure 5.21). To provide a meaningful comparison, the blank test was done using the same IDA electrode as that used to obtain the black curve, except that the poly( **1&3** ) film had been carefully removed with a cotton swab. As it can be seen from comparison of the black curve with the red, the current measured on the poly( **1&3** ) film mainly came from polarization of the solvent acetonitrile.

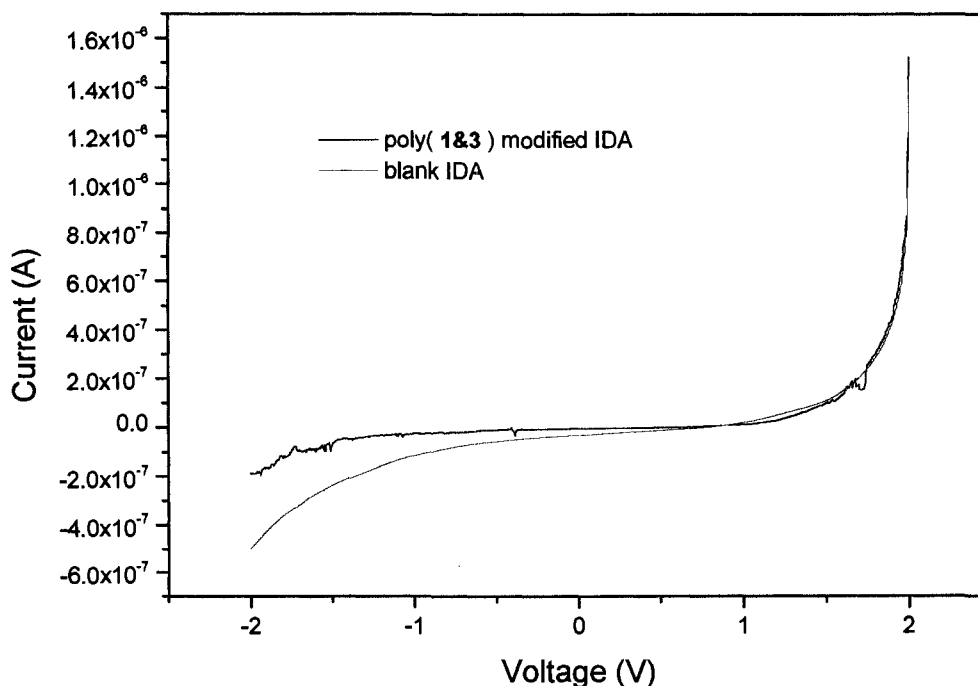


**Figure 5.21.** Voltammograms of IDA electrodes soaked in acetonitrile. The black curve is for the poly( **1&3** ) modified IDA electrode, which is the same as that used in Figure 5.20. The red curve is also for the same IDA electrode except that it was cleaned by removing the poly( **1&3** ) film with a cotton swab. Other conditions will be same as that in Figure 5.20.

## SUMMARY

During this study, polymerizable iron complexes **1**, **2** and **3** were successfully prepared and thermally polymerized on the surface of working electrodes. Redox concentration gradient was created in the polymer films utilizing a standard four electrode bipotentiostat. Attempts were made to covalently lock the redox gradient by chemically grafting the polymerizable counter ions to the polymer backbone.

However, polymer films produced this way are highly resistive ( $>10^6 \Omega$  prior to attempts to lock the gradient and  $>10^9 \Omega$  after). The main issue to be addressed in the future is to developing new polymers which have intrinsically high conductivity. Hybrid polymers containing both redox and conjugated moieties could be a good choice. According to Cameron<sup>17</sup>, coordination of metal atoms to a conjugated polymer backbone will lead to an enhancement of the rate of electron transport compared to similar polymers not having the conjugation.

For example, a hybrid polymer, bisbipyridyl osmium(II) complex of poly([6,6'-bibenzimidazole-2,2'-diyl]-2,5-pyridine), when deprotonated, exhibits an electron diffusion coefficient  $D_e$  of  $\sim 10^{-9} \text{ cm}^2/\text{s}$  at a potential around 0.4 V vs SSCE.<sup>17</sup> According to the formula  $\lambda^2 = 2D_e t$  ( $\lambda$  is the electron diffusion length  $\lambda$ ,  $t$  is the diffusion time), the electrons would be able to travel across the hybrid polymer of  $1 \mu\text{m}$  thickness within a duration of just 5 seconds, implying facile redox gradient formation upon applying a small potential bias (ca. 0.4 V) across the polymer film. By scanning the potential of the polymer in a solution of  $\text{ATA}^+ \text{APS}^-$ , cations on the deprotonated polymer backbone would be replaced by polymerizable  $\text{ATA}^+$ ; meanwhile, polymerizable anions  $\text{APS}^-$  would be added around the Co(III) centers for charge neutralization purposes. Once a

redox gradient is established, it could be permanently locked by polymerizing the incorporated electrolyte. The backbone of the hybrid polymer was formed by thermal treatment at for 125 °C 24 hour followed by 160 °C for 43 hours.<sup>17</sup> Thus, thermal polymerization of the electrolyte at 120°C would not significantly change the hybrid polymer.

- (1) Elliott, C. M.; Pichot, F.; Bloom, C. J.; Rider, L. S. *Journal of the American Chemical Society* **1998**, *120*, 6781-6784.
- (2) Maness, K. M.; Masui, H.; Wightman, R. M.; Murray, R. W. *Journal of the American Chemical Society* **1997**, *119*, 3987-3993.
- (3) Maness, K. M.; Terrill, R. H.; Meyer, T. J.; Murray, R. W.; Wightman, R. M. *Journal of the American Chemical Society* **1996**, *118*, 10609-10616.
- (4) Masui, H.; Murray, R. W. *Journal of the Electrochemical Society* **1998**, *145*, 3788-3793.
- (5) Terrill, R. H.; Hatazawa, T.; Murray, R. W. *Journal of Physical Chemistry* **1995**, *99*, 16676-83.
- (6) Terrill, R. H.; Hutchison, J. E.; Murray, R. W. *Journal of Physical Chemistry B* **1997**, *101*, 1535-1542.
- (7) Elliott, C. M.; Redepenning, J. G.; Balk, E. M. *Journal of the American Chemical Society* **1985**, *107*, 8302-4.
- (8) Kaufman, F. B.; Engler, E. M. *Journal of the American Chemical Society* **1979**, *101*, 547-9.
- (9) Kaufman, F. B.; Schroeder, A. H.; Engler, E. M.; Kramer, S. R.; Chambers, J. Q. *Journal of the American Chemical Society* **1980**, *102*, 483-8.
- (10) Ren, X.; Pickup, P. G. *Journal of Electroanalytical Chemistry* **1994**, *372*, 289-91.
- (11) Salzer, C. A. Ph. D. Thesis, Colorado State University, 2002.
- (12) Arana, C.; Keshavarz, M.; Potts, K. T.; Abruna, H. D. *Inorganica Chimica Acta* **1994**, *225*, 285-95.
- (13) Hurrell, H. C.; Mogstad, A. L.; Usifer, D. A.; Potts, K. T.; Abruna, H. D. *Inorganic Chemistry* **1989**, *28*, 1080-4.
- (14) Abruna, H. D. *Coordination Chemistry Reviews* **1988**, *86*, 135-89.
- (15) Guadalupe, A. R.; Usifer, D. A.; Potts, K. T.; Hurrell, H. C.; Mogstad, A. E.; Abruna, H. D. *Journal of the American Chemical Society* **1988**, *110*, 3462-6.
- (16) Chidsey, C. E. D.; Murray, R. W. *Science (Washington, DC, United States)* **1986**, *231*, 25-31.
- (17) Cameron, C. Ph. D. thesis Memorial University of Newfoundland 2000
- (18) Turner, J. W.; Schultz, F. A. *J. Phys. Chem. B* **2002**, *106*, 2009-2017.
- (19) Toma, H. E.; Takasugi, M. S. *Journal of Solution Chemistry* **1989**, *18*, 575-83.
- (20) Thorsteinsson, T.; Masson, M.; Kristinsson, K. G.; Hjalmarsdottir, M. A.; Hilmarsson, H.; Loftsson, T. *Journal of Medicinal Chemistry* **2003**, *46*, 4173-4181.
- (21) Fuerstner, A.; Thiel, O. R.; Ackermann, L. *Organic Letters* **2001**, *3*, 449-451.
- (22) Kang, S. K.; Kim, W. S.; Moon, B. H. *Synthesis* **1985**, 1161-2.
- (23) Babler, J. H.; Invergo, B. J. *Journal of Organic Chemistry* **1979**, *44*, 3723-4.
- (24) Chambron, J. C.; Sauvage, J. P. *Tetrahedron* **1987**, *43*, 895-904.
- (25) Jones, R. G.; Mann, M. J. *Journal of the American Chemical Society* **1953**, *75*, 4048-52.
- (26) Trofimenko, S. *Journal of the American Chemical Society* **1967**, *89*, 3170-7.
- (27) Haubold, W.; Herdtle, J.; Gollinger, W.; Einholz, W. *Journal of Organometallic Chemistry* **1986**, *315*, 1-8.
- (28) Jaekle, F.; Polborn, K.; Wagner, M. *Chemische Berichte* **1996**, *129*, 603-606.
- (29) Schilt, A. A. *Journal of the American Chemical Society* **1960**, *82*, 3000-5.

- (30) Toma, H. E.; Malin, J. M. *Inorganic Chemistry* **1973**, *12*, 1039-45.
- (31) Gameiro, P.; Pereira, E.; Garcia, P.; Breia, S.; Burgess, J.; de Castro, B. *European Journal of Inorganic Chemistry* **2001**, 2755-2761.
- (32) Trofimenko, S. *Journal of the American Chemical Society* **1967**, *89*, 3165-70.
- (33) Trofimenko, S. *Journal of the American Chemical Society* **1967**, *89*, 4948-52.
- (34) Trofimenko, S. *Journal of the American Chemical Society* **1967**, *89*, 6288-94.
- (35) Ybarra, G.; Moina, C.; Florit, M. I.; Posadas, D. *Electrochimica Acta* **2008**, *53*, 3955-3959.